Active flow control as a tool to reveal the role of the precessing vortex core in swirl flames

vorgelegt von
Master of Science (TU Berlin),
Finn Simon Lückoff,
orcid.org/0000-0002-6610-0851

an der Fakultät V – Verkehrs- und Maschinensysteme
der Technischen Universität Berlin
zur Erlangung des akademischen Grades

Doktor der Ingenieurwissenschaften
– Dr.-Ing. –

genehmigte Dissertation

Promotionsausschuss:

Vorsitzender:	Prof. Dr. rer. nat. Valentin Popov
Gutachter:	Prof. Dr.-Ing. Kilian Oberleithner
Gutachter:	Prof. Dr.-Ing. Christian Oliver Paschereit
Gutachter:	Prof. Adam Michael Steinberg
Gutachter:	Prof. Maarten Vanierschot

Tag der wissenschaftlichen Aussprache: 13. April 2021

Berlin 2021

Preface

This doctoral thesis and the accumulated publications would not have been realized without the support and help of some specific persons. First of all, I want to mention my supervisors Prof. Dr.-Ing. Kilian Oberleithner and Prof. Dr.-Ing. Christian Oliver Paschereit. Kilian, I am very thankful for the tremendous professional, friendly and motivating support you have given me during the whole project. I must also admit that I am very honored to be part of your team and enjoy helping you to further develop your department. Prof. Paschereit, you are supporting me without constraints since the beginning of the project for which I am very thankful. This includes your expertise and fresh ideas and the use of your laboratories and measurement equipment. Prof. Adam Michael Steinberg and Prof. Maarten Vaniershot, thank you very much for taking part in the committee and the evaluation of this thesis. Prof. Dr. rer. nat. Valentin Popov, I am very happy and thankful that you host the committee as a chairmen.
Besides the supervisors, there are the co-authors who supported the work with their expertise and ideas. Moritz Sieber, thank you very much for your unconditional support overcoming experimental, analytical and technical issues. Jens Müller, thank you very much for your extraordinary studies associated with this thesis which accompanied the project and support the findings of this thesis. Thomas Kaiser, thank you very much for introducing me into the world of hydrodynamic global linear stability analysis.
Moreover, I want to thank the rest of the FLOW group which includes or included: Phoebe Kuhn, Mohammad Rezay Haghdoost, Sirko Bartholomay, Jan Beuth, David Nolte, Jakob von Saldern, Moritz Reumschüssel, Bhavraj Thethy, Alexander Jaeschke and Mario Casel; and all the other colleagues who accompanied and supported me: Eric Bach, Johann Vinkeloe, Tom Tanneberger, Richard Blümner, Niclas Garan, Alessandro Orichini, Fatma Cansu Yücel, Fabian Habicht, Sebastian Schimek, Thoralf Reichel and Steffen Terhaar. Thank you all for your professional support and all the pleasant, inspiring and motivating conversations and experiences which we had and will have together. Special thanks goes out to Alexander Jaeschke for his exemplary support in the experiments of this project.
Furthermore, I want to thank our team assistants, Sandy Meinecke and Maria Lück, for their support in handling all the bureaucracy involved in the project management and for our pleasant and inspiring conversations during lunch breaks. Thank you very much, Andy Göhrs, for the technical realization and maintenance of the test rigs and your smart ideas to overcome technical issues. In this context, I also want to thank the former colleagues Robert Bahnweg, Udo Schwadtke and Heiko Stolpe for their technical support.
Last but not least, I want to thank the most important people in my life with all my heart which are: my wife, my parents, my family and friends who support and supported me with their unconditional love which means everything to me! - Thank you!

Zusammmenfassung

Die Strömung innerhalb einer Gasturbine ist typischerweise stark turbulent, wenn sie den Verdichter verlässt und den Brennereinlass erreicht. Im Inneren des Brenners passiert die Strömung typischerweise einen Drallgenerator, der die fast parallele Strömung in eine Drallströmung umwandelt. Der Grad des in der Strömung induzierten Dralls ist ausreichend hoch, so dass der vom Brennerauslass in die Brennkammer austretende Drallstrahl ein Phänomen erfährt, das als Wirbelaufplatzen (vortex breakdown) bezeichnet wird. Als Folge dieses Phänomens bildet sich um die Strahlachse eine zentrale Rezirkulationszone, die es der Flamme ermöglicht, sich innerhalb der entstehenden Scherschichten zu stabilisieren. Diese reaktive Strömungskonfiguration ermöglicht eine effiziente und emissionsarme magere Verbrennung, ist jedoch anfällig für thermoakustische und hydrodynamische Instabilitäten. Eine der bekanntesten hydrodynamischen Instabilitäten in dieser Strömungskonfiguration ist der so genannte precessing vortex core (PVC), der sich als eine spiralförmige, kohärente Struktur manifestiert, welche stromabgerichtet die Scherschichten entlang mäandert. Obwohl es bereits mehrere Studien über den PVC gibt, ist dessen Einfluss auf den Verbrennungsprozess noch nicht vollständig verstanden und beschrieben.

In der vorliegenden Arbeit wird ein aktives Strömungskontrollsystem entwickelt, das exklusive experimentelle Bedingungen schafft, um die Rolle des PVC auf den Verbrennungsprozess weiter zu untersuchen. Dieses Strömungskontrollsystem ist in die Mischsektion eines Drallbrenners integriert. Dort wird eine helikale Aktuation, nach dem zero-net-mass-flux Prinzip, realisiert, durch welche die präzedierende Bewegung des PVC nachgeahmt wird. Die Aktuation wird in jenem Bereich angewendet, in welchem die Antwort des PVC auf äußere periodische Anregung maximal ist. Dieser Bereich der höchsten Rezeptivität kann als Ursprung des PVC betrachtet werden. Aufgrund der maximalen Antwort des PVC in diesem Bereich sind nur kleine Anregungsamplituden notwendig, um eine erhebliche Kontrollwirkung zu erzielen, ohne die Strömungskonfiguration grundlegend zu verändern. Nach einem umfassenden Nachweis der Funktionalität des Regelkonzepts unter isothermen und reaktiven Betriebsbedingungen wird das Strömungskontrollsystem eingesetzt, um den PVC je nach Strömungskonfiguration anzuregen (offener Regelkreis) oder zu unterdrücken (geschlossener Regelkreis). Mit diesem Werkzeug kann der ausschließliche Einfluss des PVC auf Flammendynamik, Mischung und NO_x-Emissionen untersucht werden.

Es wird beobachtet, dass die Anregung des PVC selbsterregte thermoakustische Schwingungen erheblich dämpfen kann. Eine Erklärung für diese Beobachtung ist ein möglicher Bruch der Symmetrie der achsensymmetrischen Äquivalenzverhältnisschwankungen durch den angegereten asymmetrischen PVC. Weitere Erklärungen für diese Beobachtung werden durch zwei Kopplungsmechanismen zeitlich gemittelter Felder gegeben, die aus zeitaufgelösten Strömungsfeld- und Wärmefreisetzungsratenmessungen abgeleitet werden. Diese Mechanismen werden in Verbindung mit Messungen der Flammentransferfunktion (FTF) abgeleitet, die zeigen, dass der PVC in der Lage ist, den FTF-Gain zu reduzieren, ohne die FTF-Phase zu verändern. Dem ersten Mechanismus zufolge reduziert

der PVC die Wachstumsrate der Kelvin-Helmholtz-Instabilität, was das Wachstum der achsensymmetrischen Moden in den Scherschichten behindert. Mechanismus zwei bezieht sich auf die PVC-induzierte Änderung der mittleren Flammenform, die kompakter wird und sich stromaufwärts zum Brenneraustritt hin verschiebt. Dadurch erreichen weniger Wärmefreisetzungsratenschwankungen die empfindliche Flammenspitze, was ebenfalls zu einer Dämpfung des FTF-Gains führt. Neben diesen Erkenntnissen zum Einfluss des PVC auf die Flammendynamik wird gezeigt, dass der PVC eine großräumige Vermischung der einströmenden kalten Reaktanden mit den heißen Produkten in der zentralen Rezirkulationszone bewirkt. Diese großräumige Vermischung erhöht die Reaktionsgeschwindigkeit und befördert Radikale in das einströmende Fluid. Dadurch folgt die Flamme den PVC-induzierten Wirbeln und das Niveau der NO_x-Emissionspegel erhöht sich.

Mit dem entwickelten Strömungskontrollansatz werden einzigartige experimentelle Bedingungen geschaffen, die es erlauben, den ausschließlichen Einfluss des PVC auf den Verbrennungsprozess zu untersuchen. Darüber hinaus kann dieser Strömungskontrollansatz zur aktiven Steuerung der Stabilität und Effizienz des Verbrennungsprozesses eingesetzt werden. Um den Laboraufbau des Strömungskontrollsystems auf eine Maschine im industriellen Maßstab anzuwenden, wird ein alternatives Aktuationskonzept vorgeschlagen, das sich auf fluidische Oszillatoren stützt. Darüber hinaus ist der in der vorliegenden Arbeit untersuchte Strömungskontrollansatz auf alle Arten von Strömungen mit inhärenten globalen hydrodynamischen Moden, wie z.B. dem PVC, anwendbar.

Abstract

The flow inside a gas turbine is typically highly turbulent when it leaves the compressor and reaches the burner inlet. Inside the burner, the flow typically passes through a swirl generator which transforms the almost parallel flow into a swirling flow. The degree of the swirl induced to the flow is sufficiently high such that the swirling jet emanating from the burner outlet into the combustion chamber undergoes a phenomenon known as vortex breakdown. As a consequence of this phenomenon, a central recirculation zone forms around the jet axis which allows the flame to stabilize inside the resulting shear layers. This reacting flow configuration allows for an efficient and low-emission lean combustion, but is prone to thermoacoustic and hydrodynamic instabilities. One of the most prominent hydrodynamic instabilities in this flow configuration is the so-called precessing vortex core (PVC) which manifests as a single-helical coherent structure meandering in downstream direction along the shear layers. Although, there are already several studies about the PVC, its impact on the combustion process is not fully understood and described, yet.

In this thesis, an active flow control system is developed which creates exclusive experimental conditions to further investigate the role of the PVC on the combustion process. This flow control system is integrated into the mixing section of a swirl burner. There, helical actuation, according to the zero-net-mass-flux principle, is achieved which mimics the helical motion of the PVC. The actuation is applied in the region where the response of the PVC to external periodic forcing is maximal which can be considered as the origin of the PVC. Due to the maximal response of the PVC in this region, only small actuation amplitudes are necessary to achieve a considerable control effect without changing the flow configuration fundamentally. After a comprehensive proof of the control concept under isothermal and reacting operating conditions, the flow control system is applied to either excite a PVC via open-loop forcing or suppress it via closed-loop control depending on the flow configuration. With this tool at hand, the exclusive impact of the PVC on flame dynamics, mixing and NO_x emissions is investigated.

It is observed that the excitation of the PVC can damp self-excited thermoacoustic oscillations considerably. One explanation for this observation, is a possible break of the symmetry of axisymmetric equivalence ratio fluctuations by the skew-symmetric actuated PVC. Further explanations for this observation are given by two mean field coupling mechanisms which are derived from time-resolved flow field and heat release rate measurements. These mechanisms are derived in connection with measurements of the flame transfer function (FTF) which reveal that the PVC is capable of reducing the FTF gain without changing the FTF phase. According to mechanism one, the PVC reduces the growth rate of the Kelvin-Helmholtz instability which hinders axisymmetric modes to grow in the shear layers. Mechanism two refers to the PVC-induced change of the mean flame shape which becomes more compact and is shifted upstream towards the burner outlet. As a result, less heat release fluctuations reach the sensitive flame tip which leads as well to a damping of the FTF gain. Besides these findings regarding the impact of the

PVC on flame dynamics, it is shown that the PVC affects a large-scale mixing of incoming cold reactants with hot products from the central recirculation zone. This large-scale mixing enhances the reaction rate and entrains radicals into the incoming flow. Consequently, the flame follows the PVC-induced vortices and the NO_x emission level increases. With the developed flow control approach at hand, unique experimental conditions are generated which allow for investigating the exclusive impact of the PVC on the combustion process. Furthermore, this flow control approach can be applied to actively control the stability and efficiency of the combustion process. To apply the laboratory actuation system to a machine of industrial scale, an alternative actuation design is suggested which relies on fluidic oscillators. Moreover, the flow control approach studied in the present thesis is applicable to all types of flow with inherent global hydrodynamic modes such as the PVC.

Contents

List of Figures

Nomenclature

Latin characters

A	amplitude
a_i	SPOD coefficients
C_μ	momentum coefficient of actuation
D	nozzle diameter
$e(t)$	sensor measurement signal
FTF	flame transfer function
f	frequency [Hz]
f_{PVC}	PVC frequency [Hz]
G	actuator gain
m	azimuthal wave number
OH^*	heat release rate distribution
Q	global heat release rate
Re	Reynolds number
St	Strouhal number
S	swirl number
$s(t)$	actuator input signal
t	time [s]
u	acoustic velocity
$\mathbf{v}$	velocity vector
V_0	bulk velocity
(v_x, v_r, v_θ)	axial, radial and azimuthal velocity
$\mathbf{x}$	coordinate vector
(x, r, θ)	axial, radial and azimuthal coordinates
(x, y, z)	axial, transversal and out-of-plane coordinates

Greek symbols

α	complex axial wave number
$\Delta\varphi$	phase shift
ν_{eff}	effective viscosity
ω	complex frequency
ϕ	equivalence ratio
Φ_i	spatial SPOD mode
ρ	fluid density
φ	phase signal

Subscripts and superscripts

$(.)'$	fluctuating part

$(.)''$ stochastic incoherent part
$(.)_f$ forcing quantity
$(.)_n$ natural quantity
$\hat{(.)}$ Fourier transformed
$\overline{(.)}$ time average
$\tilde{(.)}$ coherent part

Operators

$\Im\{(.)\}$ imaginary part
$\Re\{(.)\}$ real part

Acronyms

BTM Burner Transfer Matrix
CRZ Central Recirculation Zone
FTF Flame Transfer Function
ISL Inner Shear Layer
LES Large Eddy Simulation
LSA Linear Stability Analysis
MMM Multi Microphone Method
OH-CL OH*-Chemiluminescence
ORZ Outer Recirculation Zone
OSL Outer Shear Layer
PIV Particle Image Velocimetry
PMT Photomultiplier Tube
POD Proper Orthogonal Decomposition
PVC Precessing Vortex Core
QLS Quantitative Light Sheet method
SPOD Spectral Proper Orthogonal Decomposition
TA Thermoacoustic
VB Vortex Breakdown

"Tumbling, in a world of swirl
Rumbling, in a world of swirl
In a world of swirl
Everything's hazy, everything's a blur"

Billy Gibbons (ZZ Top)
in *World of Swirl* (Album *Antenna*, 1994)

Chapter 1

Introduction

Fluid flows hide an infinite number of phenomena which can be directly observed in nature and fascinate mankind ever since. The enormous fascination of pioneers like Leonardo da Vinci (1452-1519) about e.g. water flows marks the beginning of an era of scientific description and technical exploitation of fluid flows. Da Vinci started to explore fluid flows on an experimental basis and explained his methodology in his Paris Manuscript (Ms.) E as follows (translated to English in [80]):

"First I will do some experiments before I proceeding beyond, because my intention is to cite first experience and then that reason to show why such experience is bound to behave in that way. And this is the real rule how speculators of natural effects have to proceed." (f. 55r)

His approach of gaining experience from experiments to describe and understand underlying phenomena, enabled mankind to convert the energy contained in fluid flows to usable energy for example in the form of electrical power. Modern energy technology relies especially on turbomachinery including different types of turbines, such as gas and hydro turbines, which are driven by different types of fluid flows. Whereas a gas turbine converts the thermal energy provided by the combustion of (fossil) fuels (e.g. coal, oil, natural gas), a hydro turbine converts the potential energy of a water reservoir into mechanical energy which is utilized to drive a generator. To guarantee a continuous supply of electrical energy to the growing world population, the electricity provided by such a generator is crucial. The increase of the world population affects a growing demand for electricity as shown in Fig. 1.1.
The data shown in Fig. 1.1 was recently published in the World Energy Outlook 2019, provided by the International Energy Agency (IEA) [54]. The bar charts characterize the composition of the global electricity generation in the presence (year 2018) and in the future (year 2040) according to two different scenarios. Whereas scenario one follows from the currently stated policies, scenario two results from a (more) sustainable development focusing more on renewable and new energy technologies. No matter which scenario, a

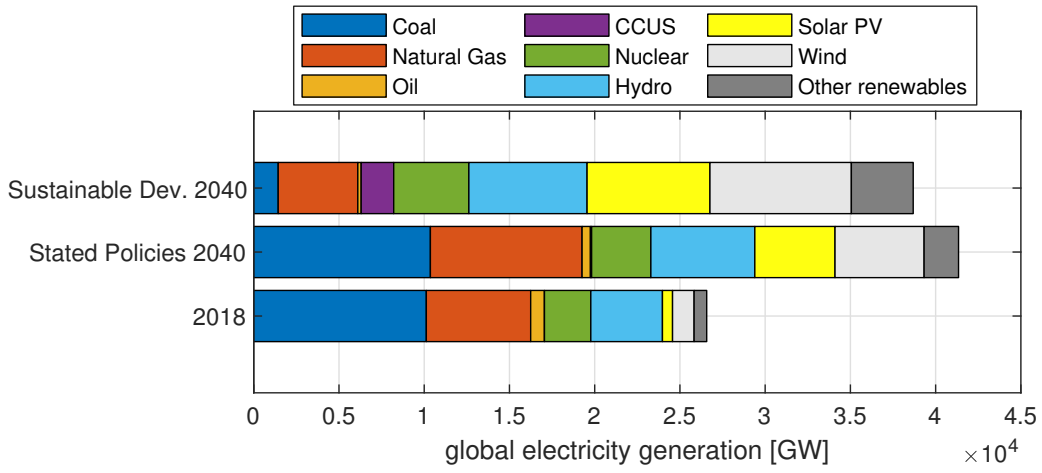

Figure 1.1: Global electricity generation by fuel and scenario, 2018, Stated Policies and Sustainable Development Scenarios 2040. Data adapted from IEA World Energy Outlook 2019. (https://www.iea.org/data-and-statistics/charts/global-electricity-generation-mix-by-scenario-2018-stated-policies-and-sustainable-development-scenarios-2040; last login: october 5 2020, 5:07pm) [53].

considerable share of the electricity will be produced by fossil fuels in year 2040 according to the World Energy Outlook 2019. In both scenarios, especially natural gas will be a key to compensate the intermittently provided energy from renewables, such as wind and solar photovoltaic (PV), to guarantee a continuous electrical energy supply. Although, mankind is facing the fight against climate change, the global electricity generation will still rely on fossil fuels in the (near) future. Therefore, scientists need to do both, increasing the efficiency of conventional technologies and developing new concepts for electricity generation. Currently, Carbon Capture Utilisation and Storage (CCUS) and electrolysis of hydrogen from renewables (power-to-gas) gain interest and importance in the energy sector. CCUS reached a high technology readiness level, however, a wide implementation in the thermal and industry sector is still missing [62]. Hydrogen, e.g. in the context of power-to-gas systems [151], becomes more and more attractive such that the gas turbine industry starts to adapt their machines to this potentially "green fuel" [12]. Although, a energy transition towards renewables has been initiated, gas turbines will play a crucial role in the medium-term future. Therefore, further research and development work on this technology is required for a best possible support of the energy transition.

Turbulent fluid flows power modern gas turbines and are thus crucial for the associated electricity generation. Before the fluid flow enters the combustion chamber, it typically passes a swirl generator which transforms the axially directed flow into a turbulent swirling flow. In premixed combustors, the following mixing section guides the turbulent swirling flow into the combustion chamber. In this mixing section, fuel is injected into the incoming air flow. The turbulent swirling flow affects an effective mixing of fuel and air yielding premixed conditions which allow for low emission combustion. Besides the quality of effective mixing, a turbulent swirling flow provides even more qualities which are beneficial for the combustion process when it emanates as a swirling jet into the combustion chamber.

If the degree of swirl is high enough, the emanating swirling jet will undergo an aerodynamic phenomenon called vortex breakdown (VB). This phenomenon generates a flow

configuration that facilitates the aerodynamic stabilization of the flame. However, this reacting flow configuration is prone to hydrodynamic instabilities which can manifest in different types of coherent flow structures. For example, the axisymmetric Kelvin-Helmholtz instability can couple with planar thermoacoustic waves, arising in a thermoacoustically unstable premixed combustion system. These thermoacoustic waves induce velocity fluctuations at the burner outlet leading to the formation of axisymmetric vortices. Their growth along the shear layers is driven by the Kelvin-Helmholtz instability resulting in large-scale coherent vortex structures which roll up the flame. Another coherent flow structure, occurring in such a flow configuration, has a helical shape and is known in the combustion community as precessing vortex core (PVC). This flow structure appears solely under certain operating conditions and is very often accompanied by bi-stable and transient flame dynamics [96, 135, 155]. Therefore, a systematic investigation of the impact of the PVC on the combustion is rather difficult. Nonetheless, such a systematic investigation appears to be important since the PVC can influence flame dynamics [128, 142], fuel-air mixing [132] and flame stability [4, 133].

1.1 Motivation and research focus

To facilitate a systematic investigation of the role of the PVC in the combustion process, an appropriate control system is necessary which allows the PVC's amplitude and frequency to be arbitrarily varied. Such a flow control system needs to exclusively target the PVC without changing other dynamical structures such that the general flow configuration is maintained. To implement such an efficient active flow control mimicking shape and dynamics of the PVC, the actuation needs to be applied in the flow region where the receptivity of the PVC is maximal. Actuating in this region directly targets the PVC and requires very small actuation amplitudes to generate a high flow response. In this way, the exclusive impact of the PVC on premixed swirl-stabilized flames can be studied. Accordingly, the first research focus of the present thesis is the development of an active flow control system which allows a direct control of the PVC without altering the flow configuration fundamentally (see publications 2.1 to 2.3).
Very important properties of the combustion process are flame stability and low levels of pollutant emission to guarantee an efficient operation of the gas turbine in accordance with environmental regulations. Both properties are relying on the flow conditions in the combustion chamber which are influenced by the PVC. A stable combustion process requires a stable flame which can have different shapes and dynamics. Accordingly, the transition from one flame shape to another, which can be promoted by coherent flow structures such as the PVC, leads to a change of the flame dynamics [4, 133]. Depending on flame shape and associated flow configuration, flame dynamics can be dominated by thermoacoustic oscillations which may jeopardize flame stability and a safe operation of the machine [75]. These thermoacoustic oscillations induce large-scale vortex structures which roll up the flame front and can interact with the PVC [83, 128, 135, 142]. Furthermore, these large-scale vortex structures can induce hot spots which increase the emission of NO_x [103, 105]. Closely connected with the NO_x emission level is the homogeneity of the

fuel-air mixture reaching the flame [30]. Large-scale vortex structures, as induced by the PVC, can enhance the mixing of fuel and air which affects the flame stability and may influence the formation of pollutant emissions [132].
As described in the previous paragraph, the PVC is closely connected to the combustion process involving: flame dynamics, flame stability, fuel-air mixing and NO_x emissions. A targeted investigation of the role of the PVC in the context of these combustion properties is very complicated since all of them are closely linked. This close link motivates the application of the active flow control system, developed in the first research focus of this thesis (see publications 2.1 - 2.3), to study the exclusive impact of the PVC on these combustion properties. Due to the lack of control opportunities of the PVC dynamics such a targeted investigation was not possible before. This approach allows for formulating the following research questions, which form the second research focus of the present thesis:

1. **How does the PVC influence the mean flame shape and flow field?**
   - see publications 2.2 - 2.5
2. **Which role does the PVC play in the context of flame dynamics?**
   - 2.1 How does the PVC interact with thermoacoustic modes?
     - see publication 2.2
   - 2.2 Is the PVC capable of damping thermoacoustic oscillations?
     - see publications 2.2 and 2.5
   - 2.3 Which mechanisms govern the impact of the PVC on the flame response?
     - see publication 2.5
   - 2.4 How to describe the interaction between PVC-induced vortices and flame?
     - see publications 2.3 and 2.4
3. **How does the PVC contribute to mixing?**
   - see publications 2.3 and 2.4
4. **In which way does the PVC influence NO_x emissions?**
   - see publication 2.4

The present manuscript is divided into three chapters which are structured as follows. In chapter 1.2 and 1.3, an introduction into the phenomenology of isothermal and reacting swirling flows is given which allows for a thorough understanding of the role of the PVC in isothermal flows and the combustion process. In this introduction, hydrodynamic phenomena (chapter 1.2) such as vortex breakdown in swirling jets (chapter 1.2.1), which is crucial for the generation of a PVC, are described. Subsequently, characteristic flow instabilities are discussed which occur in the resulting flow configurations (chapter 1.2.2). At the end of chapter 1.2, the appearance and important properties of the PVC are described for isothermal flow conditions (chapter 1.2.3). Based on the description of the

fundamental (isothermal) character of the PVC, its role and formation in premixed swirl-stabilized flames (chapter 1.3) is discussed based on the current status of research, aside from the publication accumulated in the present thesis. In this connection, the impact of the PVC on flame dynamics (chapter 1.3.1) is described, which includes the interaction with thermoacoustic instabilities and its role in flame shape transition. Moreover, the effect of the PVC on (fuel-air) mixing is discussed based on studies found in the literature (chapter 1.3.2). Related to the flame dynamics and mixing, a brief introduction into the formation of NO_x emissions in connection with coherent structures (chapter 1.4) is given. The following chapter 1.5 describes the experimental setup and methods applied in this thesis including the developed (direct) active flow control approach which is explained in chapter 1.5.1. Furthermore, the pressure (chapter 1.5.2) and optical (chapter 1.5.3) measurement techniques applied in the present thesis are introduced. The last part of chapter 1 deals with the empirical and analytical methods (chapter 1.6) applied in this thesis. These methods are divided into four groups: decomposition methods (chapter 1.6.1), hydrodynamic linear stability analysis (chapter 1.6.2), tomographic reconstruction methods (chapter 1.6.3) and the flame transfer function (chapter 1.6.4).
In chapter 2, the five journal publications are accumulated which represent the scientific work and focus of this thesis. These publications demonstrate the research progress from the design of a suitable actuation system (publication 2.1) to the investigation of the PVC's impact on the flame transfer function (publication 2.5). The first research focus of this thesis is covered by publications 2.1 to 2.3 which document the development and proof-of-concept of the direct active flow control system. With this newly developed active flow control system at hand, new insights about the impact of the PVC on: flame dynamics (publications 2.2 to 2.5), mixing (publications 2.3 and 2.4) and NO_x emissions (publication 2.4) are revealed. Upfront of each publication presented in chapter 2, a short summary is given which contextualize its positions and significance within the whole thesis.
Chapter 3 summarizes the conclusions from the obtained findings gained in publications 2.1 to 2.5 and connects them in a broader context. This allows for tackling the four research questions, stated above, which cover the second research focus of the present thesis. Based on this discussion, future steps for the application of the developed flow control approach in the scientific as well as the industrial context are suggested. Furthermore, the findings presented in the publications associated with the present thesis are connected to the drawn conclusions.

1.2 Hydrodynamics of swirling jets

A swirling jet is a superposition of an axially directed flow and a rotating fluid motion which emanates from a nozzle into an open or some sort of confined environment. Swirling jets can be found in many technical applications such as: turbomachinery (e.g. turbo-pumps, jet engines or hydro turbines), mixing devices (e.g. fuel injectors), or modern combustion chambers (e.g. in gas turbines).
Two important quantities commonly used to characterize swirling jets from a hydrodynamic point of view are the Reynolds number Re and the swirl number S. The swirl number is usually defined as the ratio of the axial flux of the angular momentum and the axial flux of the axial momentum of the flow [9, 70]. Thus, a high swirl number will be present, if there is a strong azimuthal velocity component, i.e. rotating fluid motion, compared to the axial velocity component. Accordingly, the swirl number is a measure for the swirl intensity and a similarity criterion of swirling jets originating from geometrically similar swirl generators [9]. For the sake of completeness it shall be mentioned that the Reynolds number is the ratio of inertial forces to viscous forces which characterizes i.a. the general (laminar or turbulent) state of the flow.

1.2.1 Vortex breakdown

The superimposed azimuthal velocity component v_θ, which transforms the non-swirling jet into a swirling jet, leads to the development of additional radial and axial pressure gradients. In a swirling jet, a natural radial pressure gradient occurs which is proportional to v_θ^2/r, where r is the radius. This gradient occurs because of the azimuthal velocity profile which can result in a pressure deficit near the jet axis. Due to the expansion of the

Figure 1.2: Smoke visualization of a laminar swirling jet ($Re = 1200$) undergoing vortex breakdown. Source: [107].

emanating jet, the azimuthal velocity decays in axial direction leading to a decaying radial pressure gradient in axial/streamwise direction. This decay causes an axial pressure gradient in the vicinity of the jet axis towards the burner outlet. If this pressure gradient is sufficiently strong, a phenomenon called *vortex breakdown* (VB) can occur. The VB manifests in the deceleration of the fluid on the jet axis which leads to the formation of a stagnation point and a region of reversed flow [42, 139].
A laminar swirling jet undergoing VB is shown by a smoke visualization given in Fig. 1.2. It shows the characteristic stagnating flow and the formation of a recirculation region near the jet axis. These flow features, resulting from the VB, have a severe impact on the flow field. A typical time-averaged flow field of a swirling jet undergoing vortex breakdown is shown in Fig. 1.3 [66]. In case of sufficiently high S and Re, a stable central recirculation zone (CRZ) forms around the jet axis, which is labeled with III in Fig. 1.3. At the upstream end of the CRZ, a stagnation point is formed indicated by a blue dot. In such a flow configuration, two characteristic shear layers develop: an inner shear layer (ISL, marked with II) between the jet, emanating from the nozzle, and the reversed flow of the CRZ, and an outer shear layer (OSL, marked with I) between the jet and the surrounding fluid. These flow features (I-III) yield a flow configuration which is very beneficial for technical applications.
Especially modern gas turbine combustors benefit from the phenomenon of VB and the resulting flow configuration because it allows for the aerodynamic stabilization of the flame without the necessity to introduce a solid bluff body. Such a bluff body generates

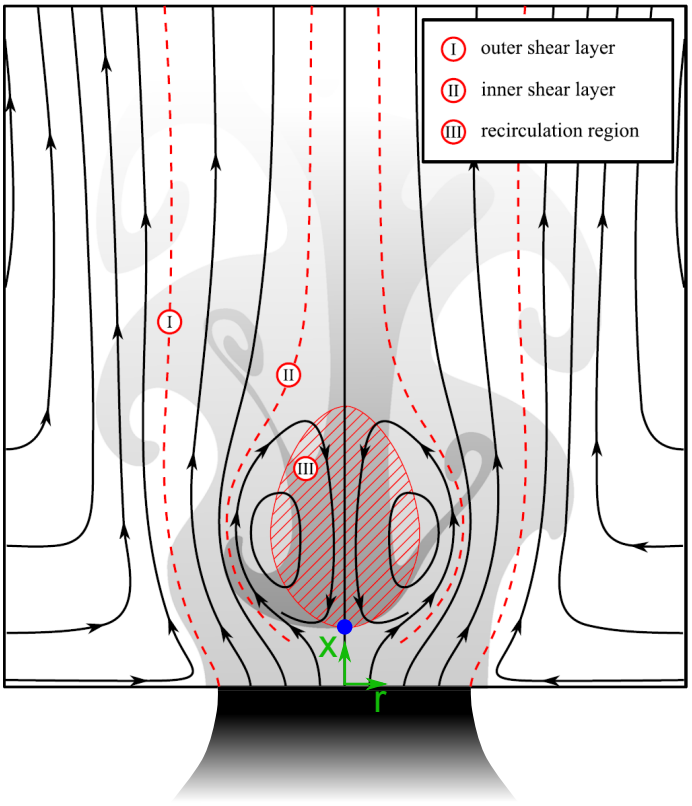

Figure 1.3: Mean flow field of a swirling jet undergoing vortex breakdown with vortex structures illustrated in gray (adopted from [66]). The blue dot indicates the upstream stagnation point.

a wake in which the flame can anchor. However, this type of flame holder is exposed to high temperature by the flame and the effect of deposition of coke. This leads to a progressing (thermal) deterioration of the material which may jeopardize a reliable combustor performance. The key feature of swirling flows is the CRZ. It contains a well mixed zone of hot combustion products and chemically active species, which facilitates flame stabilization by the ignition of incoming fuel-air mixture [9]. Moreover, the formation of ISL and OSL provides a variety of flow velocities to which the flame's burning velocity can match such that a stable flame and combustion is achieved.
In most technical applications, the swirling jet is confined. In gas turbines, this confinement is a combustion chamber where the unique phenomenon of VB is exploited. The confinement can considerably alter the size and the shape of the CRZ which changes the overall flow configuration [42, 138]. The impact of the confinement on the flow field depends on the confinement ratio of combustion chamber diameter to the swirl burner outlet diameter. The smaller the confinement ratio, the larger the influence on VB and the characteristic flow configuration. As described above, the sudden expansion downstream of the nozzle and associated entrainment effects cause a decay in azimuthal velocity, which affects the adverse pressure gradient on the jet axis, leading to the formation of the CRZ [42, 139]. Another effect of the confinement is the generation of an outer recirculation zone (ORZ). The expanding swirling jet maintains the recirculation of the fluid in the ORZ which is geometrically bounded by the walls of the confinement and the front plate around the nozzle orifice. In downstream direction, the jet confines the ORZ, which ends in the region where the jet attaches to the wall of the confinement depending on the jet angle. The additional region of recirculated fluid may influence the flame stabilization as well [139].

1.2.2 Characteristic flow instabilities

The phenomenon of VB has been the subject of research for decades as shown exemplary in [10, 34, 44, 69, 74, 91, 116]. However, the vortex breakdown has not been fully understood, yet. To further understand the dynamics and the onset of VB, current research focuses on vortical (coherent) structures that are generated by hydrodynamic instabilities which occur due axial and azimuthal shear [91]. There are various experimental [10, 74, 91, 101] and theoretical [32–34] studies revealing the destabilizing impact of swirl on helical, i.e. azimuthal, instabilities.
The azimuthal shape and orientation of instability modes and associated vortical structures is described by the azimuthal wave number m which is a real integer value indicating the azimuthal mode order. For $m > 0$ and a fixed axial location x, the corresponding mode will rotate in time in the *same* direction as the flow which is referred to as *co-rotating*. Contrarily, a mode with $m < 0$ rotates in time in the *opposite* direction of the flow which is referred to as *counter-rotating*. Accordingly, a hydrodynamic mode with azimuthal wave number $m = 1$ describes a single-helical co-rotating coherent flow structure and $m = 2$ a double helical co-rotating structure. A mode with azimuthal wave number $m = 0$ describes (ring-like) axisymmetric fluctuations without any azimuthal, i.e helical, variation.
The framework of hydrodynamic stability theory distinguishes between *local* and *global*

instabilities. While a local instability is associated with the local velocity profile, a global instability is associated the entire flow field. In the local framework, the flow is characterized as *locally absolutely unstable*, if a flow disturbance exists that grows in time. In contrast, a velocity profile is described as *locally convectively unstable* if a flow disturbance is swept away from the source and grows in space. Locally convectively unstable shear flows, such as a mixing layer [36] or a non-swirling jet [22], are called *noise amplifiers*. Contrarily, there are shear flows, e.g. bluff-body wakes such as cylinder wakes [154] or low-density jets [85], displaying intrinsic dynamics due to sufficiently large region of absolute instability. These types of flows are classified as *oscillators* [50].
Shear flows must contain a sufficiently large region of absolute instability to become globally unstable [19, 20, 50]. The resulting global modes are driven by intrinsic large-scale (global) oscillations that are synchronized to one frequency by a so-called wavemaker that is located near the region of absolute instability. For swirling jets, this region is usually associated with the reversed flow around the jet axis [74, 89, 95].

Coming back to the phenomenological explanation of the VB given above, it is evident that the occurrence of this phenomenon is predominantly a function of swirl number S [116]. However, the emergence of VB happens rather intermittent and is accompanied by the formation of azimuthal modes of different shapes ($-3 \leq m \leq 3$) [34, 74, 91]. In Fig. 1.4 the onset of VB in a turbulent swirling jet is illustrated depending on S which summarizes the results of [91]. A dominant axisymmetric $m = 0$ mode is present in the non-swirling jet ($S = 0$) which is typical for such a flow configuration [22] (compare left side of Fig. 1.4). The increase of S provokes a break of the symmetry leading to the destabilization of counter-rotating modes ($m < 0$) that become more energetic than axisymmetric and co-rotating modes. However, the flow remains globally stable and no VB arises for $S < 0.86$. Increasing S to $0.86 < S < 1.06$ results in the intermittent occurrence of VB accompanied by oscillations in axial direction at low frequency. At $S = S_{\mathrm{VB}} = 1.06$, the VB starts to

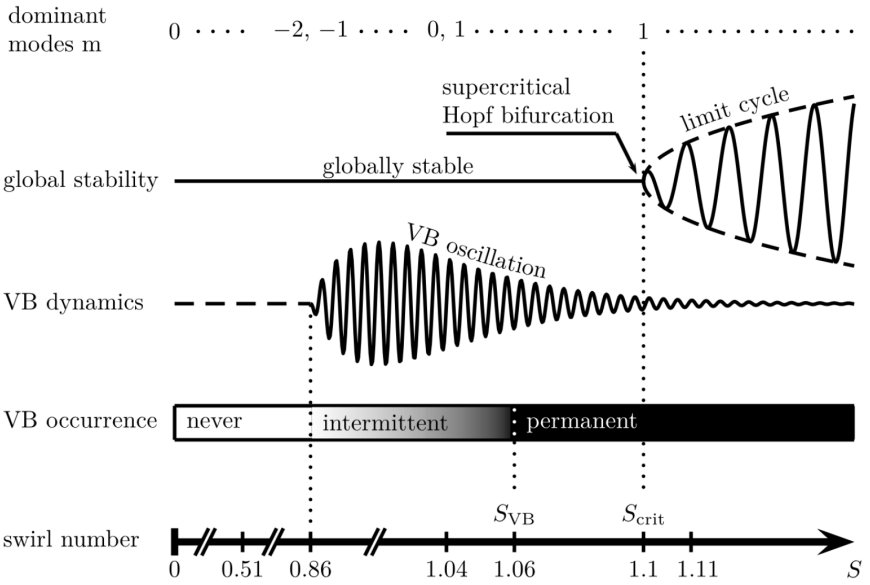

Figure 1.4: Sketch describing the onset of vortex breakdown and global instability in an experimentally investigated turbulent swirling jet. Source: [91].

appear permanently in the mean flow field but still oscillates in axial direction causing $m = 0$ modes. Moreover, $m = 1$ modes start to appear, causing a meandering CRZ. Further increasing S leads to a decay of the axial oscillation of the VB. Above this point, the CRZ grows linearly with increasing S which promotes the growth of absolute instability regions [74]. When the region of absolute instability is sufficiently large, an internal feedback mechanism starts to stimulate the CRZ to precess in the rotation direction of the main flow inducing a non-axisymmetric spiral VB. This internal feedback mechanism sets in at $S = S_{\text{crit}} = 1.1$ where the flow undergoes a supercritical Hopf-bifurcation to a self-excited global single-helical mode $m = 1$ which saturates at its limit cycle oscillation [34, 74, 113]. The growth of the CRZ saturates at $S = 1.11$. Increasing S further leads to an upstream shift of the CRZ and enhances the global oscillation [91].
The self-excited global mode manifests in a large-scale coherent structure in the ISL and OSL as shown by the vortex structures illustrated in gray in Fig.1.3. Due to the precessing motion of the vortex core around the jet axis, these helical vortices are formed in the shear layers which are a manifestation of the Kelvin-Helmholtz instability [32]. As clarified in [141], the precession of the vortex core and the helical Kelvin-Helmholtz instabilities are different manifestations of the same global mode ($m = 1$). In the field of combustion research, this entire coherent flow structure, which includes the precession of the vortex core and the helical Kelvin-Helmholtz instability, is commonly termed precessing vortex core (PVC) [139]. Accordingly, this established term is used throughout the present manuscript to refer to the entire single-helical coherent structure.
In the publications shown in this thesis (2.1 - 2.5), the swirl number is kept constant at $S = 0.7$. The resulting swirl intensity is sufficient to guarantee a stable VB and with that a stable PVC at isothermal conditions. At reacting conditions, the flame can have a considerable impact on the PVC which is discussed in chapter 1.3.

1.2.3 The PVC in isothermal swirling jets

An isothermal swirling jet featuring a stable vortex breakdown and a global mode ($m = 1$) is shown in Fig. 1.5. This figure illustrates the single-helical coherent flow structure which is called PVC in this thesis. There are three characteristic flow features: the CRZ (semi-transparent gray pathline-surface originating upstream in the center); the meandering vortex core that acts as the wavemaker for the global mode ($m = 1$) oscillations (central streak-lines and bluish streak-surface coming from the nozzle center); helical waves in the OSL that amplify near the nozzle and roll up to spiral vortices (semi-transparent greenish streak-surface) [107]. The CRZ meanders around the jet axis which induces spiral vortices in the ISL. These vortices grow and incorporate the OSL such that the outer coherent structures move in phase with the CRZ [74, 95].
The well defined oscillation frequency of the PVC (f_{PVC}) is dictated by the wavemaker at the jet center [95]. To characterize the oscillation frequency, the Strouhal number

$$\text{St} = \frac{f_{\text{PVC}} \cdot D}{V_0} \tag{1.1}$$

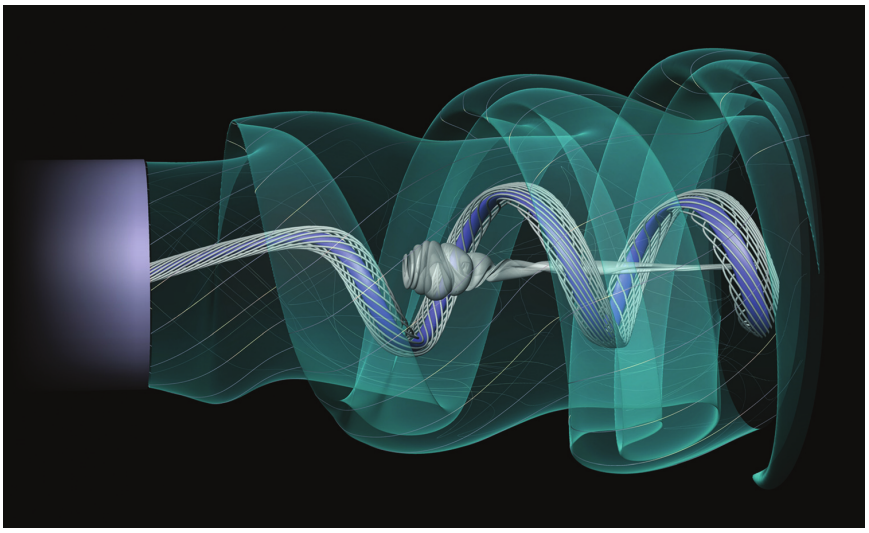

Figure 1.5: Three-dimensional visualization of the phase-averaged velocity of an isothermal swirling jet undergoing vortex breakdown ($Re = 20000$) featuring a PVC. Source: [107].

is commonly utilized, where D is a characteristic (nozzle) diameter and V_0 refers to the bulk velocity. The value of St depends especially on the geometry of the swirling jet facility, e.g. unconfined jet or swirl combustor [138]. However, for a fixed geometrical configuration and varying mass flow St remains (almost) constant, because of a weak dependence on the Re number [42]. Accordingly, the frequency of the PVC increases almost linearly with growing mass flow [28, 128, 133, 139]. Furthermore, an almost linear increase of St was shown experimentally for a growing swirl number S and constant Re number [6, 17]. As described above, swirling flows are mostly confined in technical applications which can lead to a considerable increase of St for high levels of confinement [139].
The amplitude of the PVC, as a global mode, can be characterized by a forced Landau equation which describes the amplitude evolution of a global mode at near-critical conditions in the context of a supercritical Hopf-bifurcation [50, 65]. If external forcing is absent and the flow state is near critical conditions, the limit-cycle amplitude increases proportionally to the deviation from a critical control parameter which is the critical swirl number S_{crit} in case of a swirling jet. Oberleithner et al. [91] demonstrated this trend for a turbulent swirling jet which means that the oscillation amplitude of the PVC grows with increasing $S > S_{\mathrm{crit}}$ (see Fig. 1.4). The impact of confinement and Re number on the PVC amplitude appears to be only marginal [6].
The wavemaker, which drives the oscillation of the global mode, is located upstream of the CRZ [108, 115]. Very recent publications reveal that the flow regions even further upstream are crucial for the generation of the PVC [59, 86, 87, 140]. These crucial flow regions can reach far upstream for example into the mixing section [86, 87] or the fuel injector [59, 140] of a combustion system. In a study associated with this thesis (see chapter 3.2), Müller et al. [87] showed that a region of high turbulent production is found in the mixing section of a generic combustion chamber. This region of high production is responsible for the initiation and amplification of the PVC [87]. Consequently, the origin of the PVC appears to be far upstream of the CRZ.

Axisymmetric coherent structures ($m = 0$) are typically dominant in non-swirling jets where they are formed in the shear layer due to the Kelvin-Helmholtz instability. If swirl is added to the jet, the axisymmetric modes are damped with increasing swirl level [91]. The shear layers of swirling jets undergoing a stable vortex breakdown can give rise to axisymmetric modes ($m = 0$), if axisymmetric external forcing is present. In technical applications, such as swirl combustors, these modes can be externally excited due to the thermoacoustic feedback cycle (explained in detail in section 1.3). Therefore, the interaction of a naturally occurring (self-excited) PVC and an externally forced axisymmetric mode is of particular interest to reveal possible impacts on the flow and with that on the technical performance. To isolate underlying hydrodynamic mechanisms, isothermal swirl combustors flows are investigated to reveal the shear layer response to axisymmetric forcing in the presence of a PVC [29, 81]. Mathews et al. [81] showed in their experiments that the PVC suppresses the shear layer response to axisymmetric acoustic forcing ($m = 0$). Moreover, it is shown that the confinement of the combustion chamber reduces the response to acoustic forcing due to the formation of an ORZ. Based on [81], Frederick et al. [29] discovered that the increased shear layer thickness induced by the PVC weakens the Kelvin-Helmholtz instability mechanism in the flow field. As a result, the shear layer response to acoustic forcing ($m = 0$) is reduced [29].
The findings about the shear layer response to acoustic forcing and the role of the PVC in this context are especially relevant in reacting flows where a premixed flame is stabilized in the shear layers. Such a flame affects the flow field considerably and with that the generation and dynamics of the PVC. Therefore, the following section elaborates the interaction of the PVC with important properties of premixed swirl-stabilized combustion.

1.3 The PVC in premixed swirl-stabilized combustion

The flow configuration in many modern gas turbine combustors can be described as follows: A swirling air flow is merged with a fuel flow inside a mixing section upstream of the combustion chamber. The swirling flow facilitates the mixing of air and fuel leading to a relatively homogeneous premixed mixture. This premixed fuel-air mixture propagates as a (confined) swirling jet into the combustion chamber. There, the swirling jet undergoes VB such that a premixed flame can stabilize in the resulting shear layers where the burning velocity is equal to the flow velocity (compare description above in 1.2). This type of premixed swirl-stabilized flames allows for burning at very lean conditions to realize efficient and low emission combustion [23]. The common parameter describing the air excess of the fuel-air mixture is the equivalence ratio ϕ: a lean mixture ($\phi < 1$) has an air excess, a rich mixture ($\phi > 1$) is characterized by a fuel excess; fuel and oxidizer consume each other completely at stoichiometric conditions ($\phi = 1$). Natural gas is applied as a fuel in combination with air in the publications shown in this thesis where reacting flows are investigated (publications 2.2-2.5).

In general, there are various parameters which influence the shape of a premixed swirl-stabilized flame such as: burner design, fuel type, preheating temperature, wall temperature, cooling, thermal power or the equivalence ratio [96, 142, 145]. However, in the context of this thesis, the thermal power and the equivalence ratio are the only variable experimental parameters which allow to change the shape of the flame. In Fig. 1.6, the two different flame shapes are shown which are investigated in the present thesis: attached V-flames (Fig.1.6, left) and detached M-flames (Fig.1.6, right). The photographs in the top row show both flame types as they can be observed in the combustion chamber in this thesis[1]. The V-flame is attached to the centerbody, which is placed inside the mixing tube of the burner. Compared to the detached M-flame, which stabilizes in the shear layers further downstream, the V-flame appears brighter than the M-flame. The reason for this appearance is the higher equivalence ratio and the corresponding higher thermal power applied to obtain the V-flame. In the present thesis, the equivalence ratio is the main parameter which controls the flame shape. The bottom row shows representative examples of the flow fields and the heat release rate distribution for both flame types. The heat release rate distributions indicate the reconstructed mean flame shapes which resemble the letters "V" and "M", respectively. Generally, the presence of a flame has a significant impact on the flow field because of the volume increase induced by the chemical (combustion) reaction leading to an expansion of incoming fluid. The blue line indicates the boundary of the CRZ which is considerably different comparing the two different flow fields. In this flow configuration, the CRZ associated with the V-flame does not form an upstream stagnation point as it is the case for the flow field including the M-flame. The comparison of these flow configurations shows that a change of the flame shape is typically accompanied by a considerable change of the (mean) flow field which may have a distinct impact on the flow stability.

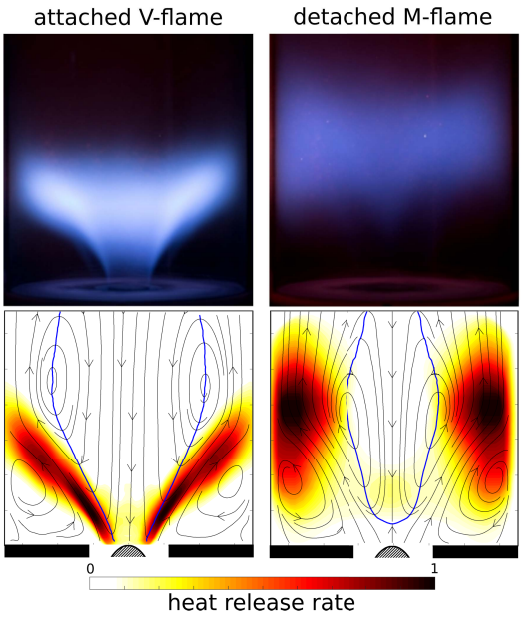

Figure 1.6: Flame shape and flow field of an attached V-flame (left) and a detached M-flame (right). (photographs adopted from [141])

Especially the stability of the global mode ($m = 1$) associated with the PVC clearly depends on the type of flame and the corresponding mean flow field. Oberleithner et al. showed that the density stratification induced by the flame in the region of the wave-maker decides whether a PVC naturally occurs in a reacting flow field or not [97]. Even if a very strong backflow is present in the CRZ, the PVC is typically damped by the strong stabilizing density gradients induced by the attached V-flame in the wave maker region around the burner outlet. However, the less steep density gradients caused by the M-flame around the burner outlet allow the PVC to be present also in reacting flows. In general, it can be stated that the occurrence of the PVC under reacting conditions depends

[1]The photographs were taken by Steffen Terhaar and are published for example in his PhD thesis [141]

especially on the flame shape and the resulting flow and density field [96, 97, 128, 142, 145]. Compared to isothermal flows, the PVC frequency is only slightly increased under reacting conditions as shown in [96, 133, 142] if the PVC is mostly located upstream in the region of unburnt reactants as shown by Stöhr et al. [133]. However, due to the expansion of the fluid over the flame front, the flow velocity is considerably increased which may lead to considerably higher PVC frequencies as reported in [128]. Furthermore, Steinberg et al. [128] showed that the amplitude of the PVC increases in reacting flows, compared to isothermal cases, which is accompanied by strong pressure oscillations. As shown in the overview table provided by Stöhr et al. in [133], the appearance of a PVC is highly dependent on the geometry of the combustor and the operating conditions. The same holds for the derived values of St numbers and PVC amplitudes [96].
In the following sections, those combustion properties are discussed which are investigated in the publications 2.2 - 2.5 regarding the impact of the PVC. The section about *flame dynamics* focuses on the interaction of the PVC mode ($m = 1$) with thermoacoustic modes ($m = 0$) (compare publications 2.2 and 2.5). Moreover, the role of the PVC in the context of *mixing* and possible effects on *NO_x emissions* are discussed briefly (compare publication 2.3 and 2.4).

1.3.1 PVC in the context of flame dynamics

The big advantage of lean premixed flames are low levels of pollutant emissions generated in the combustion process. However, this type of flame is susceptible to combustion, i.e. thermoacoustic, instabilities which can have severe influence on the flame dynamics and the performance of the combustor. The onset of thermoacoustic instabilities relies on a coupling of the perturbed flame and the acoustic field in the combustion chamber. In this context, unsteady heat release can act as an acoustic source which may resonate with the acoustic field of the combustor. This resonance can lead to even stronger acoustic perturbations which affect even stronger heat release fluctuations establishing a feedback cycle which can lead to very high acoustic pulsation amplitudes of a few percent of the static pressure in the combustor. Such a high pulsation level can have severe consequences on the mechanical integrity and the efficiency of the machine. To establish such a feedback cycle with increasing fluctuation amplitudes, energy needs to be added to the acoustic field. The necessary condition for self-excited thermoacoustic instabilities was formulated by J.W.S. Rayleigh in 1878 and is commonly known as Rayleigh's criterion [110]. Accordingly, if pressure and heat release fluctuations are oscillating in phase, energy will be added to the acoustic field. Nevertheless, a positive feedback cycle, which maintains self-excited oscillations, is only established when the energy added from the heat source is higher than the acoustic dissipation of the system.
These thermoacoustic modes (TA modes) occurring due to the described feedback cycle predominantly have an axisymmetric shape ($m = 0$) in most laboratory model combustors. Such modes lead to velocity perturbations at the burner outlet which are amplified in the shear layers due to Kelvin-Helmholtz type instabilities leading to large-scale coherent structures. These coherent structures have as well an axisymmetric shape ($m = 0$) and interact (in a nonlinear fashion) with other hydrodynamic modes such as the PVC

($m = 1$). In the following, the term "TA mode" will refer to the axisymmetric hydrodynamic coherent structure resulting from the thermoacoustic velocity perturbations.
Depending on the operating conditions, the strong interaction of TA and PVC modes was observed to lead either to suppression or excitation of the helical coherent structure [37, 38, 128, 130, 142]. As shown by Steinberg et al. [128], helical shaped dynamics induced by the PVC are dominant in detached flames. If the flame attaches to the burner nozzle, no PVC will be formed and the flame dynamics are dominated by TA modes. However, it was shown in a numerical simulation (LES) that a PVC can be generated by acoustic forcing [38]. Terhaar et al. [142] could show experimentally that acoustic forcing ($m = 0$) can excite a PVC in attached flames. They concluded that appearance or suppression of a PVC depends on changes of the mean flow field induced by the TA modes. However, in their configuration the natural PVC in a detached flame was damped by acoustic forcing. Steinberg et al. [130] revealed that the (natural) PVC either damps or drives self-excited TA instabilities depending on the relative shape of PVC and flame. Based on these findings, the authors concluded that a properly tuned PVC could be used to extract energy from the TA oscillations. In contrast to that, several studies showed that a PVC can be efficiently suppressed by acoustic forcing ($m = 0$) [60, 64, 104]. These studies show that the PVC can not only dominate the dynamics of (detached) flames; but, can influence and interact with the dynamics of TA modes and corresponding thermoacoustic oscillations. The interaction between PVC and TA modes can generate additional interaction components, i.e. interaction modes [83, 129, 130, 142]. Steinberg et al. [129] describe the resulting complex flow field dynamics as follows: The PVC is stretched and contracted in axial direction at the TA frequency. This superposition generates an interaction mode of first azimuthal order in the heat release signal with a frequency equal to the difference of the TA mode and PVC frequencies (compare as well [83]). These interaction modes describes the circumferential movement of the heat release centroid around the combustor. Due to the superimposed axial contraction and stretching, a periodic asymmetry of the flame is caused. Accordingly, the flame dynamics are considerably influenced i.a. by large-scale flame wrinkling. Moeck et al. [83] describe the heat release perturbations induced by the interaction mode as a "yin and yang" - type pattern which rotates with the interaction frequency in the direction of the mean swirl. The authors observed the interaction mode in the presence of self-excited as well as externally forced thermoacoustic oscillations. Moreover, these heat release fluctuations strongly interact with the combustor wall. The interaction mode appears to result from nonlinear processes in the flame dynamics since the spectrum of the velocity at isothermal conditions only shows a very small peak compared to the reacting cases. Interaction modes can be generated as well with an interaction frequency equal to the sum of the PVC and the (forced) TA frequency [83].

For a stable combustion process, a stable (attached or detached) flame is required which is not influenced by unfavorable flame dynamics. However, the PVC is known to drive the flame transition from an attached to a detached flame which is also called flame lift-off [4, 5, 128, 134, 135]. The process of flame lift-off is for example described by An et al. [4] as follows (compare Fig.1.7). In a turbulent swirl flame, local flame extinction near the flame base can be induced for example by a turbulent flow fluctuation. The local extinction causes a smoother density gradient which leads to the formation of a PVC [5, 97]. The asymmetric structure of the PVC increases strain-rate on the flame base such that

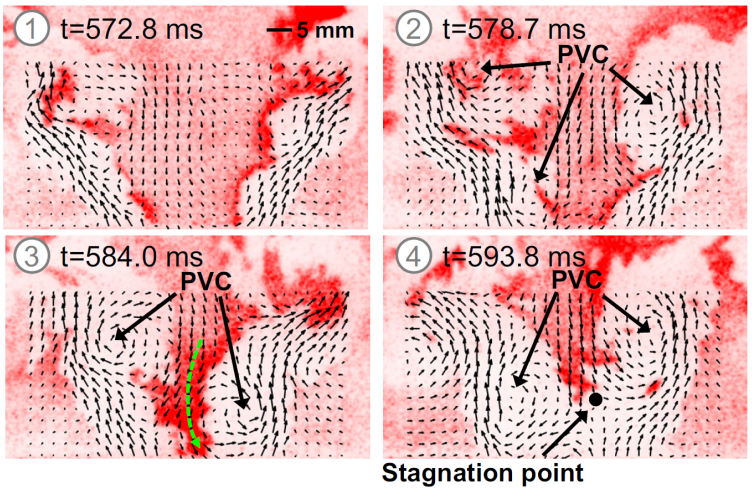

Figure 1.7: Sequence of velocity fields (black arrows from PIV) and flame front (in red from OH-PLIF) measurements showing the formation of the PVC and the subsequent detachment of the flame. (adopted from [135])

a complete extinction in that region can occur which leads to (total) flame lift-off and the formation of an upstream stagnation point. Another very comprehensive study by An et al. [5] involving variations of various experimental parameter, confirms the finding of [4] regarding the role of the PVC in the flame lift-off scenario. This study further points out that the prediction of hydrodynamic stability and extinction is important to control the attachment/detachment of the flame to maintain a stable combustion process. The role of the PVC in the flame lift-off scenario gives rise to complex transient flow-flame interactions that explain bi-stable flame transitions that have been observed in several recent studies [96, 135, 155].

In case of bi-stable flames, where the flame shape transitions intermittently, the PVC and the TA modes take competing roles governing the dynamics of the flame. As shown by Stöhr et al. [134, 135], the TA modes can trigger a flame shape transition from a detached M-flame to an attached V-flame. Consequently, the naturally present PVC is suppressed. However, an opposed transition from V-flame to M-flame, which can be initiated by the PVC and the formation of an upstream stagnation point (compare Fig.1.7), is possible as well [96, 134, 135]. The dynamics and interactions between PVC and TA modes in bi-stable flames are still part of current research. In a very recent study, a novel decomposition method could reveal a series of previously unknown dynamics governing the intermittent attachment/reattachment phenomenon. For more details, the reader is referred to [155].

Key factors for the transition of a thermoacoustically stable to an unstable flame are the flame position and vortical waves rolling up the flame front [99]. In an unstable flame, axisymmetric shear layer vortices resulting from vortex shedding at the nozzle lip reach the flame which leads to the production of heat release perturbations. The lifetime of the vortices determines the intensity of the heat release perturbations and with that the response of the flame to vortical flow perturbations [100]. Moreover, the flame response, described by the flame transfer function (compare section 1.6.4), is governed by the swirl fluctuations which are generated through the swirler under thermoacoustically unstable conditions [98]. The flow perturbations induced by the external or self-excited acoustic forcing grow in the shear layers due to the underlying Kelvin-Helmholtz instability [93].

Therefore, also the flame response to acoustic forcing depends on the growth rate of the axisymmetric ($m = 0$) vortical structures (TA modes). Another PVC-TA mode interaction mechanism appears when recalling the findings in [29, 81] which showed that the growth rate of acoustically forced modes ($m = 0$) under isothermal conditions is reduced by the PVC. These findings show (another) possibility how the PVC may reduce the flame response regarding axisymmetric acoustic forcing.
In most studies, the investigated flames are (assumed to be) axisymmetric. In this case, the global heat release is only determined by axisymmetric TA modes ($m = 0$). Helical heat release perturbations, induced e.g. by the PVC, cancel out in the global heat release of axisymmetric swirl flames [83]. If the mean flame shape is not perfectly axisymmetric, even helical modes ($m \neq 0$) can induce global heat release as shown by Acharya et al. [1, 2]. Vice versa, axisymmetric flow perturbations can cause helical heat release fluctuation in non-axisymmetric flames.

For more details regarding the dynamics of premixed swirl flames the reader is referred to these review articles [16, 48]. In the present thesis, the interaction of PVC and TA mode is investigated at various operating conditions in publication 2.2. The impact of the PVC on the flame response and the growth rate of the TA mode is studied in publication 2.5. Moreover, the effect of the PVC on the dynamics and shape of heat release rate fluctuations is discussed and illustrated in publications 2.3 and 2.4.

1.3.2 PVC in the context of mixing

To achieve a stable, efficient and low emission combustion, it is crucial to provide a well-mixed fuel-air mixture at the outlet of the mixing section. Especially for safety reasons, the fuel is injected into a mixing section (e.g. a mixing tube) which is to be found comparably close to the inlet of the combustion chamber [25, 137]. Due to the lack of mixing length, the mixture entering the combustion chamber is typically (only) partially premixed. Only in laboratory combustors, perfectly premixed mixtures are studied. Such a perfectly premixed mixture is mostly obtained by injecting the fuel far upstream of the combustion chamber [137, 143].
Generally, swirl flows are well suited to generate high degrees of mixing quality due to the stirring fluid motion. However, in technical applications partially premixed conditions are typical which lead to equivalence ratio fluctuations. These equivalence ratio fluctuations are transported through the flame where they generate heat release fluctuations which influence the flame response [25]. Therefore, there is a huge interest in controlling equivalence ratio fluctuations and with that the mixing quality. A different combustion property, which is connected to the mixing quality, are pollutant emissions which will be discussed in the section below.
Previous studies showed that the strong coherent velocity fluctuations induced by the PVC near the burner outlet enhance the mixing quality of fuel and air or incoming cold reactants and hot recirculated products [27, 31, 35, 39, 132, 136, 144]. The PVC is capable of initiating vortex-induced mixing in partially premixed combustors as shown by Stöhr

et al. [132]. In this combustor, the fuel is injected very close to the combustor outlet under partially premixed conditions (see Fig. 1.8). Accordingly, the resulting mixing length is rather short such that fuel (indicated in blue in Fig. 1.8) and air (white regions) enter the combustion chamber as separated, rather unmixed, streams (see $t = 0\,\mathrm{ms}$ in Fig. 1.8). As a PVC vortex appears at the burner outlet ($t = 0.4\,\mathrm{ms}$), the fuel is entrained by the vortex towards the center which initiates the vortex-induced mixing of fuel and air. As a result, a well-mixed region is formed ($t = 0.8\,\mathrm{ms}$) which is indicated by a broadly distributed blue-white region (upstream right) compared to the separated unmixed stream (upstream left). This homogeneously mixed region of ignitable fuel-air mixture is needed for a rapid ignition by the recirculated gas which contributes substantially to the stabilization of the flame (indicated in red in Fig. 1.8) [132, 136]. In the mixing and flame stabilization study of Galley et al. [35], the mixing pattern caused by the PVC in crosswise direction is shown which has the shape of a "comma" following the precessing motion of the vortex. The "head" of this comma is a fuel-rich region trapped in the core of the vortex. This region is followed by a well-mixed ignitable fuel-air mixture which enhances the flame stabilization. As a consequence, the stabilization point follows the motion of the PVC. This mixing and stabilization scenario is supported by LES simulations in [27].

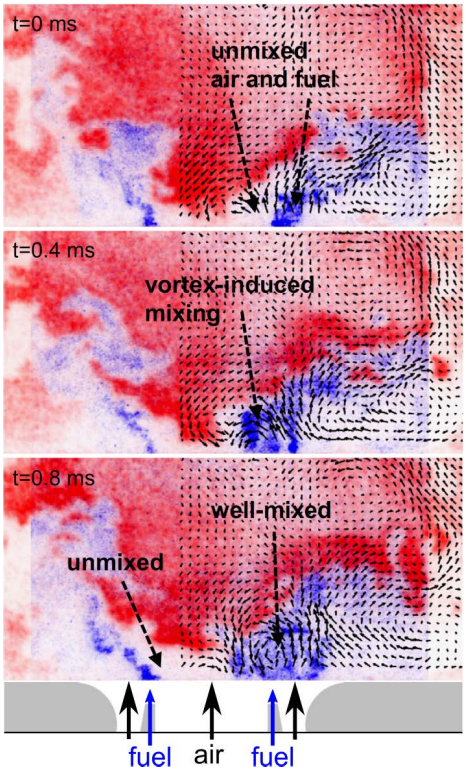

Figure 1.8: Sequence of velocity fields (black arrows from PIV), flame front (red from OH-PLIF) and fuel concentration (blue from acetone-PLIF) measurements showing the vortex-induced mixing induced by the PVC (adopted from: [132]).

Moreover, the PVC affects strong coherent mixing of the incoming cool reactants jet with the recirculated hot products [39, 144]. This coherent mixing leads to a smooth density gradient around the burner outlet which is typical for detached flames where a natural PVC is present [97, 144]. In such a detached flame, this coherent mixing of cool reactants with hot products cools down the CRZ which reduces the reactivity of the fuel-air mixture and inhibits the reattachment of the flame [144, 146].

In the present manuscript, the role of the PVC in the context of large-scale mixing is discussed in publication 2.3. Furthermore, in publication 2.4 the vortex-induced mixing between the incoming reactants and the hot products is illustrated and discussed in connection with NO_x emissions.

1.4 NO_x emissions and coherent structures

There are various (pollutant) species to be found in the exhaust gas of a premixed flame which is fired with a hydrocarbon-based fuel such as natural gas: carbon oxides (CO_2 and CO), nitric oxides (NO and NO_2), polycyclic aromatic hydrocarbons (PAH), unburnt hydro carbons and soot [56]. These emissions interact with the environment mostly in a harmful way: CO_2 enhances the greenhouse effect; PAH and soot can cause cancer [56]. In this section, the focus is on nitric oxides which are summarized under the term NO_x. These NO_x emissions are harmful for the human body and the global ecosystem as they e.g. attack the mucous membranes of the respiratory organs and cause "acid rain" [56]. Therefore, the amount of pollutant (NO_x) emissions is strictly regulated by law which makes them an important design parameter for modern combustion systems.
The formation of NO_x emissions, in the context of gas turbine combustion, is primarily described by two different formation mechanisms: the thermal NO (or Zeldovich NO) and the prompt NO (or Fenimore NO). The formation of thermal NO is connected to very high activation energies which requires high temperatures to initiate the reaction. Contrarily, prompt NO is promptly produced via the radical CH which is formed as an intermediate directly at the flame front. Compared to the thermal NO, prompt NO is also produced at lower temperatures. Both mechanisms include the nitrogen molecule which is required to be present within the oxidizer (e.g. air). The formed NO radicals further react to NO_2. For the sake of completeness, the prompt N_2O and the NNH mechanism shall be mentioned here [150]. For more details about the formation of pollutant emissions in combustion processes, the reader is referred to [56, 150].
The NO_x formation mechanism depends on thermodynamic quantities such as temperature and concentration of reactants and products. Therefore, the flow dynamics in reacting (combustor) flows can (indirectly) influence the NO_x formation. As explained above, swirling flows are well-suited to generate combustible fuel-air mixtures of high quality along the burner's mixing section. The obtained mixture quality is decisive because the better the mixing between fuel and air, the lower the level of NO_x emissions will be in lean premixed combustion [21, 30]. Beside the mixing of incoming fuel and air, the mixing of cold reactants with hot burnt products influences the reaction rates around the flame front. This includes the reaction rates of the NO_x formation mechanisms. Moreover, the mixing of reactants and products changes the composition of the radical pool which is crucial e.g. for generating prompt NO_x [18, 111, 133].
Another aspect which needs to be considered for reacting flows in the context of NO_x emissions is vortex-flame interaction [117]. Vortices, which are for example generated due to hydrodynamics instabilities such as the Kelvin-Helmholtz instability, can roll up the flame front as they propagate along the shear layers. Such a flame roll-up causes a rapid increase of the flame surface area which can lead to a heat release pulse [26, 111, 129, 131, 133]. Furthermore, an enlarged flame front increases the turbulent flame speed which is proportional to the reaction rate [56]. If vortices collide with the wall, the entrained reactants will rapidly burn and produce a heat release pulse. Such a type of wall interaction was observed for PVC vortices for example in [83]. Paschereit et al. [103, 105] observed an increase of NO_x emissions in the comparison of thermoacoustically stable and unstable partially premixed flames. Under thermoacoustically unstable conditions,

the Kelvin-Helmholtz instability causes the roll-up of symmetric vortices leading to heat release pulses. These pulses induce a small increase in (local) temperature. As the reactions rates in the thermal NO_x formation mechanism depend exponentially on temperature, such a small vortex-induced temperature increase can lead to an increase of the NO_x emission level [23].
A considerable part of the NO_x formation takes place in the (flame) reaction zone which is to be found in the ISL [13, 21]. Depending on the flow (and flame) configuration, the residence time of reactants and products can vary, for example due to the prolonged transport through the combustion chamber induced by coherent flow structures. If the time delay is increased, the thermal NO_x formation mechanism, which is relatively slow (i.e has a small reaction rate), will be promoted [56].

Previous studies comprehensively characterized the (basic) burner setup, which is utilized in the present thesis, regarding mixing behavior and NO_x emissions [40, 41]. Based on these findings, the impact of the PVC on NO_x emissions can be explained in publication 2.4.

1.5 Experimental setup and methods

This section focuses on the active flow control approach and its implementation into the experimental setup, i.e. the combustion chamber test rig. Above this, the applied measurement techniques are briefly summarized. For specific details regarding the measurement hardware and parameters, the reader is referred to the individual publications in chapter 2.

1.5.1 Active flow control approach

In this thesis, a novel active flow control approach is developed and applied to the PVC in swirl stabilized flames to investigate important combustion properties. For a successful flow control of coherent structures, such as the PVC, information about their (local) origin, the shape and dynamics are crucial.
Firstly, the (axial) actuation position within the flow needs to be chosen properly to allow for successful flow control. This choice was significantly influenced by studies about the origin of the PVC in reacting [96, 97, 102, 145] and non-reacting turbulent flows [34, 59, 86, 95, 108, 114, 140]. Even more important are the recent findings regarding global modes and their receptivity to external (open-loop) forcing [46, 79, 87, 108, 140]. Based on their adjoint (global) modes, a two-dimensional map can be derived revealing regions of high receptivity within the flow field [79, 86, 87, 108]. In these regions, external periodic forcing has the strongest influence on global modes such as the PVC. There are two studies by Müller et al. (see list of associated publications) estimating the receptivity in a generic geometry, which is somewhat similar to the configuration applied in the present thesis [86, 87]. Above this, there are studies in which the receptivity was calculated in more realistic configurations [59, 140]. All these studies have in common that the helical PVC mode shows highest receptivity values slightly upstream of the nozzle outlet around the center of the nozzle or in the vicinity of the centerbody, if present. Taking all these findings together and considering the geometry of the available swirl burner, the axial actuation position was chosen 0.45 nozzle diameters upstream of the burner outlet close to the tip of the centerbody (compare Fig. 1.9).
Actuating in the region of maximal receptivity and mimicking the shape and the dynamics of the PVC is the flow control approach which is referred to as *direct control* in this thesis. With this approach, a flow control system is realized that acts on the source of the instability driving the PVC, as derived from global adjoint linear stability theory [86, 87, 126, 140]. Actuating in the region of maximal receptivity means that only very small amplitudes are required to obtain a high response to the applied actuation. These small amplitudes and the actuation position at the origin of the PVC allow for controlling the flow efficiently such that the general flow configuration is not altered considerably. Therefore, direct control is a key enabler to investigate the impact of flow structures, such as the PVC, on the combustion process. The aim (and advantage) of direct control is to arbitrarily change the amplitude of the PVC without changing the other flow dynamics, i.e. not to excite other modes or instabilities or to change the mean flow field (except by the controlled PVC). By varying the amplitude of the PVC, the exclusive impact of the

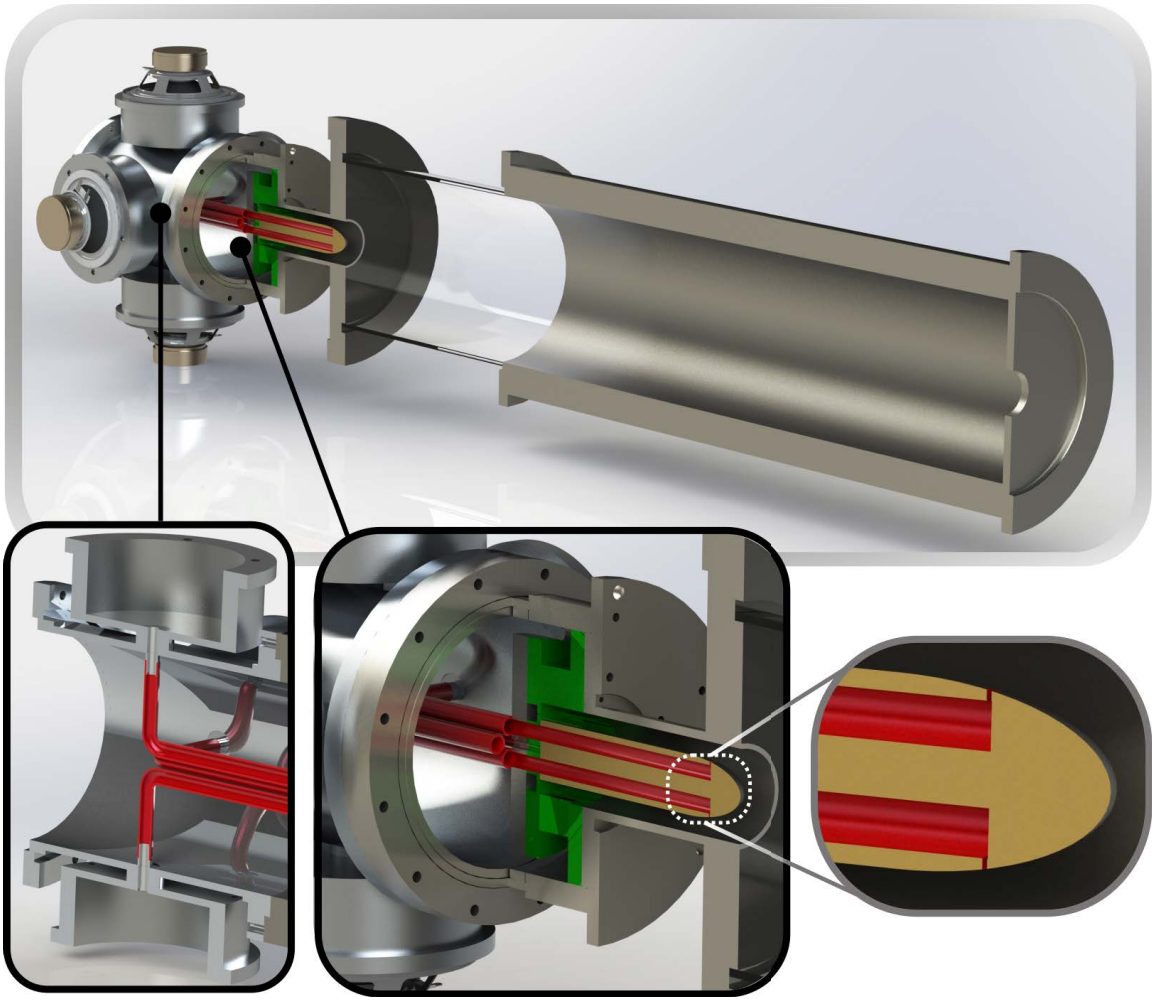

Figure 1.9: Actuator integrated into combustion chamber test rig. Details on the bottom from left to right: loudspeaker plena with connected actuation channels (red tubes), centerbody integrated into mixing tube of the burner downstream of the swirl generator (green), parabolic shape of the centerbody tip with rectangular actuation channel outlets.

PVC on other flow structures, for example axisymmetric TA modes, can be investigated in a targeted way. Moreover, the direct flow control system can be applied to either excite a PVC when it is damped, for example due to the density stratification induced by the flame, or suppress it when it is naturally present, for example in a detached flame [97]. Such a targeted excitation of the PVC allows for estimating its potential to enhance or deteriorate the combustion process.

As explained above (chapter 1.2), the PVC is a manifestation of a global hydrodynamic instability which can be adequately described by an oscillatory single-helical azimuthal ($m = 1$) mode. This description provides necessary information about the shape and the dynamics of the PVC which need to be imitated by the actuation of the flow control system to allow for targeted excitation or suppression of the PVC. Accordingly, the actuator is driven with a harmonic (sinusoidal) actuation signal which follows the dynamics of the PVC. Furthermore, the applied actuation needs to cover the single-helical shape of the PVC. This is realized by splitting one period of the actuation signal over circumferentially

arranged actuation positions. For a better comprehensibility, this arrangement is illustrated in Fig. 1.9. In this figure, the applied actuation system is shown as it is integrated into the combustor. Four loudspeakers at the upstream end (left side) force the air column to oscillate in the plena and the connected actuation channels, which are depicted by red tubes (compare bottom left in Fig.1.9). These actuation channels are attached to the swirl burner (compare bottom middle in Fig.1.9) where they continue inside a centerbody. At the tip of the centerbody, the actuation channels end in rectangular outlet slits which point in radial direction. Each of the actuation channels can be actuated individually. By shifting the phase of each of the four signals by a quarter period, a helical actuation is achieved which moves around the circumference of the centerbody and imitates the natural movement of the PVC.

In publications 2.2 - 2.5, the functionality of direct control is demonstrated in reacting flows. With this flow control system at hand, new insights into the role of the PVC in context of flame dynamics (publications 2.2 to 2.5), mixing (publications 2.3 and 2.4) and NO_x emissions (publication 2.4) are gained, which was not possible in that quality before.

Actuator design considerations

The parabolic shape of the centerbody tip, which contains the actuation channel outlets, was chosen due to aerodynamic considerations of the original cylindrical centerbody with sharped edges on the downstream end. A detailed comparison of both centerbody designs is given in publication 2.1. The parabolic shape was derived based on the aerodynamic design principle known as *boat tailing*, which is known from passive flow control at bluff bodies [49]. The boat tailing design principle aims to reduce the wake behind a bluff body. In the present case, the wake behind the centerbody shall be minimized such that no significant interaction with the flow field in the combustion chamber occurs.
The applied actuation follows the so-called *zero-net-mass-flux* principle. This means that only the air column contained in the actuation channel is used in an oscillatory manner to actuate the swirling flow through the outlet slits without adding additional fluid [55]. Typically, a zero-net-mass-flux actuator is realized with an oscillating membrane at the upstream end of the actuator. In the present case, the membrane of a loudspeaker is utilized to drive the actuator. The present actuation system was inspired by the actuators applied by Kuhn et al. [63] and Oberleithner et. al [94]. Kuhn et al. [63] used a motor-driven piston system to make a membrane oscillate which generated alternating actuation jets at the outlet of a lance. This lance was positioned at the wavemaker position of an isothermal swirling jet where the PVC could be controlled successfully. Oberleithner et al. applied eight loudspeakers circumferentially arranged around the nozzle outlet which allows for helical actuation up to an azimuthal wave number $|m| \leq 4$. The present actuator design combines the advantages of the actuators of Kuhn et al. [63] and Oberleithner et. al [94]. Accordingly, in the present actuator design, the motor-driven piston used in [63] is replaced by four loudspeakers, which are characterized by better handling and versatility. Following the design of Oberleithner et. al [94], the actuation channel outlets are arranged over the circumference of the centerbody. In the flow configuration

investigated by Kuhn et al. [63], the applied actuation lance allowed for a targeted actuation at the wavemaker position, where the response of the PVC was expected to be very high. This approach is adopted in the present actuator design by placing the outlets of the actuation channels into the centerbody tip such that the actuation is introduced in the flow region where the receptivity of the PVC is very high. The development process from an actuator with a lance, more comparable to the design of Kuhn et al. [63], to the final design is described in detail in publication 2.1.

Active (flow) control approaches are generally distinguished into two groups: open- and closed-loop approaches. The actuator used in the present thesis was designed such that both types of control can be realized. For a detailed review of the theory behind the control of turbulent flows, the reader is referred to the review article of Brunton and Noack [14]. The following paragraphs briefly describe the characteristics of open- and closed loop flow control and clarify for which purposes either of these approaches is applied in this thesis.

Open-loop control

In open loop control, an actuation signal is directly applied to the system and - in contrast to a closed loop approach - no measurement signal is fed back to the actuator, as illustrated in the generic block diagram in Fig. 1.10 . In the present case, a harmonic signal of the form

$$s(t) = A_f \sin(2\pi f_f t), \tag{1.2}$$

is used as input of the active flow control system. This sinusoidal signal contains two parameters: actuation amplitude A_f and actuation frequency f_f. They can be chosen freely, e.g. on the basis of previously performed experiments. The input signal $s(t)$ is fed into the actuator which applies a corresponding forcing to the system. In this thesis, the actuator comprises the loudspeakers and the connected apparatus for synthetic jet generation and the system consists of the swirling flow. In contrast to closed-loop control, the open-loop control approach does not contain a controller. Therefore a more appropriate and precise term for this approach would be open-loop forcing or open-loop actuation. However, the term open-loop control is often found in literature.

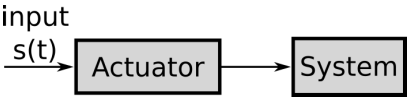

Figure 1.10: Generic open-loop control block diagram

The open-loop control approach is used for two purposes in this thesis. Firstly, it is applied to excite the PVC in flow configurations where a V-flame dampens the PVC which is the case in publications 2.2, 2.4 and 2.5. Secondly, open-loop control is applied to study the lock-in behavior of the isothermal combustor flow as shown in publication 2.1. To illustrate the lock-in behavior of a flow featuring a dominant oscillatory coherent structure such as the PVC, a generic lock-in diagram is shown in Fig.1.11 which is adopted from [71]. As shown by Terhaar et al. [142], the PVC dynamics can be well modeled by a parametric

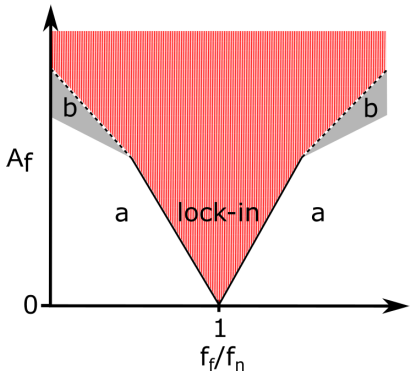

Figure 1.11: Generic lock-in diagram of a forced self-excited model oscillator showing the actuation amplitude A_f as a function of the normalized actuation frequency f_f/f_n. a: phase drifting, b: phase trapping, red-white hatched area: lock-in (phase and frequency locking) (adopted from [71])

nonlinear Van der Pol oscillator (compare section 1.2: "Characteristic flow instabilities"). The synchronization behavior of such a model oscillator, which is periodically forced, is described by the lock-in diagram shown in Fig.1.11 [71].

The lock-in diagram relates the forcing amplitude A_f to the ratio of forcing frequency f_f and natural frequency f_n which is in the present case the frequency of the naturally occurring PVC. Depending on the combination of A_f and f_f, the oscillator flow synchronizes with the forcing such that the synchronization state can be described by one of the three regions (a, b, *lock-in*) shown in this diagram. In region a, there is a *phase drifting* between forcing signal phase $\varphi_f(t)$ and the phase of the forced oscillator $\varphi_o(t)$ which means that the phase difference $\Delta\varphi(t) = \varphi_o(t) - \varphi_f(t)$ decreases or increases in time. At moderate values of A_f and f_f close to f_n, an effect called *frequency pulling* can be observed in the power spectral density which shows that f_n is pulled towards f_f with increasing A_f [71, 72]. If A_f is further increased over a critical *lock-in amplitude*, phase and frequency of the oscillator flow will fully synchronize with the forcing which means that $\Delta\varphi(t) = \mathrm{const.}$ and $f_f = f_n$. This state is called *lock-in* which means that the dynamics of the oscillator flow are following the well-defined forcing signal induced by the actuator. To reach this state of synchronization (phase and frequency locking) for f_f far from f_n, a higher value of A_f is required. Depending on the difference of f_f and f_n, the oscillator flow state can enter region b which is close to the lock-in region. In region b, frequency locking occurs whereas the phase difference $\Delta\varphi(t)$ oscillates boundedly. This state is referred to as *phase trapping*. For more details regarding the lock-in and synchronization of forced hydrodynamically self-excited jets and flames, the reader is referred to [71–73]. The phenomenon of lock-in and synchronization is used in the present thesis to study and verify the proper functionality of the newly designed actuator. Therefore, the isothermal combustor flow is studied in publication 2.1 regarding its lock-in behavior towards the forcing of the actuator. The proof of concept is fulfilled in publication 2.2 with the investigation of the impact of the forcing on the flow field.

Closed-loop control

In closed-loop control, a measurement signal is fed back to a controller, which adopts the actuation signal, corresponding to the deviation from the actual set point. A generic block diagram of this group of control approaches is shown in Fig.1.12. Compared to the open-loop control, a sensor is integrated into the block diagram which provides the measurement signal $e(t)$ containing information about the actual state of the flow. The measurement signal is fed back to the controller, which combines it with the input (reference) signal to generate an appropriate actuation.
Compared to open-loop approaches, the closed-loop control scheme is more complex. In the setup, which is used for this thesis, the controller adjusts a sinusoidal input signal $s(t)$ based on the measurements $e(t)$. For the closed-loop control applied in the present thesis (publication 2.3), the corresponding actuation signal reads as follows

$$s(t) = GA_{\mathrm{PVC}}(t)\sin(2\pi f_f t + \varphi(t) + \Delta\varphi), \tag{1.3}$$

where G stands for a gain, $A_{\mathrm{PVC}}(t)$ is the PVC amplitude, $\varphi(t)$ denotes the phase of the PVC and $\Delta\varphi$ stands for a phase shift. The current phase $\varphi(t)$ and amplitude $A_{\mathrm{PVC}}(t)$ of the PVC are estimated from the sensor signal by use of a Kalman filter, while the gain G, the forcing freq f_f and the phase lag $\Delta\varphi$ are preset by the user. The target quantity is the amplitude of the PVC, which shall be controlled in flame configurations where a PVC naturally occurs. To achieve such a type of PVC control, two time-dependent parameters need to be estimated by the controller which are: $A_{\mathrm{PVC}}(t)$, the amplitude of the PVC, and its current phase $\varphi(t)$. These two quantities are contained in the measurement signal $e(t)$ which updates the actual input signal $s(t)$. The phase shift $\Delta\varphi$ and the gain G are tuning parameters which are set by the user. The gain G adjusts the effective actuation amplitude, i.e. flow momentum, induced by the actuator to the actual flow dynamics. The phase shift $\Delta\varphi$ allows for fading between *in-phase* and *out-of-phase* actuation. To amplify the naturally present PVC, an in-phase actuation is required whereas out-of-phase actuation will damp the PVC. The maximal damping will be achieved, if the phase of the actuation signal is in opposition to the phase of the actual PVC. Above this, $\Delta\varphi$ compensates the phase lag that occurs due to the different spatial locations of sensor and actuation.

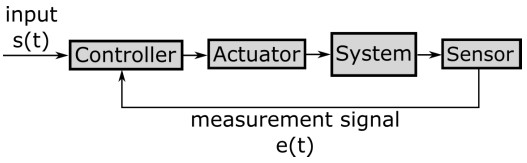

Figure 1.12: Generic closed-loop control block diagram

The controller applied in the present thesis is based on the design developed by Kuhn et al. [63]. It relies on an extended Kalman filter as state estimator [152]. The parameters of the Kalman filter were adjusted to the present burner setup such that phase-opposition control as shown in publication 2.3 could be realized. More details of the actual control design and applied technical apparatuses are given in publication 2.3. Further information about controller design is given in the review article by Brunton and Noack [14].

1.5.2 Pressure measurement techniques

The pressure measurements conducted in the present thesis can be distinguished into two groups: dynamic and acoustic pressure measurements. In this section, purpose and setup of these measurements are described.

Dynamic pressure measurements

The data provided by the dynamic pressure sensor arrangements developed in this thesis has a twofold purpose: characterizing the dynamics of the PVC in the mixing tube and the combustion chamber, and providing a suitable input signal for the closed-loop control approach. The detailed development of the sensor arrangement is given in publication 2.1.
To capture the helical motion of the PVC, the measuring points are arranged circumferentially around the burner outlet (P_1-P_4) as shown in Fig. 1.13. The round red arrow indicates the azimuthal actuation direction ($m = 1$) which is equal to the direction of rotation of the PVC investigated. The small red arrow pointing in direction of P_3 indicates an actuation jet with maximal momentum emanating from the corresponding actuator outlet at the centerbody. At the same time, the actuation channel on the opposite side is sucking air due to the inward movement of the loudspeaker membrane which leads to minimal momentum. The momentum at the actuator outlets opposite to P_2 and P_4 are zero at that time. Following the single-helical movement of the PVC ($m = 1$), the actuation momentum changes constantly in time along the circumference.
The induced actuation momentum needs to be considered for the sensor arrangement as the actuation jets may affect the pressure measurement. This influence is minimized

Figure 1.13: Circumferential sensor arrangement (P_1-P_4) with azimuthal actuation direction ($m = 1$) indicated by rounded arrow. Small red arrows exemplary indicate actuation jets generated by the four loudspeakers in the background. (View onto the burner front plate from the downstream end of combustion chamber)

when the sensors are attached to the front plate as shown in Fig. 1.13. Therefore, such an arrangement is chosen for closed-loop control applications (publication 2.3) and for clean characterization of the PVC dynamics (publications 2.1 and 2.2). In the publications accumulated in the present thesis, dynamic pressure measurements were conducted to monitor the functionality of the actuator and the dynamical behavior of the PVC.

Acoustic pressure measurements

In this thesis, acoustic pressure measurements were conducted to estimate the planar acoustic field inside the combustor. The measurements were carried out with microphone arrays mounted upstream of the burner and downstream of the combustion chamber (see for example [25, 106]). Each of these arrays consists of five microphones which are axially distributed. This experimental setup allows for decomposing the one-dimensional acoustic field into up- and downstream propagating waves (*Riemann invariants*) assuming plane acoustic waves in a duct where only the axisymmetric mode propagates. With the Riemann invariants at hand, the acoustic state variables pressure and acoustic velocity can be determined at an arbitrary location. This experimental procedure is called Multi-Microphone-Method (MMM) and was first applied in swirl-stabilized flames by Paschereit et al. [106]. The MMM allows for identifying the thermoacoustic properties of burner and flame.
Acoustic pressure measurements and MMM are applied in publication 2.5 to characterize the flame response which is further explained in section 1.6.4. More details about the derivation and implementation of the MMM are provided in the comprehensive works of Schuermans [119] and Moeck [82].

1.5.3 Optical measurement techniques

An overview of the applied optical measurement techniques is provided in this section. Technical details are given in the individual publications and are not included for brevity in the following overview.

OH*-chemiluminescence imaging (OH-CL)

The characteristic emission of OH* radicals (around 310 nm) is part of the chemiluminescence spectrum of hydrocarbon flames. This OH*-chemiluminescence is commonly used as a marker of the heat release rate in a flame [43, 45]. The emitted chemiluminescence light can be captured with an intensified camera which is used in connection with a bandpass filter. This camera setup delivers two-dimensional images of the line-of-sight integrated distribution of the heat release rate which can be used to estimate the flame shape. In the present thesis, the sampling frequency of the intensified camera is in the range of kHz which allows for time-resolved acquisition of the flame dynamics. Such an intensified high-speed camera setup is applied in the publications where the flame dynamics and the flame shape are studied (publications 2.2-2.5).

In publications 2.4 and 2.5, a photomultiplier tube (PMT), equipped with a bandpass filter, is used in addition to capture the integral OH*-chemiluminescence emitted by the flame. The perturbations induced by the PVC are captured by focusing the field of view of the PMT to a vertical plane on one side of the burner axis. This focusing is achieved with a collimator lens in front of the PMT. If the field of view is extended to the whole combustion chamber, the heat release rate fluctuations induced by the helical PVC mode will cancel out over the entire flame region due to the associated skew-symmetry [83]. This PMT setup allows for estimating the dynamics of the integral heat release rate fluctuations induced by the (actuated) PVC at a high temporal resolution ($\sim$kHz) and low memory requirements.
As reported in different studies [7, 68], the OH*-chemiluminescence is not an accurate measure for the heat release rate. The reason for this conclusion is the dependency of the OH*-chemiluminescence intensity on unsteady properties such as turbulent intensity or flame strain. Whereas the integral chemiluminescence intensity can provide rather accurate estimations of the heat release rate, spatially resolved measurements are considerably biased for example by spatially varying turbulence intensities [68]. Laborious correction procedures improve the accuracy of the OH*-chemiluminescence signal as a quantitative heat release rate marker [67, 78]. However, the application of such correction procedures is beyond the scope of the present thesis. Therefore, the shown heat release rate distributions are only considered as a qualitative marker for the flame.

Particle Image Velocimetry (PIV)

The measurement of the velocity fields inside the optical accessible combustion chamber are crucial to characterize the hydrodynamic stability, flow dynamics and shape of the PVC. Particle image velocimetry (PIV) is applied to measure the velocity fields under reacting and non-reacting conditions in the publications accumulated in this manuscript. For the PIV measurements, a pulsed high-speed laser system in connection with high-speed cameras is used such that time-resolved velocity field measurements were realized with sampling rates in the range of kHz.
Under reacting conditions, solid seeding particles are necessary, which withstand the high flame temperatures. The major disadvantage of solid particles is their tendency to stick to the combustion chamber wall which quickly deteriorates the image quality. Therefore, the application of high-speed PIV is crucial which allows for minimizing the measurement time and with that the time the wall is exposed to the injected seeding particles. This allows for conducting several measurements without cleaning the combustion chamber after every measurement. For more details regarding PIV, the reader is referred to the comprehensive textbook by Raffel et al. [109].
For hydrodynamic stability analysis, as conducted in publications 2.4 and 2.5, all three velocity field components (axial, transversal and out-of-plane) are crucial. Therefore, 3C-PIV, i.e. stereoscopic PIV, was applied to obtain the necessary data for these studies. In the measurement campaigns for publication 2.1-2.3, 2C-PIV was conducted to obtain the axial and transversal velocity components. The 2C-PIV measurements were synchronized with OH-CL measurements which allows for simultaneous acquisition of flow field and heat release rate.

Quantitative Light Sheet method (QLS)

The quantitative light sheet method (QLS) [52, 149], was applied in this thesis to estimate the density distribution in the reacting flow field. This method is relatively simple to apply in connection with PIV measurements. Depending on the local fluid density, the concentration of seeding varies and with that the amount of Mie scattering. Accordingly, the seeding distributions recorded for PIV can be used to estimate the density distribution in the combustion chamber.
In the present reacting flow configurations, the incoming cold jet has a comparably high density. This manifests in a high seeding concentration upstream of the flame leading to a high amount of Mie scattering. Over the flame front, the fluid density is rapidly decreased which reduces the seeding concentration as well. With a proper calibration procedure, involving images of a homogeneously seeded combustion chamber at isothermal conditions, reasonable density fields can be derived as shown in publication 2.3 and several other studies such as [97, 135, 145]. The density distribution is necessary to perform hydrodynamic stability analysis. Therefore, the QLS method was applied in publications 2.4 and 2.5 as well.

1.6 Empirical and analytical methods

There are some crucial empirical and analytical methods which are applied to achieve the results shown in the publications accumulated in chapter 2. These methods are briefly summarized in this section. For more details, the reader is referred to the (original) literature where the derivations of the individual methods are comprehensively presented. Corresponding references are given below.

1.6.1 Decomposition methods

The decomposition methods described in this section serve to characterize the shape and the dynamics of the PVC. These methods are crucial for the data analysis of the publications accumulated in chapter 2.

Spatial Fourier decomposition

With the circumferentially arranged pressure sensors shown in Fig. 1.13, the dynamics of the m-th azimuthal mode can be derived by decomposing the sensor signals into Fourier modes with azimuthal wave numbers as follows

$$\hat{p}_m(t) = \sum_{k=1}^{4} p_k(t) \exp\left(i\, 2\pi\, m\, \frac{k}{4}\right). \tag{1.4}$$

In Eqn. 1.4 the pressure signal of the k-th sensor is denoted by p_k. With four circumferentially arranged sensors, azimuthal modes with wave numbers $|m| = \{0, 1, 2\}$ can be detected. This decomposition is essential for investigations of the axisymmetric TA mode ($m = 0$) and the PVC mode ($m = 1$) in publications 2.1 and 2.2.
Besides the pressure signals, the two-dimensional OH-CL signal can be decomposed in spatial Fourier modes as well. The spatial modes are derived by a point-wise Fourier transform which can be written as follows

$$\widehat{\mathrm{OH}^*}(x, y) = \frac{1}{T} \int_0^T \mathrm{OH}^*(x, y, t) e^{-i2\pi f t}\, dt\,. \tag{1.5}$$

Substituting the f in Eqn. 1.5 by the frequency of the TA mode or the PVC yields a spatial Fourier mode describing thermoacoustic or PVC oscillations, respectively (compare publication 2.2).

Spectral Proper Orthogonal Decomposition (SPOD)

With the SPOD, applied in this thesis, coherent structures, here the PVC, are identified from time-resolved flow field data. The method was developed by Sieber et al. [124] and is based on the classical Proper Orthogonal Decomposition (POD) [47]. Similar to

the POD, the fluctuating part of the velocity, here exemplified with the crosswise velocity component v_y, is decomposed as follows

$$v_y(\mathbf{x},t) = \overline{v}_y(\mathbf{x}) + v'_y(\mathbf{x},t) = \overline{v}_y(\mathbf{x}) + \sum_{i=1}^{N} a_i(t)\Phi_i(\mathbf{x}). \tag{1.6}$$

As to be seen in Eqn. 1.6, the fluctuations are decomposed into a sum of spatial modes Φ_i and corresponding temporal coefficients a_i. This basis is built based on the spatial correlation among individual velocity snapshots yielding a correlation matrix. Compared to the POD, the SPOD offers a more precise selectivity which is achieved by applying a Gaussian low-pass filter to the correlation matrix. The temporal coefficients $a_i(t)$ are derived from the eigenvectors of the filtered correlation matrix and describe the dynamics of the corresponding mode Φ_i. These spatial modes are finally obtained from a projection of the snapshots onto the temporal coefficients.
More details about the derivation of the SPOD are given in [124]. Examples for the potential of this decomposition in the context of combustion are shown in [123]. In the present thesis, the SPOD is applied in all publications to identify the shape and dynamics of the PVC mode.

1.6.2 Hydrodynamic Linear Stability Analysis (LSA)

Linear stability analysis (LSA) is an analytical method applied to mean flow fields, which are measured here with stereoscopic PIV. This method allows physical construction of the coherent fluctuations (instability modes) which is fundamentally different from the empirical approach followed by the SPOD. To describe and study coherent flow structures, Hussain and Reynolds introduced the triple decomposition of the velocity field [51]. This decomposition approach can be applied for the characterization of hydrodynamic flow instabilities as shown for example in [58, 59, 95, 147]. For a velocity field $\mathbf{v}$, this decomposition reads as

$$\mathbf{v} = \overline{\mathbf{v}} + \tilde{\mathbf{v}} + \mathbf{v}'' \tag{1.7}$$

where $\overline{\mathbf{v}}$ is the mean flow field, $\tilde{\mathbf{v}}$ denotes the coherent part of the flow field and $\mathbf{v}''$ stands for the stochastic turbulent fluctuations in the flow field. Often, the coherent part $\tilde{\mathbf{v}}$ can be assumed as periodic in time and space and arising disturbances can be regarded as waves traveling in an axisymmetric shear layer. This allows for a decomposition of $\tilde{\mathbf{v}}$ into normal modes, assuming a parallel flow, in the following form (see e.g. [33, 95, 147]):

$$\tilde{\mathbf{v}}(x,r,\theta,t) = \Re\left[\hat{\mathbf{v}}(r)e^{i(\alpha x + m\theta - \omega t)}\right] \tag{1.8}$$

where α stands for the complex axial wave number, ω is the complex frequency, m denotes the real azimuthal wave number, $\hat{\mathbf{v}}$ is the radial amplitude function and $\Re$ refers to the real part (adopted from [147]). Due to the geometry of swirling jets, it is common to apply a cylindrical coordinate system to describe them which is done as well in this thesis. Accordingly, x stands for the axial coordinate, r is the radial coordinate and θ

denotes the azimuthal angle. As indicated in Fig. 1.3, the coordinate system is set to the center of the nozzle outlet, where the emanating jet starts to develop.

In order to conduct a LSA, the triple decomposition (see Eqn. 1.7) of velocity $\mathbf{v}$ and pressure field p are inserted into the incompressible Navier-Stokes equations and the momentum equation. After rearrangement and linearization, this yields separated equations of motion for the coherent part of the velocity and pressure field which reads as follows for an incompressible non-isothermal flow

$$\frac{\partial \tilde{\mathbf{v}}}{\partial t} + \tilde{\mathbf{v}} \cdot \nabla \overline{\mathbf{v}} + \overline{\mathbf{v}} \cdot \nabla \tilde{\mathbf{v}} = -\frac{1}{\overline{\rho}} \nabla \tilde{p} + \nabla \cdot (\nu_{\mathrm{eff}} (\nabla + \nabla^T) \tilde{\mathbf{v}}) \tag{1.9}$$

$$\nabla \cdot \tilde{\mathbf{v}} = 0. \tag{1.10}$$

The effective viscosity ν_{eff} is equal to the sum of the molecular and turbulent viscosity, where the latter accounts for the interaction between the random and coherent fluctuations. As a closure, Boussinesq's eddy viscosity model can be applied to calibrate the effective viscosity to the Reynolds stresses, which are obtained from PIV measurements [96, 114, 140].

Global LSA

In the framework of global LSA, the global mode ansatz

$$\tilde{\mathbf{q}}(\mathbf{x}, t) = \Re\{\hat{\mathbf{q}}(x, r) \mathrm{e}^{i(m\theta - \omega t)}\} \tag{1.11}$$

is inserted into Eqn. 1.9 and 1.10, where $\tilde{\mathbf{q}}$ stands for $\tilde{p}$ and $\tilde{\mathbf{v}}$, x denotes the axial coordinate, r is the radial coordinate and θ stands for the azimuthal angle. As the ω is complex, the real part $\Re\{\omega\}$ corresponds to the frequency and the imaginary part $\Im\{\omega\}$ to the temporal growth rate. By rearranging the resulting equations, an eigenvalue problem can be formulated with ω as the eigenvalue and $\hat{\mathbf{q}}$ as the eigenfunction. This eigenvalue problem can be numerically solved for a given m for example with the FELiCS code developed at TU Berlin which is based on Finite-Elements. For $\Im\{\omega\} > 0$ the mean flow is globally unstable and it is globally stable for $\Im\{\omega\} < 0$.
More details about the implementation and derivation of the global LSA can be found in [58, 87, 140, 148]. In the present thesis, the global LSA is applied in publication 2.4 and 2.5 for the PVC mode ($m = 1$).

Local LSA

For a local LSA, the mean flow field is sliced into velocity profiles which are analyzed separately for each (axial) location. Compared to the global LSA, the local LSA assumes a quasi parallel base flow and coherent fluctuations which are oscillating in axial direction with the complex axial wave number α. This leads to the normal mode ansatz which was

already introduced in Eqn. 1.8. This ansatz is introduced in Eqn. 1.9 and 1.10 which allows for formulating an eigenvalue problem with appropriated boundary conditions as given in [61]. It can be discretized by using, for example, a Chebyshev collocation method [95]. The eigenvalue problem can be formulated for the following three approaches: temporal, spatial and spatiotemporal analysis. The choice of the analysis approach depends on the flow configuration. In publication 2.5, a spatial analysis is conducted for $m = 0$. This approach gives insight into the spatial growth ($\Im\{\alpha\} < 0$) and decay ($\Im\{\alpha\} > 0$) of the investigated mode. For more details regarding local LSA, the reader is referred to [50, 93, 95, 142].

1.6.3 Tomographic reconstruction methods

The tomographic reconstruction methods applied in this thesis are focused on the heat release rate distribution. The two-dimensional time-resolved OH-CL measurements provide the basis for these methods, which are briefly introduced in the following paragraphs.

Abel deconvolution

The OH-CL data recorded with the intensified high-speed camera, positioned in a side-view arrangement, represent line-of-sight-integrated values. To obtain a planar representation of the heat release rate, an appropriate reconstruction method needs to be applied. If rotational symmetry of the measured configuration can be assumed, a classical Abel deconvolution can be applied to obtain a planar representation [100, 118]. For the time-averaged heat release rate distribution and axisymmetric heat release rate fluctuations induced by TA modes, the assumption of rotational symmetry is applicable in the configuration investigated in this thesis. Accordingly, the Abel deconvolution is applied in publications 2.2 to 2.5. For further detail about Abel deconvolution techniques, the reader is referred to [156].

Reconstruction of heat release fluctuations induced by helical modes

Due to its single-helical shape, the PVC induces skew-symmetric heat release fluctuations which are not covered by the assumption of rotational symmetry made for the Abel deconvolution. Therefore, an advanced reconstruction method need to be applied which was developed by Moeck et al. [84]. Most tomographic reconstruction algorithms need several cameras to obtain enough views from different angles onto the region of interest. However, in case of PVC-induced heat release fluctuations, a single stationary (OH-CL) camera is enough to generate a sufficient number of views. Exploiting the single-helical shape of the PVC, phase-averaged side-view images can be interpreted as different views of a stationary structure which allows to reconstruct the three-dimensional shape of the PVC-induced heat release fluctuations [83, 144].

This reconstruction method by Moeck et al. is applied in publications 2.2 to 2.5. For more details of the derivation and implementation of this method, the reader is referred to [84].

1.6.4 Flame Transfer Function (FTF)

A thermoacoustic system, such as a gas turbine combustor, consists of many elements (burner, flame, cooling and fuel lines etc.) which need to be modeled appropriately such that the thermoacoustic behavior of the overall system can be characterized. The complex acoustic elements, especially burner and flame, are characterized experimentally by a "black box" approach. This approach relates the acoustic state variables up- and downstream of the acoustic element via a transfer matrix or transfer function, respectively [106]. All the well-characterized acoustic elements can be put together to a network model describing the whole thermoacoustic system.
The MMM (see chapter 1.5.2) is applied to determine the burner transfer matrix (BTM) by acoustic forcing up- and downstream of the flame without combustion [106]. The acoustic velocity directly upstream of the flame is derived from the upstream microphone array in conjunction with the BTM. Applying the Rankine-Hugoniot relations in conjunction with the reconstructed acoustic velocity, the flame transfer function (FTF) can be derived assuming an acoustically compact flame [90, 120]. The FTF describes the frequency dependent flame response to acoustic forcing and is defined as

$$\mathrm{FTF}(\omega) = \frac{\hat{Q}/\overline{Q}}{\hat{u}/V_0}, \tag{1.12}$$

where ω is the frequency, $\hat{Q}$ denotes the Fourier-transformed global heat release rate, $\overline{Q}$ stands for the mean global heat release rate, $\hat{u}$ is the Fourier-transformed acoustic velocity and V_0 denotes the bulk flow velocity. Due to the application of MMM and Rankine-Hugoniot relations, the heat release rate fluctuations do not need to be measured directly.
The impact of the PVC on the FTF of a V-flame is investigated in publication 2.5. More details about the derivation of the FTF are provided in the comprehensive works of Schuermans [119] and Cosic [24].

Chapter 2

Publications

The publications accumulated in this chapter demonstrate the research progress from the design of a suitable actuation system (see publication 2.1) to the investigation of the PVC's impact on the flame transfer function (see publication 2.5). Moreover, the effects of the PVC on combustion dynamics (see publication 2.2 to 2.5), mixing (see publications 2.3 and 2.4) and NO_x emissions (see publication 2.4) are investigated by means of open- and closed-loop active flow control. Upfront of each publication printed in this chapter, a short summary is given which aims to contextualize their positions within the whole thesis. The following publications are accumulated in this chapter:

2.1 Lückoff, F., Sieber, M., Paschereit, C. O., and Oberleithner, K., **2018**; "Characterization of Different Actuator Designs for the Control of the Precessing Vortex Core in a Swirl-Stabilized Combustor". *ASME. J. Eng. Gas Turbines Power, 140(4): 041503.* https://doi.org/10.1115/1.4038039

2.2 Lückoff, F., and Oberleithner, K., **2019**; "Excitation of the precessing vortex core by active flow control to suppress thermoacoustic instabilities in swirl flames". *International Journal of Spray and Combustion Dynamics, 11.*, https://doi.org/10.1177/1756827719856237

2.3 Lückoff, F., Sieber, M., Paschereit, C. O., and Oberleithner, K., **2019**; "Phase-Opposition Control of the Precessing Vortex Core in Turbulent Swirl Flames for Investigation of Mixing and Flame Stability". *ASME. J. Eng. Gas Turbines Power., 141(11): 111008.* https://doi.org/10.1115/1.4044469

2.4 Lückoff, F., Sieber, M., Paschereit, C. O., and Oberleithner, K., **2020**; "Impact of the Precessing Vortex Core on NOx Emissions in Premixed Swirl-Stabilized Flames - An Experimental Study". *ASME. J. Eng. Gas Turbines Power, 142(11): 111010.* https://doi.org/10.1115/1.4048603

2.5 Lückoff, F., Kaiser, T. L., Paschereit, C. O., and Oberleithner, K., **2021**; "Mean field coupling mechanisms explaining the impact of the precessing vortex core on the flame transfer function". *Combustion and Flame, 223, 254–266.* https://doi.org/10.1016/j.combustflame.2020.09.019

2.1 Publication I

Characterization of Different Actuator Designs for the Control of the Precessing Vortex Core in a Swirl-Stabilized Combustor

Before the PVC can be actuated in the region, where it is most receptive to external forcing, a suitable actuator needs to be designed. The first publication documents the development process of the PVC actuator design under isothermal flow conditions. Different concepts, which are motivated by previous (helical) actuation systems [63, 94], are compared and evaluated regarding their capability of actuating and controlling the PVC inside a prototype combustion chamber. This evaluation is based on the investigation of the PVC's lock-in behavior on the actuation of the different actuator concepts. A proof of concept is provided by an actuator design allowing for reliable lock-in in connection with sufficiently high actuation amplitudes. As a result of this publication, a final actuator design is determined, which is utilized in the following studies, i.e. publications.

To facilitate closed-loop control in following studies (see publication 2.3) and characterize the dynamics of the PVC, a suitable sensor arrangement is necessary providing a representative time-resolved PVC signal. In this publication, several pressure sensor arrangements are characterized regarding their capability of resolving the PVC. Based on these findings, the sensor arrangement for non-isothermal, i.e reacting, experiments in combustion chamber test rigs is derived.

Characterization of Different Actuator Designs for the Control of the Precessing Vortex Core in a Swirl-Stabilized Combustor

Finn Lückoff[1]
Chair of Fluid Dynamics,
Hermann-Föttinger-Institut,
Technische Universität Berlin,
Müller-Breslau-Str. 8,
Berlin 10623, Germany
e-mail: finn.lueckoff@tu-berlin.de

Moritz Sieber
Chair of Fluid Dynamics,
Hermann-Föttinger-Institut,
Technische Universität Berlin,
Müller-Breslau-Str. 8,
Berlin 10623, Germany

Christian Oliver Paschereit
Chair of Fluid Dynamics,
Hermann-Föttinger-Institut,
Technische Universität Berlin,
Müller-Breslau-Str. 8,
Berlin 10623, Germany

Kilian Oberleithner
Chair of Fluid Dynamics,
Hermann-Föttinger-Institut,
Technische Universität Berlin,
Müller-Breslau-Str. 8,
Berlin 10623, Germany

The precessing vortex core (PVC) represents a helical-shaped coherent flow structure typically occurring in both reacting and nonreacting swirling flows. Until now, the fundamental impact of the PVC on flame dynamics, thermoacoustic instabilities, and pollutant emissions is still unclear. In order to identify and investigate these mechanisms, the PVC needs to be controlled effectively with a feedback control system. A previous study successfully applied feedback control in a generic swirling jet setup. The next step is to transfer this approach into a swirl-stabilized combustor, which poses big challenges on the actuator and sensor design and placement. In this paper, different actuator designs are investigated with the goal of controlling the PVC dynamics. The actuation strategy aims to force the flow near the origin of the instability—the so-called wavemaker. To monitor the PVC dynamics, arrays of pressure sensors are flush-mounted at the combustor inlet and the combustion chamber walls. The best sensor placement is evaluated with respect to the prediction of the PVC dynamics. Particle image velocimetry (PIV) is used to evaluate the passive impact of the actuator shape on the mean flow field. The performance of each actuator design is evaluated from lock-in experiments showing excellent control authority for two out of seven actuators. All measurements are conducted at isothermal conditions in a prototype of a swirl-stabilized combustor. [DOI: 10.1115/1.4038039]

Keywords: precessing vortex core, active flow control, lock-in, swirl-stabilized combustion, coherent structures, particle image velocimetry (PIV)

1 Introduction

Swirling flows are typically used in modern gas turbine combustors to aerodynamically stabilize lean premixed flames. The internal recirculation zone that is generated at high swirl intensities destabilizes a strong helical coherent structure known as the precessing vortex core (PVC) [1]. A visualization of the PVC is given in [2] and shown in Fig. 1. The origin of this coherent structure is now well understood thanks to linear hydrodynamic stability theory [3–7]. However, our current understanding of the impact of this structure on the combustion performance is still very limited.

Recent studies show that the PVC may affect the flame stability and flame dynamics [8]. It may couple with thermoacoustic instabilities [9–11] and affect the fuel–air mixing upstream of the flame [12,13], which indirectly influences the pollutant emissions. However, the fundamental interaction of the PVC with these processes is still unknown. In this context, it has not yet been clarified whether the PVC can be used in a beneficial way to reduce NO_x emissions and combustion instabilities. The only way to systematically investigate the impact of the PVC on the combustion performance is to implement an active flow control scheme that purely acts on the PVC without altering other parts of the combustion system.

A preceding study successfully applied feedback control of the PVC in a generic swirling jet setup [14]. The actuator was placed into the jet core in a region that coincides well with the sensitivity of the PVC as derived from linear stability analysis [5,6]. The present study will transfer this approach to a model combustor which has been studied in foregoing investigations [15,16]. The implementation of a feedback control system into a combustion chamber featuring reacting swirling flows poses significant challenges to the actuator and sensor design and placement. The actuator must sustain high temperatures and must be integrated into the current combustor geometries without changing the flame and flow characteristic. Likewise, the sensors must be nonintrusive and also robust with respect to high temperatures. In particular, the sensors must capture the PVC dynamics in real time in terms of amplitude and phase.

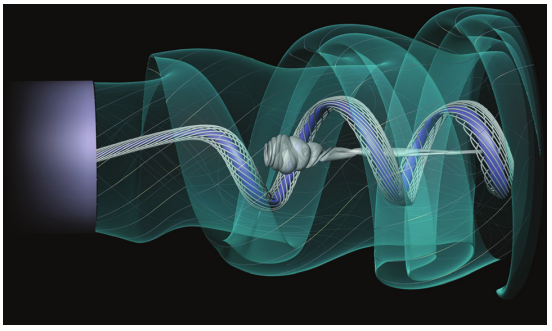

Fig. 1 Three-dimensional visualization of a velocity field including a PVC from Ref. [2]. Reconstructed from particle image velocimetry (PIV) snapshots at Reynolds number Re = 20,000. Central streak-lines surrounding a helical streak-surface depict the PVC. Spiral vortices induced by helical waves can be seen in the outer shear layer. The internal recirculation zone in the center is shown as a pathline-surface surrounded by the PVC streak surface.

[1]Corresponding author.

Contributed by the Combustion and Fuels Committee of ASME for publication in the Journal of Engineering for Gas Turbines and Power. Manuscript received July 11, 2017; final manuscript received July 31, 2017; published online October 31, 2017. Editor: David Wisler.

In this study, different actuator and sensor designs and placements are investigated as well as their ability to detect and control the PVC. The control strategy aims at forcing the flow by four independently controllable and radially or axially directed periodic jets in flow regions of high sensitivity. The four jets are arranged circumferentially to allow for the forcing of the first azimuthal mode. Such a forcing may directly lock onto the PVC oscillations which have the same mode order. In this way, we do not introduce any other mode (such as axisymmetric modes [9,10]) that would alter the overall flow dynamics. This is mandatory to investigate the explicit impact of the PVC on the combustion. Linear stability analysis further showed that the best placement for this kind of forcing is very close to the combustor inlet where the PVC is most sensitive to periodic forcing [5–7,14].

A key challenge for flow control is the placement of the actuator. It should have maximum control authority and minimum energy input. We evaluate each actuator by lock-in experiments. Here, lock-in describes the state where the dynamics of the PVC are entirely synchronized to the forcing. A suitable actuator for closed-loop control should require a minimum of amplitude to achieve lock-in [14,17]. Therefore, the lock-in behavior can be used to compare and rank the different actuator concepts. In addition, hot-wire probes are used to estimate the momentum of the actuation jets induced at the actuator channel outlets. This provides an additional ranking criterion.

Moreover, the passive impact of the actuators (without active forcing of the flow) on the mean flow and PVC dynamics needs to be investigated. This has been done via planar time-resolved PIV measurements, which allow for a detailed characterization of the baseline case. The dominant coherent structures occurring within the natural flow are characterized using spectral proper orthogonal decomposition (SPOD) analysis [18]. The SPOD is a new method that has shown excellent results with respect to the identification of coherent structures in the complex flow fields of swirl-stabilized combustors [19]. It is known that the breakdown bubble and hence the entire mean flow may substantially be modified by placing an obstacle into the flow [14,20]. To avoid any passive effect on the PVC, an actuator design needs to be employed that does not affect the mean flow.

Finally, the choice of sensors that monitor the PVC suitably is another significant challenge. We use pressure sensors placed in the mixing section of the swirler and at the combustion chamber walls. The pressure signals are used to estimate amplitude and phase of the PVC at different positions. The performance of the sensor arrays is evaluated by comparing the estimated amplitudes and the phase error with respect to the phase information from SPOD analysis.

The paper is structured as follows: We first present the test rig together with the applied measurement techniques followed by a description of the different actuator designs. Subsequently, a short introduction to the data analysis methodology is given. In Sec. 4, we first discuss the mean flow fields and the coherent structures as measured via PIV. We then evaluate the different actuator designs and sensor placements based on pressure data of the lock-in experiments and hot-wire measurements. In the concluding section, we point out which actuator concept will be used in subsequent investigations and outline our future steps.

2 Experimental Setup

In this section, the experimental arrangement with the implemented flow actuators and pressure sensors is explained. Thereafter, the different actuator designs are explained in detail.

2.1 Test Rig. The test rig is shown in Fig. 2. It consists of three different sections marked with ①–③. Section ① represents the actuation unit including four circumferentially arranged 5 in loudspeakers (rated power of 100 W). The loudspeakers are mounted on aluminum pots with an orifice at the bottom on which tubes are mounted (Fig. 2). These tubes guide the oscillating air to the outlet of the centerbodies. The loudspeakers are driven at a single frequency with relative phase shifts of $\pi/2$, which corresponds to a co-rotating mode with an azimuthal wavenumber of one. The input voltage to the speakers ranges between 0 V and 2 V and is amplified by a four-channel power amplifier (t.amp E4-130). The frequency is set relative to the natural frequency of the PVC. Accordingly, forcing frequencies were set to values corresponding to normalized frequency differences between natural and forced oscillation $\Delta f = f_f/f_n - 1$ of 8–27%. Section ② marked in Fig. 2 includes the burner, the swirl generator (inside the burner), the mixing tube with front plate and the centerbody (in the center of the mixing tube). It has exactly the same geometry as the swirl-stabilized model combustor used in foregoing investigations [15,16]. The hydraulic diameter of the mixing tube $D_h = 20$ mm is equal to the difference between the outlet ($D = 55$ mm) and the centerbody diameter ($D_{CB} = 35$ mm). In this study, the Reynolds number based on the hydraulic diameter and the plug flow velocity ranges between 13,000 and 32,000. A radial swirl generator consisting of movable blocks is used to generate the swirling flow. These blocks can be adjusted relative to each other. In this way, the theoretical swirl number Sw [21], defined as the ratio of the axial flux of tangential momentum to the axial flux of axial momentum, can be adjusted continuously between 0 and 1.5. In this study, the swirl number was set to Sw = 0.7, a value used commonly in combustion experiments [15]. To allow for rapid replacement of the dynamic pressure sensors, the mixing tube and front plate were made out of plastic. The combustion chamber (section ③ in Fig. 2) consists of a cylindrical quartz glass tube. With an inner diameter of 200 mm and a length of 300 mm, this quartz glass tube enables good optical access for flow measurements.

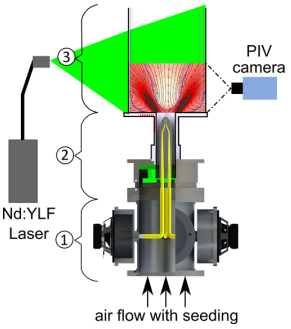

Fig. 2 Test rig with PIV setup. Section ①: actuation unit with four loudspeakers and actuation channels; section ②: burner with swirl generator, mixing tube containing centerbody inside; section ③: quartz glass combustion chamber.

2.2 Measurement Techniques. Time-resolved PIV measurements were conducted inside the cylindrical combustion chamber using a high-speed Nd:YLF diode pumped laser (Quantronix (Hamden, CT) Darwin Duo 527-100 M, 527 nm and total pulse energy of 60 mJ) in combination with a Photron SA-Z CMOS high-speed camera. The recording frequency is set to 1013.39 Hz whereby care was taken to avoid phase lock between the acquisition frequency and forcing frequency. A light sheet optic is used to achieve an appropriated laser sheet of approximately 1 mm thickness in the measurement area. Reflections of the incoming laser light at the quartz glass were minimized by utilizing beam dumps for the laser sheet and primary reflections. The laser pulse separation was set to 25 μs which corresponds to a maximum displacement of 3 pixels in the jet center. The flow is seeded with an aerosol of liquid di-ethyl-hexyl-sebacate. For each measurement, 2183 PIV snapshots with a resolution of 1024×1024 pixels were acquired. These snapshots were evaluated with a commercial PIV software. The correlation scheme employs multigrid refinement [22] with a final window size of 16×16 pixels, window overlap of 50% in combination with spline-based image deformation [23], and

subpixel peak fitting. Finally, the data were filtered for outliers and interpolated from adjacent interrogation windows. Figure 3 shows the sensor arrangements and the positions with the corresponding abbreviations (R1–R6 on the front plate; A1–A6 in the mixing tube). The pressure is measured by miniature differential pressure sensors (First Sensor HDOM010 with 1000 Pa range), which are connected to the flow via cannula tubes. These sensors allow for measuring pressure fluctuations as small as 0.1 Pa. A common reference pressure is achieved by connecting one pressure port with an ambient pressure reservoir. The pressure sensor signals are amplified with an in-house amplifier and digitized by a 16 bit A/D converter (National Instruments NI 9216, Austin, TX) at a sampling frequency of 8192 Hz.

Hot-wire anemometry is used to measure the velocities at the actuator outlets. A TSI IFA 100 hot-wire anemometer is used in combination with a single-wire probe mounted on a three-axis manual traverse. To achieve comparable conditions, the probe is traversed to those positions near the outlet where maximal velocity amplitudes are present. The signals generated by the anemometer are recorded with the before mentioned A/D converter (National Instruments NI 9215). The hot-wire probe was calibrated inside a wind tunnel with respect to a standard Prandtl tube at 42 different velocities. These measurements were approximated by a fourth-degree polynomial calibration curve.

Measuring PIV and pressure simultaneously allows for investigating the reliability of the PVC detection. This was done with the help of pressure signals which are validated by flow field data. In this connection different Reynolds numbers (as described previously), centerbody designs and sensor arrangements were studied. Accordingly, accuracy and reliability of different sensor arrangements under different flow conditions can be evaluated. In order to quantify the quality of the different actuators, pressure measurements of the forced flow were performed to gain data for lock-in evaluations. To find suitable forcing frequencies, the natural frequency of the PVC was observed for a certain parameter setting (Reynolds number, actuator design). Then, the forcing frequency was set to a value corresponding to a Δf ranging from 8% to 27%. Thus, forcing closer and further away from the natural frequency can be investigated. The hot-wire measurements serve to evaluate the momentum generated by the actuators. For all actuators, the momentum was measured for the same frequency of 100 Hz and actuation voltages between 0 and 2 V to guarantee comparability.

2.3 Actuator Designs. The results from the previous investigation suggest an actuation of the PVC close to the jet centerline in the vicinity of the upstream end of the vortex breakdown bubble [14]. This requires the use of actuation lances that are placed in this flow region. The disadvantage of such designs is the strong impact of the actuator on the mean flow, since the region around the stagnation point is highly sensitive to flow obstruction. A better option is to implement the actuator into the existing geometry and to use thin slots or holes that do not passively influence the flow. As a drawback, the placement of the actuator depends on the combustor design and must not coincide with the region of highest sensitivity. Figure 4 depicts the different actuator designs investigated in this study. For better orientation, roman numerals and small pictographs are assigned to each actuator.

The designs III, IV, and V contain tapered actuation channels with an inlet diameter of $D_c = 9$ mm and outlet diameter of 1 mm. The difference between actuators III and IV is the shape of the tip. Concept III features a flat tip in contrast to the parabolically shaped design of actuator IV. The parabolic shape is the same for all other concepts. Actuator V provides radially directed jets. In contrast, designs III and IV provide axially directed jets.

Compared to the designs described before, the actuators VI and VII have nontapered channels with constant diameter and slits with 1×9 mm^2 cross section as outlets. As to be seen at the detailed tip in Fig. 4, the slits of design VI are slightly curved following a circular line. These outlets are either radially (VII) or axially (VI) directed.

The two concepts I1/I2 and II3/II6 shown in the most left columns of the top row in Fig. 4 consist of inner channels and cannula tubes of different diameter. The tubes reach through the entire combustion chamber and can be traversed axially. This feature allows for adjusting the actuation area relatively to the wavemaker position without changing the passive influence on the flow field. Every cannula contains a 0.6 mm hole providing radially

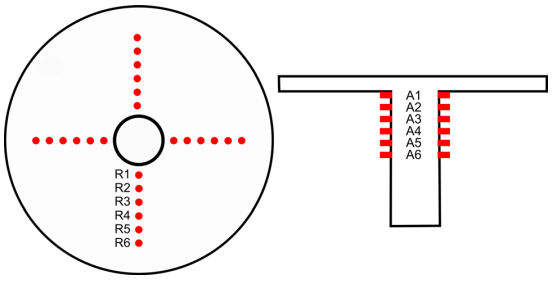

Fig. 3 Different arrangements of pressure sensors in the front plate (left) and the mixing tube (right)

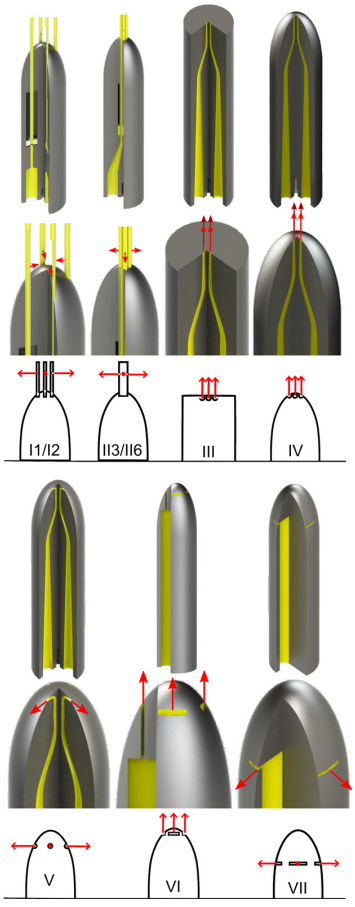

Fig. 4 Complete view, detailed tip, and equivalent pictograph of all seven centerbody designs arranged one below the other. Arrows indicate the directions of actuating jets. Each design generates four individual jets.

directed jets. Actuator I1 corresponds to the concept with four independent tubes of an inner diameter of 1.1 mm (I2 with a diameter of 2 mm). These tubes can be rotated to change the direction of the jets. The II-concepts contain a lance which consists of four cannula tubes leading to different lance diameters (3 or 6 mm) depending on the tube diameter. This design is inspired by the work of Kuhn et al. [14] where a comparable lance showed suitable performance.

3 Data Analysis Methodology

Spectral proper orthogonal decomposition is used to reconstruct the PVC dynamics and other coherent structures from the PIV data. Spatial Fourier decomposition is applied to the pressure signal in order to extract the PVC amplitude. In the following, the reader is briefly introduced to these data analysis methodologies.

3.1 Spatial Fourier Mode Decomposition. The signals recorded by four circumferentially arranged pressure sensors are decomposed into Fourier modes with azimuthal wavenumbers. Accordingly, the signal of the mth azimuthal mode can be estimated by

$$\hat{p}_m(t) = \sum_{k=1}^{4} p_k(t) \exp\left(i\, 2\pi\, m\, \frac{k}{4}\right) \tag{1}$$

where p_k is the pressure signal of the kth sensor and m is the azimuthal wavenumber. With four different circumferentially arranged sensors, azimuthal modes with wavenumber $m \in \{0, 1, 2\}$ can be detected. The Fourier coefficient $\hat{p}_m$ is complex and a function of time. In other words, the instantaneous amplitude and phase of the PVC correspond to the modulus and argument of $\hat{p}_1$, respectively.

3.2 Spectral Proper Orthogonal Decomposition (SPOD). The SPOD is a newly introduced method to identify coherent structures in flow data [18]. It is based on the classical proper orthogonal decomposition [24], but it offers a more precise selectivity, which provides benefits in complex turbulent flows like the swirling jet investigated here [19]. In the following, only a short overview of the SPOD approach is given. A detailed derivation can be found in Ref. [18]. The procedure is exemplified for the axial velocity U but holds similar for the crosswise velocity V. The SPOD provides a modal decomposition of the fluctuating part of the velocity U' that reads as follows:

$$U(\mathbf{x}, t) = \overline{U}(\mathbf{x}) + U'(\mathbf{x}, t) = \overline{U}(\mathbf{x}) + \sum_{i=1}^{N} a_i(t)\Phi_i(\mathbf{x}) \tag{2}$$

It is separated into a sum of spatial modes Φ_i and corresponding modal coefficients a_i. In order to build this basis, the spatial correlation among individual PIV snapshots is calculated, which results in the correlation matrix

$$R_{i,j} = \frac{1}{N}\int_{\Omega} U'(\mathbf{x}, t_i)U'(\mathbf{x}, t_j) + V'(\mathbf{x}, t_i)V'(\mathbf{x}, t_j)\mathrm{d}A \tag{3}$$

where Ω indicates the measured domain over which the correlation is integrated. In order to restrict the spectral content of the modes, a filter is applied to the correlation matrix resulting in a filtered correlation matrix

$$S_{i,j} = \sum_{k=-N_f}^{N_f} g_k R_{i+k,j+k} \tag{4}$$

The filter coefficients g_k are chosen to create a Gaussian low-pass filter. By adjusting the filter size N_f, the spectral constraint of the SPOD can be adjusted. A usual choice is a filter size that is between one and two periods of the dominant frequency, which is the PVC in the present case. For the presented SPOD, it is set to two periods; therefore, $N_f = 20 \approx 2f_{\mathrm{PIV}}/f_n$.

The temporal coefficients $\mathbf{a}_i = [a_i(t_1), ..., a_i(t_N)]^T$ and mode energies λ_i are obtained from the eigenvectors and eigenvalues of the filtered correlation matrix

$$\mathbf{S}\mathbf{a}_i = \lambda_i \mathbf{a}_i; \quad \lambda_1 \geq \lambda_2 \geq \cdots \geq \lambda_N \geq 0 \tag{5}$$

The subscript i refers to single eigenvalues which are sorted in descending order. The natural sorting of the modes according to their energy may sometimes hide less energetic modes among strong stochastic fluctuations. Another ranking is presented in the work of Sieber et al. [18], where the modes are sorted according to the spectral coherence of mode pairs. This ranking is used later to highlight periodic modes in the SPOD spectrum. The spatial modes are finally obtained from a projection of the snapshots onto the temporal coefficients

$$\Phi_i(\mathbf{x}) = \frac{1}{N\lambda_i}\sum_{j=1}^{N} a_i(t_j)U'(\mathbf{x}, t_j) \tag{6}$$

4 Results

In this section, the results of this study are presented starting with the flow field features of the two different basic centerbody designs utilized within the actuator designs. Thereafter, the sensor arrangement is discussed before evaluating the performances of different actuator concepts. This section ends with a proof of concept by measurements of the lock-in behavior.

4.1 Mean Flow Fields and Coherent Structures. Cylindrical centerbodies with a flat tip were typically used in foregoing studies [15,16] to achieve stable flames. But since this design also effects a wake, it may influence the occurrence of hydrodynamically self-excited modes (coherent structures), as the PVC, in an adverse way. To minimize the centerbody wake, a different design with a shaped tip is introduced. In the following, these two different centerbodies are compared concerning their impact on flow field and coherent structures.

Figure 5 shows the mean velocity fields for the two centerbody designs. The cylindrical centerbody with a flat tip is presented on the right-hand side, and the shaped tip centerbody on the left-hand side. The centerbody tip ends $0.2D$ upstream of the outlet. To generate symmetric fields, the left half was mirrored along the jet center axis to account for small asymmetries introduced by a slight misalignment of the PIV laser sheet. Bold lines indicate axial velocity equal to zero. The streamlines indicate a large inner recirculation zone (IRZ) that exists due to vortex breakdown and the outer recirculation zone (ORZ). This ORZ is generated due to the sudden area expansion between the mixing tube and the combustion chamber. A comparison of the IRZ shape between the two center body concepts leads to the observation that the shaped centerbody (left) generates a considerably broader IRZ and larger jet opening angle. Another fundamental difference appears in the flow region shortly downstream of the centerbody. As indicated by the bold contour line, the sharp-edged centerbody creates a region of reversed flow which leads to a constriction of the flow in the center of the jet (compare streamlines near $\{x/D, y/D\} = \{0, 0.2\}$). Consequently, the jet angle is reduced, whereas the ORZ is prolonged so that the region of increased fluctuations is expanded further downstream compared to the shaped centerbody. The shaped tip seems to eliminate such a wake and its consequences.

Considering the coherent structures extracted by SPOD (Fig. 6), other differences between the basic configurations arise. In both configurations, dominant PVC modes (no. 1) and their corresponding higher harmonics (nos. 2 and 3) are present. However, for the cylindrical centerbody, the Strouhal number, St, of the PVC mode is approximately 0.39 in contrast to the shaped tip

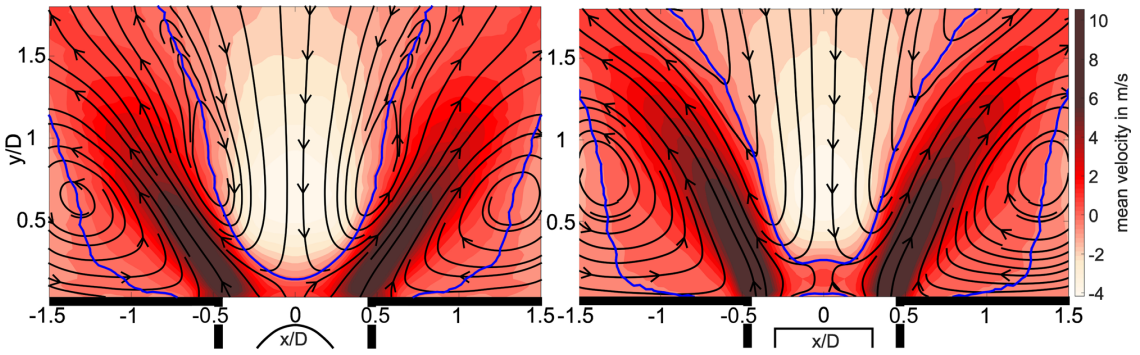

Fig. 5 Contours of the mean axial velocity component of shaped (left) and cylindrical (right) centerbody, Re = 16,000. Streamlines are derived from the mean axial and transverse velocity component. The bold lines indicate zero axial velocity.

with approximately 0.43. The spectral coherence, indicated by the size and shading of the dots in the SPOD spectrum, shows that the PVC mode and its higher harmonics are more distinct for the shaped centerbody. This implies that the PVC dynamics of the shaped centerbody are more periodic and less noisy compared to the cylindrical centerbody. Moreover, the overall energy content of the modes (nos. 1–3) is noticeably smaller in case of the cylindrical centerbody with $K_{cc,i} = \{25.18,\ 1.82,\ 0.38\}\%$ compared to $K_{sc,i} = \{32.65,\ 3.96,\ 0.77\}\%$. A reason might be additional dynamics in the wake of the cylindrical centerbody that influence the dynamics of the PVC. Most interestingly, the sharp-edged centerbody features a so-called PVC-II structure (no. 4) which is discussed in detail in Refs. [19] and [25]. For the shaped centerbody, the SPOD spectrum shows a mode (no. 4) at the same frequency as the PVC but with opposite symmetries. This mode possibly indicates small imperfection of the PVC motion which can be neglected due to its comparably small energy content.

4.2 Sensor Arrangements. The accuracy of the utilized pressure sensor arrangements is quantified with a *phase error variance*. This error corresponds to the variance of the phase difference between the SPOD coefficients a_i and the Fourier coefficients of the pressure signal $\hat{p}_1$. In the foregoing study [14], the phase of the actuation signal turned out to be the most influential parameter in terms of closed-loop control. Therefore, the applied sensor should detect the phase of the PVC mode with high accuracy.

The bar plot in Fig. 7 (right) compares the phase error variance for all actuators for three different Reynolds numbers. The error is always below 7% which appears acceptable. Related to the distance of the sensors to the mixing tube outlet (compare Fig. 3), the bar plot indicates a certain trend. The sensors closest to the outlet (R1 and A1) show the highest error, which might be attributed to disturbances coming from the centerbody wake or from fluctuations of the breakdown bubble. It is surprising that the lowest error is achieved in the mixing tube far upstream of the inlet in a region where the PVC amplitude was expected to be very low. This indicates a strong upstream influence of the PVC. The variation in the Reynolds number shows another trend. For the sensors close to the mixing tube outlet (R1–R3 and A1–A3), the error increases with higher Reynolds numbers. A reason for this trend can be stronger stochastic fluctuations due to stronger turbulence at high Reynolds numbers. The generally small error values suggest that all sensors are suitable to work within a future closed-loop system. In addition, these results provide a certain flexibility in choosing a sensor position in future experiments with combustion. Accordingly, expected influences of the flame dynamics on the pressure signals can be minimized.

Figure 7 (left) shows the amplitude of the PVC as detected from the pressure measurements. The depicted amplitude is calculated by $A_p = \mathrm{RMS}(\hat{p}_1) \cdot \sqrt{2}$. As to be expected, the amplitude grows with increasing Reynolds number. In general, the amplitudes of the sensors mounted into the mixing tube (A1–A6) reach values two times higher than the sensors at the front plate (R1–R6). For both, at the front plate and in the mixing tube, the amplitude decreases with larger distance to the mixing tube outlet. This behavior applies to all sensor arrays except the sensor array A1. Therefore, the sensor arrays at R3 or A3 will be used as a compromise between phase error and pressure amplitude in the future.

For the remainder of this study, we use the signals of sensors R1 for the following reasons. First, it is located far away from the actuator. This avoids that actuators with radially directed jets directly hit the sensors which could cause additional errors. Second, as shown in Fig. 7 by the bar plot on the left, this sensor provides the highest PVC amplitude as reconstructed from the Fourier coefficient. The high amplitude in combination with an acceptable phase error should capture the PVC dynamics at forced conditions in this study very well. For future experiments, the sensor arrangement R3 should be considered as it represents the best trade-off between phase error and amplitude.

4.3 Actuator Performance. In the following part, results from hot-wire measurements at the actuator outlet are presented and evaluated concerning actuator performance. Figure 8 shows exemplary the results of the hot-wire measurements for actuator VII in terms of momentum coefficient C_μ over input voltage (left) and maximal C_μ for all actuators (right). The momentum coefficient is defined as

$$C_\mu = G u_{\mathrm{RMS}}^2 / (U_0^2 A_h) \tag{7}$$

with the outlet area of the actuator G, the hydraulic cross section area A_h, and the RMS velocity at the actuator outlet u_{RMS} [26]. Increasing the input voltage leads to a nearly linear growth of C_μ (left). For this actuator design, C_μ reaches the highest value in this study of 0.32. This value suggests that the momentum induced by the actuator reaches the same order of magnitude as the mean flow, which seems sufficient to alter the PVC.

To decide which actuator designs perform suitably to control the PVC dynamics, an appropriate comparison needs to be carried out. One of the decisive parameters to achieve a sufficient amount of control authority is the generated actuation momentum. The plot on the right-hand side of Fig. 8 compares the maximum

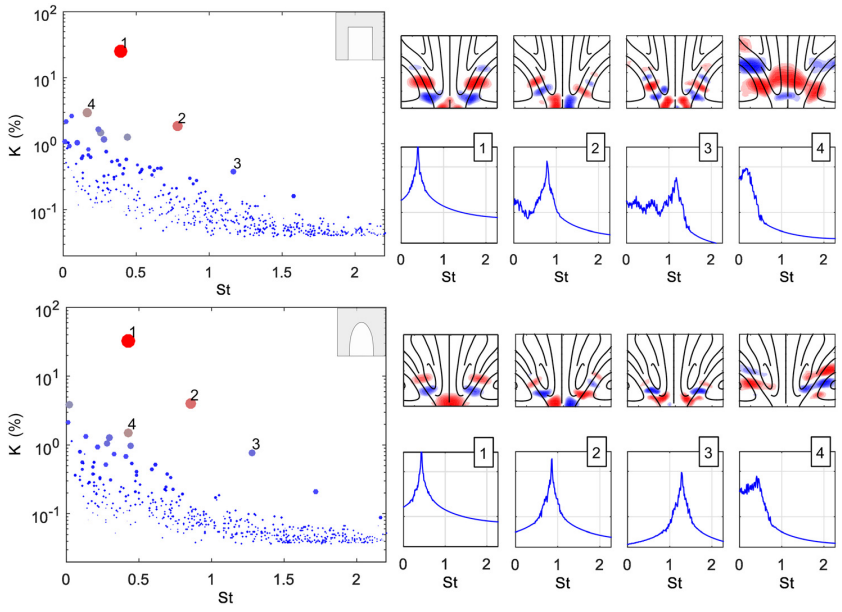

Fig. 6 SPOD results for shaped centerbody (lower row) and cylindrical centerbody (upper row). Each decomposition is represented by an SPOD spectrum (left) where a dot indicates a mode pair that is placed according to its energy and frequency. The size and shading of the dot indicate the spectral coherence of a mode pair. On the right side, the spatial structure Φ (upper row) and the power density spectrum of the coefficient *a* (lower row) are given for selected modes. The spatial mode is indicated by crosswise velocity plus streamlines of the mean flow.

momentum coefficient for all actuators. Except for the actuators VI and VII, the maximal values max(C_μ) are up to five magnitudes lower than the mean flow momentum. The significant momentum differences obviously arise from the small channel diameters (1–2 mm) and related diameter jumps resulting in much higher damping of the oscillating air. Also, tapered channels (actuators III, IV, and V) seem to cause damping which is noticeably smaller compared to the actuators I1, I2, II3, and II6. Unfortunately, once the main flow is turned on, the actuation with single tubes (I1 and I2) and lances (II3 and II6) do not show considerable effects on the swirl flow. Therefore, only the concepts III–VII are considered in the following open-loop investigation.

4.4 Lock-In Experiments. As shown in Sec. 4.3, the actuator VII achieves the highest momentum considering only the vicinity of the actuator (i.e., without main flow). To assess the ability of this actuator to control the PVC, lock-in experiments are conducted. Therefore, the actuation is set to the same mode number $m = 1$ and direction of rotation (clockwise) as the PVC but at a frequency that is slightly different than the natural PVC frequency. By increasing the actuation amplitude, lock-in is achieved once the PVC dynamics follow the excitation. Lock-in can be assessed from the spectra of the pressure signals or from the phase difference between the actuation and the natural mode (see, e.g., Ref. [27]).

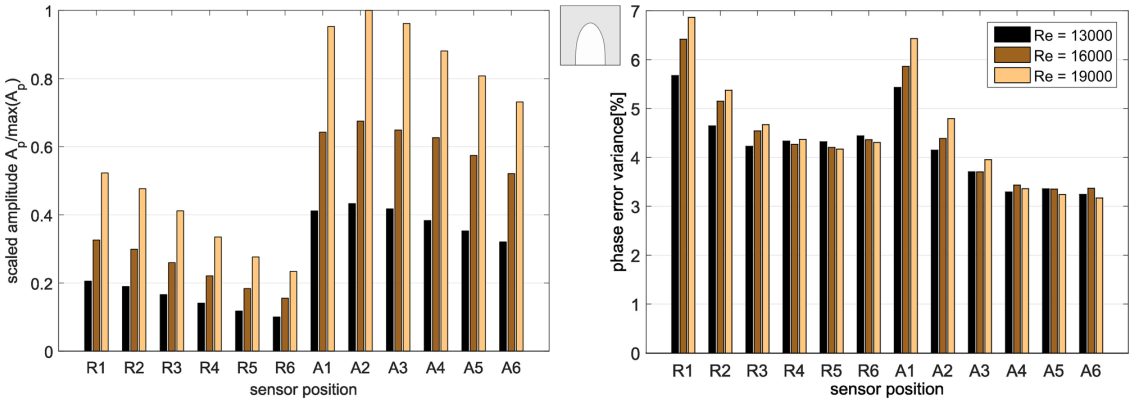

Fig. 7 Amplitudes A_p of the pressure coefficients $\hat{p}_1$ scaled with the maximum amplitude (left) and phase error variance between a_i and $\hat{p}_1$ (right) for all considered sensor positions

Figures 9 and 10 show the power spectral density spectra of the pressure signals measured during two lock-in experiments. The spectra are decomposed into the axisymmetric, the first azimuthal, and the second azimuthal modes for increasing forcing amplitudes (compare Eq. (1)). They provide a good indication of the PVC and its first harmonic to the applied forcing.

Figure 9 shows a case with $\mathrm{Re} = 16{,}000$ and a forcing frequency difference of $\Delta f = 18.5\%$. This corresponds to a forcing frequency of $f_f = 112$ Hz relative to the natural PVC frequency of $f_n = 94.5$ Hz. At the lowest forcing amplitude ($A_f = 0.25$ V), a sharp peak starts to grow at 112 Hz which indicates the actuation. It appears only in the $m = 1$ spectrum which proves that the actuator impacts only the intended mode. For slightly higher forcing ($A_f = \{0.25, 0.5, 0.75\}$ V), the natural frequency peak is marginally shifted below the natural frequency. That is not the case in Ref. [17], where f_n remains constant. Beside this, a minor peak with a frequency of approximately 130 Hz appears for low to medium forcing amplitudes ($A_f = \{0.5, 0.75, 1\}$ V). Increasing forcing amplitude damps and broadens this peak. This peak represents an interaction peak with its frequency $f_i = f_f + (f_f - f_n)$ which occurs due to the interaction between forcing and natural mode. Upon further increasing the forcing amplitude to $A_f > 0.75$ V, the frequency of the PVC is shifted to that of the forcing. This behavior is called *frequency pulling* [27]. In this case, the frequency pulling is weak because of the high Δf. Therefore, a natural and an actuated mode coexist even at highest actuation amplitudes. At the same time, the amplitude of the PVC decreases and the peak broadens. Accordingly, frequency locking does not occur although the natural mode is considerably damped. Considering the higher harmonic mode ($m = 2$), it can be seen that the natural peak is clearly damped with increasing forcing due to the decreased and broadened PVC. For high forcing amplitudes ($A_f > 1.25$ V), no natural peak can be seen beside the forced one. Furthermore, with higher forcing amplitude, a second harmonic of the forcing grows in the $m = 2$ spectrum indicating first nonlinearities. A small peak of this second harmonic is already seen for the lowest forcing amplitude as well. If the forcing amplitude is increased, a peak of the acoustic mode ($m = 0$) grows at f_f as well but remains at low values. This peak cannot be seen on the plots because it is overlying with the forced PVC mode. The reason for this peak can be vibrations of the test rig due to the loudspeaker forcing or a slight imperfection of the actuator calibration. Additionally, acoustic broadband noise occurs for frequencies above 180 Hz caused by the flow.

In Fig. 10, the actuation frequency is selected close to the natural frequency at $\Delta f = 8.7\%$. Additionally, the Reynolds number is higher with $\mathrm{Re} = 19{,}000$ which leads to a natural frequency of $f_n = 115$ Hz. This case is chosen since the process of frequency pulling is shown here distinctly. Lock-in occurs for $\mathrm{Re} = 16{,}000$ at lower Δf as well, but the corresponding spectra do not depict the frequency pulling as good as the chosen case. As seen in the $m = 1$ spectrum, the PVC frequency shifts marginally below f_n comparable to the foregoing case for low actuation amplitudes ($A_f = \{0.25, 0.5, 0.75\}$ V). Frequency pulling occurs for medium forcing ($A_f > 0.75$ V), resulting in frequency lock-in for high actuation amplitudes ($A_f \geq 1.25$ V). Furthermore, an interaction peak, as described for the case before, is present as well. The other modes ($m = \{0, 2\}$) behave in the same manner as in the plot shown before. The two cases presented here are just selected examples depicting two different phenomena, frequency lock-in and coexistence of natural and actuated modes. In order to survey the different actuator designs, the lock-in behavior for the different designs is compared in the following discussion.

Finally, the performances of the actuators with momentum coefficients above 10^{-4} without flow (Fig. 8) are compared regarding their ability to control the PVC dynamics. The Reynolds number is set to $\mathrm{Re} = 16{,}000$, $\Delta f = 8\%$, and the forcing amplitude is ranging from 0 to 2 V. Figure 11 demonstrates the influence of forcing from different actuators on the amplitude of (natural) PVC modes (left) as well as the progression of actuated mode amplitudes (right). Obviously, the forcing of actuators with small outlet holes and tapered inner channels (III, IV, and V) does not affect the natural mode remarkably, since the amplitudes remain constant on average. In contrast, the actuators VI and VII damp the natural mode by around 1.5 magnitudes already with a low actuation input amplitude of 0.75 V. The flat tip actuator III shows much lower PVC amplitudes in general, which might be due to the weaker PVC (see Fig. 6) or due to lower pressure fluctuations caused by the changed geometry.

Regarding the actuated mode, the concepts VI and VII show a considerable increase at the actuation frequency up to 0.75 V and a subsequent saturation. The concepts with axial actuation direction (III and IV) cause an actuated mode with small amplitude value saturating at 0.5 V. For actuator IV, a small amplitude increase is detectable on average. Altogether, the concepts III, IV, and V generate actuated mode amplitudes which are more than one magnitude smaller than those of designs VI and VII.

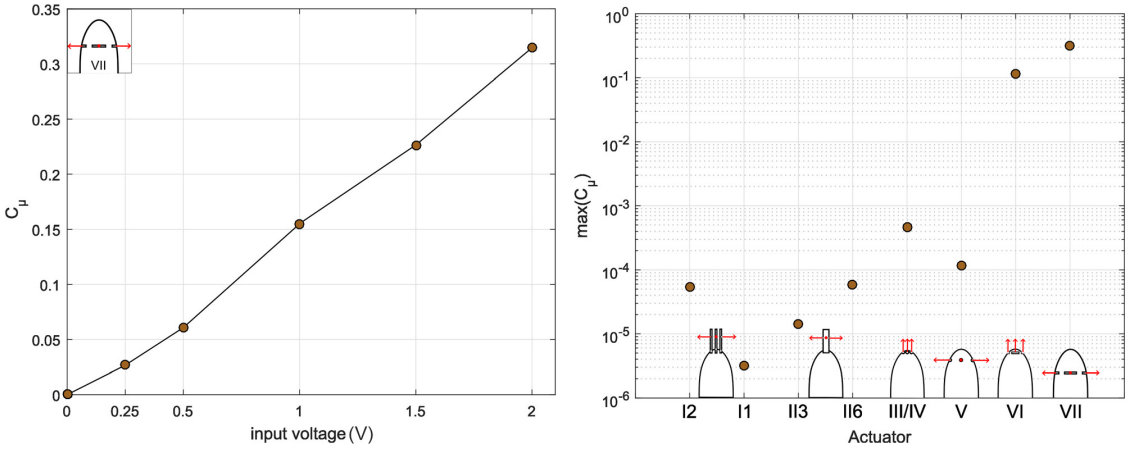

Fig. 8 C_μ ($\mathrm{Re} = 16{,}000$) for actuator VII (left) and maximum C_μ for different actuator concepts (right). The C_μ estimated for the actuator IV is also valid for actuator III, indicated by the label "III/IV" on the left, since the only difference is the outer geometry which does not influence these measurements without flow.

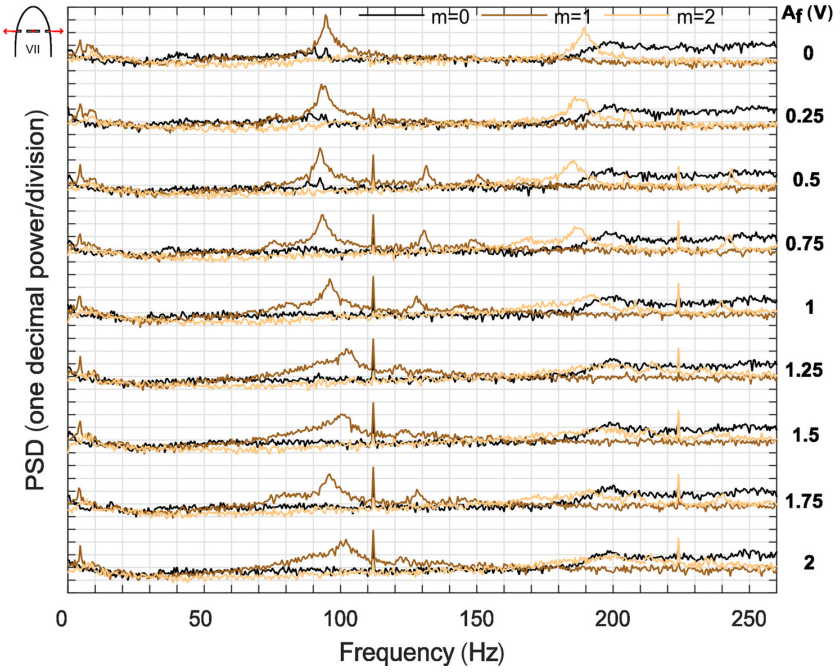

Fig. 9 Spectra of spatial Fourier modes ($m = \{0, 1, 2\}$) for different actuation amplitudes using the actuator design indicated by the small pictograph in the top-left corner. The spectra are deduced from the pressure sensors located at the combustor front plate. Forcing frequency $f_f = 112$ Hz, which is at $\Delta f = 18.5\%$ relative to the natural PVC frequency of $f_n = 94.5$ Hz at Re = 16,000.

Considering the lock-in behavior in general, it can be stated that the concepts VI and VII together with the rest of the actuation unit (amplifier, loudspeakers, pots, and actuation channels) provide a proof of concept of the entire actuation setup.

5 Conclusion

This study presents a loudspeaker-based zero-net-mass-flux actuator integrated into a swirl-stabilized combustor. The aim of

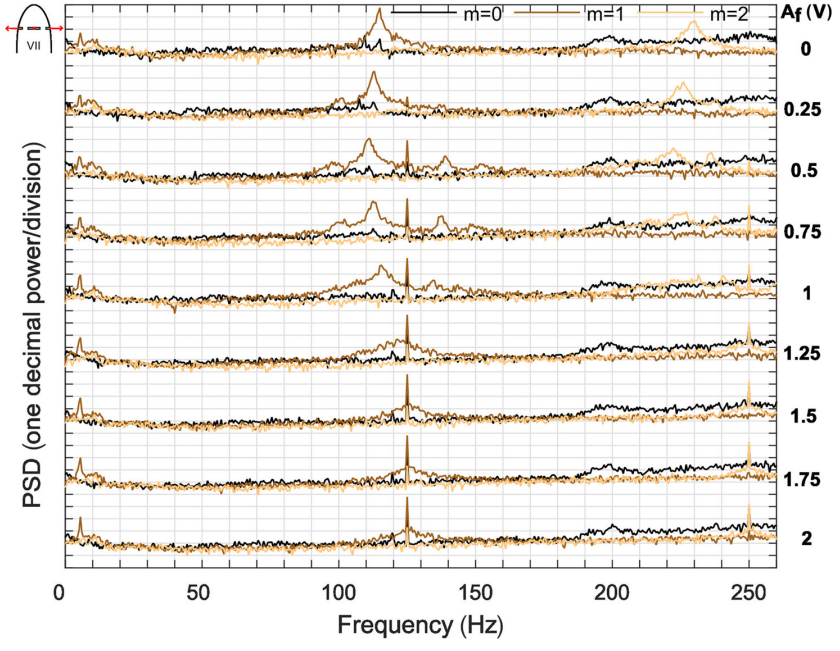

Fig. 10 Spectra of spatial Fourier modes ($m = \{0, 1, 2\}$) for different actuation amplitudes (compare Fig. 9): $f_f = 125$ Hz, $f_n = 115$ Hz, $\Delta f = 8.7\%$, and Re = 19,000

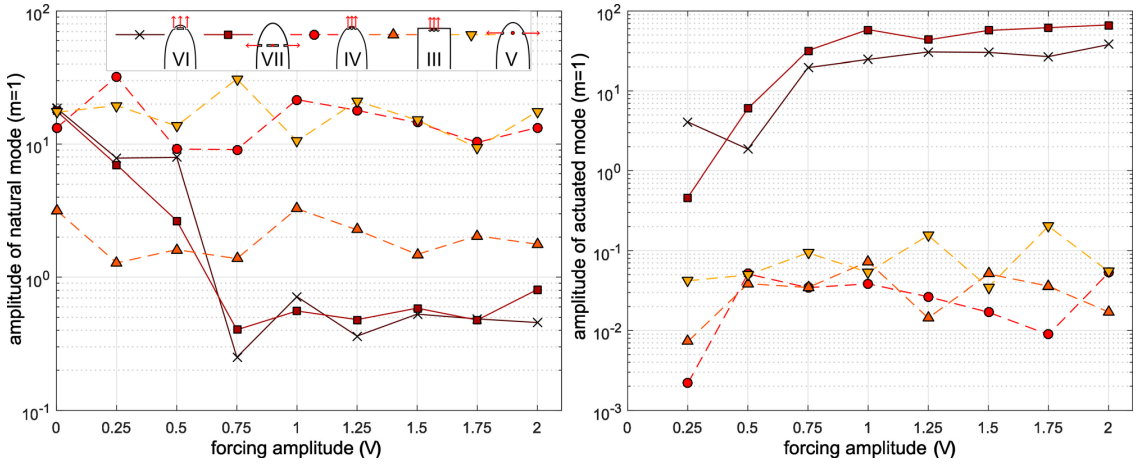

Fig. 11 Amplitude of the natural PVC mode ($m = 1$; shaped tip: $f_n = 94.5$ Hz, flat tip: $f_n = 88$ Hz) taken from power spectral density spectra over forcing amplitude (left), and amplitude of the actuated mode ($m = 1$; shaped tip: $f_f = 102$ Hz, flat tip: $f_f = 95$ Hz) depending on the forcing strength (right), Re = 16,000, $\Delta f = 8\%$, compare Figs. 9 and 10

the actuator is to control the dynamics of the PVC in a swirl-stabilized combustor. Such an actuator integrated into a closed-loop control system is necessary to study the influence of the PVC on flame dynamics, thermoacoustic instabilities, and pollutant emissions. Before a reliable closed-loop control can be implemented, a suitable actuator and a sensor design need to be developed, which is done in this study.

The actuators are integrated into a centerbody in the mixing section of the burner. In this way, the PVC can be actuated close to the region of highest sensitivity. The passive effect of two basic centerbody designs on the flow field is investigated by using time-resolved PIV measurements. These measurements in connection with dynamic pressure measurements allow for validating different sensor arrangements concerning the accuracy of reliable PVC detection. To evaluate the performance of the different actuators, hot-wire measurements at the actuator outlet are performed for different actuation amplitudes without main flow. A proof of concept of two actuator designs is shown by lock-in investigations based on pressure measurements.

The influence of two different basic centerbody shapes is investigated first. It is shown that a streamlined centerbody provides more distinct and stronger PVC dynamics. To measure the PVC phase and amplitude in real time, differential pressure sensors are embedded circumferentially in the mixing section and the combustor chamber front plate. These sensor arrangements provide a signal which matches the phase of the PVC gained from the PIV data with an acceptable error of less than 7%. As shown by Kuhn et al. [14], the phase is the most important property which needs to be detected accurately to achieve an efficient closed-loop control. The measured momentum coefficients for different actuator concepts in connection with open-loop tests (dynamic pressure measurements with flow) lead to the following design description for an effective actuator design. Actuation channels should have constant diameter D_c and a rectangular outlet ($\approx 1 \times D_c$ mm^2 slit). Such a design allows for low damping of the fluctuations induced by the loudspeakers and provides actuation over a broad azimuthal extend, which seem to be necessary for the present flow configurations.

Future investigations need to clarify the effects of the suitable actuators on the flow field. PIV measurements of the actuated flow will clarify whether the current actuator acts on the PVC only without strongly affecting the mean flow field. This study shows a certain flexibility in the sensor arrangement to detect the PVC reliably. Accordingly, different arrangements can be considered for future experiments at reacting conditions to cope especially with high temperatures. The presented lock-in results represent a huge progress within the development of an effectively performing actuator and sensor system integrated into a swirl-stabilized burner. These results serve as the basis for the development of a closed-loop system.

Acknowledgment

We would like to thank Andy Göhrs and Robert Bahnweg for their technical support and Alexander Jaeschke for supporting the experimental procedure.

Funding Data

- Deutsche Forschungsgemeinschaft (Grant No. OB 402/4-3).
- Technische Universität Berlin (Anschubfinanzierung).

Nomenclature

a = SPOD coefficients
A_f = forcing amplitude
C_μ = momentum coefficient of actuators
D = nozzle diameter
D_c = channel diameter
D_h = hydraulic nozzle diameter
f_f, f_n = forcing frequency, natural frequency
G = diameter or width of actuator outlets
K = turbulent kinetic energy
m = azimuthal mode number
N = number of snapshots
N_f = SPOD filter size
PIV = particle image velocimetry
PVC = precessing vortex core
R = correlation matrix
Re = Reynolds number
S = filter correlation matrix
SPOD = spectral proper orthogonal decomposition
St = Strouhal number
Sw = swirl number
(U, V) = axial and radial velocity component
U_0 = bulk velocity
Δf = normalized frequency difference between f_f and natural f_n
λ = SPOD mode energy
Φ = spatial mode

References

[1] Syred, N., 2006, "A Review of Oscillation Mechanisms and the Role of the Precessing Vortex Core (PVC) in Swirl Combustion Systems," Prog. Energy Combust. Sci., **32**(2), pp. 93–161.

[2] Petz, C., Hege, H.-C., Oberleithner, K., Sieber, M., Nayeri, C. N., Paschereit, C. O., Wygnanski, I., and Noack, B. R., 2011, "Global Modes in a Swirling Jet Undergoing Vortex Breakdown," Phys. Fluids, **23**(9), p. 091102.

[3] Gallaire, F., Ruith, M., Meiburg, E., Chomaz, J.-M., and Huerre, P., 2006, "Spiral Vortex Breakdown as a Global Mode," J. Fluid Mech., **549**, pp. 71–80.

[4] Oberleithner, K., Sieber, M., Nayeri, C. N., Paschereit, C. O., Petz, C., Hege, H.-C., Noack, B. R., and Wygnanski, I., 2011, "Three-Dimensional Coherent Structures in a Swirling Jet Undergoing Vortex Breakdown: Stability Analysis and Empirical Mode Construction," J. Fluid Mech., **679**, pp. 383–414.

[5] Qadri, U. A., Mistry, D., and Juniper, M. P., 2013, "Structural Sensitivity of Spiral Vortex Breakdown," J. Fluid Mech., **720**, pp. 558–581.

[6] Tammisola, O., and Juniper, M., 2016, "Coherent Structures in a Swirl Injector at $Re = 4800$ by Nonlinear Simulations and Linear Global Modes," J. Fluid Mech., **792**, pp. 620–657.

[7] Rukes, L., Paschereit, C. O., and Oberleithner, K., 2016, "An Assessment of Turbulence Models for Linear Hydrodynamic Stability Analysis of Strongly Swirling Jets," Eur. J. Mech.: B, **59**, pp. 205–218.

[8] Oberleithner, K., Stöhr, M., Im, S. H., Arndt, C. M., and Steinberg, A. M., 2015, "Formation and Flame-Induced Suppression of the Precessing Vortex Core in a Swirl Combustor: Experiments and Linear Stability Analysis," Combust. Flame, **162**(8), pp. 3100–3114.

[9] Moeck, J. P., Bourgouin, J.-F., Durox, D., Schuller, T., and Candel, S., 2012, "Nonlinear Interaction Between a Precessing Vortex Core and Acoustic Oscillations in a Turbulent Swirling Flame," Combust. Flame, **159**(8), pp. 2650–2668.

[10] Terhaar, S., Ćosić, B., Paschereit, C., and Oberleithner, K., 2016, "Suppression and Excitation of the Precessing Vortex Core by Acoustic Velocity Fluctuations: An Experimental and Analytical Study," Combust. Flame, **172**, pp. 234–251.

[11] Ghani, A., Poinsot, T., Gicquel, L., and Müller, J.-D., 2016, "LES Study of Transverse Acoustic Instabilities in a Swirled Kerosene/Air Combustion Chamber," Flow, Turbul. Combust., **96**(1), pp. 207–226.

[12] Stöhr, M., Arndt, C., and Meier, W., 2015, "Transient Effects of Fuel–Air Mixing in a Partially-Premixed Turbulent Swirl Flame," Proc. Combust. Inst., **35**(3), pp. 3327–3335.

[13] Terhaar, S., Krüger, O., and Paschereit, C. O., 2015, "Flow Field and Flame Dynamics of Swirling Methane and Hydrogen Flames at Dry and Steam-Diluted Conditions," ASME J. Eng. Gas Turbines Power, **137**(4), p. 041503.

[14] Kuhn, P., Moeck, J. P., Paschereit, C. O., and Oberleithner, K., 2016, "Control of the Precessing Vortex Core by Open and Closed-Loop Forcing in the Jet Core," ASME Paper No. GT2016-57686.

[15] Terhaar, S., Oberleithner, K., and Paschereit, C., 2015, "Key Parameters Governing the Precessing Vortex Core in Reacting Flows: An Experimental and Analytical Study," Proc. Combust. Inst., **35**(3), pp. 3347–3354.

[16] Oberleithner, K., Terhaar, S., Rukes, L., and Paschereit, C. O., 2013, "Why Nonuniform Density Suppresses the Precessing Vortex Core," ASME J. Eng. Gas Turbines Power, **135**(12), p. 121506.

[17] Li, L. K. B., and Juniper, M. P., 2013, "Lock-In and Quasiperiodicity in a Forced Hydrodynamically Self-Excited Jet," J. Fluid Mech., **726**, pp. 624–655.

[18] Sieber, M., Paschereit, C. O., and Oberleithner, K., 2016, "Spectral Proper Orthogonal Decomposition," J. Fluid Mech., **792**, pp. 798–828.

[19] Sieber, M., Paschereit, C. O., and Oberleithner, K., 2016, "Advanced Identification of Coherent Structures in Swirl-Stabilized Combustors," ASME J. Eng. Gas Turbines Power, **139**(2), p. 021503.

[20] Akilli, H., Sahin, B., and Rockwell, D., 2003, "Control of Vortex Breakdown by a Coaxial Wire," Phys. Fluids, **15**(1), pp. 123–133.

[21] Leuckel, W., 1967, "Swirl Intensities, Swirl Types and Energy Losses of Different Swirl Generating Devices," International Flame Research Foundation, Ijmuiden, The Netherlands, Technical Report No. G02/a/16.

[22] Soria, J., 1996, "An Investigation of the Near Wake of a Circular Cylinder Using a Video-Based Digital Cross-Correlation Particle Image Velocimetry Technique," Exp. Therm. Fluid Sci., **12**(2), pp. 221–233.

[23] Huang, H. T., Fiedler, H. E., and Wang, J. J., 1993, "Limitation and Improvement of PIV," Exp. Fluids, **15**(4–5), pp. 263–273.

[24] Holmes, P., Lumley, J. L., and Berkooz, G., 1998, *Turbulence, Coherent Structures, Dynamical Systems and Symmetry* (Cambridge Monographs on Mechanics), Cambridge University Press, Cambridge, UK.

[25] Terhaar, S., Reichel, T. G., Schrödinger, C., Rukes, L., Paschereit, C. O., and Oberleithner, K., 2015, "Vortex Breakdown Types and Global Modes in Swirling Combustor Flows With Axial Injection," J. Propul. Power, **31**(1), pp. 219–229.

[26] Greenblatt, D., and Wygnanski, I. J., 2000, "The Control of Flow Separation by Periodic Excitation," Prog. Aerosp. Sci., **36**(7), pp. 487–545.

[27] Li, L. K., and Juniper, M., 2013, "Phase Trapping and Slipping in a Forced Hydrodynamically Self-Excited Jet," J. Fluid Mech., **735**, p. R5.

2.2 Publication II

Excitation of the Precessing Vortex Core by Active Flow Control to Suppress Thermoacoustic Instabilities in Swirl Flames

The appropriated actuation system and sensor arrangement derived from the findings of publication I (see 2.1) are transferred from the isothermal prototype test rig into a combustion chamber test rig allowing for experiments under reacting flow conditions. With the implemented actuation system, open-loop control experiments are conducted in publication II, which is given in this section.

A lock-in investigation at the beginning of this study proves the capability of the actuation system to control a PVC in an open-loop control approach. With this actuation system, a thorough investigation is conducted which studies the PVC's impact on flame shape, flame dynamics and thermoacoustic stability of different types of flames. The actuator manages to excite a PVC in a reacting flow field which is exposed to severe self-excited thermoacoustic oscillations. This allows to study the (nonlinear) interaction between self-excited thermoacoustic modes and excited PVC modes. In case of partially premixed flames, a considerable reduction of the thermoacoustic oscillation amplitude is achieved with very small PVC actuation amplitudes.

Original Research Article

International journal of spray and combustion dynamics

International Journal of Spray and Combustion Dynamics
Volume 11: 1–23

DOI: 10.1177/1756827719856237
journals.sagepub.com/home/scd
SAGE

Excitation of the precessing vortex core by active flow control to suppress thermoacoustic instabilities in swirl flames

Finn Lückoff and Kilian Oberleithner

Abstract

In this study, we apply periodic flow excitation of the precessing vortex core at the centerbody of a swirl-stabilized combustor to investigate the impact of the precessing vortex core on flame shape, flame dynamics, and especially thermoacoustic instabilities. The current control scheme is based on results from linear stability theory that determine the precessing vortex core as a global hydrodynamic instability with its maximum receptivity to open-loop actuation located near the center of the combustor inlet. The control concept is first validated at isothermal conditions. This is of utmost importance for the proceeding studies that focus on the exclusive impact of the precessing vortex core on the combustion dynamics. Subsequently, the control is applied to reacting conditions considering lean premixed turbulent swirl flames. Considering thermoacoustically stable flames first, it is shown that the actuation locks onto the precessing vortex core when it is naturally present in the flame, which allows the precessing vortex core frequency to be controlled. Moreover, the control allows the precessing vortex core to be excited in conditions where it is naturally suppressed by the flame, which yields a very effective possibility to control the precessing vortex core amplitude. The control is then applied to thermoacoustically unstable conditions. Considering perfectly premixed flames first, it is shown that the precessing vortex core actuation has only a minor effect on the thermoacoustic oscillation amplitude. However, we observe a continuous increase of the thermoacoustic frequency with increasing precessing vortex core amplitude due to an upstream displacement of the mean flame and resulting reduction of the convective time delay. Considering partially premixed flames, the precessing vortex core actuation shows a dramatic reduction of the thermoacoustic oscillation amplitude. In consideration of the perfectly premixed cases, we suspect that this is caused by the precessing vortex core-enhanced mixing of equivalence ratio fluctuations at the flame root and due to a reduction of time delays due to mean flame displacement.

Keywords

Active flow control, precessing vortex core, thermoacoustic, swirl-stabilized combustion, flame dynamics

Date received: 20 December 2018; accepted: 10 May 2019

1. Introduction

In modern gas turbine combustors, flame stabilization is typically achieved by an aerodynamic feature of swirling flows known as vortex breakdown. This phenomenon gives rise to an inner recirculation zone (IRZ) and corresponding inner and outer shear layers. Especially, the inner shear layer is prone to a global hydrodynamic instability known as the precessing vortex core (PVC).[1] The PVC can be described as a single helical-shaped coherent structure (azimuthal wavenumber of unity) which meanders downstream along this shear layer.[2] The PVC is typically present in isothermal swirling jets. However, in reacting flows, it depends on the

Laboratory for Flow Instabilities and Dynamics, Institute of Fluid Dynamics and Technical Acoustics, Technische Universität Berlin, Berlin

Corresponding author:
Finn Lückoff, Laboratory for Flow Instabilities and Dynamics, Institute of Fluid Dynamics and Technical Acoustics, Technische Universität Berlin, Müller-Breslau-Str. 8, 10589 Berlin, Berlin.
Email: finn.lueckoff@tu-berlin.de

density stratification, and thus, the flame shape whether a PVC is present or not.[3–5]

Several studies show that the PVC considerably influences the dynamics of swirl flames.[6–8] In particular, the PVC affects vortex-flame interaction,[9] flame stabilization,[10] and flame shape transition in connection with flame lift-off.[11–14] It was shown that a PVC arises as soon as a V-shaped flame detaches from the burner outlet and transitions to a detached M-flame.[3–5,11,12] Moreover, it was further shown that the strong velocity fluctuations near the burner outlet induced by the PVC enhance the mixing of fuel and air.[15–17]

The interaction of the PVC with thermoacoustic instability is an open question and subject to several studies. Previous studies in isothermal swirling jets suggest that the PVC may modify the mean flow as such that axisymmetric shear-layer instabilities are damped,[18,19] which ultimately leads to a reduction of thermoacoustic instability.[20] Moreover, it was shown by Stöhr et al.[12] that a thermoacoustic instability may suppress the PVC in a premixed swirl-stabilized flame. Depending on the operating conditions, the strong interaction of thermoacoustic and PVC modes was observed to lead either to suppression or excitation of the helical coherent structure.[21–23] Besides this, the interaction between PVC and thermoacoustic oscillations can generate additional interaction components as well.[14,24] Moreover, it is highly plausible that the aforementioned mixing enhancement induced by the PVC has a strong effect on the attenuation of equivalence ratio fluctuations, which is a key driver for thermoacoustic instability. Furthermore, the mean flame shape plays an important role for thermoacoustic instability,[25] which can be modified by the PVC. These ideas will be further investigated in this work.

Within the analytic framework of linear stability analysis, the PVC is interpreted as the manifestation of a linear global hydrodynamic instability. Recent studies have shown that this linear framework not only predicts the PVC quantitatively correct, but allows and determines the flow regions of its origin at reacting and non-reacting conditions.[1,3–5,26–32] Moreover, the mean field stability analysis allows for the prediction of the receptivity of the global mode to open-loop actuation, which is of utmost importance for the current control approach.[28,29,33,34] This receptivity can be represented as a two-dimensional map revealing those regions of the flow where external periodic actuation has most influence on global modes.[28,32,34] This approach was applied to realistic swirling fuel injector flows that give rise to a PVC.[29,30] The authors showed that the receptivity of the helical PVC mode is highest upstream of the central recirculation zone on the jet centerline in the vicinity of the nozzle outlet and the centerbody.

These findings have motivated a new control concept that acts directly on the PVC. For this purpose, an actuator was designed that actuates a helical PVC mode in the region of highest receptivity. In a preliminary study of isothermal low-Reynolds-number flows, an actuation lance was used that allowed for excitation of mode $m = 1$ on the jet centerline upstream of the vortex breakdown bubble. Closed-loop control experiments confirmed the effectiveness of the control and reproduced the receptivity determined from linear stability theory.[35] In a next step, this control was modified so that it is applicable to highly turbulent flows of swirl-stabilized combustors at reacting conditions. For this purpose, the actuator was implemented in a centerbody upstream the flame and successfully tested at isothermal flow conditions.[36] Finally, the actuator and sensors were advanced to be heat resistant and successfully tested under reacting conditions.[37] With this newly developed technique, the idea is either to excite the PVC through open-loop control at conditions where is naturally suppressed or to damp the instability through closed-loop phasor control where it is naturally occurring. As the control applies at the most receptive region of the instability, this control works at minimal energy input.

A main disadvantage of the studies mentioned at the beginning is that the PVC, as a natural instability of the flow, cannot be controlled independently from all other flow and flame conditions. These studies, therefore, do not allow to conclude about the direct impact of the PVC on the different flame mechanisms. This leads to the motivation of this work, where flow control is applied to directly control the PVC without altering the remaining flow and flame dynamics. The control applied in this work is motivated by recent findings of linear stability theory.

The goal of the present work is to apply this control to influence and suppress thermoacoustic instabilities occurring in turbulent swirl flames. As the control exploits the natural instability of flow field, it is expected to be very effective. For this purpose, we consider thermoacoustically unstable flames where the PVC is naturally suppressed. Through open-loop actuation, we excite a PVC mode in a controlled manner and investigate its effect on thermoacoustic oscillations.

The flow and flame dynamics are measured using high-speed PIV and OH*-chemiluminescence and analyzed using temporal Fourier analysis and spectral POD.[38] Experiments are conducted at perfectly and partially premixed conditions to isolate the aforementioned effect of the PVC on mean field modifications and equivalence ratio fluctuations, respectively. The key questions that are addressed in this work are:

1. Can we excite a PVC at conditions where it is naturally suppressed?

2. Can we excite a PVC in the presence of thermoacoustic oscillations?
3. What is the influence of PVC excitation on thermoacoustic oscillations?

The paper is structured as follows: the experimental test rig is explained first, with a detailed description of the actuator unit and the applied measurement techniques. In the next section, we introduce the data analysis methodology including SPOD, Fourier analysis, and OH*-chemiluminescence-related deconvolution methods. The result section starts with the presentation of a lock-in study conducted at isothermal conditions that demonstrate the PVC actuation principal. Subsequently, we consider data from a detached M-shaped flame that naturally features a PVC and an attached V-shaped flame that features no PVC. Both flames are operated at thermoacoustically stable conditions first, and the PVC dynamics in the flame are discussed. This leads to the core of the current work dealing with the influence of the PVC actuation on the thermoacoustically unstable V-flame configuration operated at perfectly and partially premixed conditions. The identified mechanisms and control opportunities are summarized in the concluding section, and an outlook toward future investigations is given.

2. Experimental setup

In this section, the experimental setup with the integrated actuator is presented and explained. Moreover, the conducted pressure and time-resolved PIV and OH*-measurements are described including the experimental procedure and applied operating conditions.

2.1. Test rig

Figure 1 shows the test rig consisting of three sections, which are labeled in the figure with ①, ②, and ③. Section ① represents the actuation unit which is used to actuate a helical PVC mode with an azimuthal wavenumber of unity at the centerbody (Figure 2). The helical actuation is achieved by four circumferentially arranged 5 in loudspeakers (rated power of 100 W) that are driven with a phase shift of $\pi/2$ relative to one another. The loudspeakers, which are driven by a four channel power amplifier, are mounted to aluminum plenums with an orifice at the bottom to which the red tubes are connected. The air column in the red tubes is actuated by the loudspeakers at a single frequency with a constant amplitude as indicated by the red arrows. The oscillating air exits through four centerbody outlets that have a rectangular shape (9 mm wide and 1 mm high) and are placed 25 mm upstream of the mixing tube end. The parabolic shape of the centerbody provides unaffected

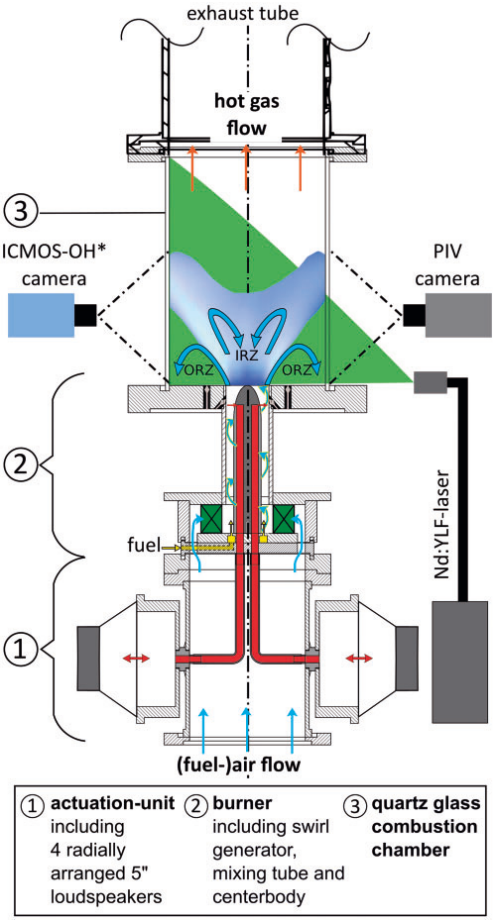

Figure 1. Test rig with measurement technique.

PVC dynamics, which is mandatory to obtain adequate experimental conditions.[36]

Section ② includes the burner, the swirl generator (green), the mixing tube with front plate, and the centerbody (in the center of the mixing tube). A detailed view of the burner setup is given in Figure 2. The yellow areas and arrows indicate the way of the fuel (natural gas) under partially premixed operating conditions. Under these operating conditions, the fuel is introduced downstream of the swirler directly into the mixing section. To achieve perfectly premixed operating conditions, the fuel is injected far upstream of the burner. The hydraulic diameter of the mixing tube $D_h = 20\,\text{mm}$ is equal to the difference between the outlet ($D = 55\,\text{mm}$) and the centerbody diameter ($D_{CB} = 35$ mm). A radial swirl generator (marked green in Figures 1 and 2) is used to generate the swirling flow. This swirler consists of movable blocks which can be adjusted relative to each other.[39] In this way, the swirl number S, defined as the ratio of the axial flux of tangential momentum to the

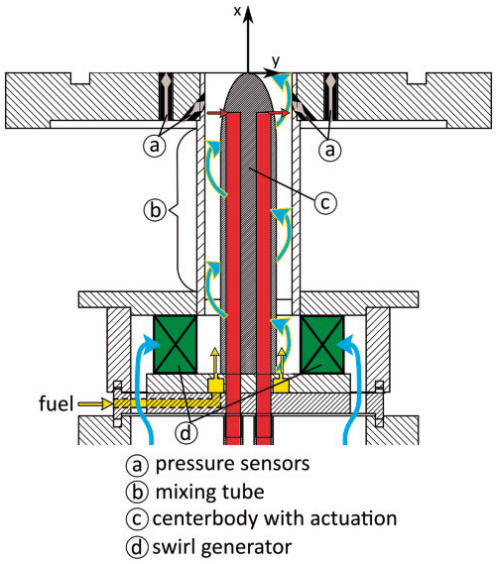

Figure 2. Detailed view of the burner.

axial flux of axial momentum, can be adjusted.[40] The swirl number was set to $S = 0.7$ in this study.

The combustion chamber (section ③ in Figure 1) consists of a cylindrical quartz glass tube with an inner diameter of 200 mm and a length of 300 mm. It provides optical access for the PIV and OH*-chemiluminescence measurements.

The origin of the coordinate system is set to the mixing tube outlet plane on the central jet axis (compare Figure 2). The x-coordinate points in axial direction, which is the main flow direction. Perpendicular to the axial coordinate, the y-coordinate describes the transverse or radial direction, respectively.

2.2. Experimental procedure

In this study, different operating conditions were investigated which are described by the equivalence ratio ϕ and the Reynolds number Re that is based on the hydraulic diameter of the mixing tube outlet and the bulk velocity at the outlet. For each operating condition, measurements were conducted with and without actuation. In case of a reacting flow, each measurement consists of time-resolved OH*-chemiluminescence and simultaneous pressure measurements.

The operating conditions are summarized in Table 1. Accordingly, a wide range of equivalence ratios were investigated. This results in different flame shapes, where only the detached flames at lean mixture naturally feature a PVC. The corresponding PVC frequencies are also listed in the table in real units and expressed as a Strouhal number based on the bulk velocity and the

Table 1. Operating conditions of reacting tests.

Reynolds number	Re	22000	26000	30000
Air mass flow [kg/h]		100	120	140
Natural PVC freq. [Hz]		118	138	163
Strouhal number	St	0.14		
Swirl number	S	0.7		
Equivalence ratio	ϕ	$0.59 \leq \phi \leq 0.74$		
Premix types	-	perfectly, partially		
Inlet temperature [K]		293		
Thermal power [kW]	P	$29 \leq P \leq 43$		

U_0 and hydraulic inlet diameter D_h. As also seen in the previous studies, the PVC frequency shows clear Strouhal number scaling with $St = 0.14$ for all cases considered.

The actuation frequencies selected in this study are close to the natural PVC frequencies to achieve optimal response by exploiting the natural instability. For the operating conditions, where the PVC is not naturally present (rich mixtures), actuation was applied at the same Strouhal numbers, assuming that the instability driving the PVC is not substantially changed. This assumption is supported by the comparison between reacting and non-reacting conditions, where the PVC frequency is quite robust showing only slight changes of less than 5%.

To quantify the actuator efficiency, it is common to relate the momentum of the actuation jets to the momentum of the main flow, yielding the momentum coefficient[41]

$$C_\mu = G u_{\mathrm{RMS}}^2 / \left(U_0^2 A_h\right) \tag{1}$$

where u_{RMS} represents the RMS velocity at the actuator outlet, which was measured with a hot-wire anemometer,[36] G the outlet area of the actuator, A_h the hydraulic cross section area, based on the hydraulic diameter of the mixing tube D_h, and U_0 the bulk velocity of the main flow. In the present work, the maximum actuation amplitude was set to $C_\mu = \{1.19, 0.83, 0.49\}\%$ for the three considered Reynolds numbers, respectively (see Table 1). These values were chosen based on preliminary open-loop experiments at isothermal conditions, and they were found to be sufficient to generate lock-in reliably without changing the mean flow considerably.

2.3. Measurement techniques

Time-resolved OH*-chemiluminescence measurements were conducted in the combustion chamber (Figure 1).

The recorded OH*-chemiluminescence images serve as a qualitative indicator for heat release rate and reveal the mean and phase-averaged flame shape. For these measurements, a high-speed CMOS camera (Photron SA 1.1) in combination with a high-speed intensifier (Lambert Instruments HiCATT 25) was used to capture line-of-sight OH*-chemiluminescence intensity snapshots. The camera was equipped with a 308 nm band pass filter to record only the OH*-chemiluminescence. The sampling rate of the camera was set to 1013 Hz to resolve the dynamics related to the PVC and occurring thermoacoustic oscillation, which are in the range of 70–180 Hz. Within a measurement time of approximately 2.1 s, 2183 snapshots with a resolution of 1024×1024 pixels were acquired.

In a separate experiment, time-resolved PIV measurements were conducted at isothermal conditions. Therefore, the same camera was used in connection with a high-speed Nd:YLF diode pumped laser (Quantronix Darwin Duo 527-100 M, 527 nm and total pulse energy of 60 mJ). A light sheet optic was used to generate an appropriated light sheet of approximately 1 mm thickness in the measurement area, which was seeded with solid TiO_2 particles. The recorded particle snapshots were evaluated with a commercial PIV software. The correlation scheme employs multigrid refinement[42] with a final window size of 16×16 pixels, window overlap of 50% in combination with spline-based image deformation,[43] and subpixel peak fitting. In the final step, the vector fields were filtered for outliers and interpolated from adjacent interrogation windows.

The pressure was measured by miniature differential pressure sensors (First Sensor HDOM010 with 1000 Pa range) which were arranged circumferentially at the outlet of the mixing tube (compare ⓐ in Figure 2). In each of the two pressure measurement planes, four sensors were mounted. In the mixing tube, the sensor orientation was shifted by 20° relative to the exit channels of the actuator to avoid interference with the actuation jets emanating from the centerbody. The pressure sensors were connected to the flow via short cannula tubes to allow for measuring pressure fluctuations as small as 0.1 Pa. All reference pressure ports of the differential sensors were connected to an ambient pressure reservoir to provide a common reference pressure. The signals were amplified with an in-house amplifier and digitized by a 16 bit A/D converter (NI 9216) at a sampling frequency of 16,384 Hz. In a previous study,[36] the accuracy of the PVC signal measured with the pressure sensors was estimated in comparison to the time coefficients of corresponding POD modes determined from time-resolved PIV measurements. The error was estimated at approximately 5% for the pressure sensor arrangement used in the present study.

3. Data analysis methodology

In the following, the reader is briefly introduced to spatial Fourier decomposition applied to the pressure signal as well as the post-processing of the PIV and OH*-chemiluminescence snapshots.

3.1. Spatial Fourier decomposition of the pressure signals

The pressure signals are used to characterize the amplitude and frequency of the PVC in the combustion chamber. The signals recorded by the four circumferentially arranged pressure sensors are decomposed into Fourier modes with azimuthal wavenumbers. Accordingly, the signal of the mth azimuthal mode is given as

$$\hat{p}_m(t) = \sum_{k=1}^{4} p_k(t) \exp\left(i 2\pi m \frac{k}{4}\right) \tag{2}$$

where p_k is the pressure signal of the kth sensor and m the azimuthal wavenumber. With four circumferentially arranged sensors, azimuthal modes with wavenumbers $m = \{0, 1, 2\}$ can be detected. The Fourier coefficient $\hat{p}_m$ is complex and a function of time, where $m = 1$ describes the PVC dynamics, and the instantaneous amplitude and phase of the PVC correspond to the modulus and argument of $\hat{p}_1$, respectively.

3.2. Spectral proper orthogonal decomposition of time-resolved PIV snapshots

The spectral proper orthogonal decomposition (SPOD) is a recently introduced method to identify coherent structures in time-resolved flow data.[44] It is based on the classical proper orthogonal decomposition (POD),[45] but it offers a more precise selectivity of relevant modes, which provide benefits in complex turbulent flows like the combustor flow investigated here.[46] In the following, only a very brief description of the SPOD approach is given. A more detailed derivation can be found in Sieber et al.[44] The procedure is exemplified for the crosswise velocity V but holds similar for the axial velocity U. The SPOD provides a modal decomposition of the fluctuating part of the velocity V' that reads as follows

$$V(\mathbf{x}, t) = \bar{V}(\mathbf{x}) + V'(\mathbf{x}, t) = \bar{V}(\mathbf{x}) + \sum_{i=1}^{N} a_i(t)\Phi_i(\mathbf{x}) \tag{3}$$

The fluctuating part of the velocity is separated into a sum of spatial modes Φ_i and corresponding modal coefficients a_i. In order to build this basis, the spatial

correlation among individual PIV snapshots is calculated, which results in a corresponding correlation matrix. In contrast to the classical POD, a Gaussian low-pass filter is applied to this correlation matrix, which puts a temporal constraint on the POD modes. The width of this filter is typically related to the convection time of the most dominant structure, in this case, the PVC. The temporal coefficients $a_i(t)$, describing the dynamics of the corresponding mode, are derived from the eigenvectors of the filtered correlation matrix. The spatial modes $\Phi_i(\mathbf{x})$ are finally obtained from the projection of the snapshots onto the temporal coefficients.

3.3. Decomposition of the OH*-signal

The global heat release rate fluctuation is an important quantity to characterize the flame response to actuation and flow perturbations. The global heat release rate $I(t)$ is obtained by integrating the OH*-signal $\mathrm{OH}^*(x, y, t)$ recorded by the camera over the entire flame area. Time averaging of this quantity provides an estimate of the mean global heat release rate $\bar{I}$ and its temporal fluctuation $I'(t) = I(t) - \bar{I}$.

To differentiate between the global heat release rate fluctuations induced by thermoacoustic fluctuations and by the PVC, we employ a special decomposition method. By assuming that the mean flame is axisymmetric, the thermoacoustic modes induce heat release fluctuations $\mathrm{OH}^{*\prime}(x, y, t)$ which are symmetric with respect to the centerline of the combustor. Accordingly, the heat release fluctuations integrated over the left ($y < 0$) and right ($y > 0$) half of the combustion chamber are in phase. Contrarily, the PVC as a single-helical flow structure generates heat release fluctuations which are antisymmetric with respect to the centerline of the combustor. Consequently, the corresponding heat release fluctuations integrated over the left ($y < 0$) and right ($y > 0$) half of the combustion chamber are 180° out of phase. Hence, the summation of the heat release fluctuations left ($\mathrm{OH}^{*\prime}(x, y < 0, t)$) and right ($\mathrm{OH}^{*\prime}(x, y > 0, t)$) of the combustors centerline eliminates antisymmetric fluctuations, which yields a representation of purely symmetric fluctuations. Vice versa, subtraction eliminates symmetric fluctuation, which yields a representation of purely antisymmetric fluctuations. The integration of these symmetric and antisymmetric fluctuations over the entire flame area provides measures for the global heat release fluctuations induced by symmetric and antisymmetric modes, I'_s and .

The global dynamics of the flame with respect to the PVC and thermoacoustic oscillations are investigated from a spectral analysis of the antisymmetric and symmetric global heat release rate fluctuations. Assuming that the thermoacoustic instability is nominally axisymmetric, the spectrum of the symmetric global heat release rate $I'_s(t)$ points out certain relevant frequencies. Likewise, assuming that the PVC is antisymmetric, the spectrum of the $I'_a(t)$ reveals the response in the flame with respect to the PVC mode. For practical conditions, the flame is typically not perfectly symmetric. This implies that symmetric velocity fluctuations also induce weak antisymmetric heat release rate fluctuations, and antisymmetric velocity fluctuations induce symmetric heat release rate fluctuations, as shown by Acharya et al.[47] Accordingly, traces of the symmetric mode may be found in the antisymmetric-decomposed spectrum and vice versa. The power spectral density (PSD) of the OH*-measurements presented in the results chapter is normalized with the averaged noise level to remove any offset due to different gain settings of the used intensifier.

For a more detailed description of the flame response, the local OH*-signal is decomposed in spatial Fourier modes. These spatial modes are estimated by a point-wise temporal Fourier transform of the OH*-intensity signal, which can be expressed as

$$\widehat{\mathrm{OH}^*}(x, y) = \frac{1}{T}\sum_{t=0}^{T-1} \mathrm{OH}^*(x, y, t) \exp\left(-\frac{i2\pi}{T} ft\right) \qquad (4)$$

Evaluating this equation at the frequency of thermoacoustic oscillations f_{TA} or the PVC frequency f_{PVC} allows to investigate the corresponding structure of the heat release rate fluctuations. The phase of the decomposed spatial modes is adjusted to the respective phase of the maximal global amplitude.

However, the OH*-signal recorded by the camera represents the line-of-sight-integrated values, and an appropriate deconvolution of the data to a planar representation must be conducted. For the symmetric part of the heat release rate, a classic Abel-deconvolution is applied. For the skew symmetric fluctuations induced by the PVC, a tomographic reconstruction technique developed by Moeck et al.[48] was employed. In contrast to conventional tomographic reconstruction techniques, this algorithm only requires one camera. Since the PVC is rotating at a well-defined rate, a phase-resolved sequence of projection images gained from the time-resolved OH*-chemiluminescence snapshots can be used for the tomographic reconstruction.

4. Results

At the beginning of this section, a lock-in study of the isothermal flow inside the combustion chamber is presented, which demonstrates the actuation principal on the basis of SPOD modes and corresponding time coefficients. Thereafter, two reacting cases are considered at

thermoacoustic stable conditions. Starting with a detached M-flame, we actuate the PVC at a frequency slightly lower than the natural frequency, which is considered as a lock-in test. Subsequently, open-loop actuation is applied to an attached V-flame to demonstrate the possibility to excite a PVC for such flame types. In the last and major part, the actuation system is applied to investigate the role of the PVC in a thermoacoustically unstable V-flame. By comparing experimental results from perfectly and partially premixed flames, the dominant interaction mechanisms between the PVC and thermoacoustic instabilities are isolated and discussed.

4.1. Lock-in study at isothermal conditions

The goal of lock-in studies is to demonstrate the principal of the control method. Lock-in describes the state where the dynamics of the PVC are entirely synchronized to the actuation. To reach this synchronization, the actuation amplitude must be increased to a critical value, known as the lock-in amplitude. In a preliminary investigate,[36] the lock-in behavior of the current setup was evaluated based on spectra of pressure measurements. Although these results already demonstrated the working principal of the actuator, the impact of the actuation on the mode shape could not be evaluated. For this purpose, PIV measurements were conducted at the lock-in state to ensure that the natural mode shape of the PVC is not disrupted by the actuation. This is of great importance to unambiguously isolate the impact of the PVC on the combustion properties.

Figure 3 shows the outcome of these PIV measurements. The left side depicts the most energetic SPOD mode (radial velocity component), and the right side depicts the power spectrum of the corresponding mode coefficient. These quantities describe the spatial structure and the dynamic of the PVC, respectively. For better orientation, streamlines derived from the mean flow data are superimposed on the mode shapes. They indicate the inner and outer recirculation zone that is typical for the flow field of a swirl-stabilized combustor. The first row in Figure 3 corresponds to the natural case where the actuator is inactive. The strong fluctuations of the radial velocity component at the jet axis near the inlet indicate the periodic displacement of the jet core which is characteristic for the PVC. The convective vortex pattern in the shear layer between the annular jet and the IRZ indicates the typical downstream propagating single-helical spiral of the PVC. The spectral content of this mode is relatively sharp with a clear peak at the natural Strouhal number.

Once the actuation is applied, an additional peak in the spectrum appears at the actuation frequency, at already very low amplitudes of $C_\mu = 0.05\%$ (see vertical dashed line in Figure 3). Upon increasing the amplitude, this peak becomes dominant, and the natural peak is pulled toward the actuation frequency. This is called frequency pulling and is known as a typical lock-in behavior.[49] At the highest actuation amplitude, the spectral peak has become extremely sharp at significantly higher energy than the natural peak, indicating that the PVC has entirely locked onto the external actuation.

For all actuation amplitudes, the shape of the SPOD modes remains very similar. A trend toward smaller wavelengths is noticeable for higher actuation amplitudes which is due to the fact the locked state corresponds to a higher frequency. Moreover, for the highest actuation amplitude, the mode shape reaches less downstream as in those cases with lower actuation amplitude. This is due to the fact that the strongly forced instabilities undergo nonlinear saturation further upstream compared to the natural case.[50] These effects are expected and of low significance. More importantly, the mode shapes clearly show that the actuator generates the same spatial structure as the natural PVC without causing any artifacts due to the actuation. Above this, the extremely low actuation amplitude of $C_\mu < 0.26\%$ required for lock-in indicates that the actuator is indeed working in a very receptive flow region.

The process of frequency pulling and lock-in can be further investigated by considering the phase difference $\Psi(t)$ between the decomposed pressure signal of the PVC mode ($\hat{p}_1$) and the actuation signal (see e.g. Li and Juniper[51]). Figure 4 shows this quantity as a function of time for the different actuation amplitudes. For the lowest actuation amplitude, the phase decay is nearly constant indicating that the flow does not follow the actuation at all. For higher actuation amplitudes, the phase decay becomes staggered, which means that the flow follows the actuation for the period of time where the phase difference is constant. This kind of behavior is characteristic for frequency pulling. As soon as the flow follows the actuation through the entire time, the state of lock-in is reached. This is characterized by a constant phase difference, as it is the case for the two highest actuation amplitudes.

Last, we address the change of the mean flow field due to the actuation. Figure 5 shows the contour of turbulent kinetic energy $\left(\mathrm{TKE} = \sqrt{\overline{u'^2} + \overline{v'^2}}\right)$ and superimposed mean flow streamlines for the natural and lock-in state. The blue lines indicate zero-mean axial velocity, which indicates the region of reversed flow of IRZ. In both cases, the major turbulent kinetic energy is present near the burner outlet and along the upstream region of the inner shear layer. The comparison of the two cases further shows that the overall

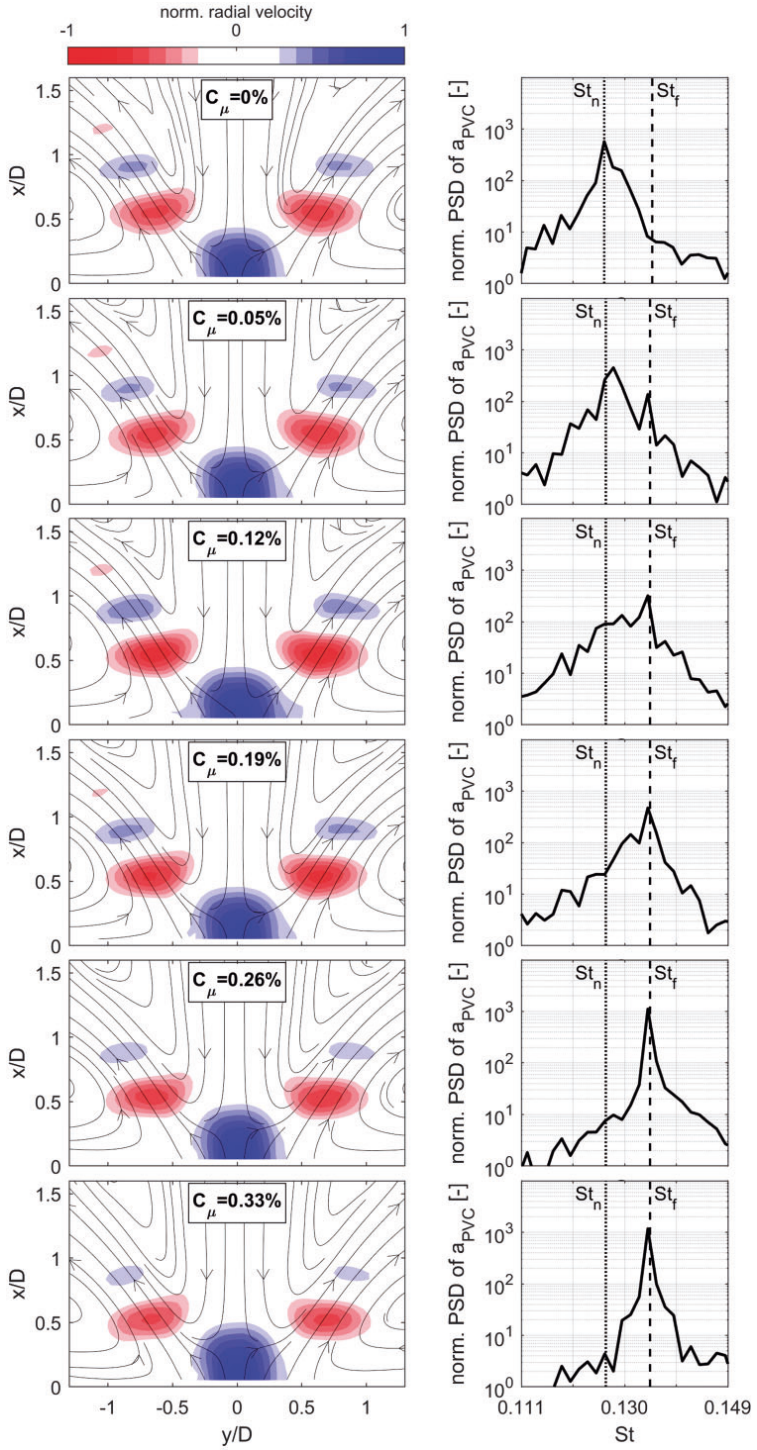

Figure 3. Lock-in study with SPOD modes Φ_{PVC} (left column) and spectra of corresponding time coefficients a_{PVC} (right column). Re = 36,000 Hz ($St_f = 0.135$) and $f_n = 180$ Hz ($St_n = 0.127$).

turbulent kinetic energy is increased due to the actuation, which is due to the strengthening of the PVC fluctuations. It is quite astonishing that the actuation at such low amplitudes causes such an immense increase of turbulent fluctuations (16.5% increase in depicted region). Considering the mean flow, a slight change of the upstream stagnation point of the IRZ is noticeable, which indicates stronger turbulent fluctuations at this location. Nonetheless, the mean flow distortion due to the actuation appears negligible for all cases considering the fact that this is the strongest actuation considered.

From these preliminary results, we can state that the actuator properly locks onto the natural PVC, and it does not cause any artifacts in the flow dynamics. Moreover, lock-in is achieved at very low actuation amplitudes of $C_\mu < 0.26\%$ at comparably high Reynolds numbers. Hence, the actuator appears to be working very efficiently in a region of high receptivity of the PVC.

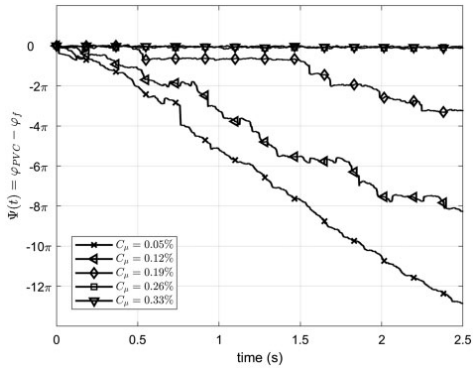

Figure 4. Phase differences $\Psi(t)$ of decomposed pressure signal $\hat{p}_1$ for different actuation amplitudes under isothermal conditions. Re = 36,000, $f_{PVC} = 189$ Hz, and $f_{nat} = 180$ Hz.

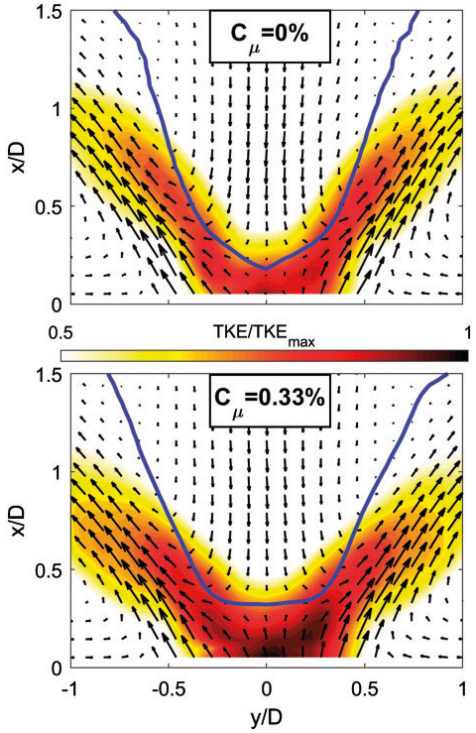

Figure 5. TKE normalized with the maximal value of both plots over the mean flow field (every second measured vector). Top plot: natural (non-actuated) case, bottom plot: actuated case in state of lock-in ($C_\mu = 0.33$) both under isothermal conditions. Re = 36,000, $f_{PVC} = 189$ Hz, and $f_{nat} = 180$ Hz.

4.2. Investigated flame shapes

In this study, two different flame shape types are investigated as depicted in Figure 6. At lean mixtures ($\phi = 0.59$), the flame is detached from the burner outlet and has a characteristic mean shape resembling the letter M, which defines its name, M-flame (left). In richer mixtures in contrast ($\phi = 0.71$), the flame is directly attached to the burner outlet and exhibits a characteristic V-shape. The letter flame therefore is referred to as V-flame in the following (see right-hand side in Figure 6).

Previous studies[3,13] pointed out that a PVC is typically present in M-flames, whereas the V-flame suppresses the PVC. The reason for this suppression is the very strong density stratification induced by the attached V-flame.[3]

The mean flame shapes in Figure 6 reveal a non-symmetric heat release rate distribution of the V-flame; however, the M-flame appears less non-symmetric. This non-symmetry plays an important role

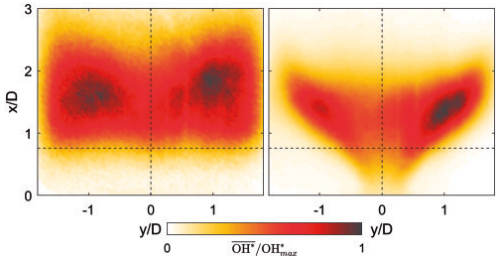

Figure 6. Time-averaged line-of-sight integrated OH*-chemiluminescence of the two basic mean flame shapes which are investigated in this study; M-flame (Re = 30,000 and $\phi = 0.59$) on the left, V-flame (Re = 30,000 and $\phi = 071$) on the right, both perfectly premixed.

in the following investigations. Possible reasons for the asymmetry can be a non-uniform cooling of the burner front plate or a not perfectly symmetric burner design.

4.3. Actuation of the PVC in the M-flame

Starting with the more simple case, we consider a detached M-flame where a PVC naturally occurs. Figure 7 shows the PVC dynamics in the M-flame measured at Reynolds number $\mathrm{Re} = 30,000$ and equivalence ratio $\phi = 0.59$ at perfectly premixed conditions. Figure 7(d) and (e) shows the deconvoluted mean flame shape at non-actuated and actuated conditions. Both resemble the typical M-shape with only minor differences in the flame shape near the wall and flame root position, with the actuated flame appearing somewhat more compact than the non-actuated one.

The pressure spectra shown in Figure 7(a) present the spectral distribution of the first helical mode ($m = 1$). The black line represents natural conditions with the PVC frequency f_{PVC} at around 163 Hz. The peak is relatively broad indicating intrinsic unsteadiness of the PVC limit cycle due to background turbulence. For the actuated flow (red line), the actuation frequency is set to 160 Hz ($St = 0.139$) with an amplitude corresponding to $C_\mu = 0.49\%$, which is above the critical lock-in amplitude. At the actuation frequency, the peak in the actuated pressure spectrum becomes more distinct compared to the natural case. The disappearance of the natural PVC peak indicates the lock-in of the reacting flow to the helical actuation.[36]

Figure 7(b) and (c) shows the spectral distribution of the symmetric and antisymmetric fluctuations $\hat{I}_s$ and $\hat{I}_a$ of the global heat release rate. For the non-actuated case, no dominant peak is visible in the spectrum of $\hat{I}_s$ that would indicate the presence of (symmetric) thermoacoustic modes. However, the spectrum of $\hat{I}_a$ displayed in Figure 7(c) shows the helical PVC mode very distinctly at the same frequency as in the pressure spectrum. When the actuation is turned on, the shape of the symmetric OH*-spectrum remains unchanged, while the antisymmetric OH*-spectrum shows a single distinct peak at the actuation frequency analog to the pressure signals (Figure 7(c)). In connection with the pressure spectrum, which is an indicator for the flow dynamics, it can be concluded that the actuation achieves lock-in of the PVC mode and corresponding heat release rate fluctuations. In the locked state, both pressure and OH*-spectra show a higher PVC amplitude compared to the natural case, which indicates a strengthening of the PVC through the actuation.

Figure 7(f) shows the spatial structure of the oscillation induced by the PVC that can be derived from a vertical slice through the tomographic reconstruction of

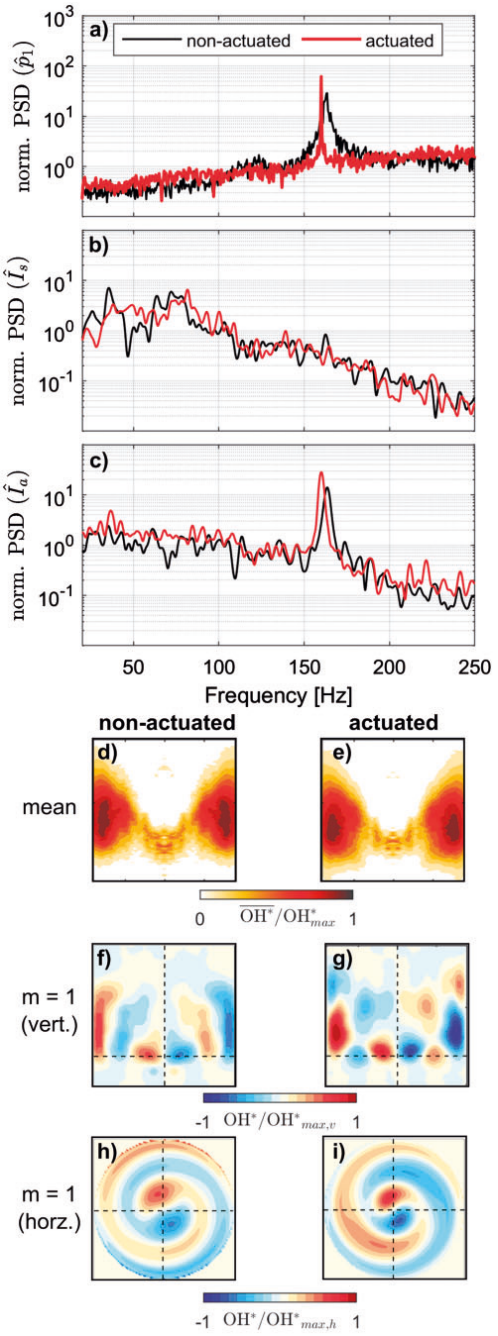

Figure 7. Actuation of M-Flame at $\mathrm{Re} = 30{,}000$ and $\phi = 0.59$, perfectly premixed: (a) spectrum of $m = 1$ pressure mode; spectrum of symmetric (b) and antisymmetric (c) global heat release rate fluctuations; deconvoluted mean OH* of non-actuated (d) and actuated (e) flame; vertical (f, g) and horizontal (h, i) view of the PVC under non-actuated and actuated conditions gained from tomographic reconstruction.

the OH*-signal.[24,48] Accordingly, the PVC acts on the flame especially around the jet axis near the flame root and in the zone of main heat release rate. The fluctuations propagate from the central jet axis, where they are initiated, to the combustor wall. Comparable conclusions can be drawn from the reconstruction at actuated conditions (Figure 7(g)), with the difference that for an actuated PVC, stronger fluctuations near the jet axis upstream and inside the main heat release rate zone appear. In both cases, the regions of strong fluctuations are elongated near the wall due to interaction with the confinement, as already reported by Moeck et al.[24] For the actuated PVC, the heat release fluctuations are stronger in this region indicating enhanced wall-flame interaction. The horizontal slices ($x/D = 0.75$, compare horizontal line in Figure 6) shown in Figure 7(h) and (i) depict a typical shape of a single helical structure, such as the PVC. Furthermore, these plots reveal that the actuated PVC leads to the same flame dynamic structure as for the natural case but the heat release is somewhat more distinct, which is in line with the more distinct pressure peak shown in Figure 7(a). This further demonstrates that the applied actuation indeed actuates a clean PVC structure without generating any additional disturbances of the flame shape.

4.4. Actuation of the PVC in the V-flame

For the V-flame configuration, the equivalence ratio is increased to $\phi = 0.71$ while all other parameters are kept the same as for the previously considered M-flame configuration.

Figure 8(d) shows the deconvoluted mean OH*-intensity illustrating the typical shape of a V-flame. In contrast to the detached M-flame, this flame is attached to the burner outlet. The mean heat release rate for the actuated V-flame (Figure 8(e)) appears more compact, with the region of maximum heat release rate being shifted upstream and inward to the flame root.

Compared to the M-flame, the V-flame does not feature a PVC naturally, which can be seen by the absence of a distinct peak in the decomposed pressure signals in Figure 8(a) for the non-actuated case (black line). The disappearance of the PVC for the V-flame is in line with the previous investigations, showing that the temperature field induced by the flame is suppressing the PVC.[3] The OH*-spectra shown in Figure 8(b) and (c) do not feature any prominent peak for the unforced flame showing no indication for either thermoacoustic instability or a PVC.

When actuation is applied, the $m = 1$ pressure spectrum depicted in Figure 8(a) shows a clear peak at the actuation frequency of 160 Hz ($St = 0.139$, $C_\mu = 0.49\%$). This peak has a similar amplitude as for the forced M-flame configuration, providing first

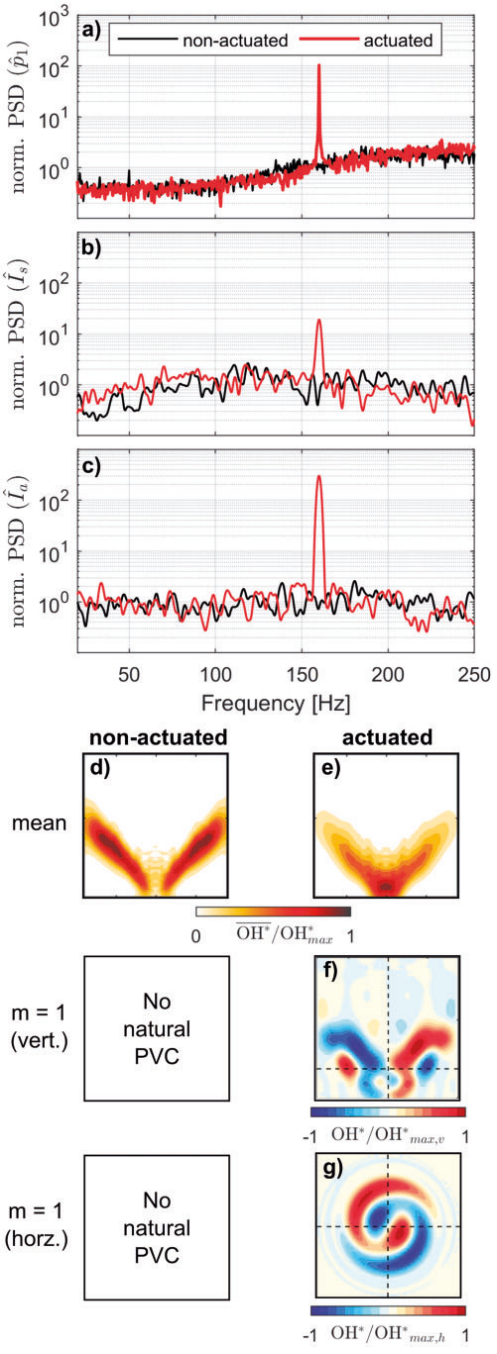

Figure 8. Actuation of V-flame at Re = 30,000 and $\phi = 0.71$, perfectly premixed: (a) spectrum of $m = 1$ pressure mode; spectrum of symmetric (b) and antisymmetric (c) global heat release rate fluctuations; deconvoluted mean OH* of non-actuated (d) and actuated (e) flame; vertical (f) and horizontal (g) view of the PVC under non-actuated and actuated conditions gained from tomographic reconstruction.

indication that the actuation is actually triggering a PVC instability.

Considering the symmetric OH*-spectrum shown in Figure 7(b), we observe a small peak at the actuation amplitude. This is surprising as it is generally expected that the antisymmetric actuation does not cause symmetric heat release rate fluctuations. This is most probably due to the fact that the V-flame is not perfectly symmetric (compare Figure 6). This is in accordance with the work by Acharya et al.,[47] who found that an axisymmetric excitation field can excite helical flame disturbances in non-axisymmetric reacting swirling flows and vice versa.

Considering the flame dynamic structures shown in Figure 7(f) and (h), no descriptive reconstructed mode can be shown for the non-actuated V-flame because it does not feature any dominant (PVC) dynamics. For the actuated case, the vertical slice through the reconstructed helical structure shows a distinct mode induced by the actuated PVC, which is present along the flame front (Figure 8(f)). The intensity appears to be considerably higher along the flame arms compared to the region of the flame root. Obviously, the fluctuations induced near the flame root seem to grow considerably in spatial extend as well as intensity when traveling downstream along the flame front. The horizontal slice shown in Figure 8(g) shows the typical helical shape of the emerging PVC in the region of the flame root.

The discussion of Figure 8(e) to (g) reveals plausible and considerable interactions between the PVC and the V-flame, which have not been observed before in such a controlled manner.[12] However, the selection of the actuation frequency and mode for the V-flame is based on the hydrodynamic instability of the M-flame, which requires some additional explanations. A previous study by Oberleithner et al.[3] revealed that the reason for the suppression of the PVC in the V-flame is not the difference in the mean flow but the difference in the density stratification. Accordingly, it has been concluded that the general hydrodynamic instability is very similar for both types of flames. Therefore, we decided to actuate the V-flame near the frequency of the natural PVC of the M-flame.

The validity of the current control scheme is further supported by the similarity of the response of the M- and V-flame to PVC actuation. The tomographic reconstruction of the helical flame fluctuations presented in Figures 7 and 8 reveals flame fluctuations that start to rise near the center jet axis, where the wavemaker of the PVC is typically found and grows along the flame front. These considerations lead to the conclusion that the actuated structures are not describing a helical response of the shear layers to the actuation but an actuated PVC.

Hence, the V-flame configuration is an appropriate case to study the direct influence of PVC on the combustion processes as it can be controlled freely from zero to large amplitudes, which is not the case for the M-flame where the PVC occurs naturally. In the following, the V-flame configuration is used to study the influence of the PVC on thermoacoustic oscillations.

4.5. Interaction of a thermoacoustic instability and the PVC in a perfectly premixed V-flame

In the literature, different interaction mechanisms between axisymmetric thermoacoustic and single-helical PVC modes are described. We address the following three mechanisms in this study:

- Frederick et al.[19] showed in their analysis that the PVC leads to a thickening of the shear layers and, hence, reduces the growth rate of the Kelvin–Helmholtz instability, which is also known as a key driver for thermoacoustic instability.[52]
- Steinberg et al.[14] associate the interaction of single helical and thermoacoustic modes with stretching and contraction of the PVC by the thermoacoustic mode. They showed that the heat release fluctuations are aligned to the interaction mode, which causes asymmetric radially detached flame patterns.
- Moeck et al.[24] concluded that the rise of an interaction mode is caused by nonlinear processes in the flame dynamics since they could not detect it in their velocity measurements under self-excited conditions.

To investigate the interaction between PVC and thermoacoustic modes, the PVC actuation is applied to a perfectly premixed flame featuring self-excited thermoacoustic oscillations at $\phi = 0.73$ and $\mathrm{Re} = 26{,}000$. The actuation frequency is set to the natural frequency of the PVC at isothermal conditions of $f_{\mathrm{PVC}} = 138$ Hz ($St = 0.14$), which is close to the PVC frequency of the M-flame at $\phi = 0.59$.

In Figure 9, the spectra of the decomposed pressure signals $\hat{p}_0$ and $\hat{p}_1$ as well as the corresponding OH*-signals $\hat{I}_s$ and $\hat{I}_a$ are compared for non-actuated and actuated conditions. The actuation amplitude is set to $C_\mu = 0.65\%$, which is the equivalent lock-in amplitude of the M-flame.

The non-actuated pressure spectrum of mode $m = 0$ shown in black in Figure 9(a) reveals a distinct peak of the dominant thermoacoustic mode at $f_{\mathrm{TA}} = 120$ Hz and minor peaks of the subharmonic and first harmonic at 60 and 240 Hz. Above this, a peak is present at 180 Hz, which represents the interaction of the fundamental and subharmonic oscillation. The corresponding spectrum of the symmetric OH*-signal in Figure 9(b) reveals the fundamental and first harmonic at the

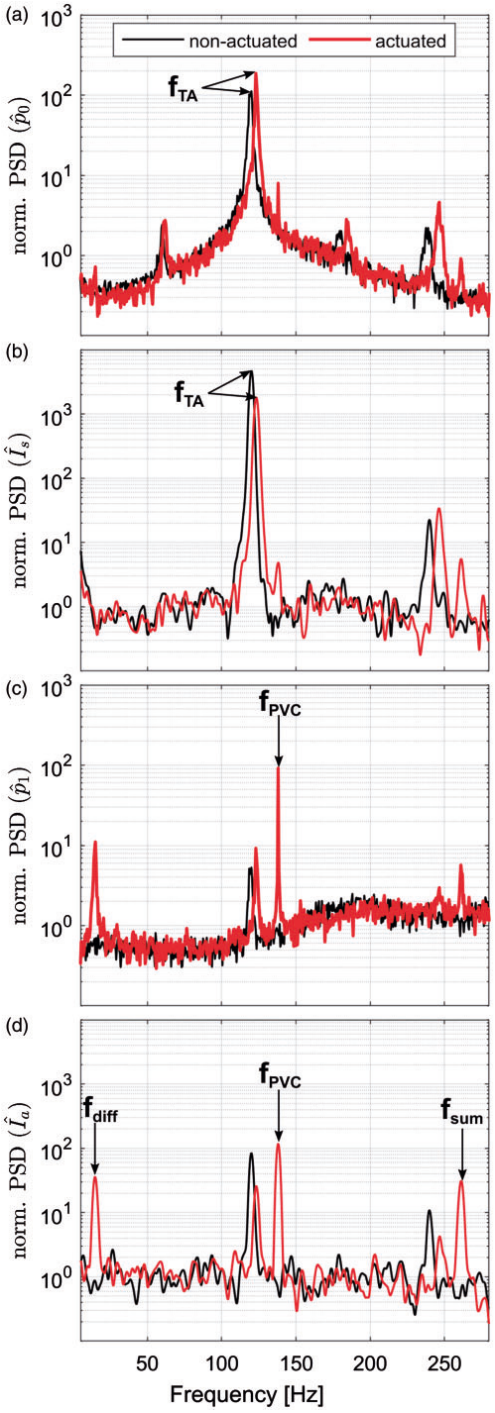

Figure 9. Effect of PVC actuation on thermoacoustic oscillations of V-flame at Re = 26,000, $\phi = 0.73$, and $C_\mu = 0.65\%$ (perfectly premixed): spectra of $m = 0$ (a) and $m = 1$ (c) pressure mode; spectra of symmetric (b) and antisymmetric (d) global heat release rate fluctuations.

same frequency as the pressure spectrum. On the contrary, the subharmonic and its interaction with the fundamental frequency are not visible in the OH*-signal. All these peaks describe the dynamics of the thermoacoustic oscillation under non-actuated conditions, whereas the subharmonic oscillation and its interaction with the fundamental are only a pressure phenomenon indicating possibly a subharmonic resonance of the shear layer.

The pressure spectrum of the helical mode in Figure 9(c) shows a small peak at the fundamental thermoacoustic frequency. This small peak is unexpected when considering axisymmetric perturbations of an axisymmetric flame. However, as discussed above, the mean flame shape of the V-flame is not perfectly axisymmetric. Therefore, the nominally axisymmetric thermoacoustic instability may indeed cause antisymmetric flame disturbances. Likewise, the antisymmetric PVC may induce symmetric (global) flame fluctuations.[47]

Compared to the pressure spectrum, the spectrum of the antisymmetric OH*-signal reveals the fundamental frequency of the thermoacoustic mode more distinctly together with the first harmonic (compare Figure 9(d)). This observation suggests that the symmetric thermoacoustic oscillations are rather affecting the dynamics of the antisymmetric flame component than the first helical pressure mode.

Considering the actuated case, both the asymmetric OH* spectrum and the $m = 1$ pressure spectrum show a clear peak at the actuation frequency (Figure 9). Hence, despite the pulsations induced by the thermoacoustic instability, the PVC actuation is effective. The spectra further show that the actuation of the PVC causes a slight shift of the thermoacoustic frequencies toward higher values. It is further noticeable that the PVC actuation causes fluctuation in the symmetric OH* spectrum, which is most probably due to the asymmetry mean flame shape.

Because of the presence of two dominant modes, PVC and thermoacoustic mode, nonlinear interactions take place between these modes. These interactions cause peaks in the spectrum at frequencies corresponding to sums or differences between the frequency of the PVC and the thermoacoustic mode. Such an interaction peak is present at $f_{\text{diff}} = f_{\text{PVC}} - f_{\text{TA}} = 15$ Hz and has been observed and analyzed in other configurations as well.[14,24] For example, Moeck et al.[24] also found interaction peaks at a frequency f_{sum} equal to the sum of f_{TA} and f_{PVC} under self-excited conditions that appeared only in the velocity signals. In the present study, such an interaction peak is present in the pressure spectrum of the first helical as well as in the antisymmetric OH* spectrum at $f_{\text{sum}} = f_{\text{PVC}} + f_{\text{TA}} = 258$ Hz, as indicated in Figure 9(d). These interaction modes are mainly

antisymmetric, which is in line with the observations of Steinberg et al.[14] and Moeck et al.[24] Therefore, these peaks are comparably larger in the antisymmetric spectra in Figure 9(c) and (d). The symmetric spectra reveal the high frequency interaction peak quite clearly; however, the low frequency interaction peak is only marginal in the spectra of the symmetric pressure and OH* signals. This leads to the conclusion that the interaction modes primarily have a helical and antisymmetric structure.

In Figure 10(a) and (b), the mean shapes of the non-actuated and actuated flames are represented. Accordingly, the actuation shifts the zone of major heat release rate from the flame tip to the flame root, whereby the whole flame becomes more compact.

Figure 10(c) and (d) reveals the structure of heat release rate fluctuations for the thermoacoustic mode ($m = 0$) that were reconstructed via point-wise Fourier transform and subsequent Abel deconvolution. The horizontal representations (e and f) are computed by rotating the vertical representation by 180° and extracting one horizontal slice at $x/D = 0.75$ (compare horizontal dotted line in Figure 10(c) and (d)). The vertical representation of mode $m = 0$ represents the axisymmetric thermoacoustic oscillations traveling along the flame. The contours are normalized by the maximal absolute value, which allows for a clear representation of the spatial shape. The vertical and corresponding horizontal shapes are slightly changed by the actuation due to the change of the mean flame. Accordingly, the spots of high fluctuation amplitude around the jet center axis in the non-actuated flame are dispersed by the PVC actuation. This leads to a broader area of constant fluctuation amplitude around the jet center axis at the flame root in the actuated case. The amplitude reduction of the strongly fluctuating spots is revealed by the horizontal representations as well. Nonetheless, in both flames, the strongest fluctuations can be seen at the flame tip.

In Figure 10(g) and (h), vertical and horizontal slices through the reconstructed OH*-fluctuations induced by the PVC are given only for the actuated flame. These plots are normalized by the maximal absolute value of the respective slice. The vertical shape of mode $m = 1$ is very similar to that in the actuated thermoacoustically stable V-flame shown in Figure 8. The major difference is the elevated fluctuation near the jet axis for the unstable flame. A reason for that can be the difference in the mean flame shape due to the thermoacoustic mode. The horizontal slice in Figure 10(h looks also very similar to the actuated stable case, revealing the typical helical shape of the PVC. This comparison shows that the flame response to the PVC actuation is qualitatively the same for the thermoacoustically stable and unstable V-flame.

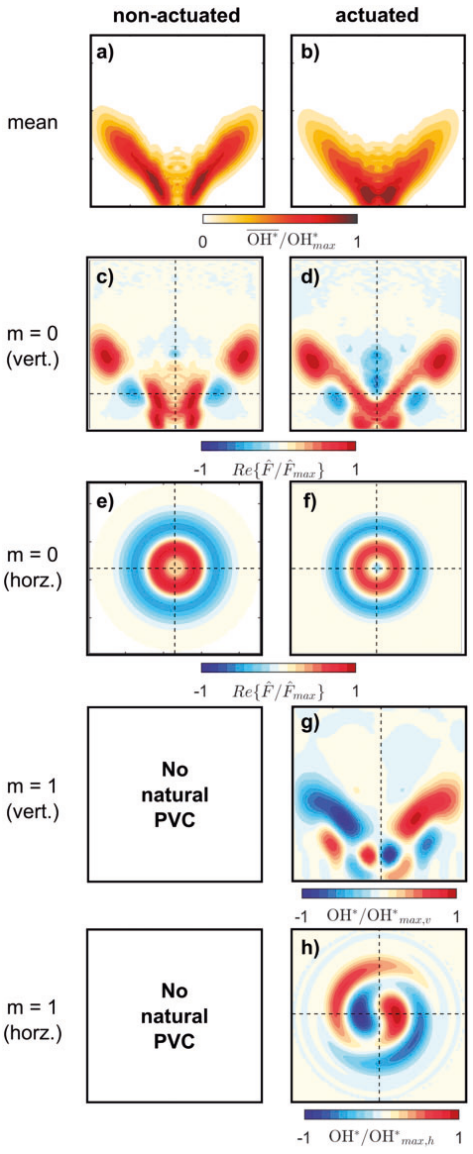

Figure 10. Effect of actuation on thermoacoustic and PVC mode shapes of V-flame at Re = 26,000 and $\phi = 0.73$ (perfectly premixed): deconvoluted mean OH* of non-actuated (a) and actuated (b) flame; thermoacoustic mode shape (Fourier mode) under natural (c) and actuated (d) conditions; horizontal view of thermoacoustic mode at $x/D = 0.75$ reconstructed from Fourier mode (e, f); vertical (g) and horizontal (h) view of the PVC under non-actuated and actuated conditions gained from tomographic reconstruction.

The various nonlinear interaction modes discussed above do not explain the change of the fundamental frequency of the thermoacoustic oscillations with applied actuation. To gain a deeper insight into this mechanisms, a parameter study was conducted where

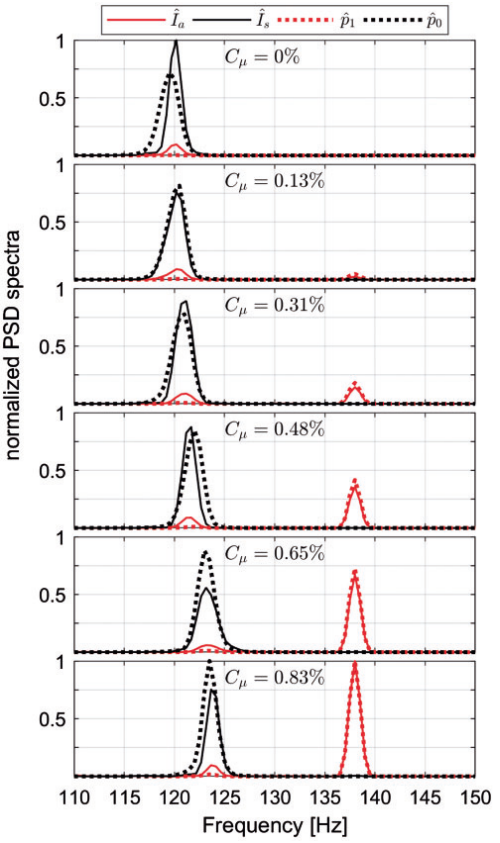

Figure 11. Spectra of global symmetric $\hat{I}_s$ (black solid) and antisymmetric $\hat{I}_a$ (red solid) OH*-signal as well as decomposed pressure spectra of mode $m = 0$ ($\hat{p}_0$, black dotted) and mode $m = 1$ ($\hat{p}_1$, red dotted) for different actuation amplitudes under thermoacoustically unstable conditions at Re = 26,000, $\phi = 0.73$, and $f_{PVC} = 138$ Hz.

the PVC actuation amplitude was step-wise increased at a constant actuation frequency of $f_{PVC} = 138$ Hz. The results are depicted in Figure 11 showing a zoom-in of the spectra of symmetric and anti-symmetric OH* fluctuations as well as the axisymmetric and helical pressure spectra for different actuation amplitudes. These spectra are generated by applying the Welch's overlapped segment averaging spectral estimation (*pwelch* Matlab command) with a segment length of sampling rate/1 s and an overlap of 50%. To allow relative comparisons, all values are normalized with respect to an overall maximum value.

For the non-actuated case (top image of Figure 11), the symmetric OH*-spectrum reveals the fundamental thermoacoustic frequency of 120 Hz. Likewise, the symmetric pressure spectrum shows a peak at this frequency. The antisymmetric OH*-spectrum also shows considerable spectral content at the frequency of the thermoacoustic instability, which is due to the slight asymmetries of the mean flame shape. These antisymmetric flame fluctuations are two magnitudes weaker than the symmetric flame fluctuations induced by the thermoacoustic mode (compare Figure 9). Apparently, the antisymmetric flame fluctuations are not strong enough to generate a prominent peak at this frequency in the normalized pressure spectrum of $\hat{p}_1$ in Figure 11.

For the actuated cases (rows two to six of Figure 11), the actuation frequency f_{PVC} is set to 138 Hz, and the actuation amplitude is step-wise increased. Comparing the amplitudes of the symmetric OH*-signal with the pressure signal of mode $m = 0$ for increasing actuation amplitude, different trends can be seen. Whereas the amplitude of the OH*-signal has its maximum at a low actuation amplitude, the pressure signal reaches its maximum at the highest actuation amplitude. Therefore, no clear trend can be drawn regarding the impact of the PVC actuation on the amplitude of the thermoacoustic mode. What is more obvious is the shift of the frequency of the thermoacoustic oscillations to higher values. From the natural frequency of 120 Hz, a gradual frequency shift toward 124 Hz takes place with increasing actuation amplitude. These results suggest that the actuation of the PVC has only minor effect on the amplitude of the thermoacoustic oscillations, but it shows an impact on the frequency of the thermoacoustic oscillations. Consequently, the results show as well that the thermoacoustic feedback cycle is not disrupted by the PVC, as the amplitude of the thermoacoustic oscillations is not affected considerably by the PVC actuation.

Frederick et al.[53] have proposed a mechanism that describes how the PVC may suppress the thermoacoustic oscillations in perfectly premixed flames. The authors suggest that the coherent Reynolds stresses induced by the PVC may lead to a thickening of the shear layers that is sufficient to significantly reduce the growth rates of the axisymmetric Kelvin–Helmholtz instability, which in turn leads to the reduction of the thermoacoustic oscillations.[52,54] To investigate on this mechanism, Figure 12 shows the the amplitude of thermoacoustic pressure oscillations against the actuation amplitude for a number of different actuation frequencies. To estimate the amplitude of the thermoacoustic oscillations (TA amplitude), the corresponding PSD spectrum of the decomposed pressure signal of mode $m = 0$ is integrated around the related peak. Finally, the amplitude is equal to the square root of this integral value. The resulting data shows only a very slight dependence of these two quantities, which demonstrates that the proposed mechanism is irrelevant for this flame. Moreover, a detailed investigation of the mean flow field measured at isothermal conditions shows that the shear layer thickness is only marginally affected by the PVC actuation (not

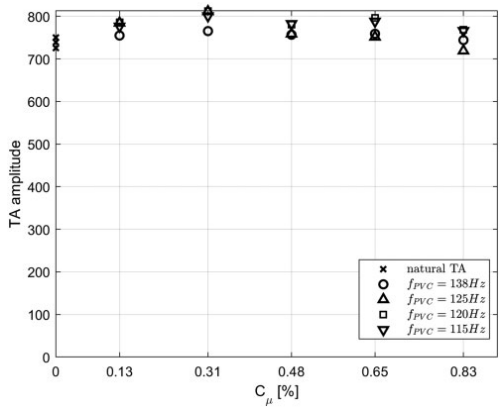

Figure 12. Amplitudes of thermoacoustic mode from integrated pressure spectrum for different actuation frequencies (f_{PVC}) and amplitudes (C_μ) at Re = 26,000 and $\phi = 0.73$–0.74.

shown here for brevity). Hence we conclude that the modification of the mean flow field through the PVC and the indirect influence on the axisymmetric Kelvin–Helmholtz instability are of minor importance for this flame.

Figure 11, however, shows a clear impact of the PVC actuation on the frequency of the thermoacoustic mode. A possible reason for this behavior might be the change of the convective time-delays within the thermoacoustic feedback loop, which might be induced by the change of the mean flame shape. The thermoacoustic feedback cycle is driven by the phase difference between the heat release rate perturbations and the pressure perturbations in the combustion chamber. These perturbations in itself are driven by the time delay between velocity perturbations at the combustor inlet and subsequent heat release rate perturbations in the flame downstream. As shown by Silva and Polifke,[55] this time delay may directly influence the thermoacoustic frequency.

To further investigate this mechanism, the mean flame position is estimated by the center of mass (COM) of one half of the deconvoluted mean OH*-field, reading[39]

$$\mathrm{COM}_y = \frac{\overline{\int \mathrm{OH}^*(x,y)x\,\mathrm{d}x}}{\overline{\int \mathrm{OH}^*(x,y)\,\mathrm{d}x}}; \quad \mathrm{COM}_x = \frac{\overline{\int \mathrm{OH}^*(x,y)y\,\mathrm{d}y}}{\overline{\int \mathrm{OH}^*(x,y)\,\mathrm{d}y}} \tag{5}$$

The estimated flame positions are shown in Figure 13(a) for different actuation frequencies and amplitudes. It illustrates the gradual movement of the mean flame in the (x,y)-plane induced by the PVC actuation. The data shows a clear trend for all considered actuation frequencies. Accordingly, the flame moves

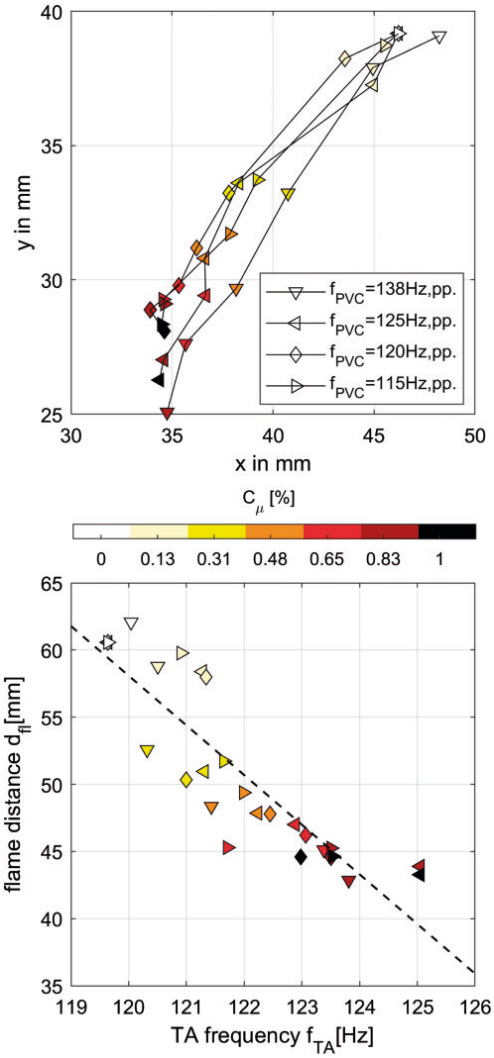

Figure 13. (a) Axial (x) and radial (y) coordinates of estimated flame position for different actuation frequencies (f_{PVC}) and amplitudes (C_μ) at Re = 26,000 and $\phi = 0.73$–0.74; (b) regression of flame distance $d_{fl} = \sqrt{x^2 + y^2}$ over thermoacoustic frequency f_{TA} for the same operating conditions as in (a).

upstream toward the burner outlet and in radial direction toward the center axis for increasing actuation amplitude. This results in a more compact flame with major heat release near the center axis, as shown for example in Figure 10. A possible reason for the upstream movement of the flame is an increase in turbulent burning velocity induced by the PVC actuation. Due to the actuation, the turbulent fluctuations are enhanced near the burner outlet, which increases the wrinkling of the flame front (compare Figure 5). The enhanced wrinkling increases the turbulent burning velocity, which causes flame anchoring more upstream

inside the inner shear layer where the increased burning velocity matches the higher flow velocity.

The coordinates of the flame position in the (x,y)-plane are condensed to one quantity by calculating the distance of the flame $d_{fl} = \sqrt{x^2 + y^2}$ to the center of the burner outlet. This flame distance is plotted over the corresponding dominating thermoacoustic oscillation frequency f_{TA} in Figure 13(b) for a number of actuation frequencies and amplitudes. The figure reveals a clear correlation between the thermoacoustic frequency and the flame distance as well as the PVC amplitude.

The distance of the flame (Figure 13(b)) can be used to estimate the convective time delay from the burner front plate to the flame using a bulk velocity estimated at 11.57 m/s based on the geometry and the fuel-air mass flow. Accordingly, the time delay τ is equal to 5.2 ms for the non-actuated flame. Together with the period duration of $T = 1/f_{TA}$, the ratio is $\tau/T = 0.63$. For the actuated cases with maximal actuation amplitude, the ratio τ/T is estimated at 0.47 equivalently to the non-actuated case. The difference of 16% causes a significant phase shift between the heat release and pressure fluctuations which may lead to a slight increase of the frequency of the thermoacoustic oscillations.[55–57] The very recent work by Silva and Polifke[55] provides a theoretical framework, which supports the increase in frequency induced by decreasing time delay.

In conclusion, the results show that the PVC actuation causes a more compact flame with the major heat release shifted upstream. This leads to smaller convective time-lags and changes in the phase relation between heat release rate and pressure in a way that higher thermoacoustic frequencies occur.

4.6. Interaction of a thermoacoustic instability and the PVC in a partially premixed V-flame

In this section, we consider a partially premixed V-shaped flame where fuel injection is applied at the swirler. For this condition, equivalence ratio fluctuations generated at the fuel injector may play a key role in the thermoacoustic feedback cycle.[58–60] The global parameters are set to Re = 22,000 and $\phi = 0.71$. As in the section before, we first consider the spectra of global OH* and decomposed pressure signal for the non-actuated flame and the flame actuated at an amplitude of $C_\mu = 0.94$ % (Figure 14). Without actuation, a dominant oscillation is clearly detected in the global OH*- and symmetric pressure spectrum, as shown in Figure 14(a) and (b), with the fundamental frequency at $f = 76.5$ Hz. The strength of the peak and the existence of higher harmonics indicate a strong thermoacoustic oscillation. Similar to the perfectly premixed flames discussed earlier, the partially premixed flame is not

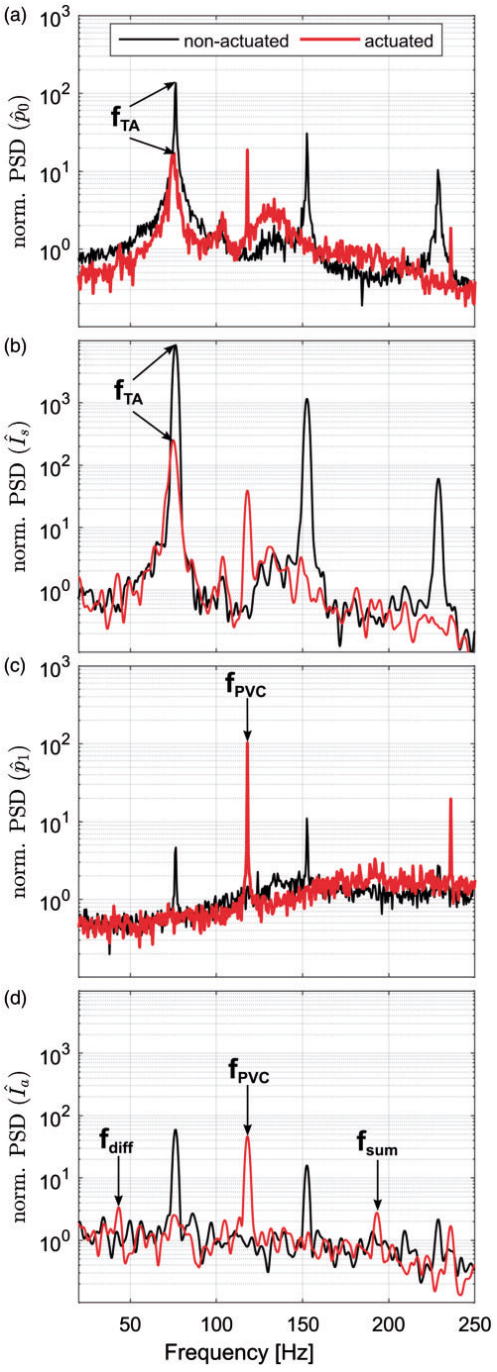

Figure 14. Effect of PVC actuation on thermoacoustic oscillations of V-flame at Re = 22,000, $\phi = 0.71$ (partially premixed): spectrum of $m = 0$ (a) and $m = 1$ (c) pressure mode; spectrum of symmetric (b) and antisymmetric (d) global heat release rate fluctuations.

perfectly symmetric, which explains the distinct contribution of the thermoacoustic oscillation at 76.5 and 153 Hz to the antisymmetric OH*-signal shown in Figure 14(d). However, compared to the symmetric OH*-spectrum, the amplitudes are two magnitudes lower. The pressure spectrum of mode $m=1$ contains only marginal peaks at the thermoacoustic frequencies, which can be seen in Figure 14(c). This underlines the fact that the antisymmetric heat release fluctuations found at the non-actuated state are not driven by a PVC, but by the asymmetry of the flame shape.

Considering the actuated case next (red lines in Figure 14), the $m=1$ pressure spectrum does not show any peaks at the frequencies of the thermoacoustic oscillation. Instead, the PVC actuation generates a dominant peak at the corresponding frequency of 118 Hz and a considerable lower one at the first harmonic at 236 Hz. Accordingly, the actuation achieves to excite a PVC even at the presence of strong thermoacoustic oscillations that occur under partially premixed conditions.

The most remarkable effect of the actuation is the considerable suppression of the thermoacoustic oscillations. This can be seen in the spectrum of the symmetric (global) OH*-spectrum, and the pressure spectrum of the symmetric mode is shown in Figure 14(a) and (b). Accordingly, the oscillations are reduced by one order of magnitude at the fundamental frequency, and the peaks at the higher harmonics are completely suppressed. The $m=0$ pressure spectrum further shows a new peak at the PVC frequency at a similar amplitude as the remaining thermoacoustic oscillation. This slight coupling between the $m=1$ actuation and the $m=0$ oscillations is most likely due to the asymmetries of the mean flame shape.

The PVC may also influence the thermoacoustic mode through a direct nonlinear interaction, as shown earlier for the perfectly premixed flame. Corresponding characteristic peaks in the antisymmetric OH*-spectrum shown in Figure 14(d) are indicative for such interactions, such as the low-frequency interaction mode oscillates at $f_{\mathrm{diff}} = 43$ Hz, which corresponds exactly to the difference of the actuation frequency $f_{\mathrm{PVC}} = 118$ Hz and the frequency of the thermoacoustic mode $f_{\mathrm{TA}} = 75$ Hz. The high-frequency mode at $f_{\mathrm{sum}} = 193$ Hz corresponds to the sum of the two frequencies. It is considerably lower than for perfectly premixed flames due to the strong damping of the thermoacoustic mode (compare Figure 9(d)).

The mean flame shape of the non-actuated and actuated cases is shown in Figure 15(a) and (b), respectively. The actuated flame exhibits distinct differences to the non-actuated flame especially concerning the concentrated shape of the zone of maximum OH*-intensity at the flame root. This difference was already observed for perfectly premixed conditions (Figure 8(b)); however, at technically premixed conditions, the flame appears even more compact, indicating better mixing at the flame root due to the PVC actuation.

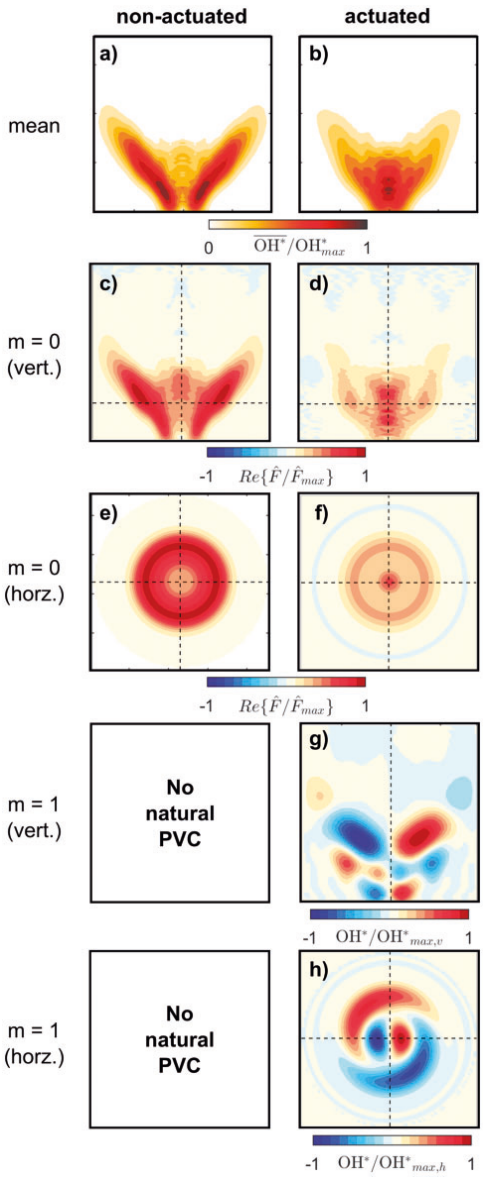

Figure 15. Effect of actuation on thermoacoustic and PVC mode shapes of V-flame at Re = 22,000 and $\phi = 0.71$ (partially premixed): deconvoluted mean OH* of non-actuated (a) and actuated (b) flame; thermoacoustic mode shape (Fourier mode) under natural (c) and actuated (d) conditions; horizontal view of thermoacoustic mode at $x/D = 0.75$ reconstructed from Fourier mode (e, f); vertical (g) and horizontal (h) view of the PVC under non-actuated and actuated conditions gained from tomographic reconstruction.

Figure 15(c) shows the symmetric heat release rate fluctuations at the fundamental frequency of the thermoacoustic oscillation. It indicates that the flame expands downstream in axial and radial direction during one cycle before it collapses and moves upstream again to repeat this periodic motion. For the actuated case, the spatial expansion and the amplitude of the thermoacoustic mode are clearly reduced (Figure 15(d)). This implies that the considerably damped remaining heat release rate fluctuations for the actuated case are now occurring near the jet center and no longer at the flame tip. The horizontal slices shown in Figure 15(e) and (f) underline this effect.

Finally, Figure 15(g) and (h) shows the reconstructed heat release rate induced by the PVC actuation. The comparison with the perfectly premixed case shown in Figure 10(g) and (h) reveals that the applied actuation is indeed causing a PVC-like structure in the flame response. Slight differences appear which can be attributed to the higher compactness of the flame at partially premixed conditions.

The present experiment reveals a significant suppression of the thermoacoustic instability through the actuation of the PVC. An explanation for the suppression of the thermoacoustic instability by the PVC is given by Frederick et al.,[19] as described above. However, our experiments conducted at perfectly premixed conditions for different actuation frequencies and amplitudes (compare Figures 10 and 11) do not support this explanation. Since the burner is operated at partially premixed conditions, one possible reason for the suppression is the improved mixing caused by the PVC actuation upstream of the flame. The improved mixing reduces the equivalence ratio fluctuations generated at the fuel injectors, which are known to be key driver for thermoacoustic oscillations.[58–60] As for the perfectly premixed flame, the change in convective time delay due to the upstream shift of the flame may influence the thermoacoustic oscillation in the partially premixed flame as well. For the partially premixed case, the time delay τ is considerably higher because the mixing tube length from the injector to the burner outlet needs to be induced as well. Therefore, the time delay is estimated at 15.9 ms for the non-actuated case, which leads to $\tau/T = 1.22$, because of the low frequency of the thermoacoustic oscillations at 76.5 Hz. For the actuated case with maximal damping of the thermoacoustic oscillation, the time delay is reduced to 14.2 ms and $\tau/T = 1.09$. The difference of 13% is comparable to that for the perfectly premixed flame. However, different from the perfectly premixed flame, the PVC actuation appears to induce a phase shift between heat release and pressure that is sufficient to push the system dynamics from an unstable state to more stable thermoacoustic conditions. Although the relative difference in time delay is equal for the perfectly premixed case, the amplitude of the thermoacoustic oscillations is not affected considerably. Therefore, we

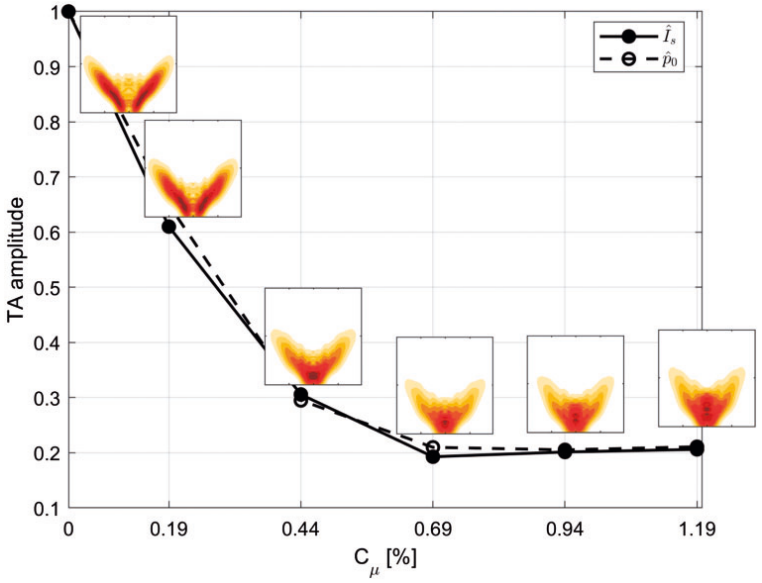

Figure 16. Amplitude of global symmetric OH*-fluctuations $\hat{I}_s$ (black solid) and decomposed pressure signals of mode $m = 0$ ($\hat{p}_0$, black dotted) for different actuation amplitudes in thermoacoustically unstable partially premixed flames at Re = 22,000, $\phi = 0.71$, and $f_{PVC} = 118$ Hz; values are normalized with respect to the non-actuated case ($C_\mu = 0$).

conclude that the impact of the PVC actuation on the equivalence ratio fluctuations is crucial as well to understand the damping mechanism for the partially premixed flame.

To further investigate the damping of the thermoacoustic oscillations through the PVC actuation, a parameter study is conducted, where the actuation amplitude was stepwise increased. Figure 16 shows the amplitude of the thermoacoustic oscillation as derived from the symmetric pressure and OH*-spectra versus the PVC actuation amplitude. The corresponding mean flame shapes are also shown revealing the movement of the major heat release zone from the flame arms to the flame root, which ends up in a more compact flame. Strikingly, even for the lowest actuation amplitude of , a reduction of the thermoacoustic pulsations of 40% is achieved. Upon further increasing the actuation amplitude, the thermoacoustic oscillations are suppressed by 80% at $C_\mu \geq 0.69\%$, which is the most remarkable effect of the actuation. The pressure and OH*-fluctuation curve are almost identical for all actuation amplitudes, which underline the overall suppression of pressure and flame fluctuations induced by thermoacoustic oscillations.

5. Conclusion

This study investigates the impact of helical open-loop PVC excitation on thermoacoustically stable and unstable swirl-stabilized flames as well as the isothermal combustor flow. The considered reacting cases are thermoacoustically stable and unstable attached V-flames without a natural PVC and stable detached M-flames with naturally occurring PVC.

The present control scheme is motivated by the recent findings from linear stability theory that determine that the PVC is a self-excited global mode. The actuator was implemented into a centerbody upstream of the flame where theory predicts the highest receptivity of the PVC mode to open-loop control. In this manner, the actuation neatly locks to the natural instability of the flow and allows for a very effective control and minimal input energy.

The isothermal combustor flow was studied first regarding the impact of the PVC actuation on mode shape and flow dynamics. This was done using SPOD of time-resolved PIV snapshots. The corresponding lock-in study serves as a proof of concept for the active flow control principal.

For the reacting cases, time-resolved OH*-chemiluminescence measurements were conducted. The symmetric and antisymmetric global OH*-fluctuation signal was Fourier decomposed and analyzed in conjunction with pressure measurements which allows for characterization of interactions between the hydrodynamic modes and the flame. To reveal the impact of the PVC actuation on the flame shape, the deconvoluted mean and Fourier-decomposed OH* distributions were considered.

From this experimental study, the following conclusions can be drawn:

1. The current control unit allows for direct actuation of the PVC at extremely low actuation amplitudes (less than 1% of total momentum). This is possible because the actuation is applied at the most sensitive region of the PVC as determined from stability theory.
2. Lock-in experiments show that the actuation is acting directly on the PVC instability, without qualitatively altering the flow dynamics.
3. The control works equally effective for reacting and non-reacting conditions.
4. The PVC can be excited even in flames subjected to severe thermoacoustic oscillations.
5. At perfectly premixed conditions, the PVC actuation causes no relevant reduction of the amplitude of the thermoacoustic oscillations. However, nonlinear interactions are observable that manifest in non-symmetric heat release.
6. PVC actuation enhances turbulence at the flame root region, which causes more compact and more upstream located flames. This leads to a slight increase of the frequency of the thermoacoustic instability due to a reduction of convective time lags and change in the phase relation between heat and pressure fluctuations.[55–57]
7. For partially premixed flames, the PVC actuation causes a reduction of the thermoacoustic instability of 80% at an actuation amplitude of less than 1%. Current experiments suggest that the suppression is caused by the mitigation of equivalence ratio fluctuations due to the PVC-enhanced mixing.

The observations regarding PVC-induced flame dynamics reported here are in line with the current literature, which shows that this flow control system is capable to generate proper experimental conditions to study flame dynamics and mode interaction in a controlled manner. Moreover, the open-loop control of the M-flame configuration and the SPOD-based lock-in study of the isothermal flow shows that the actuator does not trigger any undesired modes other than the naturally occurring PVC. This is highly important for the results of the present and follow-up studies that focus on the exclusive influence of the PVC on the combustion processes. From an application point of view, this study shows that by exploiting the PVC instability, thermoacoustic oscillations can be effectively suppressed for some flames using very little input energy. In conjunction with other studies cited above, it

appears that the PVC can be employed as a beneficial tool in reacting flows, provided that it is controlled properly. In real gas turbines, where pressure and velocity are significantly higher as in a lab-scale burner, the share of the PVC on the total energy is expected not to change. As a consequence, very strong PVC-induced fluctuation could occur. Therefore, efficient PVC control in real gas turbines can play an important role to maintain stability of the system.

Acknowledgements

Special thanks go out to Andy Göhrs and Robert Bahnweg for their technical support and Alexander Jaeschke for supporting the experimental procedure.

Declaration of Conflicting Interests

The author(s) declared no potential conflicts of interest with respect to the research, authorship, and/or publication of this article.

Funding

The author(s) disclosed receipt of the following financial support for the research, authorship, and/or publication of this article: Deutsche Forschungsgemeinschaft (DFG) within the project OB 402/4-3. We acknowledge support by the German Research Foundation and the Open Access Publication Fund of TU Berlin.

ORCID iD

Finn Lückoff https://orcid.org/0000-0002-6610-0851

References

1. Gallaire F, Ruith M, Meiburg E, et al. Spiral vortex breakdown as a global mode. *J Fluid Mech* 2006; 549: 71–80.
2. Petz C, Hege HC, Oberleithner K, et al. Global modes in a swirling jet undergoing vortex breakdown. *Phys Fluids* 2011; 23(9): 091102.
3. Oberleithner K, Terhaar S, Rukes L, et al. Why nonuniform density suppresses the precessing vortex core? *J Eng Gas Turb Power* 2013; 135(12): 121506.
4. Terhaar S, Oberleithner K and Paschereit C. Key parameters governing the precessing vortex core in reacting flows: an experimental and analytical study. *Proc Combust Inst* 2015; 35(3): 3347–3354.
5. Oberleithner K, Stöhr M, Im SH, et al. Formation and flame-induced suppression of the precessing vortex core in a swirl combustor: experiments and linear stability analysis. *Combust Flame* 2015; 162(8): 3100–3114.
6. Syred N. A review of oscillation mechanisms and the role of the precessing vortex core (PVC) in swirl combustion systems. *Prog Energy Combust Sci* 2006; 32(2): 93–161.
7. Huang Y and Yang V. Dynamics and stability of lean-premixed swirl-stabilized combustion. *Prog Energy Combust Sci* 2009; 35(4): 293–364.
8. Candel S, Durox D, Schuller T, et al. Dynamics of swirling flames. *Annu Rev Fluid Mech* 2014; 46: 147–173.
9. Stöhr M, Boxx I, Carter CD, et al. Experimental study of vortex flame interaction in a gas turbine model combustor. *Combust Flame* 2012; 159: 2636–2649.
10. Stöhr M, Arndt C and Meier W. Effects of Damköhler number on vortex–flame interaction in a gas turbine model combustor. *Proc Combust Inst* 2013; 34(2): 3107–3115.
11. An Q, Kwong WY, Geraedts BD, et al. Coupled dynamics of lift-off and precessing vortex core formation in swirl flames. *Combust Flame* 2016; 168: 228–239.
12. Stöhr M, Oberleithner K, Sieber M, et al. Experimental study of transient mechanisms of bi-stable flame shape transitions in a swirl combustor. *J Eng Gas Turbines Power* 2018; 140: 011503.
13. Stöhr M, Oberleithner K, Arndt CM, et al. Experimental study of transient coupling of PVC formation and flame shape transition in a bi-stable turbulent swirl flame. In: *Proceedings of the 7th European combustion meeting, Budapest, Hungary, 2015*.
14. Steinberg A, Boxx I, Stoehr M, et al. Flow-flame interactions causing acoustically coupled heat release fluctuations in a thermo-acoustically unstable gas turbine model combustor. *Combust Flame* 2010; 157(12): 2250–2266.
15. Terhaar S, Krüger O and Paschereit CO. Flow field and flame dynamics of swirling methane and hydrogen flames at dry and steam-diluted conditions. *J Eng Gas Turbine Power* 2015; 137: 041503.
16. Stöhr M, Arndt C and Meier W. Transient effects of fuel-air mixing in a partially-premixed turbulent swirl flame. *Proc Combust Inst* 2015; 35(3): 3327–3335.
17. Galley D, Ducruix S, Lacas F, et al. Mixing and stabilization study of a partially premixed swirling flame using laser induced fluorescence. *Combust Flame* 2011; 158(1): 155–171.
18. Mathews B, Hansford S and O'Connor J. Impact of swirling flow structure on shear layer vorticity fluctuation mechanisms. In: *ASME turbo expo 2018: turbomachinery technical conference and exposition, volume 4A: combustion, fuels and emissions*, Oslo, Norway, 11–15 June 2018. New York: ASME.
19. Frederick M, Manoharan K, Dudash J, et al. Impact of PVC dynamics on shear layer response in a swirling jet. *J Eng Gas Turb Power* 2018; 140: 061503.
20. Oberleithner K, Paschereit CO and Wygnanski I. On the impact of swirl on the growth of coherent structures. *J Fluid Mech* 2014; 741: 156–199.
21. Terhaar S, Ćosić B, Paschereit C, et al. Suppression and excitation of the precessing vortex core by acoustic velocity fluctuations: an experimental and analytical study. *Combust Flame* 2016; 172: 234–251.
22. Ghani A, Poinsot T, Gicquel L, et al. LES study of transverse acoustic instabilities in a swirled kerosene/air combustion chamber. *Flow Turbul Combust* 2016; 96(1): 207–226.
23. Steinberg A, Arndt C and Meier W. Parametric study of vortex structures and their dynamics in swirl-stabilized combustion. *Proc Combust Inst* 2013; 34: 3117–3125.
24. Moeck JP, Bourgouin JF, Durox D, et al. Nonlinear interaction between a precessing vortex core and acoustic

oscillations in a turbulent swirling flame. *Combust Flame* 2012; 159(8): 2650–2668.
25. Palies P, Ilak M and Cheng R. Transient and limit cycle combustion dynamics analysis of turbulent premixed swirling flames. *J Fluid Mech* 2017; 830: 681–707.
26. Paredes P, Terhaar S, Oberleithner K, et al. Global and local hydrodynamic stability analysis as a tool for combustor dynamics modeling. In: *Proceedings of the ASME turbo expo* 2015; 138: 021504.
27. Oberleithner K, Sieber M, Nayeri CN, et al. Three-dimensional coherent structures in a swirling jet undergoing vortex breakdown: stability analysis and empirical mode construction. *J Fluid Mech* 2011; 679: 383–414.
28. Qadri UA, Mistry D and Juniper MP. Structural sensitivity of spiral vortex breakdown. *J Fluid Mech* 2013; 720: 558–581.
29. Tammisola O and Juniper M. Coherent structures in a swirl injector at Re=4800 by nonlinear simulations and linear global modes. *J Fluid Mech* 2016; 792: 620–657.
30. Kaiser TL, Poinsot T and Oberleithner K. Stability and sensitivity analysis of hydrodynamic instabilities in industrial swirled injection systems. *J Eng Gas Turb Power* 2018; 140(5): 051506.
31. Rukes L, Paschereit CO and Oberleithner K. An assessment of turbulence models for linear hydrodynamic stability analysis of strongly swirling jets. *Eur J Mech B Fluid* 2016; 59: 205–218.
32. Müller JS, Lückoff F and Oberleithner K. Guiding actuator designs for active flow control of the precessing vortex core by adjoint linear stability analysis. *J Eng Gas Turb Power* 2018; 144(4): 041028.
33. Hill DC. Adjoint systems and their role in the receptivity problem for boundary layers. *J Fluid Mech* 1995; 292: 183–204.
34. Magri L and Juniper M. Global modes, receptivity, and sensitivity analysis of diffusion flames coupled with duct acoustics. *J Fluid Mech* 2014; 752: 237–265.
35. Kuhn P, Moeck JP, Paschereit CO, et al. Control of the precessing vortex core by open and closed-loop forcing in the jet core. In: *ASME turbo expo 2016: turbomachinery technical conference and exposition, volume 4B: combustion, fuels and emissions*, Seoul, South Korea, 13–17 June 2016. p.13.
36. Lückoff F, Sieber M, Paschereit CO, et al. Characterization of different actuator designs for the control of the precessing vortex core in a swirl-stabilized combustor. *J Eng Gas Turb Power* 2017; 140(4): 041503–041503-10.
37. Lückoff F, Sieber M and Oberleithner K. Open-loop control of the precessing vortex core in a swirl-stabilized combustor: impact on flame shape and flame stability. In: *Proceedings of ASME turbo expo 2018: turbomachinery technical conference and exposition*, Lillestrøm, Norway, 11–15 June 2018. GT2018-75472.
38. Sieber M, Ostermann F, Woszidlo R, et al. Lagrangian coherent structures in the flow field of a fluidic oscillator. *Phys Rev Fluid* 2016; 1(5): 050509.
39. Schimek S, Moeck JP and Paschereit CO. An experimental investigation of the nonlinear response of an atmospheric swirl-stabilized premixed flame. *J Eng Gas Turb Power* 2011; 133(10): 101502.
40. Leuckel W. *Swirl intensities, swirl types and energy losses of different swirl generating devices*. Technical report, Doc. No. G02/a/16, International Flame Research Foundation, Ijmuiden, The Netherlands, 1967.
41. Greenblatt D and Wygnanski IJ. The control of flow separation by periodic excitation. *Prog Aerosp Sci* 2000; 36(7): 487–545.
42. Soria J. An investigation of the near wake of a circular cylinder using a video-based digital cross-correlation particle image velocimetry technique. *Exp Therm Fluid Sci* 1996; 12: 221–233.
43. Huang HT, Fiedler HE and Wang JJ. Limitation and improvement of PIV. *Exp Fluid* 1993; 15(4–5): 263–273.
44. Sieber M, Paschereit CO and Oberleithner K. Spectral proper orthogonal decomposition. *J Fluid Mech* 2016; 792: 798–828.
45. Holmes P, Lumley JL and Berkooz G. *Turbulence, coherent structures, dynamical systems and symmetry*. Cambridge: Cambridge University Press, 1998.
46. Sieber M, Paschereit CO and Oberleithner K. Advanced identification of coherent structures in swirl-stabilized combustors. *J Eng Gas Turb Power* 2016; 139: 021503–021503-8.
47. Acharya VS, Shin DH and Lieuwen T. Premixed flames excited by helical disturbances: flame wrinkling and heat release oscillations. *J Propul Power* 2013; 29(6): 1282–1291.
48. Moeck JP, Bourgouin JF, Durox D, et al. Tomographic reconstruction of heat release rate perturbations induced by helical modes in turbulent swirl flames. *Exp Fluid* 2013; 54(4): 1–17.
49. Li LKB and Juniper MP. Lock-in and quasiperiodicity in a forced hydrodynamically self-excited jet. *J Fluid Mech* 2013; 726: 624–655.
50. Oberleithner K, Rukes L and Soria J. Mean flow stability analysis of oscillating jet experiments. *J Fluid Mech* 2014; 757: 1–32.
51. Li LK and Juniper M. Phase trapping and slipping in a forced hydrodynamically self-excited jet. *J Fluid Mech*. Epub ahead of print 29 October 2013. DOI: 10.1017/jfm.2013.533.
52. Oberleithner K, Schimek S and Paschereit CO. Shear flow instabilities in swirl-stabilized combustors and their impact on the amplitude dependent flame response: a linear stability analysis. *Combust Flame* 2014; 162(1): 86–99.
53. Frederick M, Manoharan K, Dudash J, et al. Impact of precessing vortex core dynamics on shear layer response in a swirling jet. *J Eng Gas Turb Power* 2018; 140(6): 061503.
54. Oberleithner K and Paschereit CO. Modeling flame describing functions based on hydrodynamic linear stability analysis. In: *ASME turbo expo 2016: turbomachinery technical conference and exposition, vol. 4B: combustion, fuels and emissions*, Seoul, South Korea, 13–17 June 2016. New York: ASME.
55. Silva CF and Polifke W. Non-dimensional groups for similarity analysis of thermoacoustic instabilities. *Proc Combust Inst* 2019; 37(4): 5289–5297.
56. Rayleigh. The explanation of certain acoustical phenomena. *Nature* 1878; 18(455): 319–321.

57. Juniper MP and Sujith RI. Sensitivity and nonlinearity in thermoacoustics. *Annu Rev Fluid Mech* 2018; 50: 661–689.
58. Lieuwen T and Zinn BT. Theoretical investigation of combustion instability mechanisms in lean premixed gas turbines. AIAA Paper 98-0641.
59. Lieuwen T, Torres H, Johnson C, et al. A mechanism of combustion instability in lean premixed gas turbine combustors. *J Eng Gas Turb Power* 2001; 123(1): 182–189.
60. Ćosić B, Terhaar S, Moeck JP, et al. Response of a swirl-stabilized flame to simultaneous perturbations in equivalence ratio and velocity at high oscillation amplitudes. *Combust Flame* 2014; 162(4): 1046–1062.

2.3 Publication III

Phase-Opposition Control of the Precessing Vortex Core in Turbulent Swirl Flames for Investigation of Mixing and Flame Stability

Whereas open-loop control was applied in the previous publications 2.1 and 2.2, the actuator is integrated into a closed-loop to realize phase-opposition control as shown in the work presented in this section. The strategy in this study is to continuously suppress the natural PVC in a detached M-flame such that the impact of the PVC on the flow and the flame can be investigated.

First, a proof of concept is shown for the phase-opposition control, which requires only a very low average actuation amplitude to damp the PVC considerably. This allows to study the impact of the (damped) PVC on the mean flow field and coherent as well as stochastic velocity fluctuations. Based on these findings, conclusions are drawn about the PVC impact on small- and large-scale mixing. Furthermore, the effects of the PVC on the mean flame shape, the density field and the flame dynamics are characterized.

Phase-Opposition Control of the Precessing Vortex Core in Turbulent Swirl Flames for Investigation of Mixing and Flame Stability

Finn Lückoff[1]
Laboratory for Flow Instabilities and Dynamics,
Institute of Fluid Mechanics and
Technical Acoustics,
Technische Universität Berlin,
Müller-Breslau-Street 8,
Berlin 10623, Germany
e-mail: finn.lueckoff@tu-berlin.de

Moritz Sieber
Laboratory for Flow Instabilities and Dynamics,
Institute of Fluid Mechanics
and Technical Acoustics,
Technische Universität Berlin,
Müller-Breslau-Street 8,
Berlin 10623, Germany

Christian Oliver Paschereit
Chair of Fluid Dynamics,
Institute of Fluid Mechanics
and Technical Acoustics,
Technische Universität Berlin,
Müller-Breslau-Street 8,
Berlin 10623, Germany

Kilian Oberleithner
Laboratory for Flow Instabilities and Dynamics,
Institute of Fluid Mechanics
and Technical Acoustics,
Technische Universität Berlin,
Müller-Breslau-Street 8,
Berlin 10623, Germany

The precessing vortex core (PVC) is a helically shaped coherent flow structure that occurs in reacting and nonreacting swirling flows undergoing vortex breakdown. In swirl-stabilized combustors, the PVC affects important phenomena, such as turbulent mixing and thermoacoustic oscillations. In this work, a closed-loop flow control system is developed, which allows for phase-opposition control of the PVC, to achieve appropriate conditions to systematically investigate the influence of the PVC on turbulent flames. The control consists of a zero-net-mass-flux actuator placed in the mixing section of the combustor, where the PVC is most receptive to periodic forcing. The flow control system is characterized from pressure measurements and particle image velocimetry (PIV) and the impact on flame dynamics is extracted from OH-chemiluminescence measurements. The data reveal that the PVC amplitude is considerably suppressed by the phase-opposition control without changing the overall characteristics of flow and flame, which is crucial to study the exclusive effect of the PVC on combustion processes. Moreover, the control allows the PVC amplitude to be adjusted gradually to investigate the PVC impact on turbulent mixing and flame dynamics. It is revealed that the PVC-induced flow fluctuations mainly affect the large-scale mixing, while the small scale mixing remains unchanged. This is because the suppression of the PVC allows other modes to become more dominant and the overall turbulent kinetic energy (TKE) budget remains unchanged. The destabilization of other modes, such as the axisymmetric mode, may have some implications on thermoacoustic instability.* [DOI: 10.1115/1.4044469]

Keywords: active flow control, closed-loop control, precessing vortex core, spectral proper orthogonal decomposition (SPOD), swirl-stabilized combustion, particle image velocimetry (PIV)

Introduction

In modern gas turbines, strongly swirling jets emanating into the combustion chamber are applied to achieve flame stabilization. Due to the resulting radial and axial pressure gradients, a reversed flow region and an upstream stagnation point can arise near the central jet axis. This phenomenon is called vortex breakdown and leads to the formation of an inner recirculation zone (IRZ) and corresponding inner and outer shear layers. In this flow configuration, a variety of flow velocities is present, which allow for aerodynamic flame stabilization. However, especially the inner shear layer is prone to global hydrodynamic instabilities like the precessing vortex core (PVC) [1]. The PVC can be described as a helical-shaped coherent structure, which meanders downstream along the IRZ and occurs typically in isothermal swirling jets [2]. In reacting swirling flows, the PVC can exist as long as the density stratification, induced by, e.g., a premixed swirl-stabilized flame, is mild enough near the upstream stagnation point. This is the case, for example, in lean flames, which are detached from the burner outlet [3–5].

Recent studies pointed out that the PVC influences flame dynamics regarding flame shape transition in connection with flame lift-off [6,7]. In this context, it was shown that an arising thermoacoustic instability is capable to suppress the PVC [7]. Above this, strong interaction between thermoacoustic modes and the PVC either suppress or excite helical coherent structures depending on the operating conditions [8,9]. Recent studies of isothermal swirling jets show that the growth rate of thermoacoustic modes decreases when the degree of swirl is very high [10,11]. Further studies need to clarify whether the PVC or other flow features are responsible for flow modifications, which lead to this reduction of growth rate. Nonetheless, interaction of hydrodynamic modes induced by thermoacoustic oscillations and the PVC can give rise to interaction modes [12]. Due to the strong precessing motion near the burner outlet, the mixing of fuel and air can be enhanced by the PVC, which stabilizes the flame [13–15]. In a previous study, very distinct damping of thermoacoustic oscillations was achieved by open loop actuation of the PVC under partially premixed conditions, suggesting that this damping is caused by improved mixing of fuel and air upstream of the flame [16].

According to the mentioned studies, the PVC plays an important role for several combustion properties such as flame dynamics, flame shape transition, and mixing. Therefore, further research is needed to understand the role of the PVC under reacting conditions in a quantitative manner and to use the PVC to improve the combustion systems. To investigate the PVC in the context of swirl-stabilized flames, appropriate experimental conditions are needed that enable to control the PVC. A corresponding active flow control system needs to target the PVC as direct as possible without altering the flow configuration fundamentally.

Based on linear hydrodynamic stability analysis (LSA), an appropriated flow control approach can be designed. With the

[1]Corresponding author.

Manuscript received July 1, 2019; final manuscript received July 15, 2019; published online September 16, 2019. Editor: Jerzy T. Sawicki.

help of LSA, the origin of the PVC can be described and understood thoroughly in reacting [3–5,17] and nonreacting swirling flows [18–23]. In this context, the spatial distribution of the sensitivity of hydrodynamic modes to active flow control can be derived from adjoint modes [20–22,24]. Accordingly, the best location for periodic forcing to control the PVC can be estimated. Equipped with the knowledge about the origin and the sensitivity of the PVC, an effective active flow control scheme can be realized, which acts purely on the PVC without altering other structures significantly [25].

In previous studies, we presented open-loop experiments using an active flow control system implemented in a swirl combustor, and we demonstrated its good performance at isothermal and reacting conditions [16,26]. This flow control system was designed based on studies of the sensitivity of the PVC in comparable configurations and is used in this work as well [20–22,24]. The actuation of this system is placed in the region of highest sensitivity, which allows for direct and very efficient control of the PVC.

In this study, the active flow control system is used in a closed-loop manner. The goal is to suppress the PVC through phase-opposition control. We therefore investigate an operating condition where the PVC is naturally present. With this experimental arrangement, the impact of the PVC on the flow field and the flame is investigated.

This paper is structured as follows: At the beginning of this study, the experimental setup is explained including descriptions of the closed-loop control approach, the test rig, and the applied measurement techniques. The time-resolved data for this study were obtained using synchronized OH*-chemiluminescence and particle image velocimetry (PIV) measurements as well as pressure measurements. To analyze these data properly, different analysis methods were utilized, such as spectral proper orthogonal decomposition (SPOD) [27,28], spatial Fourier decomposition, and quantitative light sheet method (QLS) [29]. These methods are shortly introduced in the second part of this paper. In the result section, the mean flow field and the turbulent kinetic energy (TKE) are analyzed under natural and controlled operating conditions. Moreover, the spatial structure and the dynamics of the PVC are analyzed with the help of SPOD, which allows to quantify the effectiveness of the phase-opposition control. Thereafter, the coherent and stochastic fluctuations are quantified under controlled and uncontrolled conditions, applying a triple decomposition [30]. Furthermore, the length scale of the smallest eddies in the flow fields is estimated based on an approximation by Taylor [31]. The result section ends with an investigation of the impact of the (un)controlled PVC on flame shape and flame dynamics. Above this, the density distribution is estimated based on PIV snapshots for different control gains. This study closes with conclusions, which detail future experiments and the opportunities of this flow control facility, which is unique to our knowledge.

Experimental Setup

In this section, the experimental setup is presented including the test rig, the actuator and the applied time-resolved pressure, and synchronized PIV and OH*-measurements. Moreover, the working principle of the phase-opposition flow control system is explained.

Test Rig. Figure 1 shows the test rig, which consists of three sections labeled with ①, ②, and ③. The air flows from bottom to top.

Section ① represents the actuation unit, which allows the actuation of a helical PVC mode at the centerbody with an azimuthal wavenumber of unity. The helical actuation is achieved by four circumferentially arranged 5 in. loudspeakers (rated power of 100 W) that are driven with a phase-shift of $\pi/2$ relative to one another. The loudspeakers, which are mounted on aluminum plenums, drive the actuator as indicated by the double arrows. The oscillation of the loudspeaker membranes induces an oscillating motion of the air column inside the actuation channels, which creates actuation jets at the channel outlets as indicated by the arrows at the tip of the centerbody. The oscillating air emanates through four outlets that have a rectangular shape (9 mm wide and 1 mm high). The outlets are placed 25 mm upstream of the downstream end of the mixing tube (more details in Ref. [26]). This loudspeaker-based actuator works on the zero-net-mass-flux principal, which means that no additional air mass flow is added by the actuation.

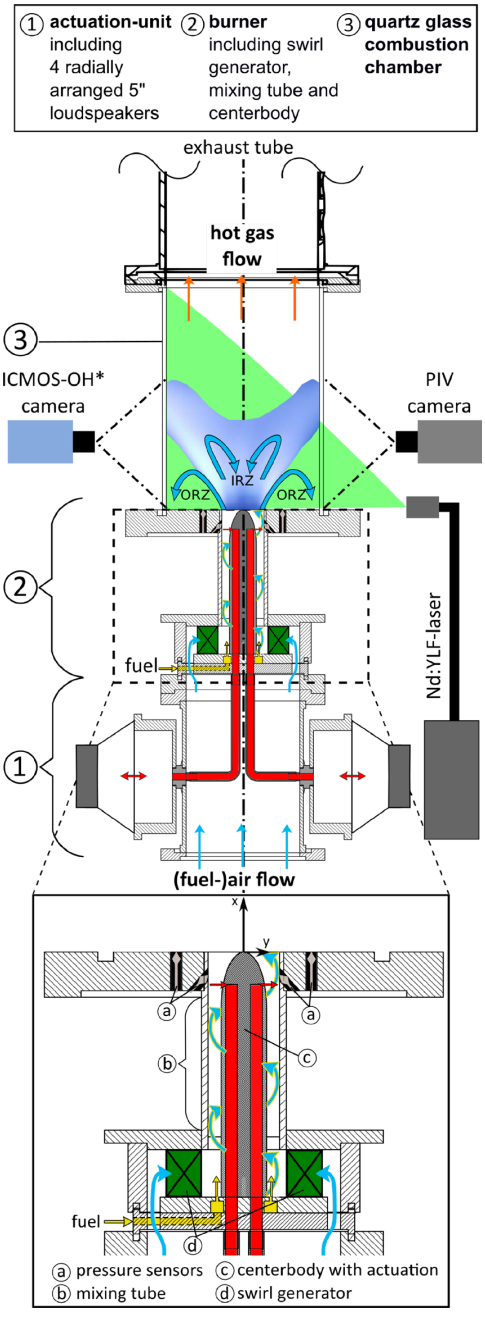

Fig. 1 Sketch of test rig with experimental setup and detailed zoom view of the burner

Section ② includes the burner, the swirl generator, the mixing tube with front plate, and the centerbody (in the center of the mixing tube). The air enters through the radial swirl generator consisting of movable blocks, which can be adjusted relative to each other. This allows to adjust the swirl number, defined as the ratio of the axial flux of tangential momentum to the axial flux of axial momentum, in a wide range [32]. The swirl number was set to 0.7 in this study. The arrows and channels at the upstream part of the burner indicate the routing of the fuel (natural gas) under partially premixed operating conditions. Under these operating conditions, the fuel is injected downstream of the swirler directly into the mixing section so that partially premixed conditions are present at the mixing tube outlet. The hydraulic diameter of the mixing tube $D_h = 20$ mm is equal to the difference between the outlet ($D = 55$ mm) and the centerbody diameter ($D_{CB} = 35$ mm). More details about the burner and actuator design can be found in Ref. [16].

The combustion chamber (section ③ in Fig. 1) consists of a cylindrical quartz glass tube with an inner diameter of 200 mm and a length of 300 mm. This glass tube provides optical access for the PIV and OH*-chemiluminescence measurements.

The operating conditions for the experiments, presented below in the result section, are kept constant as presented in Table 1.

Measurement Techniques. Time-resolved synchronized OH*-chemiluminescence and planar PIV measurements are conducted in the combustion chamber (Fig. 1) to investigate the influence of phase-opposition control on the flow and the flame at the same time. Additionally, the time-resolved dynamic pressure is measured simultaneously. The pressure signal is well suited to characterize the amplitude, the frequency, and the phase of the PVC [26]. Therefore, this signal serves as input signal for the closed-loop controller. In the following, technical properties of the aforementioned measurement techniques are given.

The OH*-chemiluminescence measurements are utilized as a qualitative indicator for the heat release rate and the mean flame shape. For these measurements, a high-speed CMOS camera (Photron (Tokyo, Japan) SA 1.1) is used in combination with a high-speed intensifier (Lambert Instruments (Groningen, Netherlands) HiCATT 25) to capture line-of-sight OH*-chemiluminescence intensity snapshots. The camera was equipped with a 308 nm bandpass filter to record nothing but the OH*-chemiluminescence. The sampling rate of the camera is set to 2 kHz, which is sufficient to resolve the dynamics of the PVC (in the range of 100–200 Hz). Within a measurement time of approximately 2.7 s, 5459 snapshots with a resolution of 1024 × 1024 pixels are acquired.

A second high-speed CMOS camera (Photron SA 1.1), without intensifier, was used in connection with a synchronized high-speed Nd:YLF diode pumped laser (Quantronix (Hamden, CT) Darwin Duo 527-100M, 527 nm and total pulse energy of 60 mJ) for time-resolved PIV measurements at the same time. The employed light sheet optic generated an appropriated light sheet of approximately 1 mm thickness in the measurement area. The reacting flow was seeded with solid TiO_2 particles, which are resistant to the high flame temperatures. The acquired particle snapshots were evaluated with a commercial PIV software (PIV-TEC GmbH (Göttingen, Germany) PIVview). The correlation scheme uses multigrid refinement [33] with a final window size of 16 × 16 pixels, window overlap of 50% in combination with spline-based image deformation [34], and subpixel peak fitting. At the end, the data were filtered for outliers and interpolated from adjacent interrogation windows.

Table 1 Operating conditions of the reacting tests

Reynolds number	Re	36,000
Air mass flow (kg/h)		170
Natural PVC frequency (Hz)		196
Strouhal number	St	0.14
Swirl number		0.7
Equivalence ratio		0.58
Premix type		Partially premixed
Inlet temperature (K)		298
Thermal power (kW)		49

The pressure is measured by miniature differential pressure sensors (First Sensor AG (Berlin, Germany) HDOM010 with 1000 Pa range). The sensors are arranged circumferentially at the outlet of the mixing tube (compare gray arrows in mixing tube and front plate in Fig. 1) to resolve the hydrodynamic properties of the PVC. In each of the two pressure measurement planes, four sensors are mounted. In the mixing tube, the sensor orientation is shifted by 20 deg relative to the exit channels of the actuator to avoid interference with the actuation jets emanating from the centerbody slits. The pressure sensors are connected to the flow via short cannula tubes. The setup allows to measure pressure fluctuations as small as 0.1 Pa. All reference pressure ports of the differential sensors are connected to an ambient pressure reservoir, which provides a common reference pressure. The signals are amplified with an in-house amplifier and digitized by a 16 bit A/D converter (National Instruments NI 9216, Austin, TX) at a sampling frequency of 16,384 Hz.

Phase-Opposition Flow Control Approach. In this study, phase-opposition flow control is applied to suppress the PVC gradually with the goal to investigate the impact of the PVC on flow and flame dynamics. To achieve such a suppression, the closed-loop control system works on the principal of phasor control, which is considered as opposition control with respect to the amplitude of the PVC. This means that the actuation aims to reduce the PVC amplitude at phases where it is effective [35]. Accordingly, the controller estimates an actuation signal, which allows the actuator to counteract against the PVC in a way that the PVC oscillation is suppressed.

The PVC observed here can be considered as an oscillatory single-helical flow structure. Therefore, a pressure sensor array, which is arranged circumferentially around the flow, is well suited to capture amplitude, flow phase, and frequency of the PVC. With these quantities, an appropriated actuation signal can be calculated. As depicted in the control scheme in Fig. 2, the control loop starts with four input signal ($P1$ to $P4$), which are provided by the pressure sensor array inside the mixing tube. The input signals are fed into a real-time controller board (dSpace DS1103 PPC controller board with 1 GHz CPU and 16-bit A/D and D/A converters), where the state of the PVC (amplitude A and phase ϕ) is estimated in real-time using a SIMULINK model. The state estimation is conducted by an extended Kalman filter (EKF) based on the pressure difference signals $x = P1-P3$ and $y = P2-P4$, which are provided by the four pressure sensors. As the single helical oscillation of the PVC is considered as a harmonic oscillator,

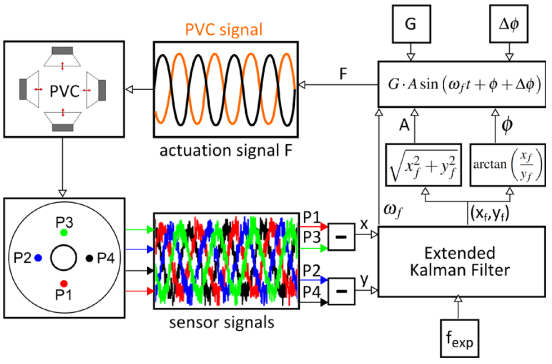

Fig. 2 Applied closed-loop scheme for phase-opposition flow control

the input signals x and y can be used to describe the PVC oscillation in the polar complex plane according to Euler's formula $e^{i\phi} = \cos\phi + i\sin\phi = y + ix$. Within the EKF, the PVC is modeled as a harmonic oscillator as well. As another input value, the expected natural PVC frequency $f_{\exp}$ is fed into the EKF, which serves as an initial guess value. This value is kept constant and was estimated under uncontrolled conditions. With the filtered output signals x_f and y_f, the current amplitude $A = \sqrt{x_f^2 + y_f^2}$ and phase $\phi = \arctan(x_f/y_f)$ of the PVC are calculated. Together with the estimated PVC frequency ω_f and the adjustable control parameters gain G and phase shift $\Delta\phi$, the (counteracting) actuation signal $F = G \cdot A\sin(\omega_f t + \phi + \Delta\phi)$ is composed. This signal is given to the actuator, which counteracts against the PVC inside the mixing tube. The resulting change of the PVC dynamics is captured by the sensor array, which closes the control loop.

Gain G and phase shift $\Delta\phi$ are the most important tuning parameters in this control approach, which need to be well adjusted to obtain a distinct control effect. The gain is necessary to adjust the actuator momentum to the incoming main flow. The additional phase shift addresses the spatial separation of actuator and sensor, the length of the cannula tubes connecting sensors and flow as well as systematic estimation errors of the controller. Moreover, it decides whether the actuator is actuating in-phase with the PVC (PVC amplification) or counteracting against it (out-of-phase). The out-of-phase actuation is applied to achieve the phase-opposition flow control, which is investigated in this study.

The influence of the phase shift on the normalized PVC energy is presented in Fig. 3 for the case of an isothermal combustor flow at a Reynolds number of Re = 36,000 and a fixed controller gain of $G = 1.6$. The PVC energy P_{PVC} is estimated by the integral of the power spectral density of the decomposed pressure signal $\hat{p}_1$ over a representative frequency band (compare Eq. (2)). Depending on the phase shift, the PVC is either amplified by 25% in case of in-phase actuation ($\Delta\phi = -0.6\pi$) or damped by 52% for counteracting out-of-phase actuation ($\Delta\phi = -1.6\pi$). These results clearly demonstrate that the present closed-loop controller is working effectively in a highly turbulent swirling flow. The comparatively low amplification observed can be explained by a nonlinear saturation of the PVC amplitude, which prevents further PVC amplification.

In order to compare different actuators and control concepts, it is common to relate the momentum of the actuation jets to the main flow to evaluate the actuation magnitude. This relation can be expressed by a momentum coefficient [36]

$$C_\mu = A_a u_{\text{RMS}}^2 / (U_0^2 A_h) \tag{1}$$

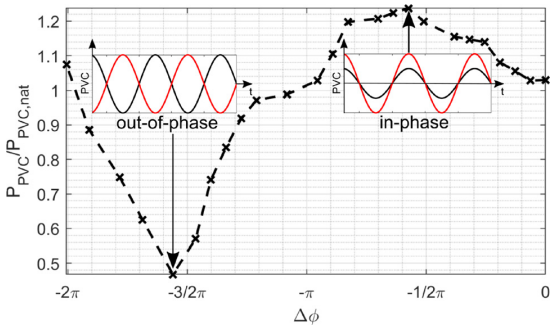

Fig. 3 PVC energy normalized by the energy of the natural case in dependence on the phase shift $\Delta\phi$. Isothermal combustor flow with Re = 36,000 and $G = 1.6$.

where u_{RMS} represents the root-mean-square (RMS) velocity at the actuator outlet, measured with a hot-wire [26], A_a the outlet area of the actuator, A_h the hydraulic cross-sectional area, based on the hydraulic diameter of the mixing tube D_h, and U_0 the bulk velocity of the main flow. The momentum coefficient describes a nondimensional quantity that quantifies the effectiveness of the control regardless of the technical specifications of the actuator. Therefore, the momentum coefficient is used in the following to quantify the actuation magnitude. In contrast to open-loop actuation [16], where the actuation signal has constant amplitude, the closed-loop signal is temporally varying due to the time-dependent estimated amplitude A. Moreover, the phase-opposition control is applied in the region of highest sensitivity, which allows for very effective flow control due to high response on small actuation momentum. Accordingly, the RMS velocity u_{RMS} is considerably low, which results in extremely low C_μ values. For the following investigations of reacting flows, C_μ varies between 0.025 and 0.055%.

Data Analysis Methodology

In the following, the reader is briefly introduced to the spatial Fourier decomposition applied to the pressure signal as well as the postprocessing of the PIV and OH*-chemiluminescence snapshots.

Spatial Fourier Decomposition of the Pressure Signals. The pressure signals recorded by the four circumferentially arranged pressure sensors are decomposed into Fourier modes with azimuthal wavenumbers. Accordingly, the signal of the mth azimuthal mode can be expressed as

$$\hat{p}_m(t) = \sum_{k=1}^{4} p_k(t)\exp\left(i2\pi m\frac{k}{4}\right) \tag{2}$$

where p_k is the pressure signal of the kth sensor and m is the azimuthal wavenumber. The Fourier coefficient $\hat{p}_m$ is complex and a function of time, where $m = 1$ describes the PVC dynamics. This function is used to calculate the instantaneous amplitude and phase of the PVC, which correspond to the modulus and argument of $\hat{p}_1$, respectively.

Spectral Proper Orthogonal Decomposition of Time-Resolved Particle Image Velocimetry Snapshots. The SPOD is a recently developed method to extract coherent structures from time-resolved flow field data [27]. It is based on the classical proper orthogonal decomposition (POD) [37], but it offers a more precise selectivity. This provides benefits especially in complex turbulent flows like reacting combustor flows investigated in this study [28]. Subsequently, only a very brief overview of the SPOD approach is given. A more detailed derivation can be found in Sieber et al. [27]. The procedure is exemplified for the crosswise velocity v, but can be applied similarly for the axial velocity u. The SPOD provides a modal decomposition of the fluctuating part of the velocity v' that reads as follows:

$$v(\mathbf{x},t) = \overline{v}(\mathbf{x}) + v'(\mathbf{x},t) = \overline{v}(\mathbf{x}) + \sum_{i=1}^{N} a_i(t)\Phi_i(\mathbf{x}) \tag{3}$$

The fluctuations are separated into a sum of spatial modes Φ_i and corresponding modal time-dependent coefficients a_i. In order to build this basis, the spatial correlation among individual PIV snapshots is calculated. This results in a corresponding correlation matrix, which is filtered by a Gaussian low-pass filter in contrast to the classical POD. The filtering helps to extract mode shape and dynamics of coherent flow structures, such as the PVC, more precisely. The temporal coefficients $a_i(t)$ describe the dynamics of the corresponding mode and are derived from the eigenvectors

of the filtered correlation matrix. From a projection of the snapshots onto the temporal coefficients, the spatial modes $\Phi_i(\mathbf{x})$ are finally obtained.

Decomposition of OH*-Chemiluminescence Data. The global heat release rate $I(t)$ is a time-dependent quantity, which characterizes the dynamical flame response to flow perturbations induced, e.g., by an actuator. It is simply obtained by integrating the recorded two-dimensional OH*-signal $\mathrm{OH}^*(x,y,t)$ over the entire flame area. The time-averaged global heat release rate $\bar{I}$ can be used to calculate temporal fluctuations $I'(t) = I(t) - \bar{I}$. These fluctuations are well suited to analyze the impact of the flow actuation on the flame dynamics.

The single-helical shape of the PVC ($m = 1$) generates heat release fluctuations, which are antisymmetric with respect to the centerline of the combustor. Accordingly, heat release fluctuations integrated over the left ($y < 0$) and right ($y > 0$) half of the combustion chamber are 180 deg out of phase. Therefore, antisymmetric fluctuations are eliminated by summation of the heat release fluctuations left ($I'(x, y < 0, t)$) and right ($I'(x, y > 0, t)$) of the combustors' centerline. The result of this summation is a representation of the purely symmetric fluctuations. Vice versa, subtraction eliminates symmetric fluctuations, which provides a representation of purely antisymmetric fluctuations.

An integration of the obtained antisymmetric fluctuations over the entire flame area can be used as a measure I'_a for the global heat release fluctuations induced by antisymmetric modes, such as the PVC.

Estimation of Density Distribution Based on Particle Image Velocimetry Snapshots (Quantitative Light Sheet). The flame within the flow field induces a density gradient where cold fresh gas collides with the hot burnt gas in the inner and the outer recirculation zones. Due to the very different fluid densities in regions of cold and hot gas, the seeding particle concentration is very different as well. Accordingly, scattered light from seeding particles, which is recorded within PIV measurements, can be used to estimate the density distribution inside the combustion chamber by a technique called QLS [29,38,39]. The scattered light intensity S is estimated by subtracting a background image S_B without seeding from the recorded scattered light intensity S_{rec}. The resulting difference signal is normalized by a time-averaged reference image S_{ref} of uniform particle distribution, which is obtained from the uniformly seeded isothermal combustor flow. This reference image corrects for inhomogeneities of the light sheet, so that

$$S(x,y,t) = \frac{S_{\mathrm{rec}}(x,y,t) - S_B(x,y)}{S_{\mathrm{ref}}(x,y) - S_B(x,y)} \tag{4}$$

Within the scope of this study, additional influences on the detected light intensity such as multiple scattering or light extinction [39] are neglected.

The light intensity and the particle concentration of the reference image with uniform particle concentration C_{ref} are further employed to receive the actual particle concentration

$$\frac{C(x,y,t)}{C_{\mathrm{ref}}} = S(x,y,t) \tag{5}$$

Since an accurate quantification of the number of particles is practically impossible, the QLS technique only provides relative information to a known quantity. Therefore, C_{ref} can be set to unity. As mentioned above, the particle concentration depends on the fluid density ρ. Within this framework, a linear influence can be assumed leading to the relation

$$\overline{\rho}(x,y) = \frac{C(x,y)}{C_{\mathrm{ref}}}\rho_{\mathrm{ref}} \tag{6}$$

including the uniform density ρ_{ref} of the isothermal reference image [29].

Results

This section deals with the results of this study starting with the flow field features and dynamics for different control gains at a fixed phase shift of $\Delta\phi = 1.34\pi$. This fixed phase shift was estimated empirically to realize phase-opposition control to suppress the PVC gradually. Subsequently, different flow scales are discussed in terms of mixing for the same control parameters. At the end of this section, the impact of the control on the flame shape, the dynamics and the density distribution is investigated. All the results presented here are derived from measurements under reacting conditions, at the operating conditions presented in Table 1.

Flow Structures and Dynamics. In the top row of Fig. 4, the natural, nonactuated flow field is depicted by streamlines (lines with arrows) and isolines (bold lines), where the axial velocity is zero. This zero-axial-velocity isoline indicates the IRZ around the central jet axis, which forms an upstream stagnation point at $x/D = 0.3$. The normalized TKE contour shows major turbulent fluctuations inside the inner shear layer, where the PVC is present. In the middle column of Fig. 4, the SPOD mode shape of the transverse velocity component represents the single-helical structure of the PVC, which is the dominating coherent structure in the SPOD spectrum. The normalized PSD (Power Spectral Density) spectrum of the corresponding time-coefficient a_{PVC} describes the PVC dynamics in the right column. It indicates that the PVC is oscillating at a distinct frequency corresponding to a Strouhal number $\mathrm{St} = 0.14$.

The middle row of Fig. 4 shows the results for applied flow control using a relatively low gain. The mean flow indicates a slight movement of the IRZ in upstream direction. The qualitative TKE distribution remains nearly unchanged; although, the TKE magnitude is slightly reduced. Regarding the SPOD mode shape, no clear deviations from the natural shape can be observed. However, the PSD spectrum of a_{PVC} shows that the frequency peak is reduced by almost 50%, which already indicates a considerable suppression of the PVC. In contrast to that, the PVC energy E_{PVC}, which is equal to the integral of the PSD spectrum over the presented frequency band, is almost the same as in the natural case. This means that the dynamics of the PVC have been distributed over a wider spectral band, but the frequency peak is strongly reduced.

The bottom row shows the impact of the phase-opposition flow control applied at high gain ($C_\mu = 0.045\%$). The PSD spectrum reveals that the spectral content is distributed over a range of frequencies without a distinct peak. Consequently, the PVC dynamic has lost its periodic oscillatory nature due to the considerable suppression of the coherent structure. The suppression of the PVC is underlined by the reduced TKE magnitude in the inner shear layer and the normalized PVC energy of $E_{\mathrm{PVC}} = 0.66$. Compared to the cases described above, the IRZ moves clearly upstream and the upstream stagnation point moves outside the measurement plane. This effect is induced by the suppressed stirring movement of the PVC, which allows the IRZ to propagate further upstream. According to our knowledge, such a direct effect of the PVC on the mean flow field was not observed before.

The effect of the controller on the flow dynamics is further investigated by considering the instantaneous dynamics of the SPOD coefficients. The two coefficients that make up the PVC dynamic are used to obtain the amplitude $A_{\mathrm{PVC}} = \sqrt{a_1^2 + a_2^2}$ and the phase $\varphi_{\mathrm{PVC}} = \arctan(a_1, a_2)$ of the PVC, where the phase is further used to get an instantaneous frequency from its time derivative

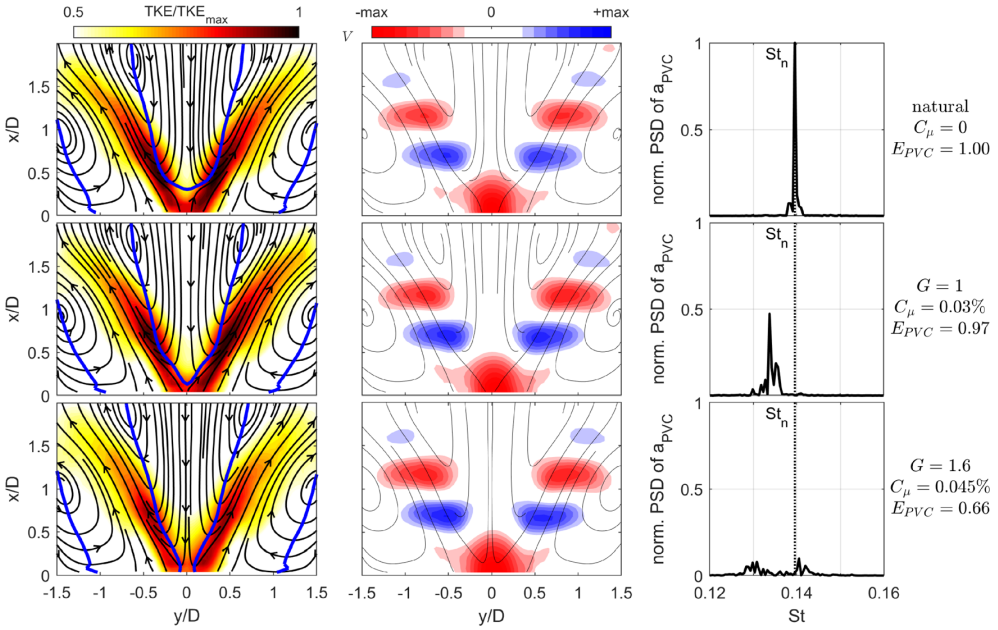

Fig. 4 Mean flow field with TKE, normalized with the spatial maximum value of the three cases, in the left column. SPOD modes of transversal velocity component describing the PVC in middle column. Normalized PSD spectrum of corresponding time coefficients. Top row: natural case, middle row: low gain ($C_\mu = 0.03\%$), bottom row: high gain ($C_\mu = 0.045\%$).

$$f_{\mathrm{PVC}} = \frac{1}{2\pi}\frac{d\varphi_{\mathrm{PVC}}}{dt} \tag{7}$$

The instantaneous frequency for different cases is shown in Fig. 5, where the selected cases can be directly compared to Fig. 4. The average amplitude at different frequencies given at the right of

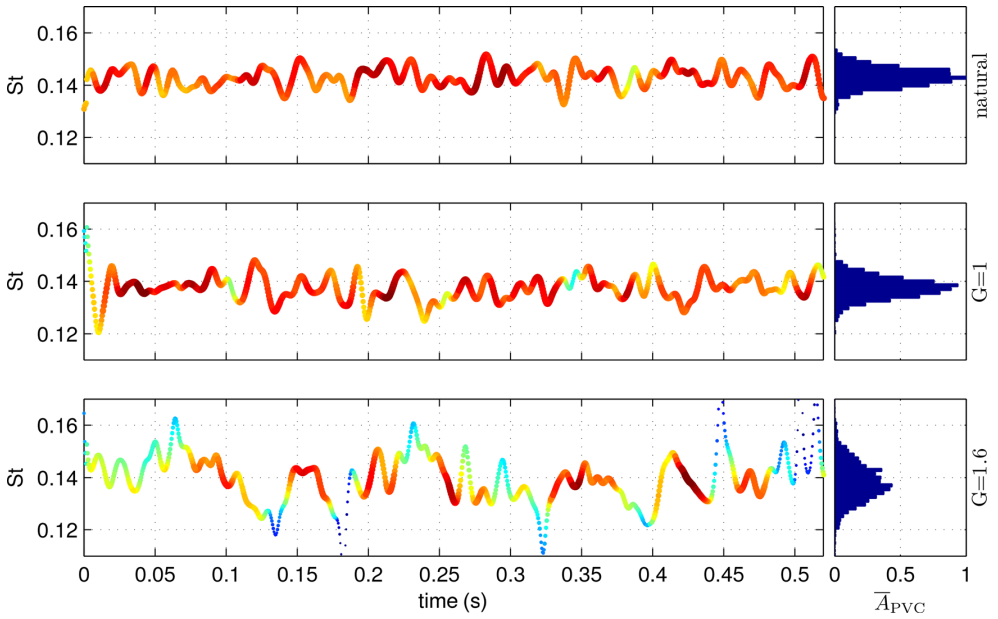

Fig. 5 Instantaneous PVC frequency (spectrogram) for the different gains presented in Fig. 4. The normalized frequency (Strouhal number) is given for a part of the measured time-series. The color and size of the markers indicate the instantaneous PVC amplitude (A_{PVC}) where the actual amplitude is arbitrary but all plots share the same axis limits and color-map range. The bar plots in the right column show the average amplitude at each Strouhal number (amplitude weighted probability density function).

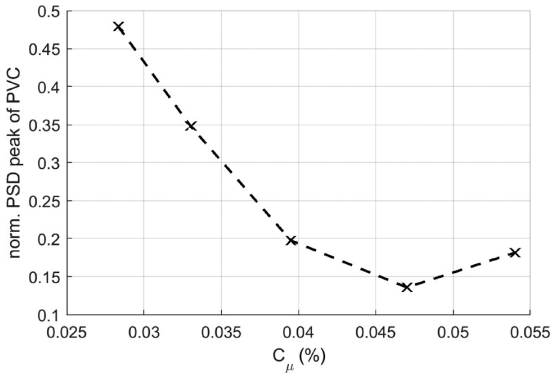

Fig. 6 Peak of the PVC as a function of actuator momentum coefficient, normalized by the uncontrolled value derived from corresponding SPOD spectra

Fig. 5 is a rotated representation of the PSD from Fig. 4. The alternative representation similarly shows an increased variation of the frequency if the PVC amplitude is reduced and a shift toward lower frequencies. However, in contrast to the PSD, there is still a distinct peak for the high gain case.

The difference between the two representations of the average spectral content can be explained by phase jumps of the PVC due to intermittent suppression. The controller causes a bias of the phase shifts toward half period due to the phase-opposition control. However, the Fourier analysis assumes a continuous progress of the phase and repeated phase shifts of half a period result in a splitting of the spectral peak. In contrast, the instantaneous frequency is not affected by these phase jumps.

The time series given in Fig. 5 shows that the suppression of the PVC due to the controller does not happen as a permanent reduction of the amplitude but as intermittent suppression. With increasing gain, there are more prolonged periods where there is no PVC present. The rekindle of the PVC is interpreted such that the controller loses track of the PVC phase at low amplitudes, which allows the PVC to recover. An improved control law might help to avoid this behavior, but the observed behavior can also be an effect of stochastic turbulent variations of the incoming flow that will also evade advanced controllers.

In general, these results demonstrate that the control system is addressing the PVC directly without altering its spatial structure. Above this, the closed-loop control system is capable to achieve a considerable suppression of the PVC in a highly turbulent reacting flow.

The PVC suppression is further underlined by Fig. 6, which shows the normalized PVC peak from PSD spectra of the SPOD coefficients a_{PVC} as a function of controller gain. Accordingly, the peak amplitude is suppressed down to 15% of the natural case at around $C_\mu = 0.045$. For the highest C_μ, the PVC peak starts to grow again because the actuation amplitude overshoots the optimal value.

Flow Fluctuations and Mixing. In this subsection, the influence of the PVC on small-scale and large-scale mixing is investigated based on the analysis of the change in the flow fluctuations and the length scales due to the suppression of the PVC. Therefore, the flow fluctuations v' are further decomposed to show the impact of the PVC on dominating coherent $\tilde{v}$ and other stochastic fluctuations $v'' = v' - \tilde{v}$. This triple decomposition was introduced by Hussain and Reynolds [30] and can be written for the transversal velocity component as

$$v(\mathbf{x},t) = \overline{v}(\mathbf{x}) + v'(\mathbf{x},t) = \overline{v}(\mathbf{x}) + \tilde{v}(\mathbf{x},t) + v''(\mathbf{x},t) \qquad (8)$$

The coherent fluctuations $\tilde{v}$ are reconstructed by the summation of the eight most energetic SPOD modes multiplied with their corresponding time-coefficients, which contain the major portion of turbulent coherent energy.

Moreover, an estimation of the average small-scale eddy size is made based on the definition of the Taylor microscale [31]

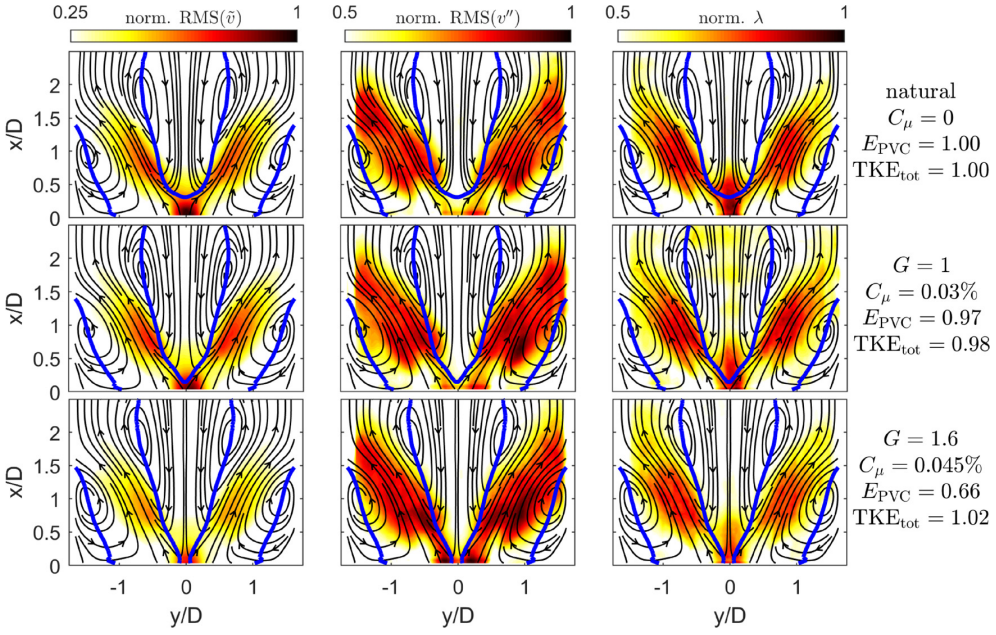

Fig. 7 Distribution of coherent fluctuations RMS($\tilde{v}$), stochastic fluctuation RMS(v'') and small-scale eddy size λ, normalized with respect to the maximum value among all cases. Top row: uncontrolled case, middle row: low controller gain ($C_\mu = 0.03\%$), bottom row: high controller gain ($C_\mu = 0.045\%$).

$$\lambda = \sqrt{\frac{2\overline{v'^2}}{\overline{\left(\frac{\partial v'}{\partial y}\right)^2}}} \tag{9}$$

The resolution of the estimated measure λ is limited by the spatial resolution of the underlying PIV measurements of $\Delta x = \Delta y = 2.55$ mm. Therefore, this measure describes the size of those small-scale eddies, which are resolved by the underlying PIV measurements.

The quantities $\tilde{v}$, v'', and λ are depicted in Fig. 7 for uncontrolled conditions (top row), as well as for the low (middle row) and high actuation gain (bottom row) cases, as normalized RMS and time-mean values. The operating and control conditions are the same as in the previous section ("Flow Structures and Dynamics"). As shown in the left column, coherent fluctuations are mainly present in the inner shear layer, where the PVC exists. In case of low actuation magnitude, a minor suppression near the burner outlet occurs. However, a very considerable suppression of the coherent fluctuations is visible for the high actuation case because of the suppressed PVC. This is in line with the reduction of TKE in Fig. 4. In contrast, the fluctuations induced by remaining coherent and stochastic fluctuations (v'') appear to grow slightly as the PVC is damped. A reason for that can be the change in the mean flow and the corresponding variation of the shear layers. Moreover, other modes, which are convectively unstable, may gain more energy due to the suppressed PVC, as the global TKE remains nearly constant. These arising modes may influence the formation of thermoacoustic modes, which needs to be clarified in future studies. Contrarily to the change in coherent and stochastic fluctuations, the small-scale eddy size changes only slightly from natural to controlled cases. This is plausible, because the small-scale eddy size is directly related to the dissipation rate, which is a function of the turbulent kinetic energy [31], which does not change considerably between the different actuation gains (compare different normalized total TKE values $\mathrm{TKE_{tot}}$ in Fig. 7).

The current results suggest some conclusions regarding the mixing enhancement induced by the PVC, which was often observed in previous investigations [13–15]. The current data show that through the reduction of the PVC, other large-scale fluctuations kick in and the total turbulent kinetic energy remains approximately unchanged. This is due to the wide range of convective instabilities that are present in swirling flows [40]. Consequently, the mixing through small-scale turbulence is not strongly affected through a suppression (or excitation) of the PVC. Accordingly, mixing induced by the PVC can be considered as a purely large-scale effect coming from the precessing motion. Due to the asymmetric nature of the PVC, its mixing may break the symmetry of equivalence ratio fluctuations, which might be a very effective mechanism to suppress thermoacoustic instability of partially premixed flames.

Flame Shape and Flame Dynamics. On the left-hand side of Fig. 8, the mean flame shape determined from Abel-deconvoluted

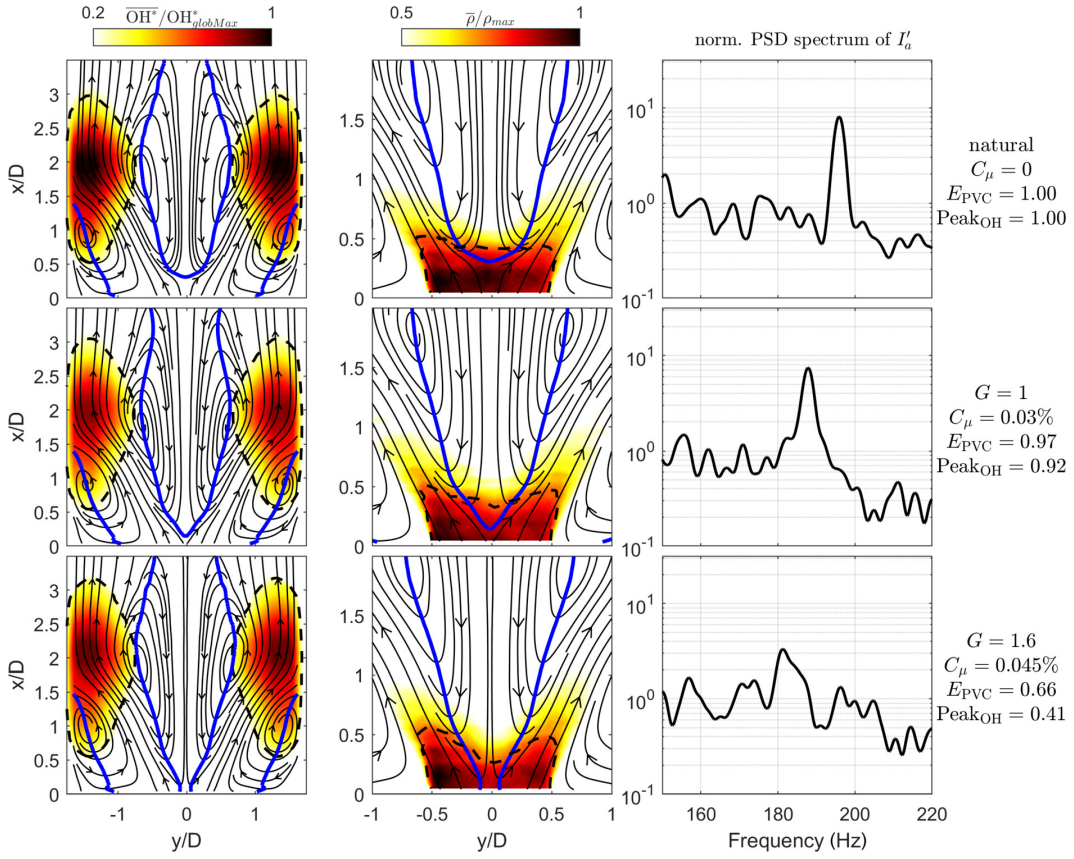

Fig. 8 Mean flame shape $\overline{OH^*}/OH^*_{globMax}$ with dashed isoline of $\overline{OH^*}/OH^*_{max} = 0.3$, mean density distribution $\overline{\rho}/\rho_{max}$ with dashed isoline of $\overline{\rho}/\rho_{max} = 0.75$ and PSD spectrum of antisymmetric OH*-fluctuations I'_a normalized by its mean noise level. Top row: natural case, middle row: low gain ($C_\mu = 0.03\%$), bottom row: high gain ($C_\mu = 0.045\%$).

OH*-chemiluminescence signals is presented for the natural (top row) and the controlled (middle and bottom row) cases. All cases show a M-shaped flame that is detached from the combustor inlet. When the control is applied, the heat release rate maximum is considerably reduced. Furthermore, the flame is elongated, which agrees with the changes in the mean flow and the corresponding shear layers (compare the dashed isolines). Therefore, the flame appears dispersed when the PVC is suppressed.

The density distribution of the natural case can be seen in the top frame of the middle column. It is almost constant in radial direction for $x/D \leq 0.5$ around the burner outlet (compare the dashed isoline). In the LSA investigation of Oberleithner et al. [3], it was shown that such a density distribution does not have a stabilizing effect on the PVC, meaning that the globally unstable nature of the PVC is maintained.

The changes in the mean flow, induced by the PVC suppression, influence the density distribution as well (compare the dashed isolines). As mentioned before, the control reduces the precessing motion of the recirculation bubble, and hence, the recirculating flow reaches further upstream. Furthermore, due to the suppressed precessing motion near the burner outlet, the flame is stabilized regarding its radial deflection, as well. Therefore, hot burnt gas is transported far more upstream inside the elongated IRZ. This leads to a radial density gradient near the burner outlet, which has a destabilizing influence on the PVC. This is plausible since the closed-loop control effectively shifts the PVC dynamics from its stable limit-cycle toward its unstable fixed point.

The right column in Fig. 8 shows the PSD spectra of the antisymmetric OH*-fluctuations I'_a. In the top spectrum, a distinct peak at 196 Hz is visible, which is equal to the natural frequency of the PVC. With the phase-opposition control applied, these PVC-induced flame fluctuations are gradually suppressed, as shown in the remaining two spectra. The peak at the PVC frequency in the depicted spectra is reduced by 8% for the low and by 59% for the high actuation gain. This declining trend is similar to the decrease of the PVC energy (E_{PVC}).

Conclusion

This study presents a novel phase-opposition flow control system, which is capable of controlling the PVC under harsh operating conditions including a high level of turbulence and combustion. The applied control approach is based on results from linear hydrodynamic stability analysis (LSA), which predict the central flow region within the combustor inlet as the most sensitive region for flow control. Therefore, the actuator is implemented in a centerbody geometry, which allows to control the PVC very accurately using low actuation amplitudes of less than $C_\mu \leq 0.05\%$. This work shows that the flow control system can be used to reduce the PVC amplitude significantly (85% peak reduction, 34% PVC energy reduction) without changing the overall characteristics of the flow and the flame. Accordingly, this system can be used as an experimental tool to investigate the influence of the PVC on important flow and combustion properties.

Within this work, this unique experimental arrangement was used to investigate the influence of the PVC on the mean flow and flame as well as flow and flame dynamics and mixing. The following conclusions can be drawn based on these results:

(1) The suppression of the PVC leads to an elongation of the mean central recirculation bubble due to the reduced precession motion of its upstream stagnation point. Possible influence on flame flashback is to be investigated further.
(2) The suppression of the PVC has no significant influence on small-scale mixing.
(3) The PVC mainly affects large-scale mixing, which is effectively controlled by the current technique.
(4) The suppression of the PVC allows other coherent fluctuations to arise, which impacts the large-scale mixing and may influence the growth of thermoacoustic modes.
(5) The PVC-induced flame fluctuations are suppressed by the control, which changes the mean flame shape as well.

These results point out some important topics, which need to be further investigated in future studies. First, there is the influence of the PVC on mixing. To study mixing processes in detail, appropriated measurement techniques, such as acetone-PLIF (Planar Laser Induced Fluorescence), need to be applied [14]. It is assumed that thermoacoustic oscillations may be damped by an actuated PVC because of mixing enhancement under partially premixed conditions [16]. In this connection, the interaction of PVC modes ($m = 1$) and axisymmetric thermoacoustic modes ($m = 0$) needs to be investigated. Regarding this, LSA tools need to be employed to clarify whether the PVC really changes the mean flow in a way that the growth rate of thermoacoustic modes can be influenced considerably [10,11]. With the help of the flow control system presented here, a new experimental opportunity is available to tackle open question regarding these phenomena.

Acknowledgment

We would like to thank the Deutsche Forschungsgemeinschaft (DFG) for funding this work within the project OB 402/4-3 (project number: 247226395). Special thanks go out to Andy Göhrs and Robert Bahnweg for their technical support and Alexander Jaeschke for supporting the experimental procedure.

Funding Data

- German Research Foundation (DFG) (OB 402/4-3, Project No. 247226395; Funder ID: 10.13039/501100001659).

Nomenclature

a_i = SPOD coefficients
C_μ = momentum coefficient of actuator
D = nozzle diameter
D_h = hydraulic diameter of the nozzle
E_{PVC} = PVC energy from SPOD time-coefficient spectrum
G = control gain
I = global heat release rate
IRZ = inner recirculation zone
LSA = linear hydrodynamic stability analysis
m = azimuthal mode number
P_{PVC} = PVC energy from $\hat{p}_1$ pressure spectrum
PIV = particle image velocimetry
PVC = precessing vortex core
QLS = quantitative light sheet method
Re = Reynolds number
RMS = root-mean-square
SPOD = spectral proper orthogonal decomposition
St = Strouhal number
TKE = turbulent kinetic energy
(u, v) = axial and radial velocity component
(x, y) = axial and radial coordinate
$\Delta\phi$ = control phase shift
λ = microscale
Φ_i = spatial mode
ρ = fluid density
$(.)'$ = fluctuating part
$(.)''$ = stochastic part
$\overline{(.)}$ = time average
$\tilde{(\cdot)}$ = coherent part

References

[1] Syred, N., 2006, "A Review of Oscillation Mechanisms and the Role of the Precessing Vortex Core (PVC) in Swirl Combustion Systems," Prog. Energy Combust. Sci., **32**(2), pp. 93–161.
[2] Petz, C., Hege, H.-C., Oberleithner, K., Sieber, M., Nayeri, C. N., Paschereit, C. O., Wygnanski, I., and Noack, B. R., 2011, "Global Modes in a Swirling Jet Undergoing Vortex Breakdown," Phys. Fluids, **23**(9), p. 091102.

[3] Oberleithner, K., Terhaar, S., Rukes, L., and Paschereit, C. O., 2013, "Why Nonuniform Density Suppresses the Precessing Vortex Core," ASME J. Eng. Gas Turbines Power, **135**(12), p. 121506.
[4] Terhaar, S., Oberleithner, K., and Paschereit, C., 2015, "Key Parameters Governing the Precessing Vortex Core in Reacting Flows: An Experimental and Analytical Study," Proc. Combust. Inst., **35**(3), pp. 3347–3354.
[5] Oberleithner, K., Stöhr, M., Im, S. H., Arndt, C. M., and Steinbergb, A. M., 2015, "Formation and Flame-Induced Suppression of the Precessing Vortex Core in a Swirl Combustor: Experiments and Linear Stability Analysis," Combust. Flame, **162**(8), pp. 3100–3114.
[6] An, Q., Kwong, W. Y., Geraedts, B. D., and Steinberg, A. M., 2016, "Coupled Dynamics of Lift-Off and Precessing Vortex Core Formation in Swirl Flames," Combust. Flame, **168**, pp. 228–239.
[7] Stöhr, M., Oberleithner, K., Sieber, M., Yin, Z., and Meier, W., 2017, "Experimental Study of Transient Mechanisms of Bi-Stable Flame Shape Transitions in a Swirl Combustor," ASME Paper No. GT2017-65003.
[8] Terhaar, S., Ćosić, B., Paschereit, C., and Oberleithner, K., 2016, "Suppression and Excitation of the Precessing Vortex Core by Acoustic Velocity Fluctuations: An Experimental and Analytical Study," Combust. Flame, **172**, pp. 234–251.
[9] Ghani, A., Poinsot, T., Gicquel, L., and Müller, J.-D., 2016, "LES Study of Transverse Acoustic Instabilities in a Swirled Kerosene/Air Combustion Chamber," Flow, Turbul. Combust., **96**(1), pp. 207–226.
[10] Frederick, M., Manoharan, K., Dudash, J., Brubaker, B., Hemchandra, S., and O'Connor, J., 2018, "Impact of Precessing Vortex Core Dynamics on Shear Layer Response in a Swirling Jet," ASME J. Eng. Gas Turbines Power, **140**(6), p. 061503.
[11] Mathews, B., Hansford, S., and O'Connor, J., 2016, "Impact of Swirling Flow Structure on Shear Layer Vorticity Fluctuation Mechanisms," ASME Paper No. GT2016-56460.
[12] Moeck, J. P., Bourgouin, J.-F., Durox, D., Schuller, T., and Candel, S., 2012, "Nonlinear Interaction Between a Precessing Vortex Core and Acoustic Oscillations in a Turbulent Swirling Flame," Combust. Flame, **159**(8), pp. 2650–2668.
[13] Terhaar, S., Krüger, O., and Paschereit, C. O., 2014, "Flow Field and Flame Dynamics of Swirling Methane and Hydrogen Flames at Dry and Steam-Diluted Conditions," ASME J. Eng. Gas Turbines Power, **137**(4), p. 041503.
[14] Stöhr, M., Arndt, C., and Meier, W., 2015, "Transient Effects of Fuel-Air Mixing in a Partially-Premixed Turbulent Swirl Flame," Proc. Combust. Inst., **35**(3), pp. 3327–3335.
[15] Galley, D., Ducruix, S., Lacas, F., and Veynante, D., 2011, "Mixing and Stabilization Study of a Partially Premixed Swirling Flame Using Laser Induced Fluorescence," Combust. Flame, **158**(1), pp. 155–171.
[16] Lückoff, F., Sieber, M., and Oberleithner, K., 2018, "Open-Loop Control of the Precessing Vortex Core in a Swirl-Stabilized Combustor: Impact on Flame Shape and Flame Stability," ASME Paper No. GT2018-75472.
[17] Paredes, P., Terhaar, S., Oberleithner, K., Theofilis, V., and Paschereit, C. O., 2015, "Global and Local Hydrodynamic Stability Analysis as a Tool for Combustor Dynamics Modeling," ASME Paper No. GT2015-44173.
[18] Gallaire, F., Ruith, M., Meiburg, E., Chomaz, J.-M., and Huerre, P., 2006, "Spiral Vortex Breakdown as a Global Mode," J. Fluid Mech., **549**(1), pp. 71–80.
[19] Oberleithner, K., Sieber, M., Nayeri, C. N., Paschereit, C. O., Petz, C., Hege, H.-C., Noack, B. R., and Wygnanski, I., 2011, "Three-Dimensional Coherent Structures in a Swirling Jet Undergoing Vortex Breakdown: Stability Analysis and Empirical Mode Construction," J. Fluid Mech., **679**, pp. 383–414.
[20] Qadri, U. A., Mistry, D., and Juniper, M. P., 2013, "Structural Sensitivity of Spiral Vortex Breakdown," J. Fluid Mech., **720**, pp. 558–581.
[21] Tammisola, O., and Juniper, M., 2016, "Coherent Structures in a Swirl Injector at Re = 4800 by Nonlinear Simulations and Linear Global Modes," J. Fluid Mech., **792**, pp. 620–657.
[22] Kaiser, T. L., Poinsot, T., and Oberleithner, K., 2018, "Stability and Sensitivity Analysis of Hydrodynamic Instabilities in Industrial Swirled Injection Systems," ASME J. Eng. Gas Turbines Power, **140**(5), p. 051506.
[23] Rukes, L., Paschereit, C. O., and Oberleithner, K., 2016, "An Assessment of Turbulence Models for Linear Hydrodynamic Stability Analysis of Strongly Swirling Jets," Eur. J. Mech. B, **59**, pp. 205–218.
[24] Müler, J. S., Lückoff, F., and Oberleithner, K., 2018, "Guiding Actuator Designs for Active Flow Control of the Precessing Vortex Core by Adjoint Linear Stability Analysis," ASME J. Eng. Gas Turbines Power, **141**(4), p. 041028.
[25] Kuhn, P., Moeck, J. P., Paschereit, C. O., and Oberleithner, K., 2016, "Control of the Precessing Vortex Core by Open and Closed-Loop Forcing in the Jet Core," ASME Paper No. GT2016-57686.
[26] Lückoff, F., Sieber, M., Paschereit, C. O., and Oberleithner, K., 2017, "Characterization of Different Actuator Designs for the Control of the Precessing Vortex Core in a Swirl-Stabilized Combustor," ASME J. Eng. Gas Turbines Power, **140**(4), p. 041503.
[27] Sieber, M., Paschereit, C. O., and Oberleithner, K., 2016, "Spectral Proper Orthogonal Decomposition," J. Fluid Mech., **792**(4), pp. 798–828.
[28] Sieber, M., Paschereit, C. O., and Oberleithner, K., 2016, "Advanced Identification of Coherent Structures in Swirl-Stabilized Combustors," ASME J. Eng. Gas Turbines Power, **139**(2), p. 021503.
[29] Göckeler, K., Terhaar, S., and Oliver Paschereit, C., 2013, "Residence Time Distribution in a Swirling Flow at Nonreacting, Reacting, and Steam-Diluted Conditions," ASME. J. Eng. Gas Turbines Power., **136**(4), p. 041505.
[30] Hussain, A. K. M. F., and Reynolds, W. C., 1970, "The Mechanics of an Organized Wave in Turbulent Shear Flow," J. Fluid Mech., **41**(2), pp. 241–258.
[31] Taylor, G. I., 1935, "Statistical Theory of Turbulence," Proc. R. Soc. London A, **151**(873), pp. 421–444.
[32] Leuckel, W., 1967, "Swirl Intensities, Swirl Types and Energy Losses of Different Swirl Generating Devices," International Flame Research Foundation, Ijmuiden, The Netherlands, Report No. G02/a/16.
[33] Soria, J., 1996, "An Investigation of the Near Wake of a Circular Cylinder Using a Video-Based Digital Cross-Correlation Particle Image Velocimetry Technique," Exp. Therm. Fluid Sci., **12**(2), pp. 221–233.
[34] Huang, H. T., Fiedler, H. E., and Wang, J. J., 1993, "Limitation and Improvement of PIV," Exp. Fluids, **15**(4–5), pp. 263–273.
[35] Brunton, S. L., and Noack, B. R., 2015, "Closed-Loop Turbulence Control: Progress and Challenges," Appl. Mech. Rev., **67**(5), p. 050801.
[36] Greenblatt, D., and Wygnanski, I. J., 2000, "The Control of Flow Separation by Periodic Excitation," Prog. Aerosp. Sci., **36**(7), pp. 487–545.
[37] Holmes, P., Lumley, J. L., and Berkooz, G., 1998, *Turbulence, Coherent Structures, Dynamical Systems and Symmetry*, Cambridge University Press, Cambridge, UK.
[38] Findeisen, J., Gnirß, M., Damaschke, N., Schiffer, H., and Tropea, C., 2005, "2D-Oncentration Measurements Based on Mie Scattering Using a Commercial PIV System," Sixth International Symposium on Particle Image Velocimetry, Pasadena, CA, pp. 21–23.
[39] Freund, O., and Rehder, H. J., Philipp, S., and Roehle, I., 2011, "Experimental Investigations on Cooling Air Ejection at a Straight Turbine Cascade Using PIV and QLS," ASME Paper No. GT2011-45296.
[40] Oberleithner, K., Paschereit, C. O., and Wygnanski, I., 2014, "On the Impact of Swirl on the Growth of Coherent Structures," J. Fluid Mech., **741**(2), pp. 156–199.

2.4 Publication IV

Impact of the Precessing Vortex Core on NO_x Emissions in Premixed Swirl-Stabilized Flames - an Experimental Study

The previous publications (2.1 to 2.3) have demonstrated that the actuation system allows to actuate a PVC such that its role in the context of swirl-stabilized combustion can be studied in a targeted way. To further investigate the impact of the PVC on important combustion properties, the actuation system is rearranged such that open-loop control of the PVC can be conducted in the following studies. A very important property of a combustion system is the amount of NO_x emissions during the combustion process. The role of the PVC in context of NO_x emissions of different types of premixed swirl-stabilized flames is elucidated based on the results shown in this publication.

At the beginning, a detailed characterization of the flow dynamics is given which are related to the changes in the mean flame shape with growing PVC actuation amplitude. The derived findings are utilized in connection with phase-resolved depictions of the PVC-induced vortex-flame interaction to explain the observed increase of the NO_x emission level with growing PVC amplitude.

Finn Lückoff[1]
Laboratory for Flow Instabilities and Dynamics,
Institute of Fluid Mechanics and Technical Acoustics,
Technische Universität Berlin,
Müller-Breslau-Str. 8,
Berlin 10623, Germany
e-mail: finn.lueckoff@tu-berlin.de

Moritz Sieber
Laboratory for Flow Instabilities and Dynamics,
Institute of Fluid Mechanics and Technical Acoustics,
Technische Universität Berlin,
Müller-Breslau-Str. 8,
Berlin 10623, Germany

Christian Oliver Paschereit
Chair of Fluid Dynamics,
Institute of Fluid Mechanics and Technical Acoustics,
Technische Universität Berlin,
Müller-Breslau-Str. 8,
Berlin 10623, Germany

Kilian Oberleithner
Laboratory for Flow Instabilities and Dynamics,
Institute of Fluid Mechanics and Technical Acoustics,
Technische Universität Berlin,
Müller-Breslau-Str. 8,
Berlin 10623, Germany

Impact of the Precessing Vortex Core on NO_x Emissions in Premixed Swirl-Stabilized Flames—An Experimental Study

The reduction of NO_x emissions remains a driving factor in the design process of swirl-stabilized combustion systems, to meet legislative restrictions. In reacting swirl flows, hydrodynamic coherent structures, such as periodic large-scale vortices in the shear layer, induce zones with increased heat release rate fluctuations in connection with temperature peaks, which lead to an increase of NO_x emissions. Such large-scale vortices can be induced by the helical coherent structure known as precessing vortex core (PVC), which influences the flow and flame dynamics under certain operating conditions. We developed an active flow control system, allowing for a targeted actuation of the PVC, to investigate its impact on combustion properties such as NO_x emissions. In this work, a perfectly premixed flame, which slightly damps the PVC, is studied in detail. Since the PVC is slightly damped, it can be precisely excited by means of open-loop flow control. In connection with time-resolved OH-chemiluminescence and stereoscopic particle image velocimetry (PIV) measurements, the impact of the actuated PVC on flow and flame dynamics is characterized. It turns out that the PVC rolls up the inner shear layer, which results in an interaction of PVC-induced vortices and flame. This interaction considerably influences the measured level of NO_x emissions, which grows with increasing PVC amplitude in a perfectly premixed flame. Nearly, the same increase is measured for partially premixed conditions. This is in contrast to previous studies, where the PVC is assumed to reduce the NO_x emissions due to vortex-enhanced mixing.*
[DOI: 10.1115/1.4048603]

Keywords: precessing vortex core (PVC), active flow control, NO_x emissions, vortex-flame interaction, finite time Lyapunov exponent (FTLE)

Introduction

The application of highly turbulent swirl flows in modern gas turbine combustors provides many advantages such as low pollutant emissions or aerodynamic flame stabilization. Due to the phenomenon called vortex breakdown, favorable flow conditions are provided for the flame to stabilize in the combustor flow field. This flow field typically contains a central recirculation zone (CRZ) around the central axis of the combustor, which generates an inner shear layer (ISL) between jet and CRZ. Moreover, an outer shear layer (OSL) is formed due to the jump in cross section from nozzle outlet to the combustion chamber. Previous studies have shown that, in particular, the ISL may give rise to a global hydrodynamic instability referred to as precessing vortex core (PVC) [1,2]. In the flow field, the PVC manifests as a single helical-shaped coherent structure of oscillatory nature, which meanders downstream along the ISL [3]. Strictly speaking, a precessing vortex core solely describes the azimuthal motion of the rotation center of the swirl flow, which may be synchronized with the single-helical coherent structure in the ISL and OSL. However, in the course of this work, the term "PVC" represents the global mode combining both features, which can be seen as cause and effect.

Generally, a PVC is present in isothermal swirling jets, whereas in reacting flows, the density stratification, defined by the flame shape, decides whether a PVC occurs or not [4–6]. Although the PVC may be damped by the flame, its characteristic stability mode can be resolved by means of linear hydrodynamic stability analysis (LSA). Apart from the spatial shape of this mode, the LSA is capable of quantitatively predicting the characteristic frequency and growth rate of coherent structures such as the PVC [1,4–14]. Furthermore, this type of mean field stability analysis can be used to estimate the receptivity of the global stability mode, describing the PVC, to open-loop forcing. In this context, the spatial distribution of the receptivity reveals where in the flow field the influence of external periodic actuation on the global mode is maximal [9,10,13–16]. Global stability analyses conducted on industrial swirling flow injectors showed that the receptivity of the PVC mode reaches its maximum upstream of the CRZ close to the nozzle outlet [10,11].

Based on the information provided by LSA, a novel active flow control concept has been developed, which targets direct control of the PVC [14,17]. This idea has been transferred from a generic isothermal experimental setup, to a swirl stabilized burner to investigate reacting flows [18]. The corresponding actuator achieves direct control by applying single-helical actuation in the region of highest receptivity. It has been shown that this actuation system is capable of exciting a PVC at operating conditions where it is naturally damped by the flame [19]. Moreover, this actuation system manages to suppress the PVC by means of closed-loop control in a reacting flow, where a PVC is naturally present [20]. Since the actuation acts in the region of highest receptivity of the PVC, only a minimal energy input is required to obtain a maximal control effect.

With the successfully tested active flow control system at hand, the PVC can be controlled independently from all other flame and flow conditions, which facilitates unique experimental opportunities. This allows for investigation of the exclusive impact of the PVC on combustion properties such as thermoacoustic oscillation [19], flame dynamics [20], or pollutant emissions.

[1]Corresponding author.
Manuscript received August 26, 2020; final manuscript received September 14, 2020; published online October 26, 2020. Editor: Jerzy T. Sawicki.

Previous studies have shown that the strong velocity fluctuations induced by the PVC near the burner outlet enhance the mixing of fuel and air [21–23]. Therefore, it appears plausible that the PVC can be helpful in reducing the amount of pollutant emissions such as NO_x because a better mixing of fuel and air typically results in lower emissions [24,25]. However, a different aspect accompanied by a dominant coherent structure such as the PVC, needs to be considered, which is vortex–flame interaction [26]. The vortices induced by the PVC may roll up the flame such that fresh reactants are transported into burning regions, while the flame surface area is increased rapidly, leading to a heat release pulse [27,28]. When these vortices collide with the combustion chamber wall, a rapid burning of the entrained reactants produces a heat release pulse. The NO_x emission level depends exponentially on temperature. Therefore, a small increase in temperature, resulting from a vortex-induced heat release pulse, may lead to an increase in the NO_x emission level. This effect can be observed in thermoacoustically unstable flames, where the Kelvin–Helmholtz-instability lead to roll-up of symmetric vortices [29,30].

The goal of this study is to investigate the impact of the PVC on the NO_x emission level in perfectly and partially premixed flames. With the novel active flow control system, appropriate experimental conditions are generated for a targeted characterization of the PVC impact on the flame and the flow field, which is related to the estimated NO_x emissions. For this purpose, stable premixed flames are studied in which the PVC is naturally damped. This allows for excitation of the PVC at arbitrary amplitude with open-loop control such that a parameter study can be conducted from which the PVC impact can be deduced.

The flow and flame dynamics are measured by means of time-resolved stereoscopic particle image velocimetry (PIV) and OH^*-chemiluminescence imaging. To analyze the corresponding snapshots, spectral proper orthogonal decomposition (SPOD) [31], the finite time Lyapunov exponent (FTLE), [32] and tomographic reconstruction [33] are applied. Above this, the NO_x emissions are measured in the exhaust gas.

The structure of this work is the following: At first, the experimental setup is presented, which includes descriptions of the flow control actuation system as well as the applied measurement techniques. Secondly, the applied advanced data analysis methodologies are briefly introduced. The following results chapter starts with the characterization of the reacting baseline flow, which is investigated further regarding flow and flame response to PVC actuation. This highlights the capability of the actuation system to excite a PVC in a flame, where it is naturally damped. By exciting a PVC with different amplitudes, its effects on the mean flow and flame are revealed. Subsequently, the interaction of PVC-induced vortices with the flame is characterized, which explains the correlation between PVC amplitude and NO_x emissions. The identified mechanisms and effects are summarized in the concluding section.

Experimental Setup

In this section, design and functionality of the burner and actuator are described in connection with the applied measurement techniques. Moreover, the applied operating conditions are given.

Burner and Actuator Design. The experiments in this study are conducted with a combustor (see Fig. 1), which consists of a radial swirl generator, a silica glass combustion chamber (200 mm diameter, 300 mm length) and an annular mixing tube duct (outlet diameter $D = 55$ mm). Inside the mixing tube, a centerbody (maximal diameter $D_{CB} = 35$ mm) is mounted, which yields a hydraulic diameter of $D_h = D - D_{CB} = 20$ mm. The parabolic shape of the centerbody avoids the formation of an unwanted wake flow, which may interfere with mode dynamics in the combustion chamber flow field. The pressure sensors, which are arranged circumferentially around the burner outlet, serve as monitoring system for the PVC and other dynamics occurring during the experiments. These

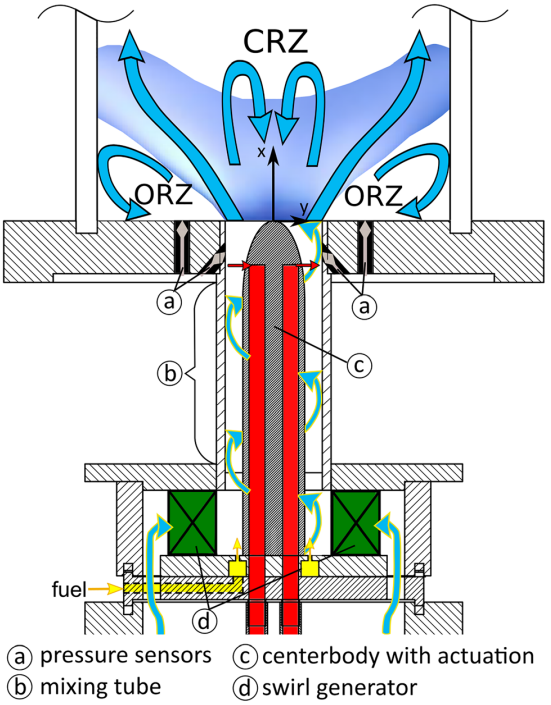

Fig. 1 Sketch of the burner with PVC actuation indicated by the small arrows at the outlets of the actuation channels

data can be used to characterize, for example, the PVC dynamics, as it was done, for example, in Refs. [18–20].

The centerbody contains four independent actuation channels with rectangular outlets (9×1 mm^2 cross section), which are arranged around the circumference, 25 mm upstream of the centerbody tip. From these outlets, actuation jets emanate in the region where previous studies reported highest sensitivity of the PVC mode [10,13,14]. These jets are generated by four individual loudspeaker (5 in. diameter, rated power of 100 W), which are each connected to one of the actuation channels. This actuator design works as a zero-net-mass-flux actuator allowing for helical actuation of the PVC by driving the loudspeakers with harmonic signals, which have a phase-shift of $\pi/2$ relative to one another. The actuator efficiency is measured by the momentum of the actuation jets related to the momentum of the main flow. This ratio is expressed as the momentum coefficient [34], $C_\mu = G u_{RMS}^2/(V_0^2 A_h)$, where u_{RMS} is the root-mean-square (RMS)-velocity at the actuator outlet, measured with a hot-wire anemometer without main airflow [18], G the area of a single actuator outlet, A_h the hydraulic cross section area (based on D_h), and V_0 the bulk velocity of the main flow. In previous studies, it was shown that this actuator can be used for open-loop control [18,19] to actuate a PVC and phase-opposition control to achieve damping of the PVC limit cycle [20]. These demanding experimental studies have shown that this control concept achieves clean and direct control of the PVC.

Applied Measurement Techniques. A water-cooled exhaust gas sampling probe is inserted into the exhaust tube, downstream of the combustion chamber, to allow for NO_x emission measurements. The cylindrical double-walled probe (10 mm outer diameter) contains an inner tube (4 mm diameter), which contains the sampling gas sucked through a 1 mm sampling orifice. This orifice is aligned to the centerline of the exhaust tube. The sampling probe is connected via a heated sample line (190 °C) to the gas

analyzer which allows for NO_x measurements on a wet basis within the subsequent chemiluminescence detector (KNESTEL CLD dual BASIC). In the wet sample line, a nondispersive infrared sensor measures CO_2 and water content to account for chemiluminescent quenching inside the CLD reaction chamber. The CLD was calibrated to a measurement range between 0 and 100 ppm using a calibration gas with a concentration of 100 ppm NO in N_2. In a parallel line, a dried gas sample is utilized in order to measure the O_2, H_2 and CO_2 content by means of a paramagnetic sensor (ABB Magnos 106, Zürich, Switzerland), a thermal conductivity sensor (ABB Caldos 27), and an nondispersive infrared sensor (ABB Uras 14), respectively. The sample gas, for both the wet and dry lines, is sucked in by gas vacuum pumps at a constant volumetric flow rate of 7.2 l/h and 60 l/h, respectively. To generate reliable mean NO_x emission values, an overall measurement time of 150 s was chosen per measurement point. This time period is divided into an initial phase (50 s), where the actuator is already running, and an effective measurement phase (100 s), where NO_x emission data are acquired with 10 Hz sampling frequency. The initial phase was necessary to account for the time delay between the changed PVC actuation condition and the arrival of the corresponding exhaust gas sample in the NO_x analyzer. The long measurement phase was chosen to obtain converged and reliable mean values.

The three components of the velocity field were measured with stereoscopic high-speed PIV at a recording rate of 2500 fps. This measurement system consists of a Nd:YLF diode pumped laser (Quantronix (Hamden, CT) Darwin Duo 527-100 M, 527 nm wavelength and total pulse energy of 60 mJ), which is synchronized with two high-speed CMOS cameras (1024 × 1024 pixels image resolution). One high-speed camera (Photron (Tokyo, Japan) SA-Z) of the measurement system was mounted perpendicular to the streamwise field of view. The second camera (Photron SA 1.1) was mounted with an angle of 40 deg to the measurement plane, due to geometrical restrictions. Moreover, this camera was equipped with a Scheimpflug adapter. To allow for an accurate estimation of the out-of-plane velocity component, a multilevel calibration target is utilized to calibrate the two camera views appropriately. A light sheet optic generates an appropriate light sheet of approximately 1 mm thickness in the measurement area. Heat-resistant solid titanium dioxide (TiO_2) seeding particles of a nominal diameter of 2 μm were introduced to the flow far upstream of the burner using a brush-based seeding generator. To evaluate the acquired particle snapshots, a commercial PIV software (PIVTEC GmbH (Göttingen, Germany), PIVview) was used applying a correlation scheme with multigrid refinement [35]. The final window size was set to 16 × 16 pixels with an overlap of 50% in combination with spline-based image deformation [36] and subpixel peak fitting. Finally, the estimated velocity field data were filtered for outliers and interpolated from adjacent interrogation windows.

Time-resolved OH^*-chemiluminescence measurements were conducted using an intensified high-speed CMOS camera (Photron SA 1.1) in combination with a high-speed intensifier (Lambert Instruments (Groningen, Netherlands) HiCATT 25) with 1024 × 1024 pixels image resolution and a recording rate of 2500 fps. Furthermore, this camera setup is equipped with a 308 nm optical bandpass filter to record only OH^*-chemiluminescence.

Moreover, a photomultiplier (PMT), equipped with a 308 nm bandpass filter, is used to capture half of the OH^*-chemiluminescence emitted by the flame, in a vertical plane, on one side of the burner axis. This is achieved by focusing the field of view of the photomultiplier, by means of a collimator, on only one half of the combustion chamber (compare Fig. 2). With this method, the antisymmetric (with respect to the combustor symmetry) global heat release rate fluctuations, induced by the PVC, are captured [37].

Operating Conditions. The reacting flow investigated in this study is generated by a premixed natural gas–air mixture with an inlet temperature of 298 K burning at an equivalence ration of 0.65. The corresponding air mass flow was set to 140 kg/h, yielding a Reynolds number, based on D_h, of 30,000 and a thermal power of 67 kW. The swirl generator was adjusted to a fixed swirl number, defined as the ratio of the axial flux of tangential momentum to the axial flux of axial momentum, of $S = 0.7$ [38]. All the experimental results presented in this study are obtained from measurements of a perfectly premixed flame, where the fuel is injected far upstream of the burner. Only the NO_x emissions, presented at the end, include results from measurements of a partially premixed flame, where the fuel is axially injected at the swirl generator (compare Figs. 1 and 2). All the other operating conditions were kept constant.

Data Analysis Methodology

In this section, three advanced methods are explained, which are used to postprocess the time-resolved velocity fields, measured

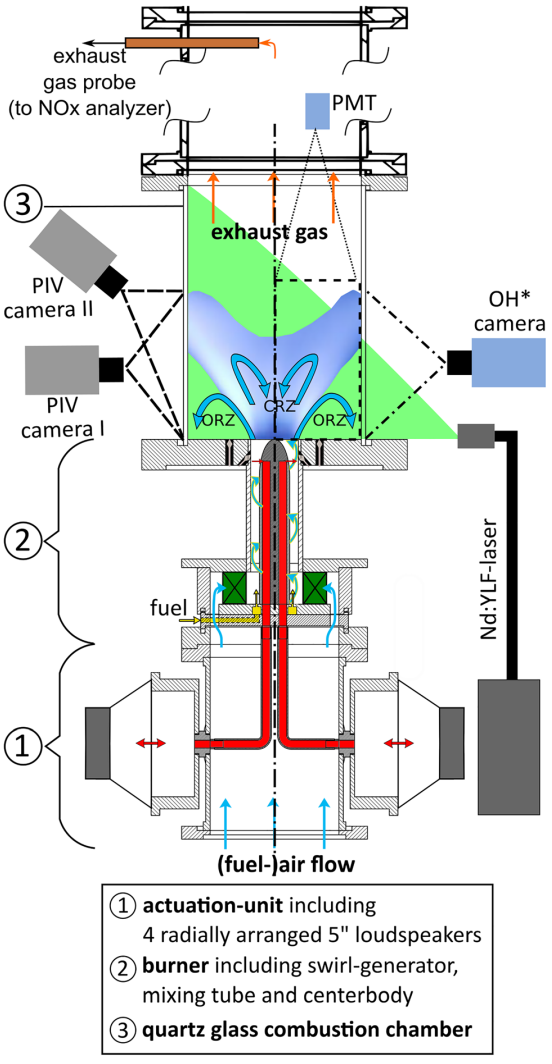

Fig. 2 Experimental setup including actuation system as well as applied measurement techniques: stereoscopic PIV, OH^*-chemiluminescence (PMT and high-speed camera) and NO_x analyzer probe

with stereoscopic PIV, as well as the OH*-chemiluminescence snapshots.

Spectral Proper Orthogonal Decomposition. With the help of the recently developed SPOD, coherent structures, such as the PVC, can be extracted from time-resolved flow field data [39]. Compared to the classical proper orthogonal decomposition (POD) [40], on which the SPOD is based, it provides enhanced selectivity. Especially in complex turbulent flows, like the reacting combustor flows investigated in this study, SPOD reveals the inherent coherent structures very distinctly [41].

In the following, a very brief overview of the SPOD approach is given. For a more detailed derivation, the reader is referred to the work of Sieber et al. [39]. SPOD provides a modal decomposition of the fluctuating part of the velocity $\mathbf{v}'$ that reads as follows:

$$\mathbf{v}(\mathbf{x},t) = \overline{\mathbf{v}}(\mathbf{x}) + \mathbf{v}'(\mathbf{x},t) = \overline{\mathbf{v}}(\mathbf{x}) + \sum_{i=1}^{N} a_i(t)\Phi_i(\mathbf{x}) \tag{1}$$

According to Eq. (1), the velocity fluctuations are decomposed into a sum of spatial modes Φ_i and corresponding time-dependent coefficients a_i. This basis is built from the calculated spatial correlation among the individual PIV snapshots. This calculation results in a corresponding correlation matrix which is, unlike the classical POD, filtered by a Gaussian low-pass filter. Due to the filtering of the correlation matrix, the mode shapes and dynamics, describing the coherent flow structures, can be extracted very precisely.

The dynamics of each spatial mode are characterized by a corresponding set of temporal coefficients $a_i(t)$. These coefficients are derived from the eigenvectors of the filtered correlation matrix. By projecting the snapshots onto the temporal coefficients, the corresponding spatial modes $\Phi_i(\mathbf{x})$ are finally obtained.

Finite Time Lyapunov Exponent. In this study, FTLE is used to visualize the vortex structures induced by the PVC. FTLE is a Lagrangian measure, which visualizes vortex structures by joint faces and reveals where fluid from different flow regions converge [32]. From a theoretical point of view, FTLE measures the divergence of path lines in the flow. These path lines can be calculated forward or backward in time. In this study, the backward time FTLE is used, which highlights repelling structures in the flow providing the vortex structures induced by the PVC as shown by Rukes et al. [42]. Time-resolved three-dimensional flow field data, which are phase-averaged in reference to the PVC oscillation, are used to reconstruct the time-resolved three-dimensional PVC structure as shown by Oberleithner et al. [8]. The reconstructed data are then used as an input for the FTLE calculations.

For the computation of the FTLE, the divergence of adjacent path lines is calculated with a fourth-order Runge–Kutta solver. The corresponding integration time was set to 1.5 periods of the PVC oscillation. The actual FTLE is derived from the distance of particles after the integration, that were initially close together. The FTLE is given by

$$\sigma = \frac{\log(d_0/d_\tau)}{\tau} \tag{2}$$

where d_0 is the initial distance and d_τ is the final distance before and after the integration time τ, respectively.

Tomographic Reconstruction of Precessing Vortex Core-Induced Flame Fluctuations. The recorded raw OH*-chemiluminescence images represent line-of-sight-integrated values. Therefore, appropriate tomographic reconstructions methods need to be applied to obtain planar representations of the flame. For the symmetric time-averaged heat release rate, a classic Abel-deconvolution is applied.

However, for the skew symmetric fluctuations, induced by the PVC, a more advanced tomographic reconstruction technique, developed by Moeck et al. [33], is employed. Conventional tomographic reconstruction techniques typically require several different camera views. This algorithm only requires a single camera view exploiting that the single-helical structure of the PVC rotates at a well-defined rate. Due to this characteristic property, a set of 36 phase-averaged projection images provide enough views to reconstruct the three dimensional structure of PVC-induced heat release fluctuations. The required phase-averaged images are calculated from time-resolved OH*-chemiluminescence snapshots of a single intensified high-speed camera (compare experimental setup).

Results

This section starts with the characterization of the reacting baseline flow, which is investigated further regarding flow and flame response to PVC actuation. Subsequently, the impact of the PVC on mean flow and flame and its role in vortex–flame interaction is revealed. Finally, the resulting effects of the PVC on the NO_x emissions are discussed.

Baseline Flow and Flame Characterization. The mean flow field depicted on the left of Fig. 3 shows typical features of a swirl flow containing a swirl-stabilized flame. Due to a high degree of swirl, the flow is undergoing vortex breakdown. As a result, a CRZ (dotted line) is formed around the jet axis, which causes a corresponding ISL between jet and CRZ. Above this, an OSL arises between jet and outer recirculation zone.

The described flow conditions allow for the stabilization of a V-shaped flame inside the ISL (Fig. 3 right). Close to the burner outlet, the resulting flame is attached to the centerbody tip. The strongest mean heat release rate is present in the upstream part of the flame ($x/D < 1$) and distributed along the ISL. Further downstream, the absolute heat release rate decreases because the flame is more dispersed and reaches into the outer recirculation zone. The mean flame ends where the jet reaches the combustor wall.

Previous studies have shown that no PVC is present in such a flame, because the density gradient at the combustor inlet suppresses the PVC [4,6,20]. This is in line with a global stability analysis conducted for this flame, which shows that the PVC mode is damped [43]. This damped PVC mode is found at a frequency of around 200.25 Hz (compare arrow in Fig. 4). Via open-loop flow control, this slightly damped PVC can be actuated [13].

Response of Flow and Flame to Precessing Vortex Core Actuation. The fact that the V-flame features a slightly damped PVC mode allows the PVC to be excited very efficiently. To verify this, a parametric study is conducted where the flow and flame response to open-loop PVC excitation is studied for various

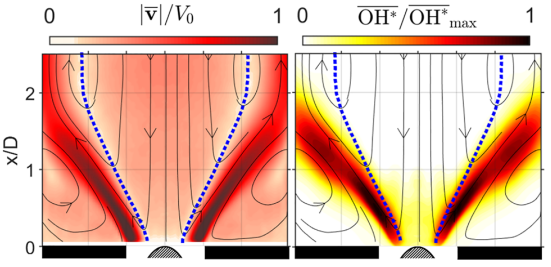

Fig. 3 Time-averaged flow field (absolute velocity $|\overline{\mathbf{v}}|$ normalized with bulk velocity) and flame shape (mean Abel-deconvoluted heat release rate $\overline{OH^*}$ normalized with maximal value) of the baseline case. The dotted line indicates the CRZ.

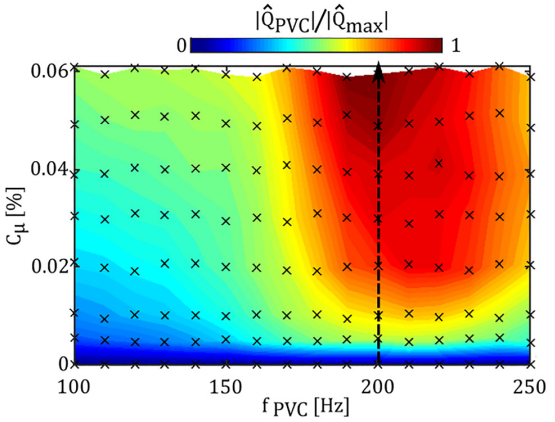

Fig. 4 Flame response to PVC actuation with different actuation frequencies (f_{PVC}) and amplitudes (C_μ) depicted by the amplitude of PVC-induced antisymmetric global heat release rate fluctuations $\hat{Q}_{PVC}$ (normalized by overall maximum)

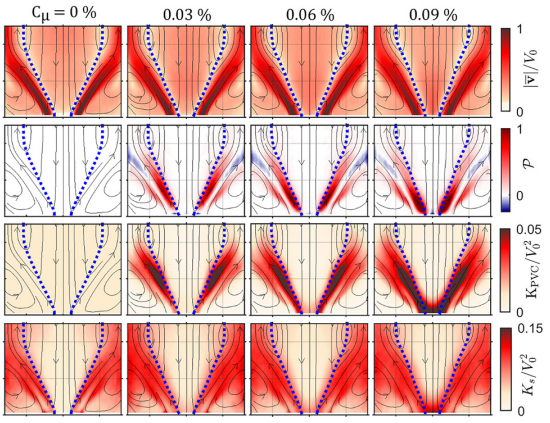

Fig. 6 Mean velocity magnitude (top) normalized with bulk velocity, production of PVC mode $\mathcal{P}$ (second row) normalized with respect to overall maximum, kinetic energy of PVC mode K_{PVC} (third row), and the kinetic energy of the stochastic flow fluctuations K_s (bottom) both normalized by the kinetic energy of the bulk flow; at different PVC actuation amplitudes

actuation amplitudes and frequencies. In the remainder of this study, the open-loop forcing is applied close to the estimated frequency of the PVC eigenmode.

The flame response is estimated from the PMT signals of one half of the flame (see experimental setup), which captures the heat release rate fluctuations induced by the (actuated) PVC. The flame response map depicted in Fig. 4 shows the amplitude $\hat{Q}_{PVC}$ describing the PVC-induced global heat release rate fluctuations for different excitation frequencies (f_{PVC}) and actuation amplitudes (C_μ). This map reveals that the highest response of the flame is registered at 200 Hz, which is very close to the frequency of the damped PVC mode as predicted from global LSA.

Figure 5 shows the flow response to the actuation applied at $f_{PVC} = 200$ Hz. It reveals the typical structure of the PVC mode, in close agreement with previous studies [4–6,11,13,20]. The mode shape does not change considerably with increasing C_μ, which indicates that the actuation does not introduce unwanted nonlinearities. The amplitude of the PVC mode grows constantly with increasing C_μ, which demonstrates that the actuation is capable of exciting a PVC of arbitrary amplitude.

Based on the findings discussed above, it can be concluded that the PVC actuation system (Figs. 1 and 2) applied in this work, is capable of exciting the PVC mode that is naturally suppressed by the V-flame. This excitation exploits the hydrodynamic stability of the flow, by targeting the PVC mode directly. Therefore, the actuation is very efficient and this can be illustrated by the fact that the PVC actuated with $C_\mu = 0.06\%$ contains 13.5% of the total turbulent kinetic energy. For the following investigations, the actuation frequency is fixed to the most responsive frequency of $f_{PVC} = 200$ Hz and only the amplitude C_μ is varied.

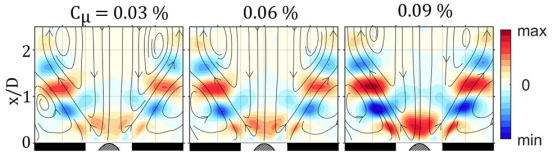

Fig. 5 Flow response to PVC actuation for $C_\mu = \{0.03; 0.06; 0.09\}$% and $f_{PVC} = 200$ Hz, depicted by the transverse velocity component of SPOD modes (normalized with overall maximum)

Influence of Precessing Vortex Core on Mean Flow and Flame. As shown in Fig. 6 (top row), the mean flow field is only slightly affected by the actuated PVC. With increasing actuation amplitude, the jet appears to be thicker, which is a result of a thickened shear layer as, for example, reported by Ref. [44].

In the second row of Fig. 6, the coherent production $\mathcal{P}$ is shown for different PVC actuation amplitudes. The production is defined as $\mathcal{P} = \overline{\tilde{v}_i \tilde{v}_j} \frac{\partial \bar{v}_i}{\partial x_j}$, where $\tilde{v}_i$ is the ith component of the velocity fluctuation of the PVC mode determined from SPOD. The coherent production $\mathcal{P}$ quantifies the energy flux between the mean field and the PVC and reveals where the PVC modifies the mean field. Accordingly, the PVC predominantly acts on the ISL in the vicinity of the burner outlet. In those regions where the coherent productions is high, the kinetic energy of the PVC (K_{PVC}) is high as well (compare middle rows in Fig. 6). The maximum of K_{PVC} is reached in the ISL and grows upstream to the burner outlet with increasing C_μ.

Besides the impact on coherent fluctuations, the impact of the PVC actuation on the remaining turbulent fluctuations needs to be considered. This is done in the bottom row of Fig. 6, where the spatial distribution of the stochastic turbulent kinetic energy

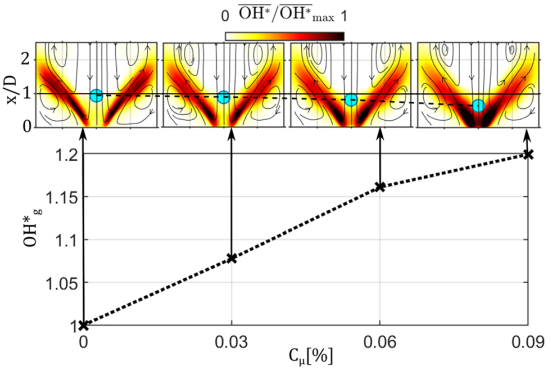

Fig. 7 Mean Abel-deconvoluted heat release rate $\overline{OH^*}$ (normalized with overall maximal value) with COM (dot in the center) at different PVC actuation amplitudes ($C_\mu = \{0; 0.03; 0.06; 0.09\}$%) (top) with corresponding global mean heat release rate of the region around the burner outlet ($x/D \leq 1$) (bottom)

(TKE) K_s is depicted, which describes the energy of all fluctuations except those induced by the PVC. With growing C_μ, no considerable increase of this energy K_s can be observed (mean increase of 6.3%). Only a slight broadening of the regions with considerable TKE can be seen. Therefore, it can be concluded that the actuation affects exclusively the dynamics of the PVC, but not the dynamics of the remaining turbulent fluctuations.

Next, the impact of the PVC actuation on the mean flame shape is discussed. Figure 7 shows mean flame shapes in the top row, which become more compact with increasing actuation amplitude. Moreover, regions of major heat release rate are concentrated more upstream with increasing C_μ. The dot on the jet axis shows the center of mass (COM) of the flame, which is calculated as follows:

$$\mathrm{COM} = \frac{\overline{\iint \overline{\mathrm{OH}^*}(x,y)xy\,\mathrm{d}x\mathrm{d}y}}{\overline{\iint \overline{\mathrm{OH}^*}(x,y)y\,\mathrm{d}x\mathrm{d}y}} \tag{3}$$

The COM serves as a measure of the flame position. Accordingly, the whole flame moves upstream with increasing C_μ. The graph in the lower diagram shows the global heat release rate of the upstream part ($x/D \leq 1$) of the flame. This value was estimated by summation of the OH^* signal weighted with the radius upstream of D. With increasing C_μ, the global heat release OH^*_g in the upstream region of the flame increases by 20%. In this region, $\mathcal{P}$ and K_{PVC} are high, which means that the PVC is predominantly interacting with the flame there. This interaction leads to PVC-enhanced flame surface wrinkling at the flame root, which increases the mean heat release rate near the burner outlet ($x/D \leq 1$). A more detailed analysis of PVC-induced flame wrinkling and its effect on $\mathrm{NO_x}$ emissions is given in the Precessing Vortex Core-Induced Vortex–Flame Interaction and Impact of Precessing Vortex Core on $\mathrm{NO_x}$ Emissions sections.

Precessing Vortex Core-Induced Vortex–Flame Interaction. Figure 8 shows how the PVC affects the flow and the flame over one period. These representations are based on three-dimensional

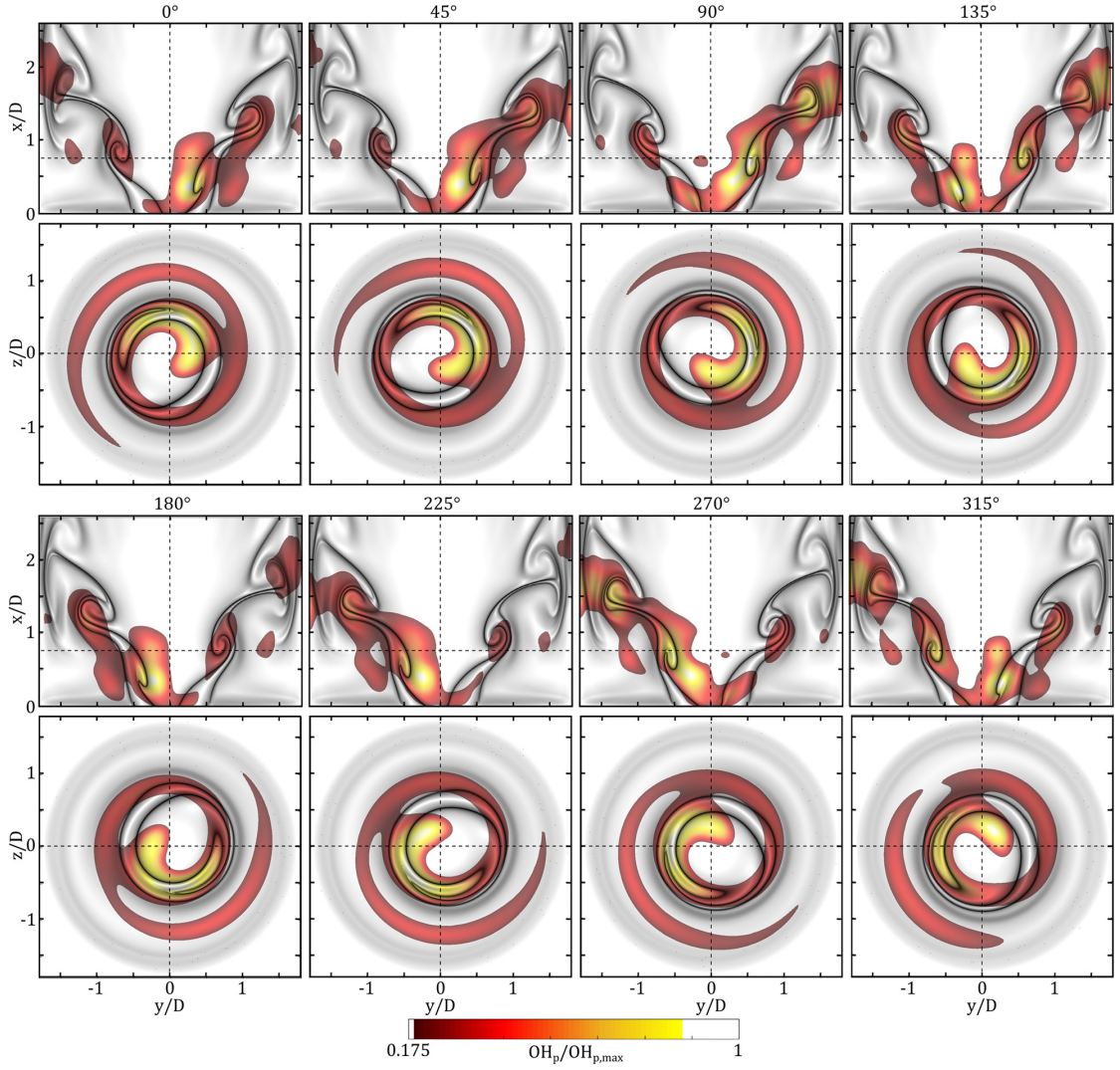

Fig. 8 Phase-averaged reconstructed flame shapes $\mathrm{OH_p}$ (normalized by the overall maximum) overlaid with the FTLE indicating the PVC-induced vortices for $C_\mu = 0.09\%$. The upper rows indicate longitudinal-section views (xy-plane) at $z = 0$, the corresponding lower rows show cross-sectional views (yz-plane) at $x/D = 0.75$.

reconstructed flow field and OH*-chemiluminescence data, which were phase-averaged in reference to the PVC oscillation. The FTLE, represented by the gray scale, is calculated to visualize the vortex pattern induced by the PVC. It is superimposed with the corresponding heat release rate fluctuations, which are the sum of the Abel-deconvoluted symmetric mean flame and the reconstructed heat release fluctuations induced by the PVC. The upper rows show a longitudinal section (xy-plane) at $z = 0$ with a horizontal line indicating $x/D = 0.75$. At this axial position, corresponding cross-sectional views (yz-plane) are presented below.

The FTLE in the xy-plane clearly indicates the vortex roll-up, which is typical for the Kelvin-Helmholtz instability. However, because of the helical shape of the PVC, alternating vortices are generated, which are connected to a helix. These vortices are convected downstream along the ISL before they collide with the combustor wall. In the cross-sectional views (yz-plane), the FTLE reveals the typical spiral pattern of the PVC, which meanders in a clockwise direction around the jet axis. Due to this pattern, the shear layer is rolled up in the azimuthal direction.

The PVC-induced vortices entrain hot burnt products from the CRZ into the jet that contains cold reactants. The entrained hot gas, containing free radicals, enhances the reaction and leads to ignition of the fresh incoming fuel–air mixture. The flame (indicated by OH_p) follows these helical vortices in the streamwise direction. As a consequence, the flame is deflected to either side of the ISL. When the antisymmetric flame patterns reach the wall, a strong interaction is evident, which results in elevated heat release rate [37]. In the crosswise section, the PVC generates a characteristic ying-yang heat release pattern, which follows the precessing motion of the PVC. This characteristic heat release pattern is a result of the considerable wrinkling of the flame, which occurs due to the PVC induced roll-up of the ISL [45,46]. As a consequence, spots of concentrated increased heat release rate, indicated by bright yellow regions, are generated. In the case of a partially premixed flame (not shown here), regions of increased (local) equivalence ratio can be formed due to the PVC induced roll-up of the ISL. The resulting PVC-induced vortex can contain a slightly richer, but still lean, fuel–air mixture, which will burn at higher temperature leading to local temperature peaks. Comparable observations have been made for axisymmetric vortex-flame roll-up due to acoustic perturbations [29,30].

The revealed PVC-induced flame wrinkling, in connection with vortex–flame interaction, explains the increase in mean heat release rate as shown in Fig. 7. The regions of concentrated heat release rate, revealed in Fig. 8, indicate a considerable impact of the PVC on the flame dynamics compared to the baseline case. The altered flame dynamics have a distinct impact on the NO_x emissions, which is discussed in the following.

Impact of Precessing Vortex Core on NO_x Emissions. The diagram in Fig. 9 shows the relative level of NO_x emissions for perfectly and partially premixed conditions as a function of PVC actuation amplitude. The plotted data reveal that the NO_x emissions increase up to 8% with increasing PVC actuation amplitude C_μ. This trend is observed independently of the premix mode for both, perfectly (pp) and technically/partially (tp) premixed conditions.

The similar increase of NO_x, independent of the premix mode, is surprising at first glance, since previous studies (e.g., Ref. [22]) report that the PVC leads to enhanced vortex-induced fuel–air mixing, which may decrease the NO_x emissions [25]. Comparing the burner setup in the work of Stöhr et al. [22] with the present design, one of the major differences is the degree of premixedness. In Ref. [22], fuel is injected close to the burner outlet (0.11 nozzle diameters upstream of burner outlet), leading to slightly partially premixed conditions [45]. However, in the present burner, fuel is injected at least three nozzle diameters upstream (partially premixed conditions) of the flame. Obviously, the partially premixed operating mode of the present setup provides

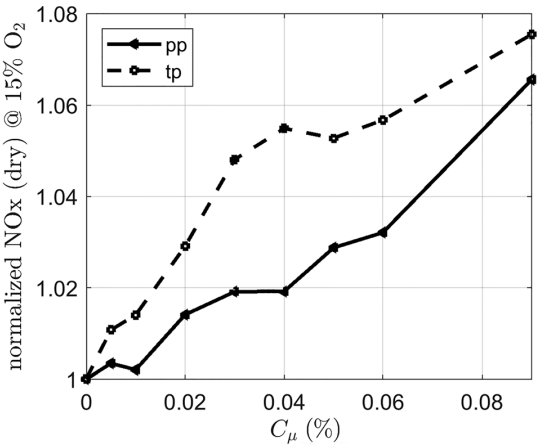

Fig. 9 NO_x emissions normalized with corresponding baseline value as a function of PVC amplitude

already a fairly premixed fuel–air mixture, which is confirmed by the study of Göke et al. [47]. Therefore, large-scale vortex-induced fuel–air mixing does not play a dominant role.

Besides the effect of the PVC on fuel–air mixing, there are other mechanisms that explain the observed increase of the NO_x emission observed in the current experiments. For example, the formation of NO_x emissions in flames can be related to different mechanisms originating from considerations of chemical reaction kinetics. These will be briefly introduced in the following in context of the present experimental setup.

To explain the NO_x formation mechanisms, previous studies are considered that comprehensively characterize the present burner regarding mixing quality and NO_x emissions [47,48]. Although the equivalence ratio (0.65) and the adiabatic flame temperature (1752 K, computed with Cantera and GRI 3.0 mechanism) are not very high in this study, a considerable contribution of the thermal NO_x formation pathway is present, as shown by Göke et al. [48]. Due to the comparably slow reaction rate of the thermal NO_x mechanism, its contribution to the overall NO_x formation is enlarged by increased residence times τ_{res}. Additionally, the formation rate of the thermal pathway grows exponentially with temperature, which implies that a small temperature perturbation can lead to a significant change of NO_x emissions [49]. A considerable part of the NO_x formation is taking place in the reaction zone, which is to be found in the ISL, where the PVC is active [24,50]. Moreover, NO_x is created further downstream via the thermal pathway, due to involved longer τ_{res} [50]. Besides the thermal pathway, there is the prompt formation mechanism, which is active in the present burner setup, too [48]. The prompt pathway requires free radicals, such as CH_x, which are contained within the burnt gas and the flame front. These radicals attack the molecular nitrogen such that nitric oxides can be build, which increases the formation of NO_x via the prompt (and the thermal) pathway [48,51].

The NO_x formation mechanism explained above can be influenced by the interactions of the PVC with the flame. As shown in Fig. 6, the PVC does not considerably influence the small-scale mixing as quantified by the incoherent turbulent kinetic energy (Fig. 6). However, the PVC leads to considerable large-scale wrinkling and roll-up of the flame due to vortex–flame interaction (compare Fig. 8). This interaction enlarges the flame surface [45,46,52]. An enlarged flame surface affects an increase of the turbulent flame speed, which is proportional to the reaction rate and fuel consumption [51].

Another factor associated with vortex–flame interaction, induced by the PVC, is the enhanced mixing of burnt and unburnt

gas, which increases the reaction rate and changes the composition of the radical pool [27,46,53]. Therefore, in the context of NO_x formation mechanisms and the vortex–flame interaction exposed in Fig. 8, possible explanations for the impact of the PVC on the global level of NO_x emissions are given as follows:

(1) An increase of the residence time τ_{res} of combustion products in the combustor, i.e., the combustion zone, where the radical concentration is high, contributes to increased formation of thermal NO_x. The increase of τ_{res} results from the roll-up of the flame front induced by the PVC, which leads to a more compact and more upstream located flame as shown in Fig. 7.
(2) Due to the overall increase of free radicals in the ISL, the NO_x formation via both pathways, prompt and thermal, are promoted. The enhanced mixing of burnt and unburnt gas involves convective transport of free radicals from the (recirculated) burnt gas to the fresh burnable mixture. Additionally, more radicals are formed due to the enlarged flame surface and corresponding increased reaction rate resulting from PVC-induced flame roll-up.
(3) In the case of a partially premixed flame, the PVC may entrain richer fuel–air mixtures into the ISL, which will burn at a higher temperature leading to a temperature peak. Such temperature fluctuations, which enhance the NO_x formation over the thermal pathway, lead to a global increase of NO_x emissions. A comparable effect was shown by Paschereit et al. for axisymmetric vortices induced by thermoacoustic oscillations [29,30]. Since this effect only occurs at partially premixed conditions, it may explain why the measured NO_x emission values for the partially premixed (tp) flame are slightly higher than those of the perfectly premixed flame (Fig. 9).

The PVC increases the global formation of NO_x via different mechanisms. Vortex–flame interaction and corresponding mixing of burnt and unburnt gas enhance these formation mechanisms, which leads to an increase of NO_x emissions in both investigated operation types. However, the degree of premixedness decides whether the PVC enhances fuel–air mixing that leads to a decrease of NO_x emissions.

Conclusion

This study investigates the role of the PVC regarding NO_x emissions in premixed swirl-stabilized flames. In order to reveal possible mechanisms affecting the emission of NO_x, the influence of the PVC on the flame and the flow field is characterized. Appropriate experimental conditions for this characterization are realized by means of an active flow control system, which allows for direct actuation of a PVC at precisely controlled amplitudes. The investigated flames slightly damp the PVC, which facilitates open-loop control of the PVC, by applying a very low actuation amplitude of $C_\mu = 0.03\%$.

In the investigated reacting swirling flow, the PVC predominantly acts on the ISL near the burner outlet, which leads to enhanced flame wrinkling. As a result, the flame is shifted slightly upstream by the PVC and takes a more compact shape with major mean heat release rate around the burner outlet.

The vortices induced by the PVC affect a considerable roll-up of the ISL and the flame, which enlarges the flame surface. The induced vortices constantly feed the incoming jet of cold reactants with hot burnt products, which enhances the reaction rate leading to increased local heat release rate in conjunction with a more compact flame that is located further upstream. These effects increase the residence time of hot products and the number of free radicals inside the ISL. As a result of these effects, an increase of NO_x emissions of around 7% can be observed for the perfectly premixed case.

Finally, the NO_x emissions of a partially premixed flame are measured, which show the same increasing trend with growing PVC amplitude as for perfectly premixed conditions but at a somewhat higher level. The latter is explained by additional temperature peaks that may occur at partially premixed flames due to PVC-induced entrainment of richer fuel–air mixture, which leads to increased local equivalence ratios.

Vortex-enhanced fuel–air mixing by the PVC that leads to a decrease of NO_x emissions, as reported for slightly premixed flames, does not play a role for the investigated fairly premixed flames [22]. Accordingly, the degree of premixedness decides which PVC driven mechanism dominates the NO_x emissions, either vortex-induced fuel–air mixing or vortex–flame interaction.

Acknowledgment

Special thanks go out to Andy Göhrs for his technical support and Alexander Jaeschke for supporting the experimental procedure.

Funding Data

- German Research Foundation (DFG) (Project 247226395 (OB 402/4-3); Funder ID: 10.13039/501100001659).

Nomenclature

a_i = SPOD coefficients
C_μ = momentum coefficient of actuator
CRZ = central recirculation zone
D = nozzle diameter
D_h = hydraulic diameter of the nozzle
FTLE = finite time Lyapunov exponent
ISL = inner shear layer
K_{PVC} = kinetic energy of PVC
K_s = kinetic energy of stochastic fluctuations
LSA = linear stability analysis
m = azimuthal mode number
OH_p = phase-averaged reconstructed flame shape
OH_g^* = global heat release rate
OSL = outer shear layer
$\mathcal{P}$ = turbulent production
PIV = particle image velocimetry
PVC = precessing vortex core
$\hat{Q}_{PVC}$ = amplitude of PVC-induced global heat release rate fluctuations
RMS = root-mean-square
SPOD = spectral proper orthogonal decomposition
TKE = turbulent kinetic energy
v = velocity vector
V_0 = bulk velocity
(x, y, z) = axial, transversal and out-of-plane coordinates
Φ_i = spatial SPOD mode
$\overline{(\cdot)}$ = time average

References

[1] Gallaire, F., Ruith, M., Meiburg, E., Chomaz, J.-M., and Huerre, P., 2006, "Spiral Vortex Breakdown as a Global Mode," J. Fluid Mech., **549**(1), pp. 71–80.
[2] Syred, N., 2006, "A Review of Oscillation Mechanisms and the Role of the Precessing Vortex Core (PVC) in Swirl Combustion Systems," Prog. Energy Combust. Sci., **32**(2), pp. 93–161.
[3] Petz, C., Hege, H.-C., Oberleithner, K., Sieber, M., Nayeri, C. N., Paschereit, C. O., Wygnanski, I., and Noack, B. R., 2011, "Global Modes in a Swirling Jet Undergoing Vortex Breakdown," Phys Fluids, **23**(9), p. 091102.
[4] Oberleithner, K., Terhaar, S., Rukes, L., and Paschereit, C. O., 2013, "Why Nonuniform Density Suppresses the Precessing Vortex Core," ASME J. Eng. Gas Turbines Power, **135**(12), p. 121506.
[5] Terhaar, S., Oberleithner, K., and Paschereit, C., 2015, "Key Parameters Governing the Precessing Vortex Core in Reacting Flows: An Experimental and Analytical Study," Proc. Combust. Inst., **35**(3), pp. 3347–3354.
[6] Oberleithner, K., Stöhr, M., Im, S. H., Arndt, C. M., and Steinberg, A. M., 2015, "Formation and Flame-Induced Suppression of the Precessing Vortex Core in a Swirl Combustor: Experiments and Linear Stability Analysis," Combust. Flame, **162**(8), pp. 3100–3114.

[7] Paredes, P., Terhaar, S., Oberleithner, K., Theofilis, V., and Paschereit, C. O., 2015, "Global and Local Hydrodynamic Stability Analysis as a Tool for Combustor Dynamics Modeling," ASME Turbo Paper No. GT2015-44173.

[8] Oberleithner, K., Sieber, M., Nayeri, C. N., Paschereit, C. O., Petz, C., Hege, H.-C., Noack, B. R., and Wygnanski, I., 2011, "Three-Dimensional Coherent Structures in a Swirling Jet Undergoing Vortex Breakdown: Stability Analysis and Empirical Mode Construction," J. Fluid Mech., **679**, pp. 383–414.

[9] Qadri, U. A., Mistry, D., and Juniper, M. P., 2013, "Structural Sensitivity of Spiral Vortex Breakdown," J. Fluid Mech., **720**, pp. 558–581.

[10] Tammisola, O., and Juniper, M., 2016, "Coherent Structures in a Swirl Injector at Re=4800 by Nonlinear Simulations and Linear Global Modes," J. Fluid Mech., **792**, pp. 620–657.

[11] Kaiser, T. L., Poinsot, T., and Oberleithner, K., 2018, "Stability and Sensitivity Analysis of Hydrodynamic Instabilities in Industrial Swirled Injection Systems," ASME J. Eng. Gas Turbines Power, **140**(5), p. 051506.

[12] Rukes, L., Paschereit, C. O., and Oberleithner, K., 2016, "An Assessment of Turbulence Models for Linear Hydrodynamic Stability Analysis of Strongly Swirling Jets," Eur. J. Mech. B. Fluids, **59**, pp. 205–218.

[13] Müller, J. S., Lückoff, F., and Oberleithner, K., 2019, "Guiding Actuator Designs for Active Flow Control of the Precessing Vortex Core by Adjoint Linear Stability Analysis," ASME J. Eng. Gas Turbines Power, **141**(4), p. 041028.

[14] Müller, J. S., Lückoff, F., Paredes, P., Theofilis, V., and Oberleithner, K., 2020, "Receptivity of the Turbulent Precessing Vortex Core: Synchronization Experiments and Global Adjoint Linear Stability Analysis," J. Fluid Mech., **888**, p. A3.

[15] Hill, D. C., 1995, "Adjoint Systems and Their Role in the Receptivity Problem for Boundary Layers," J. Fluid Mech., **292**, pp. 183–204.

[16] Magri, L., and Juniper, M., 2014, "Global Modes, Receptivity, and Sensitivity Analysis of Diffusion Flames Coupled With Duct Acoustics," J. Fluid Mech., **752**, pp. 237–265.

[17] Kuhn, P., Moeck, J. P., Paschereit, C. O., and Oberleithner, K., 2016, "Control of the Precessing Vortex Core by Open and Closed-Loop Forcing in the Jet Core," ASME Paper No. GT2016-57686.

[18] Lückoff, F., Sieber, M., Paschereit, C. O., and Oberleithner, K., 2017, "Characterization of Different Actuator Designs for the Control of the Precessing Vortex Core in a Swirl-Stabilized Combustor," ASME J. Eng. Gas Turbines Power, **140**(4), p. 041503.

[19] Lückoff, F., and Oberleithner, K., 2019, "Excitation of the Precessing Vortex Core by Active Flow Control to Suppress Thermoacoustic Instabilities in Swirl Flames," Int. J. Spray Combust. Dyn., **11**, pp. 1–23.

[20] Lückoff, F., Sieber, M., Paschereit, C. O., and Oberleithner, K., 2019, "Phase-Opposition Control of the Precessing Vortex Core in Turbulent Swirl Flames for Investigation of Mixing and Flame Stability," ASME J. Eng. Gas Turbines Power, **141**(11), p. 111008.

[21] Terhaar, S., Krüger, O., and Paschereit, C. O., 2015, "Flow Field and Flame Dynamics of Swirling Methane and Hydrogen Flames at Dry and Steam-Diluted Conditions," ASME J. Eng. Gas Turbines Power, **137**(4), p. 041503.

[22] Stöhr, M., Arndt, C., and Meier, W., 2015, "Transient Effects of Fuel-Air Mixing in a Partially-Premixed Turbulent Swirl Flame," Proc. Combust. Inst., **35**(3), pp. 3327–3335.

[23] Galley, D., Ducruix, S., Lacas, F., and Veynante, D., 2011, "Mixing and Stabilization Study of a Partially Premixed Swirling Flame Using Laser Induced Fluorescence," Combust Flame, **158**(1), pp. 155–171.

[24] Claypole, T., and Syred, N., 1981, "The Effect of Swirl Burner Aerodynamics on Nox Formation," Symp. (Int.) Combust., **18**(1), pp. 81–89.

[25] Fric, T. F., 1993, "Effects of Fluel-Air Unmixedness on No(x) Emissions," J. Propul. Power, **9**(5), pp. 708–713.

[26] Schadow, K., and Gutmark, E., 1992, "Combustion Instability Related to Vortex Shedding in Dump Combustors and Their Passive Control," Prog. Energy Combust. Sci., **18**(2), pp. 117–132.

[27] Renard, P.-H., Thévenin, D., Rolon, J., and Candel, S., 2000, "Dynamics of Flame/Vortex Interactions," Prog. Energy Combust. Sci., **26**(3), pp. 225–282.

[28] Ducruix, S., Candel, S., Durox, D., and Schuller, T., 2003, "Combustion Dynamics and Instabilities: Elementary Coupling and Driving Mechanisms," J. Propul. Power, **19**(5), pp. 722–734.

[29] Paschereit, C., Gutmark, E., and Weisenstein, W., 1998, "Structure and Control of Thermoacoustic Instabilities in a Gas-Turbine Combustor," Combust. Sci. Technol., **138**(1–6), pp. 213–232.

[30] Paschereit, C. O., and Gutmark, E. J., 2008, "Combustion Instability and Emission Control by Pulsating Fuel Injection," ASME J. Turbomach., **130**(1), p. 011012.

[31] Sieber, M., Ostermann, F., Woszidlo, R., Oberleithner, K., and Paschereit, C. O., 2016, "Lagrangian Coherent Structures in the Flow Field of a Fluidic Oscillator," Phys. Rev. Fluids, **1**(5), p. 050509.

[32] Haller, G., 2001, "Lagrangian Structures and the Rate of Strain in a Partition of Two-Dimensional Turbulence," Phys. Fluids, **13**(11), pp. 3365–3385.

[33] Moeck, J. P., Bourgouin, J.-F., Durox, D., Schuller, T., and Candel, S., 2013, "Tomographic Reconstruction of Heat Release Rate Perturbations Induced by Helical Modes in Turbulent Swirl Flames," Exp. Fluids, **54**(4), pp. 1–17.

[34] Greenblatt, D., and Wygnanski, I. J., 2000, "The Control of Flow Separation by Periodic Excitation," Prog. Aerosp. Sci., **36**(7), pp. 487–545.

[35] Soria, J., 1996, "An Adaptive Cross-Correlation Digital PIV Technique for Unsteady Flow Investigations," Proceedings of First Australian Conference on Laser Diagnostics in Fluid Mechanics and Combustion, University of Sydney, Sydney, Australia, pp. 29–48.

[36] Huang, H. T., Fiedler, H. E., and Wang, J. J., 1993, "Limitation and Improvement of PIV," Exp. Fluids, **15-15**(4–5), pp. 263–273.

[37] Moeck, J. P., Bourgouin, J.-F., Durox, D., Schuller, T., and Candel, S., 2012, "Nonlinear Interaction Between a Precessing Vortex Core and Acoustic Oscillations in a Turbulent Swirling Flame," Combust. Flame, **159**(8), pp. 2650–2668.

[38] Leuckel, W., 1967, "Swirl Intensities, Swirl Types and Energy Losses of Different Swirl Generating Devices," International Flame Research Foundation, Ijmuiden, The Netherlands, Report No. G02/a/16.

[39] Sieber, M., Paschereit, C. O., and Oberleithner, K., 2016, "Spectral Proper Orthogonal Decomposition," J. Fluid Mech., **792**(004), pp. 798–828.

[40] Holmes, P., Lumley, J. L., and Berkooz, G., 1998, *Turbulence, Coherent Structures, Dynamical Systems and Symmetry*, Cambridge University Press, Cambridge, UK.

[41] Sieber, M., Paschereit, C. O., and Oberleithner, K., 2016, "Advanced Identification of Coherent Structures in Swirl-Stabilized Combustors," ASME J. Eng. Gas Turbines Power, **139**(2), p. 021503.

[42] Rukes, L., Sieber, M., Paschereit, C. O., and Oberleithner, K., 2016, "Methods for the Extraction and Analysis of the Global Mode in Swirling Jets Undergoing Vortex Breakdown," ASME J. Eng. Gas Turbines Power, **139**(2), p. 022604.

[43] Lückoff, F., Kaiser, T., Paschereit, C. O., and Oberleithner, K., 2020, "Mean Field Coupling Mechanisms Explaining the Impact of the Precessing Vortex Core on the Flame Transfer Function," Combust. Flame (in press).

[44] Frederick, M., Manoharan, K., Dudash, J., Brubaker, B., Hemchandra, S., and O'Connor, J., 2018, "Impact of Precessing Vortex Core Dynamics on Shear Layer Response in a Swirling Jet," ASME J. Eng. Gas Turbines Power, **140**(6), p. 061503.

[45] Steinberg, A. M., Boxx, I., Stöhr, M., Carter, C. D., and Meier, W., 2010, "Flow-Flame Interactions Causing Acoustically Coupled Heat Release Fluctuations in a Thermo-Acoustically Unstable Gas Turbine Model Combustor," Combust. Flame, **157**(12), pp. 2250–2266.

[46] Stöhr, M., Boxx, I., Carter, C. D., and Meier, W., 2012, "Experimental Study of Vortex Flame Interaction in a Gas Turbine Model Compbustor," Combust. Flame, **159**(8), pp. 2636–2649.

[47] Göke, S., Göckeler, K., Krüger, O., and Paschereit, C. O., 2010, "Computational and Experimental Study of Premixed Combustion at Ultra Wet Conditions," ASME Paper No. GT2010-23417.

[48] Göke, S., Füri, M., Bourque, G., Bobusch, B., Göckeler, K., Krüger, O., Schimek, S., Terhaar, S., and Paschereit, C. O., 2013, "Influence of Steam Dilution on the Combustion of Natural Gas and Hydrogen in Premixed and Rich-Quench-Lean Combustors," Fuel Process. Technol., **107**, pp. 14–22.

[49] Correa, S. M., 1993, "A Review of No(x) Formation Under Gas-Turbine Combustion Conditions," Combust. Sci. Technol., **87**(1–6), pp. 329–362.

[50] Bradley, D., 1998, "Premixed Turbulent Flame Instability and NO Formation in a Lean-Burn Swirl Burner," Combust. Flame, **115**(4), pp. 515–538.

[51] Joos, F., 2006, *Technische Verbrennung*, Springer Press, Berlin.

[52] Steinberg, A. M., and Driscoll, J. F., 2009, "Straining and Wrinkling Processes During Turbulence–Premixed Flame Interaction Measured Using Temporally-Resolved Diagnostics," Combust. Flame, **156**(12), pp. 2285–2306.

[53] Cetegen, B. M., 2006, "Scalar Mixing in the Field of a Gaseous Laminar Line Vortex," Exp. Fluids, **40**(6), pp. 967–976.

2.5 Publication V

Mean Field Coupling Mechanisms explaining the Impact of the Precessing Vortex Core on the Flame Transfer Function

Beside the NO_x emission level (see publication 2.4), the flame transfer function (FTF) represents another important quantity for swirl-stabilized combustion systems. It characterizes the thermoacoustic stability of a combustion system towards acoustically forced axisymmetric modes. The fifth publication provides different coupling mechanisms which explain why and how the PVC affects the FTF of the investigated perfectly premixed swirl flame. These coupling mechanisms are revealed with the help of open-loop flow control of the PVC and incorporate changes of the mean flow field and the mean flame shape.

This publication starts with a global linear stability analysis revealing a stable PVC mode in the reacting base flow which contains an attached V-flame. It is shown that this PVC mode can be directly excited with the helical open-loop actuation system. The analysis of the PVC-induced mean flow changes as well as the related changes of the mean flame shape provide the basis for phenomenological explanations of the observed decrease of the FTF gain. With the help of a FTF-model, which is based on a local stability analysis of the mean flow, the decrease of the FTF gain can be partially explained in a hydrodynamic sense. However, to fully explain the FTF gain reduction, the changes of the mean flame as well as the intensity of the local heat release fluctuations induced by the acoustically excited axisymmetric modes need to be considered. Finally, two related mean field coupling mechanisms are derived which explain the FTF gain reduction induced by the PVC and the reason for the constant FTF phase.

Combustion and Flame 223 (2021) 254–266

Contents lists available at ScienceDirect

Combustion and Flame

journal homepage: www.elsevier.com/locate/combustflame

Mean field coupling mechanisms explaining the impact of the precessing vortex core on the flame transfer function

Finn Lückoff[a,*], Thomas Ludwig Kaiser[a], Christian Oliver Paschereit[b], Kilian Oberleithner[a]

[a] Laboratory for Flow Instabilities and Dynamics, TU Berlin, Müller-Breslau-Strasse 8, Berlin 10623, Germany
[b] Chair of Fluid Dynamics, TU Berlin, Müller-Breslau-Strasse 8, Berlin 10623, Germany

ARTICLE INFO

Article history:
Received 12 May 2020
Revised 16 September 2020
Accepted 16 September 2020

Keywords:
Precessing vortex core (PVC)
Swirl flames
Flame transfer function (FTF)
Active flow control
Global hydrodynamic stability

ABSTRACT

The flame transfer functions (FTF) is a key quantity to assess the thermoacoustic properties of combustion systems. It is known to depend on the hydrodynamic instabilities of the combustor flow. This work investigates how the FTF is affected by a global flow instability known as the precessing vortex core (PVC) which is often observed in swirl flames. To study the exclusive effect of the PVC on the FTF, a perfectly premixed swirl flame is considered where the PVC mode is damped with a close to zero growth rate. An active flow control system is applied in the region of high receptivity to excite the PVC at precisely controlled amplitudes. The conducted experiments show that the excited mode corresponds to the least stable global mode predicted from mean field stability analysis and that the most responsive frequency is equal to the predicted global mode frequency, which brings credibility to the control approach. FTF measurements conducted at different PVC actuation amplitudes show that the FTF gain decreases significantly with increasing PVC amplitude while the FTF phase remains unchanged. The FTF gain reduction is explained by two mechanisms: the reduction in gain of the Kelvin–Helmholtz instability through mean field modifications and the upstream movement of the flames center of mass due to enhanced coherent fluctuations at the flame root. The unchanged FTF phase is traced back to an unchanged location of the most influential heat release rate fluctuations at the flame tip. This study suggests that the control of the PVC is an effective way to avoid or mitigate thermoacoustic instabilities. The control is thereby very efficient as it exploits the natural global hydrodynamic instability of the flow.

1. Introduction

Many modern gas turbines employ highly turbulent swirling flows to stabilize the flame through an aerodynamic phenomenon called vortex breakdown. This phenomenon leads to the formation of a central recirculation zone (CRZ) and corresponding shear layers. In case of a confined flow, as to be found in a gas turbine combustion chamber, an inner shear layer (ISL), between the jet and the central recirculation zone and an outer shear layer (OSL), between jet and outer recirculation zone (ORZ), occur. These shear layers are prone to hydrodynamic instabilities. This includes the precessing vortex core (PVC, azimuthal wavenumber $m = 1$) as a global self-excited instability and a convective Kelvin–Helmholtz (KH) type instability.

The KH-instability is receptive to external forcing and couples well with planar acoustic waves that occur due to thermoacoustic (TA) oscillations in the combustor [1–5]. As a consequence, axisymmetric ($m = 0$) large-scale coherent flow fluctuations grow in the shear layers and interact with the flame, which leads to flame roll-up and global heat release rate fluctuations [5]. Therefore, the growth of the vortical structures impinging the flame has a significant impact on the flame transfer function (FTF) [2]. The FTF describes the linear response of global heat release rate fluctuations to acoustic perturbations and represents an important quantity to predict TA instability [6,7]. Beside the KH-instability, swirl fluctuations represent a second hydrodynamic parameter that influences the FTF. They are generated in the swirler and propagate into the flame leading to global heat release rate fluctuations [2].

Unlike the KH-instability, the PVC is driven by an intrinsic hydrodynamic feedback occurring at strong swirl, which leads to global hydrodynamic instability driving the self-sustained oscillations [8]. From a phenomenological viewpoint, the PVC represents the azimuthal periodic motion of the rotation center of the swirl flow. However, this motion is typically synchronized with Kelvin–Helmholtz-type helical coherent structures that form in the inner and outer shear layers and that are shed downstream. In this study, the term “PVC” corresponds to the global mode that describes the entire synchronized flow oscillations.

* Corresponding author.
E-mail address: finn.lueckoff@tu-berlin.de (F. Lückoff).

https://doi.org/10.1016/j.combustflame.2020.09.019
0010-2180/

Nomenclature

A_h	hydraulic cross section area
a_i	SPOD coefficients
C_μ	momentum coefficient of actuation
D	nozzle diameter
D_h	hydraulic diameter of the nozzle
FTF	flame transfer function
f	frequency [Hz]
F_u	velocity transfer function
G	area of actuator outlet
K_{PVC}	turbulent kinetic energy of PVC
m	azimuthal mode number
N_f	SPOD filter size
OH*	heat release rate distribution
$\mathcal{P}_{\mathrm{coh}}$	coherent production
$\mathcal{P}_{\mathrm{turb}}$	turbulent production
Q	global heat release rate
q	local heat release rate
u_{RMS}	RMS velocity at outlet of actuator
$\mathbf{v}$	velocity vector
V_0	bulk velocity
(v_x, v_y, v_z)	axial, transversal and out-of-plane velocity
(x, y, z)	axial, transversal and out-of-plane coordinates
Φ_i	spatial SPOD mode
$(.)'$	fluctuating part
$(.)''$	incoherent part
$\hat{(.)}$	Fourier decomposed
$\overline{(.)}$	time average
$\tilde{(.)}$	coherent part
AF	Acoustic Forcing
CRZ	Central Recirculation Zone
ISL	Inner Shear Layer
KH	Kelvin–Helmholtz
LSA	Linear Stability Analysis
OSL	Outer Shear Layer
PIV	Particle Image Velocimetry
PMT	Photomultiplier Tube
PVC	Precessing Vortex Core
RMS	Root Mean Square
SPOD	Spectral Proper Orthogonal Decomposition
TA	Thermoacoustic
TKE	Turbulent Kinetic Energy

In an isothermal flow, the global hydrodynamic instability causing the PVC is driven by the strong backflow of the CRZ, which is caused by vortex breakdown associated to a strong swirling flow rotation [8,9]. At reacting non-isothermal conditions, the PVC may be suppressed by the flame even at the presence of very strong backflow. Typically, the PVC is damped for attached V-flames, due to the stabilizing effect of the density field at the combustor inlet [9–12], while it remains unstable for detached M-flames. The connection between flame anchoring and PVC occurrence gives rise to complex transient flow-flame-interactions that explain bi-stable flame transitions that have been observed in several recent studies [13–16].

The role of the PVC in the context of TA stability is still subject of current research. In contrast to axisymmetric (planar) TA modes, the PVC induces skew-symmetric (helical) perturbations in the flame, which do not contribute to the global heat release rate fluctuations [5,17,18]. Therefore, the PVC cannot directly couple with axisymmetric TA modes. However, nonlinear interactions between PVC and TA modes are possible, which generate interaction modes oscillating at the sum or the difference of PVC and TA frequencies [17,19,20]. Moreover, mean field changes induced by high amplitude TA oscillations may lead to the suppression or excitation of the PVC [11,17,21,22]. Other indirect interaction opportunities are connected to the flame shape transition induced by the PVC [10,13–16]. Thereby, the change of flame shape may lead to a destabilization of TA modes that in turn interact with the PVC. This results in a complex loop of events that explain the occurrence of bi-stable flame dynamics [14,23].

Another possible PVC-TA-interaction is based on the fact that the flame response to acoustic forcing (AF), or the FTF, is to a large extend determined by the spatial growth of flow perturbations in the shear layers [4]. As was hypothesized in recent studies [24,25], the PVC may thicken the shear layers by enhancing the production of kinetic energy from the coherent fluctuations, which is commonly referred to as coherent production. The thickening of the shear layers in turn reduces the spatial growth rate of the axisymmetric KH-type instability, which directly affects the gain of the FTF. With the attempt to verify this hypothesis, experiments in combination with a spatial linear stability analysis of the KH-mode was conducted for non-reacting flows at different swirl numbers [24,25]. These studies show a substantial reduction of the growth rate of the KH-mode with high swirl, which was attributed to the PVC. However, due to the substantial change of the overall flow field with increasing swirl, the exclusive impact of the PVC on the KH-mode remains unrevealed from these experiments. Moreover, these experiments were conducted in non-reacting conditions, and hence, the impact of the PVC on the flame response (and the FTF) could not be assessed.

To validate the hypothesis of [24,25] and to overcome the shortcoming of the previous experiments, active flow control is applied in this work. This allows for a direct control of the PVC without altering any other influencing parameters at reacting and non-reacting conditions. The key is to develop a flow control that acts on the source of the instability driving the PVC, which can be determined from global adjoint linear stability theory [26–29]. Several recent studies have shown that this methodology is now ready to be applied for highly turbulent reacting swirling flows, as considered here [30–33]. The development and benchmarking of the active flow control system employed in this work was focus of previous works [12,20,30]. Accordingly, it allows for an efficient open- and closed loop control of the PVC at reacting and non-reacting conditions without changing the remaining system dynamics. It therefore fulfills the requirements to investigate the exclusive influence of the PVC on TA-instabilities of swirl flames and to investigate on the potential of active PVC control for TA-instability mitigation purpose.

In this work, a turbulent swirl flame is investigated experimentally. We consider an attached V-shaped flame that features no PVC, a configuration commonly used in gas turbine combustion. The active control unit is used to excite a PVC in an open-loop fashion. The control thereby exploits the intrinsic global hydrodynamic instability of the flow as it is verified by a global linear stability analysis. Acoustic FTF measurements are conducted for a range of PVC actuation amplitudes and the flow and flame dynamics are captured simultaneously via time-resolved PIV and OH-chemiluminescence measurements. The experimental arrangement allows for a controlled characterisation of the impact of the PVC on the FTF, and reveals the coupling mechanisms between the PVC and TA instabilities through mean flame and mean flow modifications. It further allows to verify the hypothesis of the PVC reducing the growth rate of the axisymmetric KH-mode as it was formulated in previous works.

The present study is structured as follows. First, the experimental (2) and theoretical (3) methods are explained, which are applied to analyze the chosen stable reacting base flow. This base flow is used as input for a global linear stability analysis (4.1).

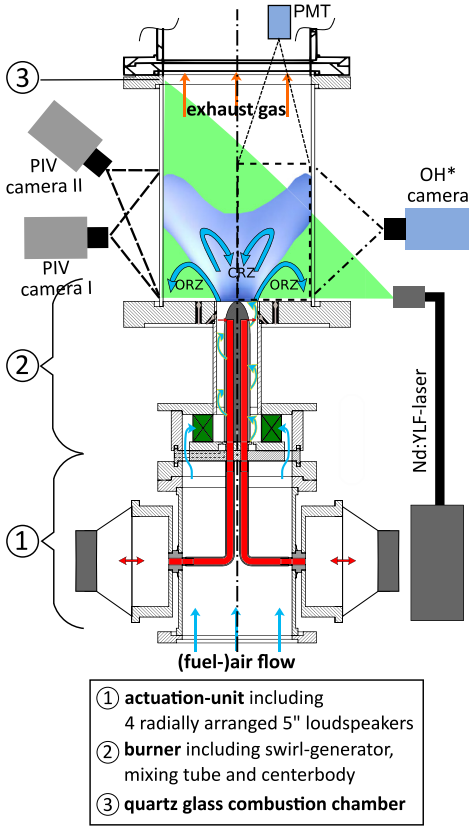

Fig. 1. Experimental setup with applied measurements techniques.

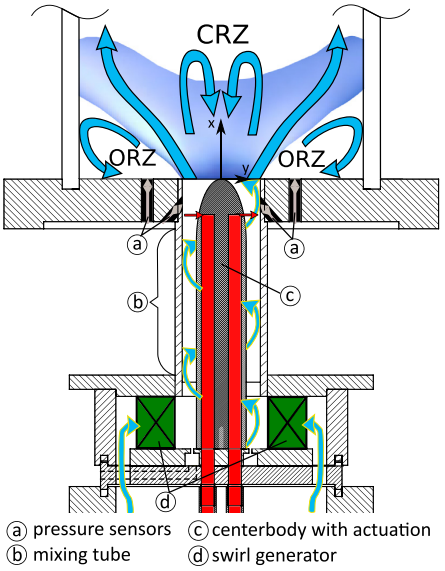

Fig. 2. Detailed sketch of the burner with PVC actuation indicated by the small arrows at the outlets of the actuation channels.

Next, the effect of the PVC actuation is analyzed with respect to flow dynamics and modifications of the temporally averaged mean flow (4.2). Finally, FTF measurements are presented for the same conditions and the influence of PVC actuation is discussed (4.3). Two different scenarios are derived, taking into account changes of the mean flow (4.3.1) and the mean flame (4.3.2). It explains the observed impact of the PVC on the FTF.

2. Experimental setup and methods

2.1. Burner and actuator design

Experiments are conducted with a swirl-stabilized combustor (see Fig. 1), which consists of a swirl generator, a silica glass combustion chamber and an annular mixing tube duct (hydraulic diameter $D_h = 20$ mm). The centerbody inside the mixing duct contains four independent actuation channels with rectangular outlets at the centerbody tip. Previous studies conducted in different geometries revealed that the highest sensitivity of the PVC mode is to be found slightly upstream of the burner outlet and the central recirculation zone, where the actuator outlets are placed [27–29,31]. Each actuation channel is connected to an individual loudspeaker, which facilitates helical actuation of the PVC according to the zero-net-mass-flux principle (Figs. 1 and 2). According to this principle, no additional fluid is added to the main flow. As a measure of actuator efficiency, the momentum of the actuation jets is related to the momentum of the main flow, yielding the momentum coefficient [34],

$$C_\mu = G u_{\mathrm{RMS}}^2 / (V_0^2 A_h),$$

where u_{RMS} refers to the RMS of the velocity fluctuations at an individual actuator outlet, which was measured with a hot-wire anemometer without main airflow [30], G refers to the area of a single actuator outlet, A_h refers to the hydraulic cross section area based on D_h, and V_0 refers to the bulk velocity of the main flow. Besides characterizing the actuators efficiency, the C_μ value is also a measure for the actuation amplitude, which is used in this study to distinguish different levels of PVC actuation. In previous studies, it was shown that this actuator can be used for phase-opposition control to achieve damping of the PVC limit cycle amplitude [12]. This is an important prerequisite for the current study as it demonstrates the capability of the control concept.

2.2. Operating conditions

The perfectly premixed fuel–air mixture with an inlet temperature of 293 K was burned at an equivalence ratio of 0.65. The air mass flow was set to 140 kg/h, which corresponds to an Reynolds number of 30,000 based on D_h and a thermal power of 67 kW. The swirl generator was adjusted to a fixed geometrical swirl number of $S = 0.7$. Air and fuel (natural gas) were premixed far upstream of the burner to ensure perfectly premixed conditions.

2.3. Measurement of flame transfer function (FTF)

The FTF describes the ratio between the global heat release rate fluctuations to the acoustic velocity perturbations at the combustor inlet. This ratio is defined as

$$\mathrm{FTF} = \frac{\hat{Q}/\overline{Q}}{\hat{u}/V_0}, \tag{1}$$

with the Fourier-transformed global heat release rate $\hat{Q}$, the mean global heat release rate $\overline{Q}$, the Fourier-transformed acoustic velocity $\hat{u}$ and the bulk flow velocity V_0.

The multi-microphone-method (MMM) was applied to reconstruct the plane wave acoustic velocities upstream and downstream of the flame [6]. Based on the reconstructed acoustic velocities, the FTF was derived by applying the Rankine–Hugoniot relation assuming acoustically compact flames [35,36].

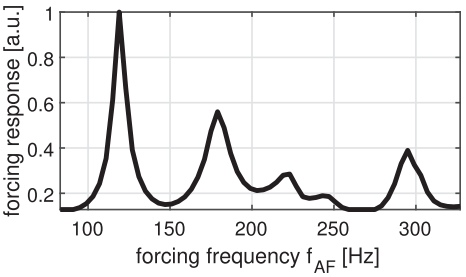

Fig. 3. Acoustic forcing response of the combustion system derived from the estimated the amplitudes of the voltage signal, which was fed to the loudspeakers, to achieve an acoustic velocity of 10% of the bulk velocity.

The burner with the PVC actuation system was implemented into an atmospheric combustion test rig that allows for measurements of the FTF [11,35]. Measurements were conducted using five condenser microphones flushmounted in the plenum upstream of the burner and another five water-cooled microphones in the exhaust tube. The microphone signals were recorded at a sampling rate of 8192 Hz for a time series of 16 s. Four 18-inch speakers connected to the plenum were used to generate acoustic forcing. The flame was acoustically forced at frequencies between 83 and 327 Hz with an increment of 4 Hz. The amplitude of the voltage signal fed to the 18-inch speakers was adjusted to achieve an acoustic forcing amplitude of $\hat{u}/V_0 = 0.1$, which assures linearity of the flame response. Thus, at resonance frequencies of the rig, the amplitude of the loudspeaker voltage signals were minimal. The corresponding frequency dependent voltage signal amplitudes were derived in an iterative procedure prior to the ultimate measurements. The normalized reciprocal of the derived amplitudes yields a measure for the response of the combustion system to the acoustic forcing, which is shown in Fig. 3. The peaks in the plot mark those frequencies at which the forcing is most effective. The considered range of acoustic forcing frequencies support only planar ($m = 0$) acoustic waves, with the aim to mimic perturbations originating from TA modes. In this study, all quantities referring to the acoustic forcing have AF as index.

2.4. Flow and flame diagnostics

The three components of the velocity field were measured with stereoscopic high-speed particle image velocimetry (PIV) at a recording rate of 2500 fps. One camera of the measurement system was mounted perpendicular to the streamwise field of view and another camera with an angle of 40° to the measurement plane. Seeding was introduced to the flow upstream of the burner using a brush-based seeding generator with titanium dioxide (TiO_2) particles of a nominal diameter of 2 μm. The light emitted by the PIV seeding particles was used to estimate the mean fluid density, using a quantitative light sheet technique [37,38].

Time-resolved OH^* chemiluminescence measurements were conducted using an intensified high-speed CMOS camera equipped with a 308 nm optical bandpass filter recording at a rate of 2500 fps. The recorded images were phase-averaged with respect to the acoustic actuation and Abel-deconvoluted to obtain the spatial distribution of heat release rate fluctuations. Moreover, a photomultiplier tube (PMT), equipped with a 308 nm bandpass filter, focused to only one half of the combustion chamber, captured the antisymmetric (with respect to the combustor symmetry) global heat release rate fluctuations induced by the PVC [17]. The time-resolved PIV and OH^* measurements had to be conducted sequentially because of geometrical restrictions around the test rig. Further details about the experimental setup and the actuator design can be found in [20].

3. Empirical and analytic methods

This section provides a brief introduction to the methodology applied to characterize the stability and dynamics of the flame and the flow.

3.1. Spectral proper orthogonal decomposition (SPOD)

The time-resolved velocity field snapshots measured in this study with PIV were post-processed using SPOD. It is an empirical mode decomposition method to extract the spatial shape and dynamic of coherent flow structures, such as the PVC [39]. The fundamental basis of the SPOD is formed by the classical proper orthogonal decomposition (POD) [40]. In contrast to the POD, the SPOD provides enhanced selectivity in complex turbulent flows such as the reacting combustor flows investigated in this study [41].

Within the framework of the SPOD, velocity fluctuations $\mathbf{v}'$ are decomposed as

$$\mathbf{v}(\mathbf{x},t) = \overline{\mathbf{v}}(\mathbf{x}) + \mathbf{v}'(\mathbf{x},t) = \overline{\mathbf{v}}(\mathbf{x}) + \sum_{i=1}^{N} a_i(t)\Phi_i(\mathbf{x}), \tag{2}$$

with spatial modes Φ_i and corresponding time-dependent coefficients a_i. This mode basis is, analog to classic POD, derived from an eigenvalue decomposition of the correlation matrix $\mathbf{R}$.

In contrast to the classical POD, the matrix $\mathbf{R}$ is filtered by a Gaussian low-pass filter, which leads to the filtered correlation matrix

$$\mathrm{S_{i,j}} = \sum_{k=-N_f}^{N_f} g_k \mathrm{R_{i+k,j+k}}\,. \tag{3}$$

The vector g_k contains the filter coefficients and N_f describes the filter width. The standard deviation of the filter is chosen such that it gives the same cut-off frequency as a box filter of half the length [41]. The filter width N_f is a crucial parameter of this SPOD approach, because it allows to switch between the classical POD ($N_f = 0$) and a pure discrete Fourier transform (N_f = number of samples) [39]. It is recommended to set N_f equivalent to one to two periods of the investigated mode, which is the PVC in the present case [41]. Accordingly, in this study N_f should be in the range of 12 to 25 samples. The corresponding cut-off is related to the filter width by $f_c \propto \frac{1}{N_f}$ [39]. In this study, N_f is set to 20, which enables an unambiguous separation of the PVC mode and the remaining turbulent fluctuations.

The SPOD-based filtering allows for extracting the mode shapes and dynamics of coherent flow structures in a defined frequency range, and it avoids a distribution of the PVC dynamics over several modes. This is especially important in those cases where the PVC is comparably weak. The temporal coefficients $a_i(t)$, which are corresponding to the eigenvectors of the filtered correlation matrix, describe the dynamics of the corresponding spatial mode. The spatial modes $\Phi_i(\mathbf{x})$ are derived from a projection of the snapshots onto the corresponding temporal coefficients. For more details regarding the derivation of the SPOD, the reader is referred to the work of Sieber et al. [39].

3.2. Mean field linear stability analysis

Linear stability analysis (LSA) is applied to the measured mean fields for two reasons. First, a global LSA is conducted to investigate the stability of the PVC mode at the uncontrolled state and to verify the control scheme. Second, a local spatial LSA is conducted

to predict the growth rates of the axisymmetric KH-instability in the shear layers at different levels of PVC actuation.

To conduct LSA of a turbulent flow, the pressure and velocity components are formally decomposed into three parts: a time-averaged mean part, $\bar{\mathbf{v}}$, a coherent part (the difference between the mean and the phase-average), $\tilde{\mathbf{v}}$, and an incoherent turbulent part, $\mathbf{v}''$. This reads exemplary for the velocity vector $\mathbf{v} = \bar{\mathbf{v}} + \tilde{\mathbf{v}} + \mathbf{v}''$. By inserting this ansatz into the Navier–Stokes equations for an incompressible non-isothermal flow and subsequent rearrangement and linearization, one arrives at the governing equations for the coherent part

$$\frac{\partial \tilde{\mathbf{v}}}{\partial t} + \tilde{\mathbf{v}} \cdot \nabla \bar{\mathbf{v}} + \bar{\mathbf{v}} \cdot \nabla \tilde{\mathbf{v}} = -\frac{1}{\bar{\rho}} \nabla \tilde{p} + \nabla \cdot (\nu_{\text{eff}} (\nabla + \nabla^T) \tilde{\mathbf{v}}) \tag{4}$$

$$\nabla \cdot \tilde{\mathbf{v}} = 0. \tag{5}$$

It is important to note that the equations are effectively weakly nonlinear as they account for the modification of the mean field through nonlinear coherent Reynolds stresses [42]. Moreover, the effective viscosity ν_{eff} consists of the sum of the molecular and the turbulent viscosity, where the latter accounts for the interaction between the random and coherent fluctuations. Using the Boussinesq approximation [10,27], the effective viscosity is calibrated to the Reynolds stresses, which are obtained from PIV measurements.

Solving this equation within the framework of global LSA, the global mode ansatz $\tilde{\mathbf{q}}(\mathbf{x}, t) = \Re\{\hat{\mathbf{q}}(x, r) e^{i(m\theta - \omega t)}\}$ is inserted in Eqs. (4) and (5), where $\tilde{\mathbf{q}}$ stands for $\tilde{p}$ and $\tilde{\mathbf{v}}$, x for the axial coordinate, r the radial coordinate and θ the azimuthal angle. The real part $\Re\{\omega\}$ of the complex ω is the frequency, the imaginary part $\Im\{\omega\}$ the temporal growth rate, $\hat{\mathbf{q}}(x, r)$ is the amplitude function, and m the azimuthal wavenumber of the global mode. The equations are rearranged to an eigenvalue problem with ω as the eigenvalue and $\hat{\mathbf{q}}$ as the eigenfunction and solved numerically for a given m using the FELiCS code developed at TU Berlin. The code takes advantage of the open source Finite-Element software package FEniCS in order to discretize Eqs. (4) and (5). In the framework of this paper, a mixed formulation was applied using second order continuous Galerkin elements for all velocity components and corresponding first order elements for the pressure. The mean flow is globally unstable if $\Im\{\omega\} > 0$ and globally stable if $\Im\{\omega\} < 0$. The global LSA is conducted for $m = 1$ to determine the global mode corresponding to the PVC.

The framework of local stability analysis extends the assumptions of the global stability approach described above. The base flow is assumed to be quasi parallel and the coherent fluctuations are locally periodic in the axial direction with the complex axial wavenumber α, which leads to the normal mode ansatz $\tilde{\mathbf{q}}(\mathbf{x}, t) = \Re\{\hat{\mathbf{q}}(r) e^{i(m\theta + \alpha x - \omega t)}\}$. A spatial analysis is applied, where ω and m are real and fixed to the value of interest and α is the complex eigenvalue. Coherent fluctuations are spatially growing where $\Im\{\alpha\} < 0$ and spatially decaying where $\Im\{\alpha\} > 0$. Since in local stability analysis, the analysis is performed on the radial velocity profile only, the analysis must be repeated for every axial position in the domain. Finally, a complex valued *velocity transfer function* $F_u(x, \omega)$ can be computed by integrating α along the axial coordinate [35], leading to

$$F_u(x, \omega) = \exp\left[i \int_0^x \alpha(\xi, \omega) \mathrm{d}\xi \right]. \tag{6}$$

The local analysis is employed in this work for $m = 0$ to determine the spatial growth rate of the KH-instability that couples with the planar acoustic forcing.

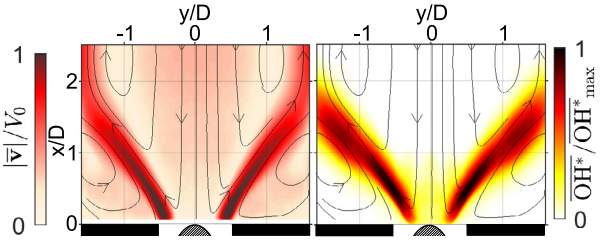

Fig. 4. Mean velocity magnitude (left) and mean Abel-deconvoluted flame shape (right) with superimposed mean streamlines for the baseline case; $\overline{OH^*}$ normalized with overall maximum.

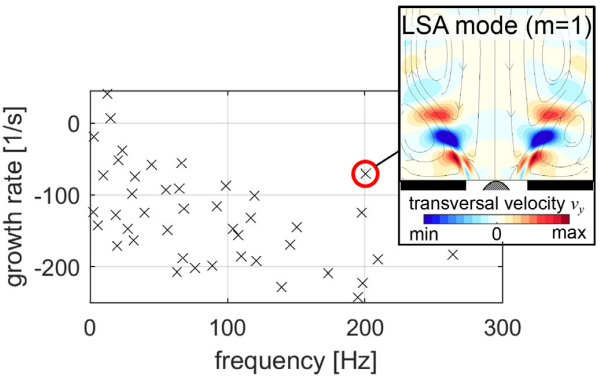

Fig. 5. Global mode spectrum of baseline case derived from LSA conducted for $m = 1$ showing a single separated eigenvalue (circled) with an eigenmode resembling a PVC-like structure.

4. Results

At the beginning of this sections, the baseline case, without actuation, is characterized, including a global LSA. Based on this analysis, PVC actuation is applied over a wide range of actuation frequencies and amplitudes and the response of the flow and the flame is characterized. Based on these studies, the PVC actuation frequency that leads to maximal response is selected and is kept constant throughout the remaining study. Thereafter a parametric study is performed where the actuation amplitude is varied to reveal the impact of the PVC on the FTF and the involved mean field coupling mechanisms.

4.1. Baseline characterisation

The mean fields shown in Fig. 4 reveal the typical features of a swirl-stabilized flame. The flow is undergoing vortex breakdown, which leads to a central recirculation zone around the jet axis and a corresponding inner shear layer between the jet and the central recirculation zone. Moreover, an outer shear layer is formed between the jet and the outer recirculation zone. A V-shaped flame (Fig. 4, right) is stabilized inside the inner shear layer, which is attached to the centerbody tip close to the outlet of the burner. The major mean heat release rate is distributed along the entire inner shear layer upstream of the location where the jet reaches the combustor wall.

As typical for this type of flames [9,10,12], the PVC is not present as it has been assured by a SPOD of PIV snapshots. This is due to the stabilizing effect of the mean density stratification in the flame-root region as detailed in previous studies [9,43].

To asses the stability of the baseline configuration and to unveil the presence of a damped PVC mode, a global stability analysis is conducted. The resulting eigenvalue spectrum is shown in Fig. 5

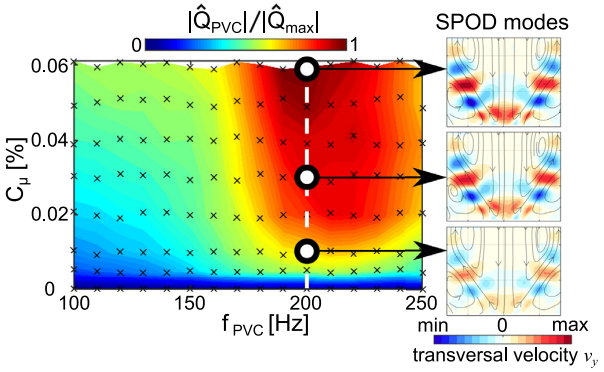

Fig. 6. Flame response to different actuation frequencies (f_{PVC}) and amplitudes (C_μ) depicted by the amplitude of PVC-induced antisymmetric global heat release rate fluctuations $\hat{Q}_{PVC}$ (normalized by overall maximum). Black crosses indicate data points. Flow response modes are shown on the right for C_μ equal to 0.01, 0.03 and 0.06 and $f_{PVC} = 200$ Hz, depicted by the transversal velocity component of SPOD modes (normalized with overall maximum).

for the $m = 1$ mode. It reveals a continuous spectrum and a few discrete eigenvalues standing aloof. The figure furthermore shows the mode shape corresponding to the least stable of the discrete modes at around 200 Hz (see circle in Fig. 5). The mode shape indicates a helical coherent structure located in the inner and outer shear layer that meanders in downstream direction.

The depicted transversal velocity component v_y reveals these structures by symmetric fluctuations in y-direction. These fluctuations indicate the resulting periodic displacement of the jet in either crosswise direction, as shown for example in [9,12,23,29,41,43,44]. The shape and frequency of this mode is very similar to the PVC occurring naturally at a slightly different operating condition featuring a detached M-flame [22,45,46]. Overall the global LSA reveals a discrete eigenmode that resembles characteristics of the PVC mode and which is slightly damped.

4.2. Flow and flame response to PVC actuation

The global LSA reveals a stable global PVC-like mode at around 200 Hz, which is close to the stability limit. According to linear stability theory, the flow response to PVC actuation should, therefore, be strongest at around this frequency [26]. This is verified by a parametric study, where the PVC response was measured for various actuation frequencies and amplitudes.

4.2.1. Flow and flame dynamics

The contour plot shown on the left of Fig. 6 reveals the antisymmetric global heat release rate as a function of PVC actuation frequency and amplitude. This quantity was derived from the antisymmetric OH* signal obtained from the PMT (compare Fig. 1). It serves as a metric for the flame response to the PVC actuation, which is closely related to the flow response [20].

The largest flame response to the PVC actuation appears at around 200 Hz. This agrees very well with the frequency of the least stable global mode identified in the LSA spectrum (Fig. 5). The white dots in Fig. 6 indicate cases where PIV measurements were conducted and the corresponding SPOD modes (transversal velocity component v_y) are shown. As discussed above in connection with the global LSA spectrum, the shape of these SPOD modes indicates the same PVC-induced periodic displacement of the jet in either crosswise direction. Moreover, these modes clearly reveal fluctuations on the jet axis, which is a clear indication of the PVC and a single helical mode ($m = 1$). Different studies revealed very similar mode shapes of the PVC in non-reacting [29,47,48] and reacting swirl flows [9,12,22,23,41,43–46], whereby the same burner was used in [9,43,46].

The comparison of Figs. 5 and 6 shows that the shape of the SPOD and global LSA mode is very similar. Moreover, the frequency of strongest response to PVC actuation measured experimentally agrees very well with the frequency of the PVC mode determined from LSA. This provides empirical evidence that the actuation system successfully excites the PVC mode, which is close to the stability limit. However, there are small deviations regarding the mode shape in the region of the combustion chamber inlet. As shown in previous studies [28,29,31,33], the PVC starts to evolve in the flow region upstream of the combustion chamber inlet. To achieve perfect agreement at the inlet region, flow field data in the mixing tube would be required, which cannot be obtained with the available combustion chamber test rig. Nonetheless, the agreement of the spatial SPOD and LSA mode shapes is reasonably well and, in connection with the excellent agreement between the frequency of the least stable global mode and the measured maximum response, the idea is strongly supported that the actuator excites the damped PVC mode, making use of a naturally existing, but damped global instability.

The efficiency of the flow control can be estimated by relating the energy contained in the SPOD modes to the actuation amplitude. For an actuation amplitude of $C_\mu = 0.06\%$, the PVC-induced flow oscillations contain 13.5% of the total turbulent kinetic energy. This very high efficiency is due to the inherent natural global instability that is exploited by this flow control. Moreover, additional analysis of the flow response data reveals no other coherent structure at either different frequency or azimuthal modenumber that is accidentally excited by the actuation. Hence, this flow control system is applicable for targeted investigations of the PVC influence on combustion properties such as FTF and flame dynamics.

4.2.2. PVC-induced mean field corrections

The actuation of the PVC causes coherent fluctuations which act on the mean field through coherent Reynolds stresses. This section, therefore, considers modifications of the mean flow state due to the response of the flow to PVC actuation.

Figure 7 (left column) depicts the mean fields at different PVC actuation amplitudes indicating slight modifications. The jet spreading appears to be enhanced with increasing actuation amplitude, which is the result of enhanced shear layer growth. Consequently, the backflow in the CRZ is accelerated, which is indicated by the narrowed streamlines and the slightly increased velocity magnitude level around the jet axis near the burner outlet.

To illustrate these observations more distinctly, the axial velocity profiles at $x/D = 0.5$ for different PVC actuation amplitudes are shown in Fig. 8a. This axial location corresponds to high levels of coherent production and strong modifications of the mean flow due to PVC actuation are expected. The figure shows that the maximal velocity remains unaffected by the actuation, but the backflow velocity in the IRZ increases substantially with higher C_μ. Moreover, the jet becomes broader, which indicates an enhanced spreading and shear layer growth

To evaluate the shear layer growth, the shear layer thickness of the ISL is estimated. The thickness of the ISL was chosen, because the PVC is expected to be primarily active in that region. As a measure for the shear layer thickness, the momentum thickness [49]

$$\delta = \int_{y_{0.1}}^{y_{0.9}} \frac{\overline{v}_x}{V_0}\left(1 - \frac{\overline{v}_x}{V_0}\right) dy \tag{7}$$

is determined from the measured velocity fields. The integration limits are chosen such that the ISL is captured in that area between CRZ and the jet, where the mean axial velocity $\overline{v}_x$ is between 10% ($y_{0.1}$) and 90% ($y_{0.9}$) of the maximal axial velocity at this

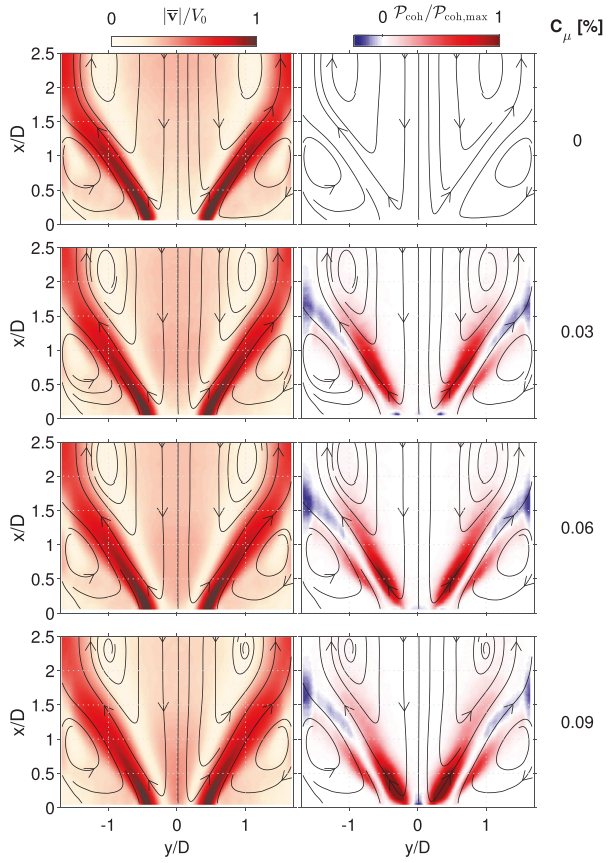

Fig. 7. Mean velocity magnitude (left), normalized with bulk velocity, and production $\mathcal{P}_{coh}$ (right), normalized with respect to overall maximum, of the PVC mode for different PVC actuation amplitudes C_μ.

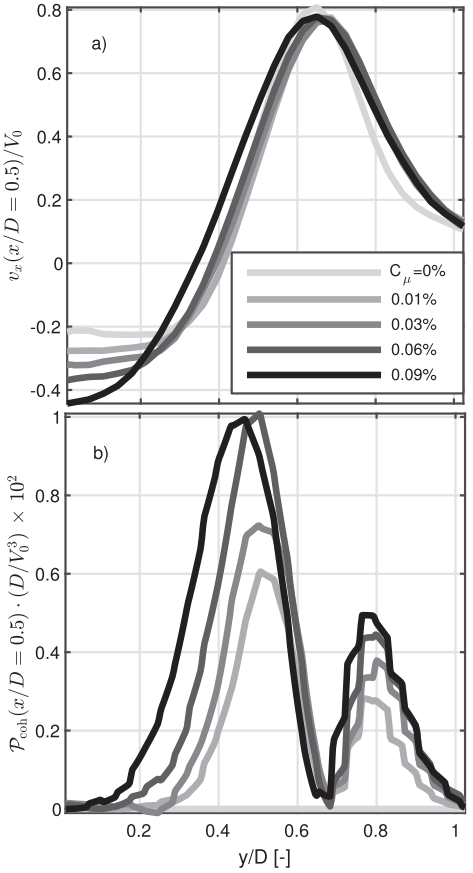

Fig. 8. Axial mean velocity a) and production profiles b) at $x/D = 0.5$ for different C_μ.

Table 1
Momentum thickness of axial shear layer, δ, determined from velocity profiles measured at $x/D = 0.5$ for different PVC actuation amplitudes, and percentage of increase, $\Delta\delta$, with respect to the uncontrolled case.

C_μ	0%	0.01%	0.03%	0.06%	0.09%
δ	1.88	2.00	2.17	2.16	2.32
$\Delta\delta$	0	6%	13.4%	13%	19%

streamwise location. In Table 1, values for the shear layer thickness at $x/D = 0.5$ and the relative growth ($\Delta\delta$) are given. These values show that the ISL grows of up to 19% due to the applied PVC actuation.

The mean flow changes induced by the PVC actuation are a direct consequence of increased coherent production $\mathcal{P}_{coh}$. This quantity is shown in right column of Fig. 7. It is defined as $\mathcal{P}_{coh} = \overline{\tilde{v}_i\tilde{v}_j}\frac{\partial\bar{v}_i}{\partial x_j}$, where $\tilde{v}_i$ is the ith component of the velocity fluctuation of the PVC mode determined from SPOD. $\mathcal{P}_{coh}$ quantifies the energy flux between the mean field and the fluctuating field induced by the PVC, and it indicates where the PVC modifies the mean field. Accordingly, substantial coherent production occurs in the inner and outer shear layer and close to the combustor inlet which coincides well with the enhanced shear layer growth observed in these regions. For the high actuation amplitudes, the production in the inner shear layer close to the combustor inlet is very high, indicating strong activity of the PVC in this region.

The radial profiles of the coherent production at $x/D = 0.5$ are presented in Fig. 8b. They show that coherent production occurs primarily in the region of the ISL, where the maximal value grows with increasing PVC actuation amplitude. Moreover, the increasing spread of these profiles illustrates the shear layer growth due to the PVC actuation. For the highest actuation amplitude of $C_\mu = 0.09\%$, the maximal production does not grow any further but is shifted slightly to the jet center, which potentially indicates a nonlinear saturation process.

In order to evaluate the distribution of the coherent production in axial direction, the coherent production $\mathcal{P}_{coh}$ is integrated in radial direction and plotted over the axial coordinate x, as shown in Fig. 9a). The resulting curves show a continuous increase in streamwise direction which corresponds to the spatial growth of the PVC-induced shear layer oscillations. The location where coherent production reaches its maximum value moves upstream with increasing actuation amplitude, which is expected as the saturation amplitude of the spatially growing structures is reached earlier for higher initial forcing amplitudes [50]. For actuation amplitudes above $C_\mu = 0.06\%$, the overall coherent production does not increase any further, which has already been observed in Fig. 8b, and which is likewise attributed to the saturation process at high amplitudes.

In Fig. 9b, the radial integral of the overall turbulent production $\mathcal{P}_{turb} = \overline{v_i'v_j'}\frac{\partial\bar{v}_i}{\partial x_j}$ is shown, where $v_i' = \tilde{v}_i + v_i''$ are the total velocity fluctuations, including stochastic as well as coherent fluctuations. There is a clear offset between the curves with actuated PVC and

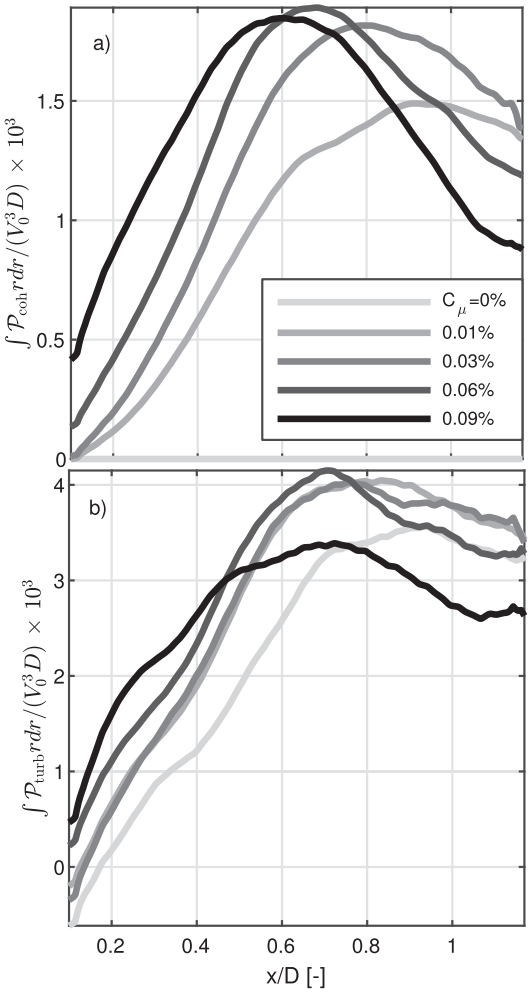

Fig. 9. Radial integral of coherent production (top) and of total turbulent production (bottom) as a function of the axial coordinate x and PVC actuation amplitude C_μ.

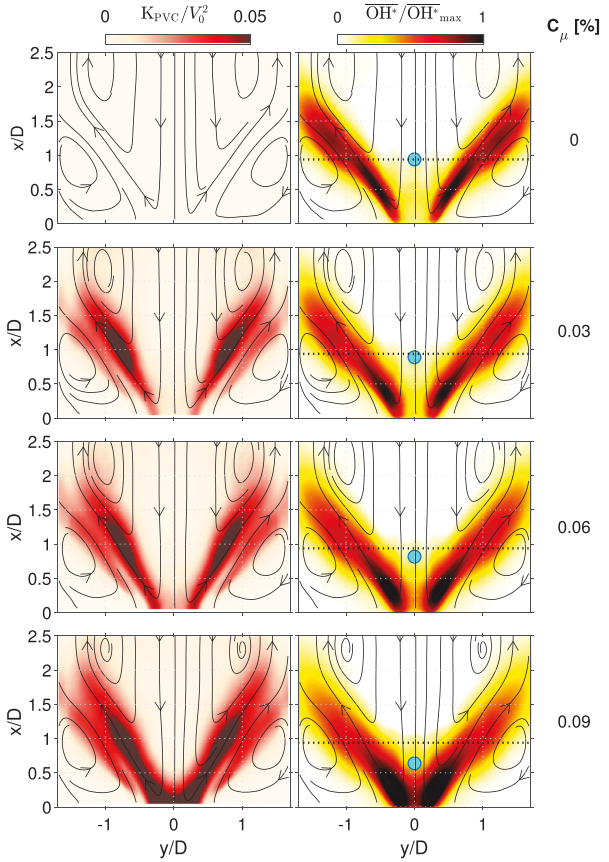

Fig. 10. Kinetic energy of PVC mode (left), normalized by kinetic energy of bulk flow, and mean Abel-deconvoluted heat release rate (right), normalized by overall maximum, for different PVC actuation amplitudes.

the baseline case, which demonstrates a considerable contribution of the actuated PVC to the total turbulent production. For all cases, except for the highest actuation amplitude, saturation sets in at around $x/D = 0.7$, whereby the increasing PVC actuation shifts the saturation point slightly upstream. In case of the highest actuation amplitude, the shape of the curve deviates from the others, which is probably because of a substantial change of the mean flow field and flame (as will be discussed later), which cannot be explained solely based on the turbulent and coherent production.

Before analyzing the impact of the PVC on the mean flame shape, those regions in the flow are revealed where the PVC induces high velocity fluctuations. In this context, the (coherent) kinetic energy distribution K_{PVC} of the PVC mode, which is determined from the SPOD, serves as a suitable quantity to illustrate these regions. It is shown in the left column of Fig. 10. For all actuation amplitudes, the region of highest fluctuation energy is located in the ISL, with a maximum occurring approximately around $x/D = 1$. This is somewhat downstream of the regions of highest coherent production, which is due to the mean convection of turbulence intensity. For the highest PVC actuation amplitude, a region of high fluctuation energy appears at the combustor inlet at the jet centerline. It indicates a strong precessing motion of the vortex core, which is the result of an enhanced coherent production near the jet axis close to the burner outlet (confirm with Figs. 7–9).

Summarizing the results from the analyses above, the main effect of the PVC-actuation on the flow field is the enhancement of the coherent production in the inner and outer shear layers. This enhancement leads to increased turbulent fluctuations, especially in the ISL, which enhances the shear layer growth. These effects are expected to affect primarily the growth of KH-instabilities [24,25]. For high C_μ values, enhanced coherent production induces an increase of fluctuation energy in the region close to the burner outlet. As a result, the actuated PVC constricts the CRZ, which leads to the accelerated backflow observed in Figs. 7 (left) and 8. The observed effects in the shear layers and close to the burner outlet will have a strong impact on the mean flame shape as will be shown in the following section.

4.2.3. PVC-induced mean flame changes

In the right column of Fig. 10, the mean flame shape is depicted for different PVC actuation amplitudes. Most noticeable, the PVC causes a more compact flame with the region of major heat release rate located closer to the combustor inlet. This shift is further quantified by the flame's center of mass (COM), calculated as

$$\mathrm{COM} = \frac{\overline{\int\int \mathrm{OH}^*(\mathrm{x},\mathrm{y})\mathrm{xy}\,\mathrm{dxdy}}}{\int\int \overline{\mathrm{OH}^*}(\mathrm{x},\mathrm{y})\mathrm{y}\,\mathrm{dxdy}}, \tag{8}$$

which is illustrated by a turquoise dot in Fig. 10. The upstream shift is most significant when increasing the actuation amplitude beyond $C_\mu = 0.06\%$. This correlates well with the observed increase of kinetic energy of the PVC in the same region as shown in the left column of Fig. 10. This suggests that the PVC-induced flame surface wrinkling at the flame root is the main driver for heat release rate in this region and therefore the upstream shift of the COM of the flame.

The mean heat release rate distribution in the flame tip region is also affected by the PVC actuation. A thickening of the flame brush is observed and a reduction of overall heat release rate. The first observation correlates well with the observed thickening of the inner shear layer due to PVC-induced coherent production. The second observation is presumably attributed to the enhanced reaction taking place at the flame root, which links back to the enhanced PVC-induced flame wrinkling at this location.

Overall, we observe a significant PVC-induced mean flame changes with the tendency to a more compact and further upstream located flame. Together with the observed mean field modifications, we expect a significant influence of the PVC on the flame response to acoustic perturbations, which is the focus of the next section.

4.3. Influence of PVC actuation on the FTF

Figure 11 shows the gain and phase of the FTF measured at different PVC actuation amplitudes. Considering the baseline case first (black dotted dashed line), the characteristic shape of the FTF gain indicates the superposition of two mechanisms driving the flame response. These are for such type of flame the swirl fluctuations and the vortex roll-up due to KH-instability [2,35]. Swirl fluctuations are axial vorticity waves that are generated when the acoustic waves impinge on the swirl generator. These perturbations propagate from the swirl generator to the flame root at a velocity related to the mean flow and induce global heat release rate fluctuations mainly at the flame root. The KH-instability waves are excited in the shear layers downstream of the combustor inlet. They form large-scale axisymmetric coherent structures that propagate to the flame tip where they induce global heat release rate fluctuations [2,4,51,52]. Difference in propagation velocity and travel distances for both mechanisms result in different convective time delays between the acoustic perturbations and global heat release rate fluctuations. This results in the interference pattern of the FTF gain with levels exceeding unity.

Considering the FTF at increasing PVC actuation amplitude (Fig. 11 colored dotted-dashed lines), a clear change of the gain can be observed. Note that the PVC actuation was applied at $f_{\mathrm{PVC}} = 200$ Hz, which is equal to the frequency of the (damped) PVC mode at the uncontrolled state and which revealed maximum flow response. Reduction in FTF gain is observed over the entire FTF frequency range with a reduction of 47% around $f_{\mathrm{AF}} = 300$ Hz and a reduction around the peaks at $f_{\mathrm{AF}} = \{130, 260\}$ Hz of 11 and 21%, respectively. In these frequency regions, a detailed analysis of the flame and flow response is presented in the following Sections 4.3.1 and 4.3.2. In sharp contrast to the gain, the phase of the FTF, and hence, the convective time delays are unaffected by the PVC actuation, which is surprising in light of the substantial changes of the mean flame location that are observed.

The FTF gain curve exhibits a minimum at around 200 Hz, due to destructive interference of heat release oscillations caused by KH-instability waves and swirl fluctuations. The proximity of the frequency at the FTF gain minimum to the frequencies of PVC's highest receptivity (compare Fig. 6) and the (damped) PVC mode (compare Fig. 5) is a pure coincidence. Actuating the PVC at a slightly different frequency would have an equal impact on the FTF gain but would require a larger actuation amplitude. To further investigate the correlation between the FTF gain curve and the PVC, an extensive parameter study would be required, which is beyond the scope of the present study. Such a future parameter study should include for instance varying swirler positions and different PVC actuation frequencies.

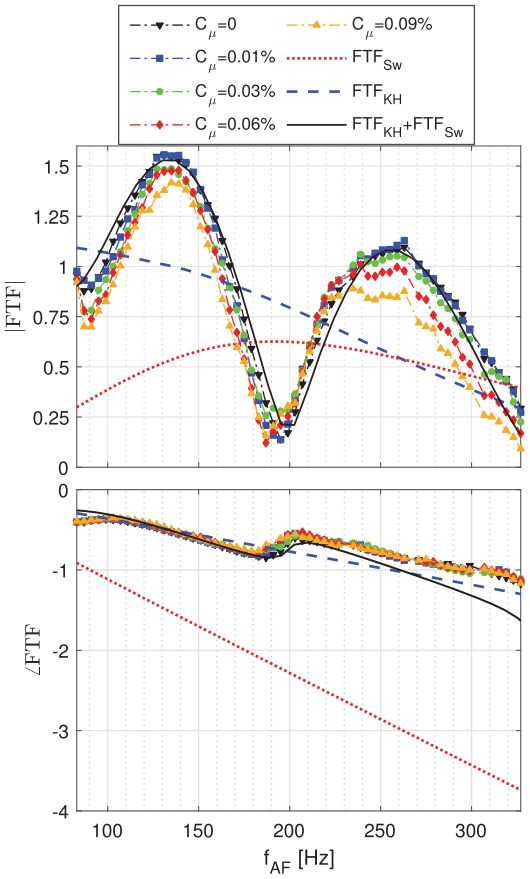

Fig. 11. Measured FTFs for different PVC actuation amplitudes C_μ equal to 0, 0.01, 0.03, 0.06 and 0.09% (markers with dashed lines) and modeled FTF (solid line) as super position of the contributions of the KH-instability $\mathrm{FTF_{KH}}$ (dashed line) and swirl fluctuations $\mathrm{FTF_{Sw}}$ (dotted line). The top plot shows the gain and the bottom plot shows the corresponding phase.

The observation of the FTF at varying PVC amplitudes leads to the central question of the following analysis: What mechanism causes the gain of the FTF to decrease with increasing PVC amplitude while the phase remains unchanged?

In general, the PVC may act on the FTF either through a direct nonlinear interaction between the TA mode and the PVC or through an indirect interaction via the mean fields. A direct linear interaction between a symmetric acoustic modes ($m = 0$) and the PVC mode ($m = 1$) is not possible due to the fundamentally different mode shape. Moreover, a direct nonlinear interaction would require high amplitude acoustic oscillations [17] which is not the case in the present study where the acoustic forcing for the FTF measurements were assured to be within the linear limit. This was verified by a detailed investigation of the mode spectrum based on OH*-chemiluminescence and pressure recordings showing no significant interaction modes. Therefore, the first mechanism can be excluded. This leaves mean field coupling mechanisms as the remaining option which will be investigated in the following.

4.3.1. Interaction mechanism via mean flow field

To assert the impact of the mean flow changes on the FTF, a model based on mean field LSA is employed [35]. Thereby, the FTF is decomposed into two parts,

$$\mathrm{FTF} = \mathrm{FTF_{KH}} + \mathrm{FTF_{Sw}}, \tag{9}$$

where the first part refers to the contribution of the KH-instability and the second to the swirl fluctuations.

The first part is modeled as

$$\mathrm{FTF_{KH}}(\omega) = \frac{\int_0^{x_{\max}} I(x) F_u(x,\omega)\mathrm{d}x}{\int_0^{x_{\max}} I(x)\mathrm{d}x} \tag{10}$$

where F_u refers to a velocity transfer function of the KH-instability determined from local LSA (see Eq. (6)). F_u is weighted by the radially integrated mean flame intensity, $I = \int_0^{r_{\max}} \overline{\mathrm{OH}^*} r \mathrm{d}r$, and spatially integrated to translate the gain and the phase of the KH-instability to the one of the FTF.

For the second part of the FTF, a convective time-lag model is employed, reading

$$\mathrm{FTF_{Sw}} = \mathrm{e}^{-i\omega\tau_1}\mathrm{e}^{-i\omega^2\sigma_1^2} - \mathrm{e}^{-i\omega\tau_2}\mathrm{e}^{-i\omega^2\sigma_2^2}, \tag{11}$$

with two convective time lags τ_1 and τ_2 and two standard deviations σ_1 and σ_2. Komarek and Polifke [53] introduced this model in the context of swirl fluctuations, consulting numerical observations of the flame response to tangential velocity fluctuations. The model parameters are optimized to achieve the best match with the measured FTF, yielding $\tau_1 = 11.4$ ms, $\tau_2 = 11.6$ ms, $\sigma_1 = 0.7$ ms, and $\sigma_2 = 1.8$ ms. The mean value of the two convective time delays corresponds approximately to the time the swirl fluctuations need to travel from the swirler to the flame. The difference of the two time delays corresponds to the time between the heat release increase due to swirl fluctuations and the heat release decrease as explained in [53].

As shown in Fig. 11, the model captures the measured FTF very well in terms of phase and gain. Moreover, the two parts of the FTF depicted in the same figure demonstrate that the FTF gain is largely determined by the interference of the KH-instability and the swirl fluctuations, which was already inferred by previous investigations [2]. Overall, this model quantifies the link between the KH-instability and the measured FTF, which is important for the following analysis.

The influence of the PVC actuation on the KH-instability is shown in Fig. 12. It compares the velocity transfer function F_u determined from LSA based on the mean flows at increasing PVC excitation amplitudes for three selected acoustic forcing frequencies (f_{AF}). Accordingly, the phase of F_u remains unaffected by the PVC actuation, which implies that the propagation velocity of the KH-instability remains unaffected by the mean field changes. However, the gain of the flow transfer functions is affected quite significantly for the moderate and high frequencies. Accordingly, the changes of the mean flow field induced by the PVC actuation substantially reduce the growth rates of the KH-instability. This can be explained by the PVC-induced enhanced turbulent production and related thickening of the inner shear layer which was deduced from Figs. 7 to 9. The region of high coherent production thereby coincides very well with the region of high spatial growth of the KH-instability, which makes this effect quite substantial. The reduction of the KH-instability gain, however, saturates at a PVC forcing amplitude of $C_\mu = 0.03\%$, while the FTF reveals still substantial gain reduction also for higher forcing amplitudes. Hence, the exceeding FTF gain reduction measured in the experiment remains to be addressed in the following paragraph.

4.3.2. Interaction mechanism via mean flame

To explain the FTF gain reduction encountered at PVC actuation amplitudes higher than $C_\mu = 0.03\%$, this section will elucidate

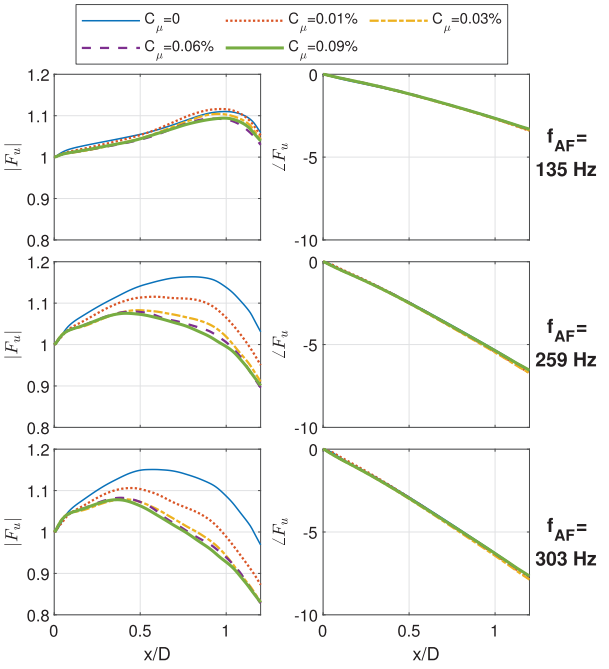

Fig. 12. Velocity transfer function F_u of the KH-instability determined from local LSA at acoustic forcing frequencies (f_{AF}) based on mean fields measured at different PVC actuation amplitudes (C_μ). The left column shows the gain and the right column gives the corresponding phase.

a second coupling mechanism: The modification of the mean flame shape. The phenomena described in Section 4.2.3 show that the PVC changes the mean flame shape in such a way that the main heat release rate is not distributed over the whole flame length anymore but concentrated near the burner outlet (compare Fig. 10, right). Consequently, the reaction zone is concentrated at the flame root in case of a sufficiently high PVC actuation amplitude. Due to the concentrated reaction zone, more fuel is consumed near the flame root, where the PVC is predominantly active, as explained above (compare Fig. 10, left). As a consequence, less fuel can be consumed downstream of the flame root, where the acoustically forced modes are predominantly acting at the sensitive flame tip. This phenomenological explanation for the measured decrease of the FTF gain will be investigated in more detail in the following.

To facilitate a more detailed investigation of the influence of the PVC on the FTF, the spatial distributions of heat release rate fluctuations induced by acoustic forcing were calculated for different PVC actuation amplitudes. For this purpose, the OH* chemiluminescence data was phase-averaged with respect to the acoustic forcing signal. Figure 13 shows contours of the RMS of this quantity, $\mathrm{RMS}(\tilde{q}_{AF})$, for three different acoustic forcing frequencies. It describes the intensity and spatial location of the flame response to acoustic perturbations. The selected frequencies are around the highest FTF gain values ($f_{\mathrm{AF}} = \{135, 259\}$ Hz) and in the region of highest relative gain reduction due to the PVC actuation ($f_{\mathrm{AF}} = 303$ Hz) as can be verified from Fig. 11. The top row of Fig. 13 shows $\mathrm{RMS}(\tilde{q}_{AF})$ for the baseline case without PVC actuation, while the rows below show the quantify for increasing PVC actuation amplitude with each column corresponding to a single acoustic forcing frequency.

For the case without PVC actuation (top row in Fig. 13), two significant regions of heat release rate fluctuations stand out. Region A is located in the inner shear layer at the flame root. It is known to be particularly sensitive to swirl fluctuations [1]. Region B is lo-

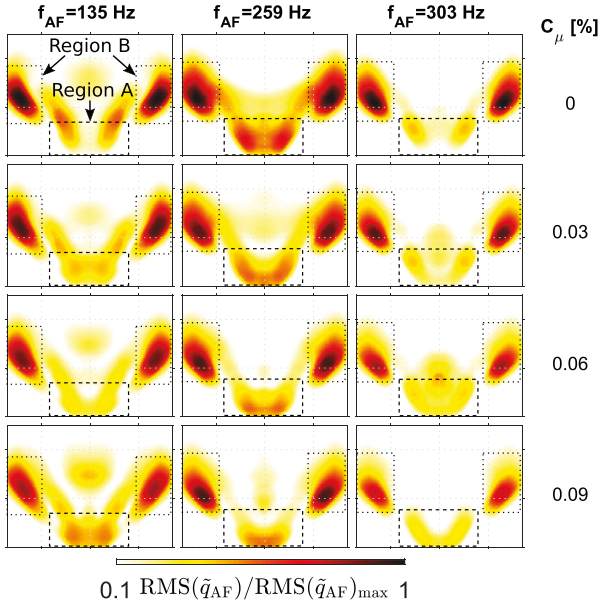

Fig. 13. Contours of intensity of local heat release rate fluctuations, RMS($\tilde{q}_{AF}$), induced by acoustic forcing at three different frequencies f_{AF} (columns) under influence of increasing PVC actuation amplitudes (rows), normalized with respect to overall maximum value.

cated at the flame tip, further downstream and at higher radial positions. Previous studies showed that heat release rate fluctuations in this region arise mainly due to KH waves interacting with the flame tip [1,54].

In region A, the flame response to acoustic perturbations at the flame root move upstream with growing PVC actuation. This upstream movement is connected to the upstream shift of the mean flame (compare Fig 10, right). Furthermore, RMS($\tilde{q}_{AF}$) slightly decreases in region A, especially for 259 Hz and 303 Hz, although the mean heat release rate increases in this region for growing PVC amplitudes. As concluded before, this increase of mean heat release is attributed to strong PVC-induced flame-front wrinkling due to a high kinetic energy of the PVC in region A (compare Fig 10, left). The damping of RMS($\tilde{q}_{AF}$) in region A has a rather small impact on the FTF gain, since the major heat release rate fluctuations are to be found at the flame tip.

Region B is expected to primarily determine the FTF gain and phase, because there the strongest heat release rate fluctuations are observed. With increasing PVC actuation amplitude, RMS($\tilde{q}_{AF}$) decreases in this region for all considered acoustic forcing frequencies. This decrease confirms the phenomenological explanation, which was given at the beginning of this section. The upstream shift of the COM of the mean flame with increasing PVC amplitude (compare Fig. 10, right) indicates the concentration of the mean flame near the flame root. Accordingly, the (mean) flame is moved away from region B, i.e. the flame tip, which is sensitive to acoustically forced modes. As a consequence, the reaction zone is also shifted upstream such that relatively more fuel is consumed near the flame root. Therefore, incoming flow perturbations, induced by acoustic forcing, are hindered to act on the flame tip (in region B) as distinctly as in the baseline case. This leads to lower RMS($\tilde{q}_{AF}$) in this region, which affects a reduced gain in the global flame response.

Local LSA has shown that the hydrodynamic response of the KH-mode to acoustic forcing remains unaffected by an additional increase of the PVC actuation amplitude for $C_\mu > 0.03\%$ (see

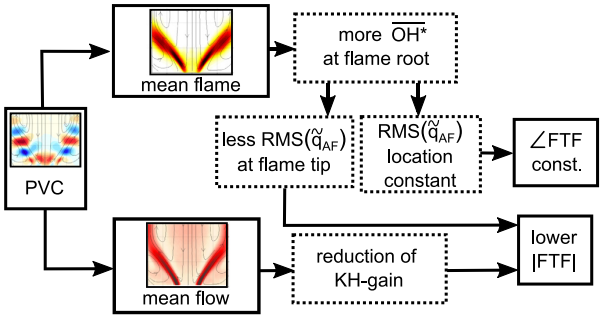

Fig. 14. Flow chart with identified interaction mechanisms explaining the damping influence of the PVC on the FTF.

Fig. 12). For these amplitudes, however, the PVC continues to shift the flame's COM away from region B, where the KH-instability perturbs the flame the most. Thus, the PVC-induced modification of the mean flame supersedes the hydrodynamic damping mechanism for high PVC actuation amplitudes. This explains the reduction of FTF gain observed for PVC actuation amplitudes higher than $C_\mu = 0.03\%$.

Finally, the independence of the FTF phase lag with respect to the PVC actuation is addressed. Intuitively, one might expect that an upstream shift of the COM of the flame should cause a decrease of the time delay and therefore have a significant impact on the phase of the FTF. As illustrated in Fig. 11 however, the phase remains rather unaffected by the PVC actuation. This contradiction can be resolved by adducing Fig. 13. The figure shows that despite the upstream shift of the mean flame, the location where the KH-mode induces the strongest heat release rate fluctuations remains the same with increasing PVC actuation (region B). Furthermore, the flow transfer functions deduced from the LSA show that the propagation velocity of the KH-mode remains likewise unaffected by the PVC actuation. And since the phase of the FTF is mainly depending of the convective time delay of the KH-wave from the burner outlet to the flame tip, it remains unaffected by the PVC actuation as well.

5. Conclusions

In this study, active flow control is applied to excite a PVC mode in a turbulent perfectly premixed swirl flame. Open-loop control is applied in a region of high receptivity and it is shown to excite the natural global instability that is damped by the flame and does not appear naturally. This provides excellent experimental conditions to investigate the exclusive impact of the PVC on the FTF and related heat release rate fluctuations. It is observed that PVC actuation leads to a significant reduction of the FTF gain but leaves the phase unaffected.

Based on the experimental data and linear stability analysis, the mechanisms leading to the change of the FTF are investigated. As the PVC is a helical-shaped coherent structure, it generates no global heat release rate fluctuations and hence cannot contribute directly to the FTF. Therefore, the mechanisms at hand are more indirect and act via the mean field or mean flame.

Figure 14 summarizes the interaction mechanisms identified in this work. In the first mechanism (lower branch in Fig. 14), the PVC modifies the mean flow due to coherent production. This leads to a reduced sensitivity of the shear layers to axisymmetric acoustic perturbations and thus to a reduction in the FTF gain, which support the hypothesis proposed in [25]. The second mechanism (upper branch in Fig. 14) is related to the change of the mean flame shape due to an increase of PVC-induced velocity fluctua-

tions near the flame root. Hereby, the reacting zone is located further upstream and the flame becomes more compact leading to weaker fluctuations of heat release rate at the flame tip, which is most influential for the FTF gain. Despite the change of the flame shape, the location of influential heat release rate fluctuations remains unchanged, which explains why the PVC does not affect the FTF phase.

In summary, this study quantifies and explains the impact of the PVC on the response of swirl flames to acoustic perturbations, which is a key for prediction and control of TA instabilities. The identified mechanisms explain how the PVC can damp TA modes as it was observed in a previous study [20]. Active flow control was thereby a key enabler to isolate the exclusive impact of the PVC, and to validate recently proposed research hypotheses. The study further shows that such a control is extremely efficient as it exploits the natural amplification of flow perturbations due to an inherent global hydrodynamic instability.

The focus of the present study is to explain how the PVC reduces the gain of the FTF via the change of the mean flow and the mean flame in the present combustion system. The study, however, raises further questions that need to be addressed in future studies: First, the general significance of the PVC in the context of the FTF and associated flame dynamics needs to be evaluated by applying the approach to other combustors. Furthermore, LES should be performed, which will provide additional insight into the physical mechanisms at play and yield flow data which is inaccessible to experimental measurements, as, for example, the region upstream of the burner outlet. In combination with global stability/sensitivity analysis of the PVC, these numerical simulations will additionally yield measures to optimize the actuation of the PVC and therefore the FTF gain reduction.

The current experiments were conducted at a model gas turbine combustor test rig, which was designed for industrial-scale investigations under atmospheric conditions. It is expected that the current findings are applicable to high pressure conditions, as well. As shown in [55,56], the PVC remains a key factor for combustion dynamics at elevated pressure for example in the context of PVC-induced mixing and thermoacoustic oscillations. Therefore, the results and developed methodologies of the present study should be directly applicable to the development of future flow control schemes suited for real gas turbine combustors. However, for industrial applications the transfer from the present active to a passive control scheme is the next logical step to contribute to the development of more stable combustion in future gas turbines.

Declaration of Competing Interest

The authors declare that they have no known competing financial interests or personal relationships that could have appeared to influence the work reported in this paper.

Acknowledgments

The funding of the German Research Foundation (grant number 247226395) is acknowledged. Special thanks go out to Andy Göhrs, Alexander Jaeschke and Mario Casel for supporting the experimental and analytical work.

References

[1] P. Palies, D. Durox, T. Schuller, S. Candel, The combined dynamics of swirler and turbulent premixed swirling flames, Combust. Flame 157 (9) (2010) 1698–1717.
[2] P. Palies, T. Schuller, D. Durox, L.Y.M. Gicquel, S. Candel, Acoustically perturbed turbulent premixed swirling flames, Phys. Fluids 23 (3) (2011) 037101-1–037101-15.
[3] K. Oberleithner, C.O. Paschereit, I. Wygnanski, On the impact of swirl on the growth of coherent structures, J. Fluid Mech. 741 (2014) 156–199.
[4] K. Oberleithner, S. Schimek, C.O. Paschereit, Shear flow instabilities in swirl-stabilized combustors and their impact on the amplitude dependent flame response: a linear stability analysis, Combust. Flame 162 (1) (2014) 86–99.
[5] S. Candel, D. Durox, T. Schuller, J.-F. Bourgouin, J.P. Moeck, Dynamics of swirling flames, Annu. Rev. Fluid Mech. 46 (1) (2014) 147–173.
[6] C.O. Paschereit, B. Schuermans, W. Polifke, O. Mattson, Measurement of transfer matrices and source terms of premixed flames, J. Eng. Gas Turb. Power 124 (2) (2002) 239–247.
[7] M.P. Juniper, R. Sujith, Sensitivity and nonlinearity of thermoacoustic oscillations, Annu. Rev. Fluid Mech. 50 (1) (2018) 661–689.
[8] F. Gallaire, M. Ruith, E. Meiburg, J.-M. Chomaz, P. Huerre, Spiral vortex breakdown as a global mode, J. Fluid Mech. 549 (2006) 71–80.
[9] S. Terhaar, K. Oberleithner, C. Paschereit, Key parameters governing the precessing vortex core in reacting flows: an experimental and analytical study, Proc. Combust. Inst. 35 (3) (2015) 3347–3354.
[10] K. Oberleithner, M. Stöhr, S.H. Im, C.M. Arndt, A.M. Steinberg, Formation and flame-induced suppression of the precessing vortex core in a swirl combustor: Experiments and linear stability analysis, Combust. Flame 162 (8) (2015) 3100–3114.
[11] S. Terhaar, B. Ćosić, C. Paschereit, K. Oberleithner, Suppression and excitation of the precessing vortex core by acoustic velocity fluctuations: an experimental and analytical study, Combust. Flame 172 (2016) 234–251.
[12] F. Lückoff, M. Sieber, C.O. Paschereit, K. Oberleithner, Phase-opposition control of the precessing vortex core in turbulent swirl flames for investigation of mixing and flame stability, J. Eng. Gas Turb. Power 141 (11) (2019) 111008-1–111008–111010.
[13] A. Steinberg, C. Arndt, W. Meier, Parametric study of vortex structures and their dynamics in swirl-stabilized combustion, Proc. Combust. Inst. 34 (2) (2013) 3117–3125.
[14] M. Stöhr, K. Oberleithner, M. Sieber, Z. Yin, W. Meier, Experimental study of transient mechanisms of bi-stable flame shape transitions in a swirl combustor, J. Eng. Gas Turb. Power 140 (2018) 011503.
[15] Q. An, W.Y. Kwong, B.D. Geraedts, A.M. Steinberg, Coupled dynamics of lift-off and precessing vortex core formation in swirl flames, Combu. Flame 168 (2016) 228–239.
[16] Q. An, A.M. Steinberg, The role of strain rate, local extinction, and hydrodynamic instability on transition between attached and lifted swirl flames, Combust. Flame 199 (2019) 267–278.
[17] J.P. Moeck, J.-F. Bourgouin, D. Durox, T. Schuller, S. Candel, Nonlinear interaction between a precessing vortex core and acoustic oscillations in a turbulent swirling flame, Combust. Flame 159 (8) (2012) 2650–2668.
[18] V. Acharya, Shreekrishna, D.-H. Shin, T. Lieuwen, Swirl effects on harmonically excited, premixed flame kinematics, Combust. Flame 159 (3) (2012) 1139–1150.
[19] A. Steinberg, I. Boxx, M. Stöhr, C. Carter, W. Meier, Flow – flame interactions causing acoustically coupled heat release fluctuations in a thermo-acoustically unstable gas turbine model combustor, Combust. Flame 157 (12) (2010) 2250–2266.
[20] F. Lückoff, K. Oberleithner, Excitation of the precessing vortex core by active flow control to suppress thermoacoustic instabilities in swirl flames, Int. J. Spray Combust. 11 (2019), doi:10.1177/1756827719856237.
[21] C.O. Paschereit, E.J. Gutmark, W. Weisenstein, Excitation of thermoacoustic instabilities by the interaction of acoustics and unstable swirling flow, AIAA J. 38 (2000) 1025–1034.
[22] A.M. Steinberg, I. Boxx, M. Stohr, W. Meier, C.D. Carter, Effects of flow structure dynamics on thermoacoustic instabilities in swirl-stabilized combustion, AIAA J. 50 (4) (2012) 952–967.
[23] Z. Yin, M. Stöhr, Time–frequency localisation of intermittent dynamics in a bistable turbulent swirl flame, J. Fluid Mech. 882 (2019) A30–1-A30-42.
[24] B. Mathews, S. Hansford, J. O'Connor, Impact of swirling flow structure on shear layer vorticity fluctuation mechanisms, ASME Turbo Expo, Volume 4A: Combustion, Fuels and Emissions, 2016. V04AT04A026
[25] M. Frederick, K. Manoharan, J. Dudash, B. Brubaker, S. Hemchandra, J. O'Connor, Impact of precessing vortex core dynamics on shear layer response in a swirling jet, J. Eng. Gas Turb. Power 140 (6) (2018) 061503.
[26] D. Sipp, O. Marquet, P. Meliga, A. Barbagallo, Dynamics and control of global instabilities in open-flows: a linearized approach, Appl. Mech. Rev. 63 (3) (2010) 030801.
[27] O. Tammisola, M.P. Juniper, Coherent structures in a swirl injector at Re = 4800 by nonlinear simulations and linear global modes, J. Fluid Mech. 792 (2016) 620–657.
[28] J.S. Müller, F. Lückoff, K. Oberleithner, Guiding actuator designs for active flow control of the precessing vortex core by adjoint linear stability analysis, J. Eng. Gas Turb. Power 141 (4) (2018) 041028.
[29] J.S. Müller, F. Lückoff, P. Paredes, V. Theofilis, K. Oberleithner, Receptivity of the turbulent precessing vortex core: synchronization experiments and global adjoint linear stability analysis, J. Fluid Mech. 888 (2020) A3.
[30] F. Lückoff, M. Sieber, C.O. Paschereit, K. Oberleithner, Characterization of different actuator designs for the control of the precessing vortex core in a swirl-stabilized combustor, J. Eng. Gas Turb. Power 140 (4) (2017) 041503–041503–10.
[31] T.L. Kaiser, T. Poinsot, K. Oberleithner, Stability and sensitivity analysis of hydrodynamic instabilities in industrial swirled injection systems, J. Eng. Gas Turb. Power 140 (2018) 051506-1–051506-10.
[32] T.L. Kaiser, L. Lesshafft, K. Oberleithner, Prediction of the flow response of a turbulent flame to acoustic pertubations based on mean flow resolvent anal-

ysis, J. Eng. Gas Turb. Power 141 (11) (2019) 111021-1–111021-8, doi:10.1115/1.4044993.
[33] T.L. Kaiser, K. Oberleithner, L. Selle, T. Poinsot, Examining the effect of geometry changes in industrial fuel injection systems on hydrodynamic structures with BiGlobal linear stability analysis, J. Eng. Gas Turb. Power 142 (1) (2019) 011024-1–011024-8, doi:10.1115/1.4045018.
[34] D. Greenblatt, I.J. Wygnanski, The control of flow separation by periodic excitation, Prog. Aerosp. Sci. 36 (7) (2000) 487–545.
[35] K. Oberleithner, C.O. Paschereit, Modeling flame describing functions based on hydrodynamic linear stability analysis, ASME Turbo Expo, Volume 4B: Combustion, Fuels and Emissions, 2016. V04BT04A009
[36] B. Schuermans, F. Guethe, D. Pennell, D. Guyot, C.O. Paschereit, Thermoacoustic modeling of a gas turbine using transfer functions measured under full engine pressure, J. Eng. Gas Turb. Power 132 (11) (2010). 2010
[37] P. Voigt, R. Schodl, P. Griebel, Using the laser light sheet technique in combustion research, 90th Symposium of AGARD-PEP on Advanced Non-intrusive Instrumentation for Propulsion Engines, 1997. Oct. 20–24, Bruessel, 1997
[38] I. Roehle, R. Schodl, P. Voigt, C. Willert, Recent developments and applications of quantitative laser light sheet measuring techniques in turbomachinery components, Meas. Sci. Technol. 11 (2000) 1023.
[39] M. Sieber, C.O. Paschereit, K. Oberleithner, Spectral proper orthogonal decomposition, J. Fluid Mech. 792 (2016) 798–828.
[40] P. Holmes, J.L. Lumley, G. Berkooz, C.W. Rowley, Turbulence, Coherent Structures, Dynamical Systems and Symmetry, Cambridge Monographs on Mechanics, 2nd, Cambridge University Press, 2012.
[41] M. Sieber, C.O. Paschereit, K. Oberleithner, Advanced identification of coherent structures in swirl-stabilized combustors, J. Eng. Gas Turb. Power 139 (2016) 021503–021503–8.
[42] D. Barkley, Linear analysis of the cylinder wake mean flow, Europhys. Lett. 75 (2006) 750–756.
[43] K. Oberleithner, S. Terhaar, L. Rukes, C.O. Paschereit, Why nonuniform density suppresses the precessing vortex core, J. Eng. Gas Turb. Power 135 (() (2013). 121506 (9 pages)
[44] M. Stöhr, R. Sadanandan, W. Meier, Phase-resolved characterization of vortex-flame interaction in a turbulent swirl flame, Exp. Fluids 51 (2011) 1153–1167.
[45] M. Stöhr, I. Boxx, C.D. Carter, W. Meier, Experimental study of vortex flame interaction in a gas turbine model combustor, Combust. Flame 159 (2012) 2636–2649.
[46] S. Terhaar, K. Oberleithner, C.O. Paschereit, Impact of steam-dilution on the flame shape and coherent structures in swirl-stabilized combustors, Combust. Sci. Technol. 186 (7) (2014) 889–911.
[47] K. Oberleithner, M. Sieber, C.N. Nayeri, C.O. Paschereit, C. Petz, H.-C. Hege, B.R. Noack, I. Wygnanski, Three-dimensional coherent structures in a swirling jet undergoing vortex breakdown: stability analysis and empirical mode construction, J. Fluid Mech. 679 (2011) 383–414.
[48] L. Rukes, M. Sieber, C. Oliver Paschereit, K. Oberleithner, Methods for the extraction and analysis of the global mode in swirling jets undergoing vortex breakdown, J. Eng. Gas Turb. Power 139 (2) (2016) 022604.
[49] H. Schlichting, Boundary Layer Theory, 6th, McGraw-Hill, New York, 1968.
[50] K. Oberleithner, L. Rukes, J. Soria, Mean flow stability analysis of oscillating jet experiments, J. Fluid Mech. 757 (2014) 1–32.
[51] S. Terhaar, B. Ćosić, C.O. Paschereit, K. Oberleithner, Impact of shear flow instabilities on the magnitude and saturation of the flame response, J. Eng. Gas Turb. Power 136 (7) (2014) 071502.
[52] B. Ćosić, S. Terhaar, J.P. Moeck, C.O. Paschereit, Response of a swirl-stabilized flame to simultaneous perturbations in equivalence ratio and velocity at high oscillation amplitudes, Combust. Flame 162 (4) (2015) 1046–1062.
[53] T. Komarek, W. Polifke, Impact of swirl fluctuations on the flame response of a perfectly premixed swirl burner, J. Eng. Gas Turb. Power 132 (6) (2010) 061503-1–061503-7, doi:10.1115/1.4000127.
[54] K. Oberleithner, S. Schimek, C.O. Paschereit, On the impact of shear flow instabilities on global heat release rate fluctuations: Linear stability analysis of an isothermal and a reacting swirling jet, ASME Turbo Expo 2012: Turbine Technical Conference and Exposition. Volume 2: Combustion, Fuels and Emissions, Parts A and B (2012), pp. 1307–1320.
[55] C.D. Slabaugh, I. Boxx, S. Werner, R.P. Lucht, W. Meier, Structure and dynamics of premixed swirl flames at elevated power density, AIAA J. 54 (3) (2016) 946–961.
[56] R. Zhang, I. Boxx, W. Meier, C.D. Slabaugh, Coupled interactions of a helical precessing vortex core and the central recirculation bubble in a swirl flame at elevated power density, Combust. Flame 202 (2019) 119–131.

Chapter 3

Discussion and Conclusions

In this chapter, the findings gathered in publications 2.1 to 2.5 are discussed, summarized and related to each other. This discussion, which is the first major part of this chapter, intends to present the publications, accumulated in this thesis, as a whole. Moreover, in the second part of this chapter, concluding remarks will be given which include a suggestion of future steps based on the findings shown in the present manuscript.

3.1 Discussion

This section follows the chronological order of the publications presented above. Firstly, the active flow control approach is discussed (chapter 3.1.1). This includes the design of the actuator and sensor setup, the theoretical control approach and alternative actuator designs which could be derived from the one developed in this thesis. Secondly, the findings obtained with the active PVC control regarding flame dynamics are discussed and related to each other (chapter 3.1.2). Besides the impact of the PVC on the mean flame shape, the role of the PVC in interactions with axisymmetric TA modes and the effect on the FTF are discussed. Finally, the impact of the PVC on mixing of fuel and air as well as the mixing of products and reactants is addressed (chapter 3.1.3) which stands in close connection to NO_x emissions (chapter 3.1.4).

3.1.1 Active flow control approach

The first step in the course of this thesis is the development of an active flow control approach, which allows for controlling the PVC. The primary purpose of this control system is to realize experimental conditions which enable a targeted investigation of the impact of the PVC on the combustion process. The development of such a flow control system involves the definition of an actuator and sensor design which follows a certain control approach.
In the following sections the development of the flow control system based on the first

publication 2.1 is discussed. Subsequently, the control approach is addressed which involves findings from studies associated with the present thesis [86, 87]. In this context, a proof of concept is given for the flow control system which refers to the second publication 2.2 as well. At the end of this section, an alternative actuator design will be discussed which is based on fluidic oscillators. This alternative design was investigated in two master theses [3, 8], which are associated with this thesis.

Sensor arrangement

A reliable sensor setup is required to control the PVC, especially in a closed-loop approach. Due to the single-helical shape of the PVC, which meanders around the jet axis, a pressure sensor array arranged around the circumference of the nozzle appears to be suitable to detect the dynamics of the PVC. Therefore, circumferential sensor arrangements at different radii on the front plate (R1-R5) and axial positions in the mixing tube (A1-A5), as shown in Fig. 3 of publication 2.1, are tested and compared regarding their capabilities of resolving the PVC dynamics accurately. The pressure signals very close to the area jump from mixing tube to combustion chamber show a slightly higher phase error compared with the phase information obtained from flow field measurements. However, in both regions, at the front plate and in the mixing tube, the PVC can be reliably detected. Accordingly, there is a certain flexibility in the sensor arrangement to guarantee a reliable PVC detection. Therefore, one sensor array close to position A3 inside the mixing tube and one array at the front plate close to position R3 are implemented into the experimental setup that allows for realizing reacting conditions with flame.
The sensors inside the mixing tube are used especially in cases with high thermal power where the sensor arrays at the front plate are exposed to high temperatures which can cause malfunction. Inside the mixing tube, the sensors are slightly tilted to avoid a direct interference with the actuation jets (compare e.g. Fig. 2 in publication 2.2). Furthermore, the sensors are cooled with pressurized air to withstand high temperatures under reacting conditions.

Actuator design

The actuator designs studied in publication 2.1 are integrated into a centerbody which is a main component of the burner utilized in this thesis [118]. The original centerbody has a cylindrical shape with a sharp edged tip (compare design III in Fig. 4 of publication 2.1 or [118]). The blunt trailing edge of this axisymmetric bluff body generates a wake flow which might have a stabilizing effect on the flame (see Fig. 5 of publication 2.1). However, such a wake typically exhibits large-scale (helical) vortex shedding modes, whereat single-helical modes ($m = \pm 1$) appear to be the most energetic ones [15, 112, 121]. To avoid an interaction of these wake modes with the PVC, the shape of the trailing edge was modified from a blunt trailing edge to a parabolic tip such that the size of the wake, and with that the dynamical impact, is minimized. The shape of this parabolic tip (compare Fig. 4 of publication 2.1 or Fig. 1.9) follows the boat-tailing design rules which are typically applied to bluff bodies to minimize the wake formation [49]. The comparison

of the two different centerbody designs, depicted in Fig. 6 of publication 2.1, confirms that the parabolic shape provides more distinct PVC dynamics which is traced back to the wake reduction and involved vortex shedding. With the newly developed centerbody shape, appropriate experimental conditions are provided which allow for studying the exclusive impact of the PVC on the combustion process.

The actuator is driven by four loudspeakers which generate synthetic jets, according to the zero-net-mass-flux principle [55], at the outlets of the actuation channels. Different actuation channel designs are tested in publication 2.1 which can be categorized into two groups: lance-based and integrated channels. The lance-based designs (compare design I and II in Fig. 4 of publication 2.1) are inspired by the actuator design successfully tested by Kuhn et al. [63] for closed-loop control of the PVC. The idea behind the lances is a targeted actuation of the wavemaker which is expected to be slightly upstream of the CRZ. With the lances, the actuation position can be adjusted to the wavemaker location which was successfully shown in [63]. However, the lance-based design has an intrusive effect on the flow field and would be exposed to a harsh environment under reacting conditions which makes a reliable operation of the actuator potentially very difficult. Therefore, the second group is tested which consists of centerbodies with integrated actuation channels (compare design III to VII in Fig. 4 of publication 2.1). This design is inspired by the actuator applied by Oberleithner et al. [94, 95] to study coherent structures in a turbulent swirling jet undergoing vortex breakdown. The eight loudspeakers driving this actuator are arranged circumferentially around the nozzle outlet allowing for a helical actuation of modes up to an azimuthal order of $m = \pm 4$. This concept is reduced to four loudspeakers in the actuator applied in this thesis because of geometrical restrictions. However, the actuation of a PVC mode is possible in a non-intrusive manner and the harsh environment induced by the flame under reacting conditions does not directly influence the performance of the actuator.

The momentum induced by the individual actuator designs is decisive for successful actuation of the PVC. Based on hotwire measurements at the outlets of the actuation channels, it is shown, in publication 2.1 (Fig. 8 and 11), that the lance-based actuators generate actuation jets with a negligible momentum. As reasons for this result, the small outlet and channel diameters in connection with comparably large channel lengths from loudspeaker plenum to the outlet need to be mentioned. Such channel geometries generate a high pressure loss compared to those actuator designs where the actuation channel diameter is kept constant until the outlet as it has been realized in designs VI and VII (compare Fig. 4 in publication 2.1). Accordingly, designs VI and VII generate a considerably higher actuation momentum which is very similar for both designs.

However, design VII is chosen for further investigations and is utilized in publications 2.2 to 2.5. The choice is made due to the following considerations. The actuation jets generated by design VII are directed in radial direction which is similar to previous successfully tested actuator designs [63, 94]. Compared to design VI, azimuthal actuation is realized over a larger circumference with design VII which leads to a larger radius of action. Furthermore, the direct impact on the mean flow field of the axially directed actuation jets generated by design VI appears to be considerably higher since the jets directly hit the shear layers and the CRZ. This configuration is expected to contradict the direct PVC control approach which aims to actuate only the PVC without altering the general flow configuration. Nonetheless, it would be worth further investigating design VI which

is beyond the scope of the present study.
The radially directed jets of design VII are expected to actuate the flow in a region inside the mixing section where the receptivity of the PVC mode is expected to be high [59, 140]. This contradicts the approach of Kuhn et al. [63] where the actuation is applied close to the wavemaker which is close to the upstream end of the CRZ. Further discussions about the control approach are given in the next paragraph.

Control approach and proof of concept

Associated with the publications accumulated in the present manuscript are two studies by Müller et al. [86, 87] which were conducted in parallel (compare list of associated publications). These studies investigate the receptivity of the PVC in a generic turbulent swirling jet which is comparable to the isothermal combustor flow analyzed in the present thesis. The receptivity is derived based on a global adjoint LSA which solves the adjoint eigenvalue problem derived from the continuous form of the adjoint equations of Eqs.1.9 and 1.10 [79, 86, 87]. The adjoint LSA of the non-actuated mean flow delivers adjoint modes which can be interpreted as two-dimensional representations of the receptivity of the PVC to (periodic) open-loop forcing. Accordingly, the adjoint modes show where in the flow field an appropriate actuator should be positioned to achieve the maximal forcing response. The theoretically derived receptivity is experimentally validated by a lock-in study, where the actuation position is shifted in axial direction along the generic mixing tube. As the actuator approaches the predicted region of highest receptivity, the lock-in amplitude decreases as expected from the adjoint modes.
Both studies [86, 87] show that the region upstream of the CRZ is crucial for the formation of the PVC. Accordingly, a finite region upstream of the nozzle outlet (inside the mixing tube) is identified where the PVC is very receptive. This region is comparably close to the actuator position in the experimental setup applied in this thesis. Therefore, it can be concluded that the actuation is induced in the region of highest receptivity which means that only small actuation amplitudes are required to achieve a large (control) effect on the PVC. The region of high receptivity correlates with the region of high turbulent production which is responsible for the initiation and the amplification of the PVC [87]. These findings can be further interpreted such that the region of highest receptivity describes the origin of the PVC. Accordingly, the findings of Müller et al. [86, 87] suggest that the actuation applied in this thesis follows the direct control approach which aims to actuate the PVC at its origin.
Admittedly, the flow configuration investigated by Müller et al. [86, 87] is not exactly the same as the one studied here in which a centerbody is positioned inside the mixing tube. From an experimental point of view, such an adjoint LSA study could not be realized in the combustion chamber test rig utilized in this thesis. Due to geometrical restrictions, optical access to the flow region upstream of the burner outlet cannot be provided to the extent required for appropriate PIV measurements. Alternatively, an extensive LES calculation of the reacting flow configuration could be conducted to determine the necessary flow information upstream of the burner outlet which is crucial for a global adjoint LSA, but beyond the scope of the present thesis. Nonetheless, there are different studies, analyzing even more complex geometries as the one investigated in [86, 87], which revealed

comparable results regarding the shape of the adjoint modes reaching into the nozzle [59, 140]. Therefore, the findings of Müller et al. [86, 87] are assumed to be applicable to the present flow configuration.
The results obtained by Müller et al. [86, 87] demonstrate that the global adjoint LSA is a valid and valuable tool for the design process of future active flow control approaches as it provides information about the optimal actuator position and forcing direction. These findings support the control approach followed in this thesis and reveal new insights into the generation and the origin of the PVC. Since the adjoint LSA relies on a theoretical framework by solving the (linearized) Navier-Stokes equations, it can be applied to any other global instability which needs to be controlled. The adjoint mode intrinsically quantifies the receptivity of a global mode to any type of periodic forcing. Therefore, the receptivity can be applied to tailor a closed-loop control approach as well, which aims e.g. to suppress the global mode via phase-opposition control [87].

The proof of the direct control concept consists of experiments and corresponding analyses, which are spread over all publications. A summary and discussion of the proof of concept is given in the following four steps:

1. In the first step towards the proof of the direct control concept, the actuator performance is tested in a lock-in study (compare chapter 1.5.1 and publication 2.1). In this lock-in experiment, an isothermal flow featuring a natural PVC is actuated at a frequency slightly higher than the natural PVC frequency. The pressure signal is decomposed such that the PSD spectrum for the first azimuthal mode can be derived. This spectrum reveals a broader peak at the natural frequency describing the oscillatory dynamics of the natural PVC and a rather sharp peak at the actuation frequency. By continuously increasing the actuation amplitude, a typical synchronization effect can be observed (compare [71, 72, 86, 87]): the natural frequency is continuously *pulled* towards the actuation frequency until both frequencies overlay and lock-in occurs. The capability of the actuator to achieve lock-in is a first indicator that the whole control system is capable of controlling the PVC directly. The lock-in study based on the pressure signal is continued in publication 2.2 where Fig. 4 shows that phase locking between the actuation signal and the PVC occurs for high actuation amplitudes. Phase-locking is a sufficient condition for synchronization of the PVC with the actuation signal [71]. In connection with the observations from the PSD spectra in publication 2.1, it can be concluded, based on the pressure measurements, that the actuation system appears to be capable of controlling the PVC.

2. To further verify the direct control approach, the impact on the flow field, especially the PVC mode, needs to analyzed. In publication 2.2, the lock-in study is accompanied by PIV measurements which allows for calculating the SPOD mode and corresponding time coefficients describing the PVC shape and dynamics (see Fig. 3 of publication 2.2). The PSD spectra of the SPOD time coefficients for increasing actuation amplitude confirm the lock-in behavior observed in the decomposed pressure measurements. The shape of the SPOD modes remains almost constant with increasing actuation amplitude and no other dominant modes are generated by the

actuation. For high actuation amplitudes above the lock-in amplitude, the mean flow changes especially at the upstream end of the CRZ, which is pushed slightly downstream by the strengthened PVC. As shown in publications 2.3-2.5, only very small actuation amplitudes are required to either suppress the PVC with phase-opposition control or excite a damped PVC in V-flame configurations. Accordingly, the impact on the mean flow field is rather small for typically applied actuation amplitudes. These findings further confirm the capability of the actuator to realize direct control of the PVC.

3. The third step of the proof of concept is shown in publication 2.3 where closed-loop control is successfully applied, as phase-opposition control, to suppress the PVC in isothermal and reacting flows with naturally present PVC. Besides the suppression of the PVC (out-of-phase actuation), this control approach allows for strengthening of the naturally present PVC (in-phase actuation) as shown in Fig. 3 of publication 2.3 for the isothermal and highly turbulent combustor flow. Moreover, the phase-opposition control preserves the shape of the PVC mode and dampens its amplitude also under harsh reacting conditions, in connection with a M-flame, as shown in Fig. 4 of publication 2.3. The necessary (effective) actuation amplitudes to suppress the PVC are very low because the actuation is applied in the region of highest receptivity. Furthermore, these closed-loop tests demonstrate that the pressure sensor arrays on the front plate and in the mixing section, which provide the measurement signal for the controller, are capturing the PVC dynamics very accurately. Without this accuracy, successful phase-opposition control, as shown in publication 2.3, would not be possible.

4. The fourth step of the proof of concept is given in publication 2.5 where a global LSA is conducted for a non-actuated reacting mean flow containing a V-flame which dampens the PVC (compare Fig. 4 and 5 in publication 2.5). The least stable mode revealed by the global LSA at around 200 Hz is very similar to the SPOD modes which are derived from the actuated flow with the same frequency (see Fig. 6 in publication 2.5). This actuation frequency was empirically derived from the maximal flame response to different PVC actuation frequencies and amplitudes (open-loop control) which provides a certain experimental validation of the theoretically derived stability mode (see Fig. 6 in publication 2.5 and Fig. 4 in publication 2.4). These consistent empirical and theoretical findings show that the flow control system is capable of exciting a damped PVC which is a key enabler to isolate the exclusive impact of the PVC on the reacting flow field and corresponding combustion phenomena. Moreover, the flow control system can excite a PVC even in flames subjected to severe thermoacoustic oscillations as shown in publication 2.2. This allows for investigations of the interaction between the PVC and TA modes.

Taking together the four steps discussed above, the developed flow control system passes the proof of concept since it allows for direct control of the PVC as defined above. The pressure sensor arrays reliably capture the PVC dynamics such that even closed-loop control can be conducted with the pressure signals used as controller input. The small amplitudes required for PVC suppression or excitation indicate that the actuation is taking place in the region of high receptivity, which is the origin of the PVC. This makes the

control approach very efficient because it exploits the natural amplification of flow perturbations given by an inherent global hydrodynamic instability. Above this, the actuator is capable of synchronizing the PVC with the actuation signal without changing the flow configuration fundamentally, e.g. by exciting other global modes. Accordingly, the flow control system developed in this thesis realizes experimental conditions which allow for studying the exclusive impact of the PVC on: flame, flow and related combustion phenomena.

Alternative actuator design

The flow control system developed and applied in this thesis primarily serves as a tool to investigate the impact of the PVC on the combustion process in swirl flames. However, such an efficient tool can be exploited to control the PVC in industrial applications to improve the performance of a machine which relies on turbulent (reacting) swirling flows such as a gas turbine. For such an application, the actuator design needs to be considerably modified to make it applicable to a real machine. A first step into this direction is made in the master theses by Barkowski [8] and Adhikari [3], which are associated with this thesis. They investigated the potential of fluidic oscillators to control the PVC in the isothermal flow field of the combustor investigated in the present thesis.
A fluidic oscillator is a device without moving parts which generates an oscillating jet at the nozzle outlet (see Fig. 3.1 left). The frequency of the oscillating jet emanating from a generic fluidic oscillator design as shown in Fig. 3.1 (left) linearly depends on the mass flow entering the device [153]. Accordingly, the amplitude of the jet increases with mass flow and frequency. With such a generic design, Barkowski [8] shows that a fluidic oscillator is capable of synchronizing the naturally present PVC with the oscillating jet such that lock-in occurs. However, such a generic design is rather unsuitable for active flow control since frequency and amplitude cannot be controlled individually. Therefore, Adhikari [3]

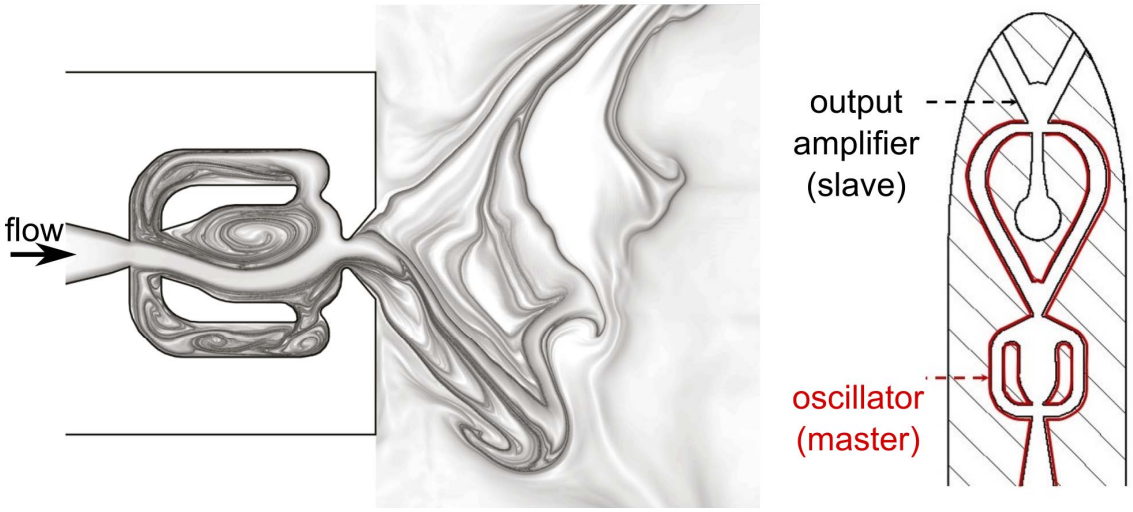

Figure 3.1: Flow field of a fluidic oscillator represented by the finite-time-Lyapunov coefficient on the left (adopted from [122]). Master-slave configuration of a fluidic oscillator integrated into the centerbody on the right (adopted from [3]).

developed a master-slave configuration consisting of an oscillator (master) and an output amplifier (slave) which allows for controlling frequency and amplitude separately (see Fig. 3.1 right). This separate control is realized with two separate air ducts which feed the oscillator and output amplifier. The more complex actuator design is capable of achieving lock-in as already shown with the generic design [8]. As a next step, this design needs to be tested under reacting conditions in an open-loop control approach to excite the PVC in a V-flame.
Since this type of actuator works without moving parts and can be easily controlled via two separate air ducts, it appears to be more suitable for industrial applications as the loudspeaker-based actuator used in the present thesis. However, the fluidic oscillators do not follow the zero-net-mass-flux principle which means that additional mass flow is added to the main flow. This can have considerable influence on the mean flow field which needs to be clarified in future studies. As suggested by Müller et al. [87], this type of fluidic oscillator could be integrated into the walls of the mixing section at a position where the receptivity of the PVC is high. Accordingly, very small actuator mass flows should be sufficient to excite a PVC if necessary. Whether the PVC can be a desirable flow feature under reacting conditions is studied in this thesis and will be discussed in the following sections.

3.1.2 Flame dynamics

The findings gathered in publications 2.2 to 2.5 regarding the impact of the PVC on flame dynamics are discussed in this section. This includes the effect of the PVC on the time-averaged (mean) flame shape, the interaction of the PVC with TA modes and the impact of the PVC on the flame transfer function.

Effect of the PVC on the mean flame shape

The PVC is responsible for increased velocity fluctuations in the vicinity of the burner outlet as shown e.g. in Fig. 6 of publication 2.4. This hydrodynamic effect counts for both, attached V-flames and detached M-flames. Both flame types are investigated in this thesis and the impact of the PVC on these different flame types is discussed in the following paragraphs.
Attached V-flames are investigated in publications 2.2, 2.4 and 2.5 by applying open-loop control of the PVC. As a consequence of the increased velocity fluctuations around the burner outlet, induced by the PVC, the flame surface at the flame root is wrinkled considerably (see Fig. 8 in publication 2.4). This flame front wrinkling increases the mean heat release rate around the burner outlet which leads to an upstream shift of the mean flame (see Fig. 7 in publication 2.4 or Fig. 13 in publication 2.2). This upstream shift is observed in both, thermoacoustically stable (publications 2.4 and 2.5) and (self-excited) unstable flames (publications 2.2) under partially and perfectly premixed conditions. In connection with the upstream shift, the flame appears more compact if a strong PVC is present. The increased compactness is an effect of the PVC-induced flame front wrinkling which increases the turbulent burning velocity around the burner outlet leading to

a concentration of the heat release rate in that region.
Detached M-flames feature a natural PVC in the combustor investigated in this thesis. Therefore, closed-loop control needs to be applied to suppress the PVC such that its impact on the mean flame shape can be studied. The suppression of the PVC allows the CRZ to reach further upstream which changes the corresponding shear layers. The flame follows the changes of the mean flow field leading to an elongated and more dispersed mean flame (compare Fig. 8 in publication 2.3).
In a publication by Lückoff et al. [77], which is associated with this thesis (see list of associated publications), a comprehensive flame shape study is shown for varying Reynolds numbers Re and equivalence ratios ϕ. The results of this study are shown in Fig. 3.2 for non-actuated (a) and actuated (b) conditions whereat the actuation amplitude is kept constant and the actuation frequency is set to the natural PVC frequency. The light red and green backgrounds indicate detached M-flames or attached V-flames, respectively. Under non-actuated conditions, the M-flame appears only at very lean conditions. Applying the open-loop actuation, which strengthens the PVC, shifts the flame shape transition to richer mixtures, i.e. higher critical ϕ values. As described in the introduction and shown for example in [4, 5, 135], the V-M flame transition, i.e. lift-off, is intermittently triggered by the PVC which forms due to a random turbulent event. The higher critical ϕ values achieved by the strengthened PVC underline the importance of the PVC in flame transition scenarios. With the synchronization of the PVC dynamics to the actuation, the intermittency of the PVC appearance, which was observed in previous studies [4, 5, 135],

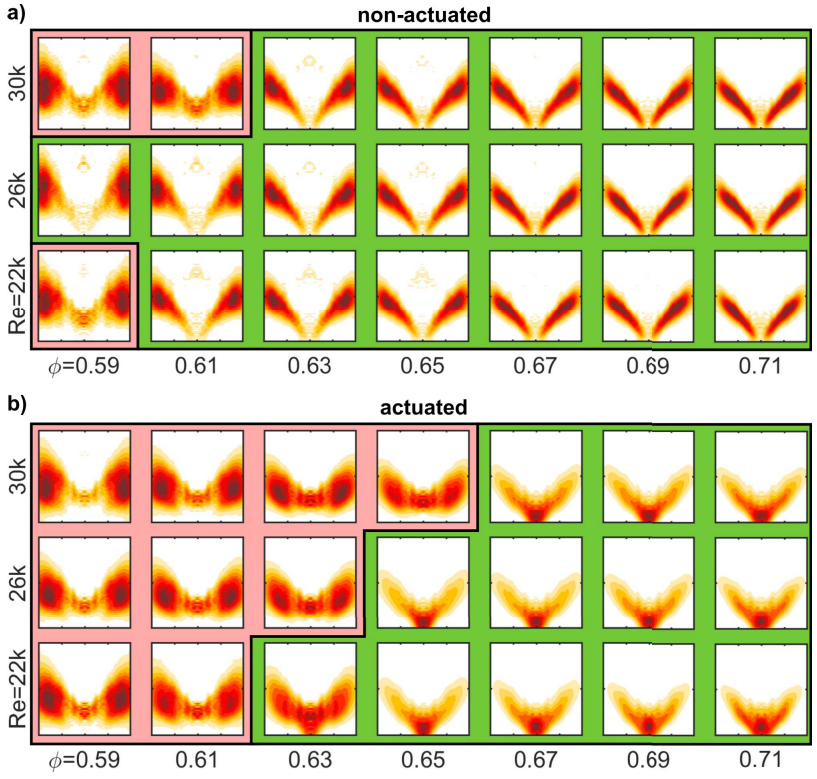

Figure 3.2: Influence of PVC on mean flame shape transition at perfectly premixed conditions; deconvoluted heat release rate fluctuations at natural (a) and actuated (b) conditions; M-flame highlighted with red, V-flame highlighted with green background (Source: [77] (associated publication, see 3.2))

is reduced. Therefore, the open-loop PVC actuation can be used to control flame shape transition. Moreover, the PVC actuation allows for generating detached flames in richer mixtures, further away from the lean blow out limit, which enhances flame stability.

Impact of PVC on the flame transfer function

To estimate the impact of the PVC on the flame transfer function (FTF), the flow control system is included into a combustion chamber test rig which allows for forcing TA modes with amplitudes in the linear regime ($|\hat{u}|/V_0 \approx 0.1$). In the combustion chamber, a stable turbulent perfectly premixed V-flame is generated and TA modes at different frequencies are forced which allows for estimating the FTF of the baseline case. The flow control system excites the damped PVC at the frequency derived from global LSA and flame response measurements (compare Fig. 5 and 6 in publication 2.5). Combining the TA forcing and the PVC excitation, the impact of the PVC on the FTF can be exclusively estimated.
Very small PVC actuation amplitudes are sufficient to significantly reduce the FTF gain whereby the phase remains unaffected (see Fig. 11 in publication 2.5). To explain this observation, two mechanisms are derived based on experimental data and LSA which are summarized in Fig. 14 in publication 2.5. These mechanisms indirectly act via the mean flow field or the mean flame shape because the single-helical PVC does not generate global heat release fluctuations and hence cannot contribute directly to the FTF.
The first mechanism relies on mean flow field modifications due to coherent production which is induced by the PVC (compare Fig. 7 to 9 in publication 2.5). The velocity transfer functions, shown in Fig. 12 in publication 2.5, reveal that the sensitivity of the shear layers to axisymmetric TA perturbations is reduced by the PVC. In other words, the growth rate of the Kelvin-Helmholtz instability is reduced by the PVC which supports the hypothesis given in [29, 81]. As a consequence of this growth rate reduction also the gain of the FTF is reduced.
The second mechanism refers to the changes of the mean flame which is shifted upstream and becomes more compact due to the increased PVC-induced velocity fluctuations at the flame root as explained above. Because of these mean flame changes, the heat release rate fluctuations induced by the TA mode at the flame tip become weaker as shown in Fig. 13 in publication 2.5. Especially, the flame tip is very sensitive to fluctuations induced by axisymmetric TA modes which is most influential for the FTF gain [93, 98]. Although the location of the mean flame, i.e. the main heat release rate, is shifted upstream, the location of the influential heat release rate fluctuations does not change. Therefore, the convective time delays of perturbations reaching the influential flame region do not change which explains why the PVC does not affect the FTF phase.
These two mean field mechanisms explain the impact of the PVC on the flame response to acoustic perturbations. The derived mechanisms extend the knowledge about the interaction of coherent flow structures in the context of flame dynamics which can help to predict and control TA instabilities more efficiently. However, the experiments in publication 2.5 were conducted in the linear regime, which means that the acoustic forcing amplitudes are comparably small. Contrarily, self-excited TA instabilities are characterized by very large (limit-cycle) oscillation amplitudes which lead to nonlinear interactions

between TA and PVC modes [83, 129, 130]. This type of interaction is discussed in the following paragraph based on the observations gathered in publication 2.2.

Interaction of the PVC with TA modes

The nonlinear interaction of the excited (single-helical) PVC ($m = 1$) with self-excited axisymmetric TA modes ($m = 0$) generates dominant interaction modes which can be seen in the antisymmetric pressure and heat release rate spectra (see Fig. 9 and 14 in publication 2.2). These antisymmetric interaction modes are generated under both, perfectly and partially premixed conditions. However, certain differences are observed between perfectly and partially premixed conditions regarding the impact of the actuated PVC on the amplitude of the TA mode. Under perfectly premixed conditions, the changes of the mean flame shape induced by the PVC, which are described above, lead to a slight increase of the frequency of the TA mode. This frequency increase can be explained with the corresponding change of convective time lags, based on the mean flame position, which modifies the phase relation between heat release and pressure fluctuations [57, 110, 125]. The amplitude of the TA oscillation remains almost constant under perfectly premixed conditions. In contrast to that, the TA mode amplitude is decreased significantly (by 80%) under partially premixed conditions at small PVC actuation amplitudes. A possible explanation for this very considerable damping of the TA oscillation amplitudes under partially premixed conditions could be the mitigation of equivalence ratio fluctuations due to PVC-enhanced mixing as stated in publication 2.2.
In publication 2.5, however, a nonlinear interaction between the PVC and the forced TA modes does not occur, due to very small TA forcing amplitudes, which are in the linear regime. However, the mechanisms derived in connection with the FTF gain reduction (see above in section "Impact of PVC on the flame transfer function") need to be discussed in the context of nonlinear mode interaction. Apparently, the actuated PVC is not capable of considerably damping the self-excited TA mode in the perfectly premixed flame shown in Fig. 10 in publication 2.2. To investigate this observation, the mean flame shapes of the non-actuated and actuated stable V-flame are compared (compare Fig. 8d and e in publication 2.2). It can be observed that the PVC actuation changes the mean flame shape considerably such that it appears even more compact and concentrated as in the FTF study in publication 2.5. The reason for this increased compactness is the considerably higher PVC actuation amplitude ($C_\mu = 0.49\%$ vs. $C_\mu = 0.09\%$), whereby the momentum coefficient C_μ (ratio between actuation and main flow momentum) is a measure of the relative actuation amplitude (compare e.g. publication 2.1). However, for the unstable case, the self-excited TA mode shifts the zones of major heat release in upstream direction and generates a more compact flame compared to the stable case (compare Fig. 10a and 8a in publication 2.2). As a consequence, the PVC actuation can not modify the mean flame shape as distinctly as in the stable case. This allows the self-excited TA mode to further persist as shown by the Fourier modes in Fig. 10c and d in publication 2.2. Moreover, the FTF study in publication 2.5 revealed that a considerably reduction of the FTF gain appears only in certain frequency ranges. Hence, the frequency of the self-excited TA oscillation may be outside of the frequency range where flame and flow field are sensitive to considerable mean field changes. Higher acoustic forcing amplitudes outside

the linear regime would allow further investigations of this phenomena by analyzing the flame describing function as it was done for example in [25]. Furthermore, the study of PVC-flame interaction in the nonlinear regime is essential to investigate the PVC's full potential for damping TA oscillation.
Under partially premixed conditions without PVC excitation, the mean flame shape appears even more compact under thermoacoustically unstable conditions compared to the unstable perfectly premixed flame (compare figures 15a and 10a in publication 2.2). However, the actuated PVC changes the mean flame shape fundamentally to a very compact flame with an almost homogeneous distribution of heat release rate at the flame root, which is the first difference compared to the perfectly premixed flame. Another difference is to be found by comparing the shapes of the Fourier modes ($m = 0$) which are fundamentally different (compare figures 15d and 10d in publication 2.2). The axial and radial extent is considerably smaller and maximal values are more upstream and closer to the jet axis in case of partially premixed conditions. Hence, the major portion of the TA mode ($m = 0$) is situated close to the burner outlet region where the influence of PVC on the mean fields (flow and flame) is maximal (see Fig. 7 and Fig. 10 in publication 2.5). Therefore, the mean field mechanisms derived in publication 2.5, and described above, are more effective under the studied partially premixed conditions. Above this, there is a third difference, which are equivalence ratio fluctuations occurring exclusively at partially premixed conditions. Acoustic waves passing the fuel injector, cause fluctuations of the equivalence ratio which are transported by the main flow into the flame and in turn cause fluctuations of the heat release. This mechanism is one of the influential branches within the TA feedback cycle which appears to be cut by the actuated PVC explaining the considerable damping of the TA oscillations. The impact of the PVC on the equivalence ratio fluctuations mechanisms is supported by the fact that the mean flame shape changes only slightly for small PVC actuation amplitudes whereas the TA amplitude already decreases by 40% as shown in Fig. 16 in publication 2.2. Due to the anti-symmetric shape of the PVC and its precessing motion, the symmetry of the axisymmetric equivalence ratio fluctuations, induced by TA modes, might be broken by the PVC actuation leading to a very effective suppression of TA oscillations. According to figure Fig. 16 in publication 2.2, the mean field mechanisms appear to set in at medium PVC actuation amplitudes as the mean flame shape changes considerably. Note that the maximum momentum coefficient C_μ, is considerably higher in case of the partially premixed flame ($C_\mu = 1.19\%$ vs. $C_\mu = 0.49\%$) which allows for more distinct mean field modifications compared to the perfectly premixed case.
To study the interaction between the PVC and high amplitude TA modes under partially premixed conditions in greater detail, a study of the flame describing function needs to be conducted as suggested above. This study should include time-resolved equivalence ratio measurements to further characterize the interaction between PVC and the equivalence ration fluctuation branch within the TA feedback cycle.

3.1.3 Role of the PVC in Mixing

The PVC is a large-scale coherent structure as shown e.g. by the SPOD modes in Fig. 4 in publication 2.3. Thus, large vortices induced by the PVC enhance the mixing of fuel and

air within large domains, as shown by Stöhr et al. [132] (see Fig. 1.8). Accordingly, the PVC is associated with large-scale mixing processes relying on its precessing motion around the jet axis, acting as a stirrer, and vortex-induced mixing. To further characterize the impact of the PVC on the mixing process based on fluid dynamical quantities, the findings of publication 2.3 and 2.4 are discussed in this paragraph.
The study presented in publication 2.3 shows how coherent and stochastic turbulent fluctuations as well as the small-scale eddy size change with the suppression of the PVC (compare Fig. 7 in publication 2.3). These results, in conjunction with findings from publication 2.4, allow to describe the impact of the PVC on the mixing process as follows. The suppression of the PVC leads to a significant reduction of coherent fluctuations (compare Fig. 7 (left) in publication 2.3) and a slight increase of stochastic fluctuations, which include all the turbulent fluctuations except those associated with the PVC. The growth of these stochastic fluctuations can be traced back to mean flow modifications due to the PVC suppression (compare Fig. 8 in publication 2.5). This modified mean flow allows other large-scale structures, which are convectively unstable, to arise keeping the global turbulent kinetic energy constant [92]. Moreover, the small-scale eddy size is nearly unaffected by the PVC suppression. By combining these findings, it can be concluded that the PVC mainly effects the large-scale mixing, which can be controlled with the flow control system developed in this thesis.
The visualization of the PVC-induced vortices, shown in Fig. 8 in publication 2.4, is obtained from phase-averaged PIV and OH-CL measurements in a V-flame which damps the natural PVC. With the active flow control system, a PVC was excited in this flow configuration facilitating the investigations of vortex-flame interaction. The obtained visualizations reveal that the PVC rolls up the ISL which constantly mixes, i.e. entrains, the incoming jet of cold reactants with the hot products trapped in the CRZ. As a result, the flame is following the PVC vortices due to enhanced reaction rates in those regions where the PVC mixes hot products with cold reactants. Accordingly, the excitation of a PVC in a stable V-flame can improve the flame stability due to enhanced mixing of incoming reactants with hot products leading to a more compact flame.
The effect of the PVC on mixing of hot products and incoming cold reactants is investigated indirectly in this thesis based on fluid dynamical quantities such as: coherent (large-scale) and stochastic turbulent fluctuations, small-scale eddy size and vortex structure visualizations. For direct (local) mixing studies, more sophisticated experimental methods would be needed which include comprehensive modifications of the test rig and laser-induced fluorescence measurement techniques as shown for example in [132]. Unfortunately, an implementation of such experimental methods was not possible within the time horizon of this thesis.

3.1.4 Impact of the PVC on NO_x emissions

The NO_x emission level can serve as a quantity which indirectly characterizes the PVC impact on the fuel-air mixing. Typically, the NO_x emissions correlate with the degree of mixing quality of fuel and air: the better the mixing of fuel and air, the lower the NO_x emissions will be in lean premixed flames [21, 30]. Therefore, premixed flames typically

emit less NO_x than diffusion flames where fuel and air are entering the combustion chamber via two separate lines. The study by Stöhr et al. [132] shows that the PVC considerably enhances the fuel-air mixing in a slightly premixed flame configuration (see Fig. 1.8). This finding motivates to investigate the impact of the PVC on the NO_x emission level in partially and perfectly premixed V-flames. To estimate a correlation between PVC amplitude and NO_x emission level, the PVC is excited with open-loop control at different actuation amplitudes as shown in publication 2.4.

As described above, the PVC predominantly acts on the ISL near the burner outlet which enhances the flame-wrinkling in this region leading to a more compact and upstream shifted flame. The PVC-induced vortices considerably roll up the ISL entraining hot products from the CRZ which locally enhances the reaction rate such that the flame follows the trajectory of the PVC (see Fig. 8 in publication 2.4). As a result, the residence time of hot products and the number of free radicals increases in the ISL, which explains the observed increase of NO_x emissions under perfectly premixed conditions as shown in Fig. 9 in publication 2.4. Under partially premixed conditions, the PVC acts on flame and flow in the same way as in the case of perfectly premixed conditions. Based on the findings regarding PVC-vortex-enhanced fuel-air mixing by Stöhr et al. [132], one could expect that the PVC effects a decrease of the NO_x emission level by homogenizing the fuel-air mixture. But instead of reducing NO_x emissions, the PVC increases the NO_x emission level in a similar trend as under perfectly premixed conditions. Moreover, an offset to slightly higher NO_x emission values is observed for the partially premixed case. This offset is explained by additional temperature peaks that can occur under partially premixed conditions because of PVC-induced entrainment of richer fluid leading to locally increased equivalence ratios [117]. In the works of Paschereit et al. [103, 105], similar observations of increasing NO_x emission levels have been made in connection with vortices induced by TA modes. The authors showed that the increase of vorticity associated with the symmetric vortices formed at the burner outlet, due to the Kelvin-Helmholtz instability, led to a NO_x emission level rise. Consequently, the control of these symmetric coherent structures also allowed to control the NO_x emissions [103, 105]. These findings support the conclusion from above that PVC-induced vortices are responsible for the observed increase of NO_x emissions.

However, it needs to be clarified why vortex-enhanced mixing, as described by Stöhr et al. [132], does not apply to the present burner configuration under partially premixed conditions such that the NO_x emission level decreases with growing PVC amplitude. In the present burner configuration, fuel is injected approximately three nozzle diameters upstream of the burner outlet into the mixing tube under partially premixed conditions. The resulting mixing length provides a fairly (nearly perfectly) premixed fuel-air mixture as shown in a study by Göke et al. [41], which investigated the present burner regarding its mixing quality under partially and perfectly premixed conditions. Contrarily, the burner setup investigated by Stöhr et al. [132], with its comparably short mixing length, provides a mixture with large regions where fuel and air are almost unmixed, as shown in Fig. 1.8. The large-scale mixing associated with the PVC, as discussed in the paragraph before, applies very well to this rather unmixed fuel-air mixture. However, it does not apply to the fairly premixed mixture provided by the present burner because the regions where fuel and air are almost unmixed are rather small, so that the comparably large PVC-induced

vortices are incapable of further improving the mixing quality. Consequently, the degree of the premixedness of a fuel-air mixture decides whether vortex-enhanced mixing applies, which may decrease the NO_x emission level. Naturally, both vortex-enhanced mixing and vortex-flame interaction can occur in a partially premixed flames such that it depends on the degree of premixedness which phenomenon dominates.

3.2 Conclusions

Active flow control of the precessing vortex core (PVC) opens up new opportunities to investigate and control the combustion process of swirl-stabilized flames. On the one hand, the exclusive impact of the PVC on flame dynamics, mixing and pollutant emissions can be studied in detail; and on the other hand, the flow control system can be used to develop strategies to control important combustion properties such as thermoacoustic oscillations or pollutant emissions. Certain requirements need to be fulfilled to ensure that such an active flow control system can be applied to investigate the exclusive role of the PVC in swirl-stabilized combustion. Therefore, a major part of this thesis deals with the developed active flow control approach and its proof of concept that is summarized and discussed in section 3.1.1. The newly developed and proven active flow control system is used as a tool to investigate the impact of the PVC on: flame dynamics (section 3.1.2), mixing (section 3.1.3) and NO_x emissions (section 3.1.4). In this concluding section, the findings obtained in this thesis are summarized and evaluated regarding their potential to promote the research in turbulent fluid dynamics and combustion. Moreover, future steps are suggested that show how the developed control approach can be appropriately applied.

The *direct* control approach followed in the development of the active flow control system aims to actuate the PVC at its origin where the receptivity is maximal. In this region, the response to periodic forcing is maximal allowing for a very effective actuation with very small actuation amplitudes. Due to this targeted and low-amplitude actuation, the general flow configuration will be rather unaffected such that the exclusive impact of the PVC on the (reacting) flow field can be investigated. The spatial location of maximal receptivity is estimated by means of adjoint (global) linear stability analysis of the mean flow field. Several studies, closely associated with this thesis, revealed that the maximal receptivity of the PVC mode is typically to be found slightly upstream of the nozzle outlet inside the mixing section of the burner. Accordingly, the actuator is designed such that helical actuation of the PVC mode is realized inside the mixing section which allows for controlling the PVC in open- and closed-loop approaches. In this context, open-loop forcing is applied in flame configurations where the PVC is damped and closed-loop control is utilized if a PVC is naturally present. With this control strategy, the exclusive impact of the PVC on flow and flame is investigated by varying the PVC amplitude and keeping the other operating conditions constant. The proof of the flow control concept is delivered by different empirical and analytical methods, such as: spectral proper orthogonal decomposition (SPOD), linear stability analysis (LSA) and Fourier analysis. The results

derived with these methods verify that the PVC can be successfully controlled with very small actuation amplitudes and without fundamentally changing the flow configuration. More details about the proof of concept and the design of the flow control system are given in section 3.1.1.

With the proven flow control system at hand, it is shown for a partially premixed attached flame that low-amplitude excitation of the PVC is capable of damping self-excited (high-amplitude) thermoacoustic oscillations by up to 80%. This observation is partly explained by two mean field coupling mechanisms that are derived for thermoacoustic (TA) modes forced in the linear regime (small amplitude). Mechanism one describes the consequences of slight mean flow modifications induced by the PVC that reduce the growth rate of the Kelvin-Helmholtz instability such that the evolution of axisymmetric vortex structures, induced by the TA oscillation, is impeded. Mechanism two refers to the PVC-induced changes of the mean flame which is shifted upstream and becomes more compact with increasing PVC amplitude. Consequently, the heat release fluctuations at the flame tip, which is very receptive to TA oscillations, are reduced. The result of both mechanisms is a reduction of the flame transfer function (FTF) gain in certain TA frequency regions. Since the location of major heat release rate fluctuation induced by the TA oscillation remains constant, also for comparably high PVC amplitudes, the FTF phase remains also constant. However, these two mechanisms are not sufficient to explain the considerable damping of self-excited TA oscillations in the partially premixed flame because they do not include the effect of the PVC on equivalence ratio fluctuations. Therefore, future studies need to involve equivalence ratio measurements to characterize the interaction between PVC and the equivalence ratio fluctuation branch within the TA feedback cycle. Since TA modes induce axisymmetric equivalence ratio fluctuations, the skew-symmetric PVC may break their symmetry which possibly explains the considerable damping effect. Furthermore, the interaction of the PVC with high-amplitude TA modes needs to be investigated further to reveal nonlinear interaction mechanisms. These investigations need to be transferred to other combustors as well, which will help to evaluate the generality of the mechanisms derived regarding the impact of the PVC on the FTF.

Besides the interaction of TA and PVC modes in attached flames, the role of the PVC in flame shape transition from a detached flame, with natural PVC, to an attached flame without natural PVC is investigated based on active flow control. In this flame transition study, it is shown that a PVC, strengthened by active flow control, is capable of shifting the flame transition to richer fuel-air mixtures. This underlines the importance of the PVC in the context of flame lift-off. For more details regarding the role of the PVC in flame dynamics, the reader is referred to section 3.1.2.

Based on fluid dynamical quantities and appropriate vortex visualizations, the mixing capabilities of the PVC are analyzed in connection with open- and closed-loop control. This analysis shows that the PVC induces large coherent vortex structures that enhance large-scale mixing. These vortices are primarily active in the inner shear layer where they entrain hot products from the central recirculation zone into the incoming jet of cold reactants. This enhances the reaction rate such that the flame follows the PVC-induced vortices. For quantitative mixing studies, more sophisticated experimental methods are needed which are for example based on laser induced fluorescence to track the fuel distribution. By varying the PVC amplitude and the degree of premixedness, a threshold can

be derived above which the PVC is capable of improving the fuel-air mixing. More details about the impact of the PVC on mixing are given in section 3.1.3.
The degree of premixedness is very relevant to the formation of NO_x emissions, because the more homogeneous the fuel-air mixture is, the lower the NO_x emissions are expected to be in lean premixed flames. In the present thesis, the impact of the PVC on the NO_x emission level of perfectly and partially premixed flames is investigated. It turns out that for both types of premixing, the NO_x emissions increase with the PVC amplitude. Since the present burner provides a fairly well-mixed fuel-air mixture, without any larger inhomogeneities already under partially premixed conditions, the PVC is incapable of further enhancing the mixing. Consequently, no decrease of NO_x emission level due to vortex-enhanced mixing can be expected. The increased vorticity originating from the excited PVC enhances the reaction rates and increases residence times of radicals and hot products such that the NO_x formation is enhanced. A more detailed investigation of the impact of the PVC on NO_x formation should involve a complex reactor model of the flow configuration including the PVC, as suggested by Claypole and Syred [21]. With the active flow control at hand, the required input parameters for such a model can be obtained for different operating conditions with an arbitrarily conditioned PVC. Moreover, the PVC control enables to validate the derived model experimentally. For more details about the role of the PVC in context of NO_x emissions, the reader is referred to section 3.1.4.

All the findings achieved with the active flow control system at hand reveal the high potential of direct control as a tool to investigate the role of the PVC in swirl-stabilized combustion. In this thesis, first successful steps in active flow control-based investigations of the PVC's impact on flame dynamics, mixing and pollutant emissions are made which should be continued in following projects focusing on more specific topics. These future studies should be accompanied by LES computations, which would increase the level of detail and provide additional insight into the physical mechanisms at play. Additionally, such simulations can provide flow data in regions which are inaccessible for experimental methods. Such flow data will increase the accuracy of results obtained from LSA and empirical methods.
Furthermore, the findings of the present thesis open up new vistas for control methods of mixing, flame stabilization and TA instabilities. By exploiting the hydrodynamic stability and receptivity of the swirl flow and applying the methodologies applied in this thesis, very efficient flow control methods with low energy consumption can be developed for industrial applications. One possible path to a flow control system that might be applicable on an industrial scale leads to fluidic oscillators, as explained in section 3.1.1. This path should be further explored in future studies because the PVC remains a key factor for combustion dynamics at elevated pressure, e.g. in the context of PVC-induced mixing and thermoacoustic oscillations [127, 157]. Moreover, the PVC appears to be even stronger in multi-nozzle configurations where it enhances the mixing of recirculated and incoming gas, but could jeopardize flame stability [11].
The control approaches developed in this thesis are not limited to the application in

swirl-stabilized combustors. A PVC can also be observed in the draft tube of hydro turbines, especially Francis turbines, downstream of the runner at off-design operating conditions [76, 88]. In hydro turbines, the PVC needs to be suppressed because the accompanied pressure pulsations can resonate with the whole system such that structural damage can be the consequence. However, hydro turbines are going to be used more frequently at off-design conditions in the future electrical energy market to flexibly compensate for the intermittent supply from renewable energy resources such as wind or solar power. Therefore, a transfer of the control methodologies developed in the present thesis from swirl-stabilized combustors to hydro turbines is necessary to increase their flexibility and efficiency for the future. In general, the flow control approach followed in this thesis can be applied to any flow featuring a global mode, such as the PVC, which makes direct control to some sort of universal flow control approach.

Although renewable energy resources are gaining ground and promote the green energy revolution, the energy market appears to rely on gas turbine combustion technology for the next decades (see Fig. 1.1). Alternative fuels such as hydrogen or synthetic fuels could even extend the existence of swirl-stabilized gas turbine combustors into the far future. In these machines, the PVC can play a key role in the control of a stable and efficient combustion process. Likewise, future turbomachinery, for example hydro turbines, whose share in the future energy market is predicted to increase (see Fig. 1.1), will rely on turbulent flows that can become globally unstable and need to be efficiently controlled. Therefore, the active flow control approach developed and applied in this thesis may serve to facilitate the development of high performance and efficient turbomachinery in the future.

Bibliography

[1] Acharya, V., and Lieuwen, T., 2016. "Premixed flame response to helical disturbances: Mean flame non-axisymmetry effects". *Combustion and Flame,* **165**(Supplement C), pp. 188 – 197.

[2] Acharya, V. S., Shin, D.-H., and Lieuwen, T., 2013. "Premixed Flames Excited by Helical Disturbances: Flame Wrinkling and Heat Release Oscillations". *Journal of Propulsion and Power,* **29**(6), Nov., pp. 1282–1291.

[3] Adhikari, A., 2020. "Development of a Fluidic Actuator with IndependentFrequency and Amplitude Modulation for Control of aPrecessing Vortex Core". Master's thesis, TU Berlin.

[4] An, Q., Kwong, W. Y., Geraedts, B. D., and Steinberg, A. M., 2016. "Coupled dynamics of lift-off and precessing vortex core formation in swirl flames". *Combustion and Flame,* **168**, pp. 228 – 239.

[5] An, Q., and Steinberg, A. M., 2019. "The role of strain rate, local extinction, and hydrodynamic instability on transition between attached and lifted swirl flames". *Combustion and Flame,* **199**, jan, pp. 267–278.

[6] Anacleto, P. M., Fernandes, E. C., Heitor, M. V., and Shtork, S. I., 2003. "Swirl flow structure and flame characteristics in a model lean premixed combustor". *Combustion Science and Technology,* **175**(8), pp. 1369–1388.

[7] Ayoola, B., Balachandran, R., Frank, J., Mastorakos, E., and Kaminski, C., 2006. "Spatially resolved heat release rate measurements in turbulent premixed flames". *Combustion and Flame,* **144**(1), pp. 1 – 16.

[8] Barkowski, D., 2019. "Open-Loop Kontrolle des präzidierenden Wirbelkerns (PVC) einerisothermen Drallströmung in einer Modellbrennkammer mit einemfluidischen Oszillator". Master's thesis, TU Berlin.

[9] Beér, J., and Chigier, N., 1972. *Combustion Aerodynamics*. Fuel and energy science series. Applied Science Publishers Limited.

[10] Billant, P., Chomaz, J.-M., and Huerre, P., 1998. "Experimental study of vortex breakdown in swirling jets". *J Fluid Mech,* **376**, pp. 183–219.

[11] Boehm, B., Dreizler, A., Gnirss, M., Tropea, C., Findeisen, J., and Schiffer, H.-P., 2007. "Experimental Investigation of Turbulence Structure in a Three-Nozzle Combustor".

In Volume 2: Turbo Expo 2007, Vol. Volume 2: Turbo Expo 2007 of *Turbo Expo: Power for Land, Sea, and Air*, ASMEDC, pp. 55–64.

[12] Bothien, M. R., Ciani, A., Wood, J. P., and Fruechtel, G., 2019. "Sequential Combustion in Gas Turbines: The Key Technology for Burning High Hydrogen Contents With Low Emissions". *Proceedings of the ASME Turbo Expo 2019: Turbomachinery Technical Conference and Exposition*, jun.

[13] Bradley, D., 1998. "Premixed turbulent flame instability and NO formation in a lean-burn swirl burner". *Combustion and Flame,* **115**(4), dec, pp. 515–538.

[14] Brunton, S. L., and Noack, B. R., 2015. "Closed-Loop Turbulence Control: Progress and Challenges". *Applied Mechanics Reviews,* **67**(5), Aug., pp. 050801–050801.

[15] Bury, Y., and Jardin, T., 2014. "Wake Instabilities behind an Axisymmetric Bluff Body at Low Reynolds Numbers". In *Notes on Numerical Fluid Mechanics and Multidisciplinary Design*. Springer Berlin Heidelberg, pp. 31–37.

[16] Candel, S., Durox, D., Schuller, T., Bourgouin, J.-F., and Moeck, J. P., 2014. "Dynamics of Swirling Flames". *Annu Rev Fluid Mech,* **46**, pp. 147–173.

[17] Cassidy, J. J., and Falvey, H. T., 1970. "Observations of unsteady flow arising after vortex breakdown". *Journal of Fluid Mechanics,* **41**(4), pp. 727 – 736.

[18] Cetegen, B. M., 2006. "Scalar mixing in the field of a gaseous laminar line vortex". *Experiments in Fluids,* **40**(6), apr, pp. 967–976.

[19] Chomaz, J. M., Huerre, P., and Redekopp, L. G., 1988. "Bifurcations to local and global modes in spatially developing flows". *Phys Rev Lett,* **60**, pp. 25–28.

[20] Chomaz, J.-M., Huerre, P., and Redekopp, L. G., 1991. "A frequency selection criterion in spatially developing flows". *Stud Appl Math,* **84**, pp. 119–144.

[21] Claypole, T., and Syred, N., 1981. "The effect of swirl burner aerodynamics on NOx formation". *Symposium (International) on Combustion,* **18**(1), pp. 81 – 89. Eighteenth Symposium (International) on Combustion.

[22] Cohen, J., and Wygnanski, I., 1987. "The evolution of instabilities in the axisymmetric jet. Part 1. The linear growth of disturbances near the nozzle". *J Fluid Mech,* **176**, pp. 191–219.

[23] Correa, S. M., 1993. "A Review of NO(x) Formation Under Gas-Turbine Combustion Conditions". *Combustion Science and Technology,* **87**, pp. 329–362.

[24] Ćosić, B., 2014. "Nonlinear Thermoacoustic Stability Analysis of a Gas Turbine Combustion Chamber". PhD thesis, TU Berlin.

[25] Ćosić, B., Terhaar, S., Moeck, J. P., and Paschereit, C. O., 2015. "Response of a swirl-stabilized flame to simultaneous perturbations in equivalence ratio and velocity at high oscillation amplitudes". *Combustion and Flame,* **162**(4), pp. 1046 – 1062.

[26] Ducruix, S., Candel, S., Durox, D., and Schuller, T., 2003. "Combustion Dynamics and Instabilities: Elementary Coupling and Driving Mechanisms". *J. Propul. Power,* **19**(5), sep, pp. 722–734.

[27] Duwig, C., Ducruix, S., and Veynante, D., 2012. "Studying the Stabilization Dynamics of Swirling Partially Premixed Flames by Proper Orthogonal Decomposition". *Journal of Engineering for Gas Turbines and Power,* **134**(10), aug.

[28] Fokaides, P., Weiss, M., Kern, M., and Zarzalis, N., 2009. "Experimental and Numerical Investigation of Swirl Induced Self-Excited Instabilities at the Vicinity of an Airblast Nozzle". *Flow, Turbulence and Combustion,* **83**, pp. 511–533. 10.1007/s10494-009-9205-3.

[29] Frederick, M., Manoharan, K., Dudash, J., Brubaker, B., Hemchandra, S., and O'Connor, J., 2018. "Impact of Precessing Vortex Core Dynamics on Shear Layer Response in a Swirling Jet". *Journal of Engineering for Gas Turbines and Power,* **140**(6), jan, p. 061503.

[30] Fric, T. F., 1993. "Effects of Fluel-Air Unmixedness on NO(x) Emissions". *Journal of Propulsion and Power,* **9**, pp. 708–713.

[31] Froud, D., O'Doherty, T., and Syred, N., 1995. "Phase averaging of the precessing vortex core in a swirl burner under piloted and premixed combustion conditions". *Combust Flame,* **100**(3), pp. 407 – 412. <ce:title>25th Symposium (International) on Combustion Papers</ce:title>.

[32] Gallaire, F., and Chomaz, J.-M., 2003. "Instability mechanisms in swirling flows". *Phys Fluids,* **15**, pp. 2622–2639.

[33] Gallaire, F., and Chomaz, J.-M., 2003. "Mode selection in swirling jet experiments: a linear stability analysis". *J Fluid Mech,* **494**, pp. 223–253.

[34] Gallaire, F., Ruith, M., Meiburg, E., Chomaz, J.-M., and Huerre, P., 2006. "Spiral vortex breakdown as a global mode". *J Fluid Mech,* **549**, pp. 71–80.

[35] Galley, D., Ducruix, S., Lacas, F., and Veynante, D., 2011. "Mixing and stabilization study of a partially premixed swirling flame using laser induced fluorescence". *Combust Flame,* **158**(1), pp. 155 – 171.

[36] Gaster, M., Kit, E., and Wygnanski, I., 1985. "Large-scale structures in a forced turbulent mixing layer". *J Fluid Mech,* **150**, pp. 23–39.

[37] Ghani, A., Poinsot, T., Gicquel, L., and Müller, J.-D., 2016. "LES Study of Transverse Acoustic Instabilities in a Swirled Kerosene/Air Combustion Chamber". *Flow, Turbulence and Combustion,* **96**(1), pp. 207–226.

[38] Giauque, A., Selle, L., Gicquel, L., Poinsot, T., Buechner, H., Kaufmann, P., and Krebs, W., 2005. "System identification of a large-scale swirled partially premixed combustor using LES and measurements". *J Turbul,* **6**, p. 21.

[39] Göckeler, K., Terhaar, S., and Oliver Paschereit, C., 2013. "Residence Time Distribution in a Swirling Flow at Nonreacting, Reacting, and Steam-Diluted Conditions". *ASME. J. Eng. Gas Turbines Power,* **136**(4), dec.

[40] Göke, S., Fueri, M., Bourque, G., Bobusch, B., Goeckeler, K., Krueger, O., Schimek, S., Therhaar, S., and Paschereit, C. O., 2013. "Influence of steam dilution on the combustion of natural gas and hydrogen in premixed and rich-quench-lean combustors". *Fuel Processing Technology,* **107**, pp. 14–22.

[41] Göke, S., Göckeler, K., Krüger, O., and Paschereit, C. O., 2010. "Computational and Experimental Study of Premixed Combustion at Ultra Wet Conditions". In Volume 2: Combustion, Fuels and Emissions, Parts A and B, ASMEDC.

[42] Gupta, A. K., Lilley, D. G., and Syred, N., 1984. "Swirl flows". *Tunbridge Wells, UK; Abacus Press*.

[43] Haber, L. C., Vandsburger, U., Saunders, W. R., and Khanna, V. K., 2000. "An Examination of the Relationship Between Chemiluminescent Light Emissions and Heat Release Rate Under Non-Adiabatic Conditions". Vol. Volume 2: Coal, Biomass and Alternative Fuels; Combustion and Fuels; Oil and Gas Applications; Cycle Innovations of *Turbo Expo: Power for Land, Sea, and Air*, American Society of Mechanical Engineers. V002T02A041.

[44] Hall, M. G., 1972. "Vortex Breakdown". *Annu Rev Fluid Mech,* **4**, pp. 195–218.

[45] Higgins, B., McQuay, M., Lacas, F., Rolon, J., Darabiha, N., and Candel, S., 2001. "Systematic measurements of OH chemiluminescence for fuel-lean, high-pressure, premixed, laminar flames". *Fuel,* **80**(1), pp. 67 – 74.

[46] Hill, D. C., 1995. "Adjoint systems and their role in the receptivity problem for boundary layers". *J Fluid Mech,* **292**, pp. 183–204.

[47] Holmes, P., Lumley, J. L., and Berkooz, G., 1998. *Turbulence, Coherent Structures, Dynamical Systems and Symmetry*. Cambridge University Press.

[48] Huang, Y., and Yang, V., 2009. "Dynamics and stability of lean-premixed swirl-stabilized combustion". *Prog. Energy Combust. Sci.,* **35**(4), pp. 293 – 364.

[49] Hucho, W.-H., 2012. *Aerodynamik der stumpfen Körper*. Vieweg + Teubner Verlag.

[50] Huerre, P., and Monkewitz, P., 1990. "Local and global instabilities in spatially developing flows". *Annu Rev Fluid Mech,* **22**, pp. 473–537.

[51] Hussain, A. K. M. F., and Reynolds, W. C., 1970. "The mechanics of an organized wave in turbulent shear flow". *J Fluid Mech,* **41**, pp. 241–258.

[52] I Roehle, R Schodl, P. V., and Willert, C., 2000. "Recent developments and applications of quantitative laser light sheet measuring techniques in turbomachinery components". *Meas. Sci. Technol.,* **11**, p. 1023.

[53] IEA, 2019. Global electricity generation mix by scenario, 2018, Stated Policies and Sustainable Development Scenarios 2040, https://www.iea.org/data-and-statistics/charts/global-electricity-generation-mix-by-scenario-2018-stated-policies-and-sustainable-development-scenarios-2040. Tech. rep., IEA, Paris,.

[54] IEA, 2019. World Energy Outlook 2019. Tech. rep., IEA, Paris, Paris.

[55] III, L. N. C., and Sheplak, M., 2011. "Actuators for Active Flow Control". *Annual Review of Fluid Mechanics,* **43**(1), pp. 247–272.

[56] Joos, F., 2006. *Technische Verbrennung*. Springer Berlin Heidelberg.

[57] Juniper, M. P., and Sujith, R. I., 2018. "Sensitivity and nonlinearity in Thermoacoustics". *Annual Review of Fluid Mechanics,* **50**, pp. 661–689.

[58] Kaiser, T. L., Oberleithner, K., Selle, L., and Poinsot, T., 2019. "Examining the Effect of Geometry Changes in Industrial Fuel Injection Systems On Hydrodynamic Structures with Biglobal Linear Stability Analysis". *Journal of Engineering for Gas Turbines and Power,* **142**(1), sep.

[59] Kaiser, T. L., Poinsot, T., and Oberleithner, K., 2018. "Stability and Sensitivity Analysis of Hydrodynamic Instabilities in Industrial Swirled Injection Systems". *Journal of Engineering for Gas Turbines and Power,* **140**(5), 01. 051506.

[60] Khalil, S., Hourigan, K., and Thompson, M. C., 2006. "Response of unconfined vortex breakdown to axial pulsing". *Phys Fluids,* **18**, p. 8102.

[61] Khorrami, M. R., Malik, M. R., and Ash, R. L., 1989. "Application of spectral collocation techniques to the stability of swirling flows". *J Comput Phys,* **81**(1), pp. 206–229.

[62] Koytsoumpa, E. I., Bergins, C., and Kakaras, E., 2018. "The CO 2 economy: Review of CO 2 capture and reuse technologies". *The Journal of Supercritical Fluids,* **132**, feb, pp. 3–16.

[63] Kuhn, P., Moeck, J. P., Paschereit, C. O., and Oberleithner, K., 2016. "Control of the Precessing Vortex Core by Open and Closed-Loop Forcing in the Jet Core". In ASME Turbo Expo 2016: Turbomachinery Technical Conference ans Exposition, Volume 4B: Combustion, Fuels ans Emissions, p. 13.

[64] Lacarelle, A., Faustmann, T., Greenblatt, D., Paschereit, C. O., Lehmann, O., Luchtenburg, D. M., and Noack, B. R., 2009. "Spatiotemporal Characterization of a Conical Swirler Flow Field Under Strong Forcing". *J. Eng. Gas Turb. Power,* **131**(3), pp. 031504–1 bis 031504–12.

[65] Landau, L., and Lifshitz, E., 1987. *Fluid Mechanics, Vol. 6*. Pergamon Press Ltd.

[66] Lang, H. M., Oberleithner, K., Paschereit, C. O., and Sieber, M., 2017. "Measurement of the fluctuating temperature field in a heated swirling jet with BOS tomography". *Experiments in Fluids,* **58**(7), jun.

[67] Lauer, M., 2011. "Determination of the Heat Release Distribution in Turbulent Flames by Chemiluminescence Imaging". PhD thesis, TU München.

[68] Lauer, M., and Sattelmayer, T., 2010. "On the Adequacy of Chemiluminescence as a Measure for Heat Release in Turbulent Flames With Mixture Gradients". *Journal of Engineering for Gas Turbines and Power,* **132**(6), p. 061502.

[69] Leibovich, S., 1978. "The structure of vortex breakdown". *Annu Rev Fluid Mech,* **10**, pp. 221–246.

[70] Leuckel, W., 1967. Swirl intensities, swirl types and energy losses of different swirl generating devices. Tech. rep., Doc. No. G02/a/16, International Flame Research Foundation, Ijmuiden, The Netherlands.

[71] Li, L. K., and Juniper, M., 2013. "Phase trapping and slipping in a forced hydrodynamically self-excited jet". *J. Fluid Mech.,* **735**.

[72] Li, L. K., and Juniper, M. P., 2013. "Lock-in and quasiperiodicity in hydrodynamically self-excited flames: Experiments and modelling". *Proceedings of the Combustion Institute,* **34**(1), pp. 947 – 954.

[73] Li, L. K. B., and Juniper, M. P., 2013. "Lock-in and quasiperiodicity in a forced hydrodynamically self-excited jet". *J. Fluid Mech.,* **726**, 007, pp. 624–655.

[74] Liang, H., and Maxworthy, T., 2005. "An experimental investigation of swirling jets". *J Fluid Mech,* **525**, pp. 115–159.

[75] Lieuwen, T. C., and Yang, V., 2005. *Combustion Instabilities in Gas Turbine Engines*, Vol. 210 of *Progress in Astronautics and Aeronautics*. AIAA, Inc.

[76] Litvinov, I., Shtork, S., Gorelikov, E., Mitryakov, A., and Hanjalic, K., 2018. "Unsteady regimes and pressure pulsations in draft tube of a model hydro turbine in a range of off-design conditions". *Experimental Thermal and Fluid Science,* **91**, feb, pp. 410–422.

[77] Lückoff, F., Sieber, M., and Oberleithner, K., 2018. "Open-Loop Control of the Precessing Vortex Core in a Swirl-stabilized Combustor: Impact on Flame Shape and Flame Stability". In Proceedings of ASME Turbo Expo 2018: Turbomachinery Technical Conference and Exposition, no. GT2018-75472, American Society of Mechanical Engineers.

[78] M. Lauer, T. S., 2008. "Heat Release Calculation in a Turbulent Swirl Flame from Laser and Chemiluminescence Measurements". In 14th Int Symp on Applications of Laser Techniques to Fluid Mechanics, Lisbon, Portugal, 07-10 July.

[79] Magri, L., and Juniper, M., 2014. "Global modes, receptivity, and sensitivity analysis of diffusion flames coupled with duct acoustics". *Journal of Fluid Mechanics,* **752**, pp. 237 – 265.

[80] Marusic, I., and Broomhall, S., 2020. "Leonardo da Vinci and Fluid Mechanics". *Annual Review of Fluid Mechanics,* **53**(1), jul.

[81] Mathews, B., Hansford, S., and O'Connor, J., 2016. "Impact of Swirling Flow Structure on Shear Layer Vorticity Fluctuation Mechanisms". In Volume 4A: Combustion, Fuels and Emissions, ASME.

[82] Moeck, J. P., 2010. "Analysis, Modeling, an Control of Thermoacoustic Instabilities". PhD thesis, TU Berlin.

[83] Moeck, J. P., Bourgouin, J.-F., Durox, D., Schuller, T., and Candel, S., 2012. "Nonlinear interaction between a precessing vortex core and acoustic oscillations in a turbulent swirling flame". *Combust Flame,* **159**(8), pp. 2650–2668.

[84] Moeck, J. P., Bourgouin, J.-F., Durox, D., Schuller, T., and Candel, S., 2013. "Tomographic reconstruction of heat release rate perturbations induced by helical modes in turbulent swirl flames". *Exp. Fluids,* **54**(4), pp. 1–17.

[85] Monkewitz, P. A., and Sohn, K. D., 1988. "Absolute instability in hot jets". *Aiaa J,* **26**, pp. 911–916.

[86] Müller, J. S., Lückoff, F., and Oberleithner, K., 2018. "Guiding Actuator Designs for Active Flow Control of the Precessing Vortex Core by Adjoint Linear Stability Analysis". *Journal of Engineering for Gas Turbines and Power,* **141**(4), dec, p. 041028.

[87] Müller, J. S., Lückoff, F., Paredes, P., Theofilis, V., and Oberleithner, K., 2020. "Receptivity of the turbulent precessing vortex core: synchronization experiments and global adjoint linear stability analysis". *Journal of Fluid Mechanics,* **888**, p. A3.

[88] Nishi, M., 1984. "Surging characteristics of conical and elbow type draft tubes". In Proc. 12th IAHR Symposium on Hydraulic Machinery and System, Stirling, 1984, pp. 272–283.

[89] Oberleithner, K., 2012. "On Turbulent Swirling Jets: Vortex Breakdown, Coherent Structures, and their Control". PhD thesis, TU Berlin.

[90] Oberleithner, K., and Paschereit, C. O., 2016. "Modeling Flame Describing Functions Based on Hydrodynamic Linear Stability Analysis". In Volume 4B: Combustion, Fuels and Emissions, ASME.

[91] Oberleithner, K., Paschereit, C. O., Seele, R., and Wygnanski, I., 2012. "Formation of Turbulent Vortex Breakdown: Intermittency, Criticality, and Global Instability". *Aiaa J,* **50**, pp. 1437–1452.

[92] Oberleithner, K., Paschereit, C. O., and Wygnanski, I., 2014. "On the impact of swirl on the growth of coherent structures". *J Fluid Mech,* **741**, 2, pp. 156–199.

[93] Oberleithner, K., Schimek, S., and Paschereit, C. O., 2015. "Shear flow instabilities in swirl-stabilized combustors and their impact on the amplitude dependent flame response: A linear stability analysis". *Combustion and Flame,* **162**(1), pp. 86 – 99.

[94] Oberleithner, K., Sieber, M., Nayeri, C. N., and Paschereit, C. O., 2011. "On the control of global modes in swirling jet experiments". *J. Phys: Conf. Ser.,* **318**(3), p. 032050.

[95] Oberleithner, K., Sieber, M., Nayeri, C. N., Paschereit, C. O., Petz, C., Hege, H.-C., Noack, B. R., and Wygnanski, I., 2011. "Three-dimensional coherent structures in a swirling jet undergoing vortex breakdown: stability analysis and empirical mode construction". *J Fluid Mech,* **679**, pp. 383–414.

[96] Oberleithner, K., Stöhr, M., Im, S. H., Arndt, C. M., and Steinberg, A. M., 2015. "Formation and flame-induced suppression of the precessing vortex core in a swirl combustor: experiments and linear stability analysis". *Combust Flame,* **162**(8), aug, pp. 3100–3114.

[97] Oberleithner, K., Terhaar, S., Rukes, L., and Paschereit, C. O., 2013. "Why Nonuniform Density Suppresses the Precessing Vortex Core". *J. Eng. Gas Turb. Power,* **135(12)**, p. 121506 (9 pages).

[98] Palies, P., Durox, D., Schuller, T., and Candel, S., 2010. "The combined dynamics of swirler and turbulent premixed swirling flames". *Combust Flame,* **157**(9), pp. 1698–1717.

[99] Palies, P., Ilak, M., and Cheng, R., 2017. "Transient and limit cycle combustion dynamics analysis of turbulent premixed swirling flames". *Journal of Fluid Mechanics,* **830**, oct, pp. 681–707.

[100] Palies, P., Schuller, T., Durox, D., Gicquel, L. Y. M., and Candel, S., 2011. "Acoustically perturbed turbulent premixed swirling flames". *Phys Fluids,* **23**(3), p. 037101.

[101] Panda, J., and McLaughlin, D. K., 1994. "Experiments on the instabilities of a swirling jet". *Phys Fluids,* **6**, pp. 263–276.

[102] Paredes, P., Terhaar, S., Oberleithner, K., Theofilis, V., and Paschereit, C. O., 2015. "Global and Local Hydrodynamic Stability Analysis as a Tool For Combustor Dynamics Modeling". In Proceedings of the ASME Turbo Expo 2015, no. GT2015-44173.

[103] Paschereit, C., Gutmark, E., and Weisenstein, W., 1998. "Structure and Control of thermoacoustic instabilities in a gas-turbine combustor". *Combust Sci Technol,* **138**, pp. 213–232.

[104] Paschereit, C. O., Gutmark, E., and Weisenstein, W., 2000. "Excitation of Thermoacoustic Instabilities by Interaction of Acoustics and Unstable Swirling Flow". *Aiaa J,* **38**, pp. 1025–1034.

[105] Paschereit, C. O., and Gutmark, E. J., 2008. "Combustion instability and emission control by pulsating fuel injection". *Journal of Turbomachinery,* **130**(1), p. 011012 (8 pages).

[106] Paschereit, C. O., Schuermans, B., Polifke, W., and Mattson, O., 2002. "Measurement of Transfer Matrices and Source Terms of Premixed Flames". *Journal of Engineering for Gas Turbines and Power,* **124**(2), Mar., pp. 239–247.

[107] Petz, C., Hege, H.-C., Oberleithner, K., Sieber, M., Nayeri, C. N., Paschereit, C. O., Wygnanski, I., and Noack, B. R., 2011. "Global modes in a swirling jet undergoing vortex breakdown". *Phys Fluids,* **23**(9), p. 091102.

[108] Qadri, U. A., Mistry, D., and Juniper, M. P., 2013. "Structural sensitivity of spiral vortex breakdown". *J Fluid Mech,* **720**, pp. 558–581.

[109] Raffel, M., Willert, C., Wereley, S., and Kompenhans, J., 2007. *Particle Image Velocimetry, A Practical Guide*, 2 ed. Springer press.

[110] Rayleigh, J. W. S., July 18, 1878. "The Explanation of certain Acoustical Phenomena". *Nature*, pp. 319–321.

[111] Renard, P.-H., Thévenin, D., Rolon, J., and Candel, S., 2000. "Dynamics of flame/vortex interactions". *Progress in Energy and Combustion Science,* **26**(3), pp. 225–282.

[112] Rigas, G., Oxlade, A. R., Morgans, A. S., and Morrison, J. F., 2014. "Low-dimensional dynamics of a turbulent axisymmetric wake". *Journal of Fluid Mechanics,* **755**, aug.

[113] Ruith, M. R., Chen, P., Meiburg, E., and Maxworthy, T., 2003. "Three-dimensional vortex breakdown in swirling jets and wakes: direct numerical simulation". *J Fluid Mech,* **486**, pp. 331–378.

[114] Rukes, L., Paschereit, C. O., and Oberleithner, K., 2016. "An assessment of turbulence models for linear hydrodynamic stability analysis of strongly swirling jets". *Eur. J. Mech. B. Fluids,* **59**, pp. 205 – 218.

[115] Rukes, L., Sieber, M., Paschereit, C., and Oberleithner, K., 2015. "Effect of initial vortex core size on the coherent structures in the swirling jet near field". *Experiments in Fluids,* **56**(10).

[116] Sarpkaya, T., 1971. "Vortex Breakdown in Swirling Conical Flows". *Aiaa J,* **9**, pp. 1792–1799.

[117] Schadow, K., and Gutmark, E., 1992. "Combustion instability related to vortex shedding in dump combustors and their passive control". *Progress in Energy and Combustion Science,* **18**(2), pp. 117 – 132.

[118] Schimek, S., Moeck, J. P., and Paschereit, C. O., 2011. "An Experimental Investigation of the Nonlinear Response of an Atmospheric Swirl-Stabilized Premixed Flame". *Journal of Engineering for Gas Turbines and Power,* **133**(10), p. 101502.

[119] Schuermans, B., 2005. "Modeling and control of thermoacoustic instabilities". PhD thesis, Lausanne, EPFL.

[120] Schuermans, B., Guethe, F., Pennell, D., Guyot, D., and Paschereit, C. O., 2010. "Thermoacoustic Modeling of a Gas Turbine Using Transfer Functions Measured Under Full Engine Pressure". *Journal of Engineering for Gas Turbines and Power,* **132**(11), aug.

[121] Sevilla, A., and Martínez-Bazán, C., 2004. "Vortex shedding in high Reynolds number axisymmetric bluff-body wakes: Local linear instability and global bleed control". *Physics of Fluids,* **16**(9), aug, pp. 3460–3469.

[122] Sieber, M., Ostermann, F., Woszidlo, R., Oberleithner, K., and Paschereit, C. Oliver, 2016. "Lagrangian coherent structures in the flow field of a fluidic oscillator". *Phys. Rev. Fluids,* **1**(5), p. 050509.

[123] Sieber, M., Paschereit, C. O., and Oberleithner, K., 2016. "Advanced Identification of Coherent Structures in Swirl-Stabilized Combustors". *J. Eng. Gas Turbines Power,* **139**, pp. 021503–021503–8.

[124] Sieber, M., Paschereit, C. O., and Oberleithner, K., 2016. "Spectral proper orthogonal decomposition". *J. Fluid Mech.,* **792**, 004, pp. 798–828.

[125] Silva, C. F., and Polifke, W., 2019. "Non-dimensional groups for similarity analysis of thermoacoustic instabilities". *Proceedings of the Combustion Institute,* **37**(4), pp. 5289–5297.

[126] Sipp, D., Marquet, O., Meliga, P., and Barbagallo, A., 2010. "Dynamics and Control of Global Instabilities in Open-Flows: A Linearized Approach". *Appl Mech Rev,* **63**(3), p. 030801.

[127] Slabaugh, C. D., Boxx, I., Werner, S., Lucht, R. P., and Meier, W., 2016. "Structure and Dynamics of Premixed Swirl Flames at Elevated Power Density". *AIAA Journal,* **54**(3), mar, pp. 946–961.

[128] Steinberg, A., Arndt, C., and W, M., 2013. "Parametric study of vortex structures and their dynamics in swirl-stabilized combustion". *Proceedings of the Combustion Insitute,* **34**, pp. 3117–3125.

[129] Steinberg, A., Boxx, I., Stoehr, M., Carter, C., and Meier, W., 2010. "Flow-flame interactions causing acoustically coupled heat release fluctuations in a thermo-acoustically unstable gas turbine model combustor". *Combust Flame,* **157**(12), pp. 2250–2266.

[130] Steinberg, A. M., Boxx, I., Stohr, M., Meier, W., and Carter, C. D., 2012. "Effects of Flow Structure Dynamics on Thermoacoustic Instabilities in Swirl-Stabilized Combustion". *AIAA Journal,* **50**(4), apr, pp. 952–967.

[131] Steinberg, A. M., and Driscoll, J. F., 2009. "Straining and wrinkling processes during turbulence–premixed flame interaction measured using temporally-resolved diagnostics". *Combustion and Flame,* **156**(12), dec, pp. 2285–2306.

[132] Stöhr, M., Arndt, C., and Meier, W., 2015. "Transient effects of fuel-air mixing in a partially-premixed turbulent swirl flame". *Proc. Combust. Inst.,* **35**(3), pp. 3327 – 3335.

[133] Stöhr, M., Boxx, I., Carter, C. D., and Meier, W., 2012. "Experimental study of vortex flame interaction in a gas turbine model combustor". *Combust Flame,* **159**, pp. 2636 – 2649.

[134] Stöhr, M., Oberleithner, K., Arndt, C. M., Steinberg, A. M., and Meier, W., 2015. "Experimental study of transient coupling of PVC formation and flame shape transition in a bi-stable turbulent swirl flame.". In Proceedings of the 7th European Combustion Meeting, Budapest, Hungary.

[135] Stöhr, M., Oberleithner, K., Sieber, M., Yin, Z., and Meier, W., 2018. "Experimental Study of Transient Mechanisms of Bi-Stable Flame Shape Transitions in a Swirl Combustor". *Journal of Engineering for Gas Turbines and Power,* **140**, p. 011503.

[136] Stöhr, M., Sadanandan, R., and Meier, W., 2009. "Experimental study of unsteady flame structures of an oscillating swirl flame in a gas turbine model combustor". *Proceedings of the Combustion Institute,* **32**(2), pp. 2925 – 2932.

[137] Stöhr, M., Yin, Z., and Meier, W., 2017. "Interaction between velocity fluctuations and equivalence ratio fluctuations during thermoacoustic oscillations in a partially premixed swirl combustor". *Proceedings of the Combustion Institute,* **36**(3), pp. 3907–3915.

[138] Syred, N.; Beer, J. M., 1974. "Combustion in Swirling Flows: A Review". *Combust Flame,* **23**, pp. 143–201.

[139] Syred, N., 2006. "A review of oscillation mechanisms and the role of the precessing vortex core (PVC) in swirl combustion systems". *Prog. Energy Combust. Sci.,* **32**(2), pp. 93 – 161.

[140] Tammisola, O., and Juniper, M., 2016. "Coherent structures in a swirl injector at Re=4800 by nonlinear simulations and linear global modes". *J Fluid Mech,* **792**, pp. 620–657.

[141] Terhaar, S., 2015. "Identification and Modelling of Coherent Structures in Swirl-Stabilized Combustors at Dry and Steam-Diluted Conditions". PhD thesis, TU Berlin.

[142] Terhaar, S., Ćosić, B., Paschereit, C., and Oberleithner, K., 2016. "Suppression and excitation of the precessing vortex core by acoustic velocity fluctuations: An experimental and analytical study". *Combust. Flame,* **172**, pp. 234 – 251.

[143] Terhaar, S., Ćosić, B., Paschereit, C. O., and Oberleithner, K., 2014. "Impact of Shear Flow Instabilities on the Magnitude and Saturation of the Flame Response". *J. Eng. Gas Turb. Power,* **136**(7), p. 071502.

[144] Terhaar, S., Krüger, O., and Paschereit, C. O., 2015. "Flow Field and Flame Dynamics of Swirling Methane and Hydrogen Flames at Dry and Steam-Diluted Conditions". *J. Eng. Gas Turbines Power,* **137**, p. 041503.

[145] Terhaar, S., Oberleithner, K., and Paschereit, C., 2015. "Key parameters governing the precessing vortex core in reacting flows: An experimental and analytical study". *Proc. Combust. Inst.,* **35**(3), pp. 3347 – 3354.

[146] Terhaar, S., Oberleithner, K., and Paschereit, C. O., 2014. "Impact of Steam-Dilution on the Flame Shape and Coherent Structures in Swirl-Stabilized Combustors". *Combust Sci Technol,* **186**(7), pp. 889–911.

[147] Terhaar, S., Reichel, T. G., Schrödinger, C., Rukes, L., Paschereit, C. O., and Oberleithner, K., 2015. "Vortex Breakdown Types and Global Modes in Swirling Combustor Flows with Axial Injection". *J Propul Power,* **31**(1), pp. 219–229.

[148] Theofilis, V., 2003. "Advances in global linear instability analysis of nonparallel and three-dimensional flows". *Prog Aerosp Sci,* **39**, pp. 249–315.

[149] Voigt, P., and Schodl, R., 1997. "Using the laser light sheet technique in combustion research". In AGARD conference proceedings, AGARD, pp. 48–1.

[150] Warnatz, J., Maas, U., and Dibble, R. W., 2006. *Combustion*. Springer-Verlag GmbH.

[151] Weidner, S., Faltenbacher, M., François, I., Thomas, D., Skùlason, J., and Maggi, C., 2018. "Feasibility study of large scale hydrogen power-to-gas applications and cost of the systems evolving with scaling up in Germany, Belgium and Iceland". *International Journal of Hydrogen Energy,* **43**(33), aug, pp. 15625–15638.

[152] Welch, G., and Bishop, G., 2006. An Introduction to the Kalman Filter. UNC-Chapel Hill, TR 95-041, July.

[153] Woszidlo, R., Ostermann, F., Nayeri, C. N., and Paschereit, C. O., 2015. "The time-resolved natural flow field of a fluidic oscillator". *Experiments in Fluids,* **56**(6), jun.

[154] Yang, X., and Zebib, A., 1989. "Absolute and convective instability of a cylinder wake". *Phys Fluids,* **1**, pp. 689–696.

[155] Yin, Z., and Stöhr, M., 2019. "Time–frequency localisation of intermittent dynamics in a bistable turbulent swirl flame". *Journal of Fluid Mechanics,* **882**, nov.

[156] Yuan, Z.-G., 1995. "The filtered Abel transform and its application in combustion diagnostics". *NASA/C–2003-212121*.

[157] Zhang, R., Boxx, I., Meier, W., and Slabaugh, C. D., 2019. "Coupled interactions of a helical precessing vortex core and the central recirculation bubble in a swirl flame at elevated power density". *Combustion and Flame,* **202**, apr, pp. 119–131.

Associated publications

[1] Lückoff, F., Sieber, M., Paschereit, C. O., and Oberleithner, K., 2018; "Characterization of Different Actuator Designs for the Control of the Precessing Vortex Core in a Swirl-Stabilized Combustor". *ASME. J. Eng. Gas Turbines Power, 140(4): 041503.*

[2] Lückoff, F., Sieber, M., and Oberleithner, K., 2018. "Open-Loop Control of the Precessing Vortex Core in a Swirl-stabilized Combustor: Impact on Flame Shape and Flame Stability". In Proceedings of ASME Turbo Expo 2018: Turbomachinery Technical Conference and Exposition, no. GT2018-75472.

[4] Müller, J. S., Lückoff, F., and Oberleithner, K., 2018. "Guiding Actuator Designs for Active Flow Control of the Precessing Vortex Core by Adjoint Linear Stability Analysis". *ASME. J. Eng. Gas Turbines Power, 141*(4), dec, p. 041028.

[3] Lückoff, F., and Oberleithner, K., 2019; "Excitation of the precessing vortex core by active flow control to suppress thermoacoustic instabilities in swirl flames". *International Journal of Spray and Combustion Dynamics, 11.*

[5] Lückoff, F., Sieber, M., Paschereit, C. O., and Oberleithner, K., 2019; "Phase-Opposition Control of the Precessing Vortex Core in Turbulent Swirl Flames for Investigation of Mixing and Flame Stability". *ASME. J. Eng. Gas Turbines Power., 141(11): 111008.*

[6] Müller, J. S., Lückoff, F., Paredes, P., Theofilis, V., and Oberleithner, K., 2020. "Receptivity of the turbulent precessing vortex core: synchronization experiments and global adjoint linear stability analysis". *Journal of Fluid Mechanics, 888*, p. A3.

[7] Lückoff, F., Sieber, M., Paschereit, C. O., and Oberleithner, K., 2020; "Impact of the Precessing Vortex Core on NOx Emissions in Premixed Swirl-Stabilized Flames - An Experimental Study". *ASME. J. Eng. Gas Turbines Power, 142(11): 111010.*

[8] Lückoff, F., Kaiser, T. L., Paschereit, C. O., and Oberleithner, K., 2021; "Mean field coupling mechanisms explaining the impact of the precessing vortex core on the flame transfer function". *Combustion and Flame, 223, 254–266.*